CONTROLLED SELF-ASSEMBLY OF *p*-PHENYLENEETHYNYLENE DERIVATIVES TO DIVERSE SUPRAMOLECULAR ARCHITECTURES

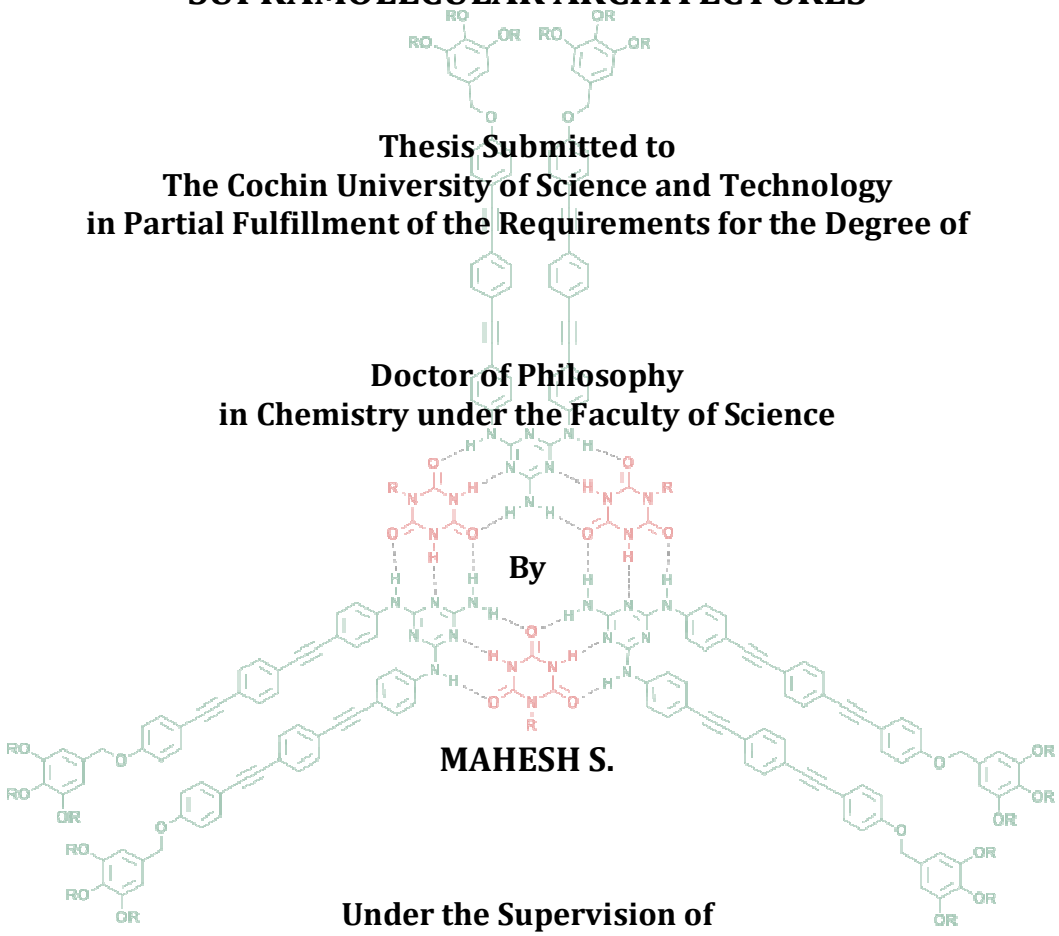

Thesis Submitted to
The Cochin University of Science and Technology
in Partial Fulfillment of the Requirements for the Degree of

Doctor of Philosophy
in Chemistry under the Faculty of Science

By

MAHESH S.

Under the Supervision of
Dr. A. AJAYAGHOSH

Photosciences and Photonics Section
Chemical Sciences and Technology Division
National Institute for Interdisciplinary Science and Technology (NIIST)
(*Formerly*, Regional Research Laboratory), CSIR,
Trivandrum- 695 019, Kerala

DECEMBER 2009

Dedicated to My Family…..

DECLARATION

I hereby declare that the matter embodied in the thesis entitled: **"Controlled Self-assembly of *p*-Phenyleneethynylene Derivatives to Diverse Supramolecular Architectures"** is the result of the investigations carried out by me at the Photosciences and Photonics Section, Chemical Sciences and Technology Division, National Institute for Interdisciplinary Science and Technology (NIIST), CSIR, Trivandrum, under the supervision of Dr. A. Ajayaghosh and the same has not been submitted elsewhere for any other degree.

In keeping with the general practice of reporting scientific observations, due acknowledgement has been made wherever the work described is based on the findings of other investigators.

Mahesh S.

National Institute for Interdisciplinary Science and Technology (NIIST)

(Formerly Regional Research Laboratory)

Council of Scientific & Industrial Research (CSIR)

Industrial Estate P.O., Trivandrum - 695 019
Kerala, INDIA

A. Ajayaghosh, F. A. Sc.
Scientist & Head
Chemical Sciences and Technology Division

Tel: 91-471-2515 306
Fax: +91-471-2491 712
E-mail: ajayaghosh62@gmail.com

December 31, 2009

CERTIFICATE

This is to certify that the work embodied in the thesis entitled: **"Controlled Self-assembly of *p*-Phenyleneethynylene Derivatives to Diverse Supramolecular Architectures"** has been carried out by Mr. Mahesh S. under my supervision at the Photosciences and Photonics Section of the National Institute for Interdisciplinary Science and Technology (NIIST), CSIR, Trivandrum and the same has not been submitted elsewhere for a degree.

A. Ajayaghosh
(Thesis Supervisor)

ACKNOWLEDGEMENTS

It is with great pleasure that I extend my deep sense of gratitude to Dr. A. Ajayaghosh, my thesis supervisor, for suggesting the research problem, for his constant guidance, support and encouragement, leading to the successful completion of this work.

I would like to express my gratitude to Prof. M. V. George for his constant encouragement, inspiration and useful discussions during my stay at NIIST.

I thank Dr. Suresh Das, Director, NIIST, Trivandrum, for providing me the necessary facilities and infrastructure of the laboratory for carrying out this work.

I take this opportunity to thank the former Directors of NIIST, in particular Dr. G. Vijay Nair, Dr. B.C. Pai and Prof. T.K. Chandrasekhar for supporting my research activities at NIIST.

My Sincere thanks are also due to:

- *Dr. K. R. Gopidas, Dr. D. Ramaiah, Dr. K. George Thomas, and Dr. A. Sreenivasan, Scientists of the Photosciences and Photonics Section, for their help and valuable suggestions.*
- *Prof. A. Kitamura, Dr. Shiki Yagai, Chiba University, Japan and Dr. Kikkawa, AIST, Tsukuba, Japan, for fruitful collaboration and also for their help and support during my visit under DST-JSPS programme at Chiba University.*
- *Dr. E. Arunkumar, Dr. Subi J. George, Dr. Priya Carol, Dr. V. K. Praveen, Dr. C. Vijayakumar, Dr. P. Chithra and Dr. S. Santhosh Babu, former members of the Photosciences and Photonics Group for their help and advice.*
- *Mr. S. Sreejith, Mr. S. Srinivasan, Ms. K. P. Divya and Mr. S. Prasanthkumar, Mr. Thirumalai Kumaran, Mr. Ansar Babu, Mr. Krishnan Kartha, Mr. P. Anees, Mr. Sandeep, and other members of Photosciences and Photonics Section for their help and cooperation.*

- *Ms. Saumya Cyriac, Mr. P. Rakesh, Ms. Vidya. K, Mr. Ziyad, Ms. Meera Mohan and other former associates of my research group.*
- *Mr. Robert Philip, Mrs. Sarada Nair, and Dr. J. D. Sudha, for their support.*
- *Mrs. Saumini Mathew for NMR spectra, Mrs. S. Viji for HRMS, Ms. Priya A. Nair and Ms. Sreenakumari for GC-MS and IR spectra, Mr. P. Prabhakar Rao and Mr. M. R. Chandran for SEM, Dr. U. Shyamaprasad and Mr. P. Guruswamy for XRD, Mr. D. Sanjay of RGCB for TEM, Mr. Willi Paul of SCTIMST for DLS and Dr. Prasad, NIIST for TEM measurements.*
- *All my friends at NIIST for their love and support.*
- *All my teachers for their encouragement at different stages of my academic career.*
- *All my family members for their love and support.*
- *CSIR, UGC, JSPS and DST for financial assistance.*

Mahesh S.

Trivandrum

December, 2009

CONTENTS

PREFACE

Control of the self-assembly of synthetic molecules for the creation of nanosized, complex architectures, by exploiting the principles of supramolecular chemistry is a topic of considerable importance. In this context, self-assembly of oligo(*p*-phenylenevinylene)s (OPVs) and oligo(*p*-phenyleneethynylene)s (OPEs) have received considerable attention. The first chapter of the thesis is a brief overview of multiple H-bonded and photochromic self-assemblies.

The second chapter of the thesis describes the self-assembly of photoisomerizable azobenzene linked phenyleneethynylene derivatives. Even though, only far related to the complex biological photomorphogenesis, a comparable but simple process of light triggered supramolecular structural evolution in the molecular self-assembly of two isomeric photochromic molecules is described in this chapter. Precisely, two isomers of the same photochromic system initially self-assemble to form different architectures which upon photoirradiation independently lead to the hierarchical evolution of supramolecular flakes and rods. We have exploited the *E-Z* isomerization of azobenzene derivatives to induce a polarity difference which triggers the hierarchical assemblage of the initially

formed supramolecular ensembles, resulting in a well-defined final morphology.

Utilization of complementary multiple H-bonding modules such as melamines and cyanurates play a key role in controlling the self-assembly of π-conjugated oligomers. Aggregation of these modules leads to rosette (macrocyclic) and tape-like (linear or crinkled) architectures. Superstructures, hierarchically organized from rosette and other related supramolecular macrocycles reported so far are limited to extended columnar architectures. In the third chapter we describe an unprecedented self-organization of H-bonded rosette assemblies of an oligo(*p*-phenyleneethynylene) (OPE) attached melamine and a cyanurate derivative in aliphatic solvent, leading to the formation of toroidal objects of nanometer dimension. This is a new procedure for synthesizing nanometer-sized toroids (donut-shaped) objects via hierarchical self-assembly of rosettes.

The last chapter of the thesis describes the synthesis, photophysical and self-assembly behavior of a melamine substituted OPE. The aggregation of this molecule in methylcyclohexane was monitored by variable temperature fluorescence measurements. The absence of significant solvent dependence on the flouresence maximum suggests that this compound exists as monomeric species under low concentration. When aliquots of a complementary H-bonding molecule was added to the solution, the initially formed

opaque and weak gels turned in to transparent and stable gel with distinct physical properties.

In summary, the work described in this thesis deals with the self-assembly of *p*-phenyleneethynylene type π-conjugated system with the help of complementary H-bonding interaction and photochromic azobenzene moiety. Self-assembly of these systems has resulted in the formation of supramolecular architectures such as nanoparticles, flakes, rods, donuts and fibers. Moreover, the morphologies of these structures showed significant dependency on the structure of the building blocks, concentration of the solutions and photoirradiation. The different chapters of the thesis describe the details of these investigations and the data presented illustrate the intriguing properties of phenyleneethynylene derivatives during their self-assembly.

Chapter 1

Diverse Self-assembled Architectures of Hydrogen-Bonded and Photoresponsive Systems: An Overview

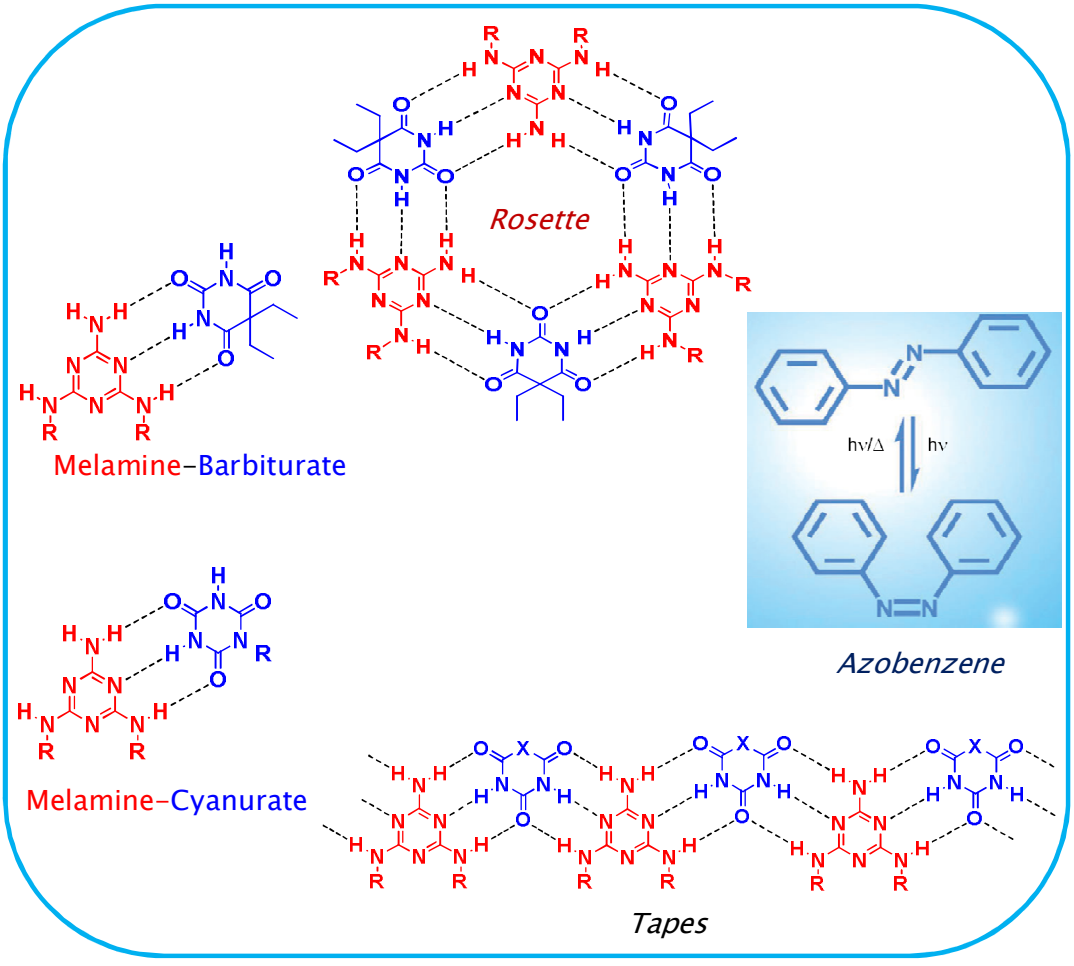

1.1. Abstract

Beyond scientific curiosity, molecular self-assembly is currently recognized as the most powerful strategy in the development of new functional materials requiring nanometer scaled molecular manipulation that is not achievable by a conventional top-down approach. The creation of hierarchical assemblies of π-conjugated systems by a supramolecular approach combines the advantages of small molecules and of polymers. Recently, several new approaches have been reported to construct self-organized π-conjugated systems into various supramolecular architectures of different size, shape and properties. However, controlled organization of self-assembled objects is extremely difficult and hence challenging. A comprehensive knowledge of intermolecular interactions is necessary to the design of molecular systems that form controlled assemblies on specific surfaces. In this chapter, an overview of the self-assembly of π-conjugated systems into morphologies of different size and shape is presented with emphasis on complementary hydrogen bonded and photoresponsive systems. Finally, the aim and the approach to the thesis are presented.

1.2. Introduction

Molecular self-assembly has emerged as a powerful tool for the construction of well-defined nanoarchitectures and for the tailoring of physical properties of small molecular building blocks.[1-3] The dynamic nature of self-assembly due to the reversibility of noncovalent interactions has been of interest to chemists for the creation of multicomponent self-assemblies, which can be regulated by external stimuli.[4] These studies have been targeted on the fabrication

of smart functional materials where physical properties and functions emerging from large molecular ensembles could be controlled at will. Moreover, the reversibility of these noncovalent interactions will allow self-correction during the organization process, leading to well defined supramolecular architectures. Supramolecular species can be constructed by means of noncovalent forces such as electrostatic, hydrophobic, van der Waals, hydrogen-bonding and donor-acceptor interactions. These interactions can be of attractive and repulsive in nature with interaction energy ranging from 4-400 kJ mol^{-1}. Compared to covalent bonds, noncovalent interactions are generally weak and vary from less than 5 kJ mol^{-1} for van der Waals forces, to approximately 50 kJ mol^{-1} for hydrogen bonds, and 250 kJ mol^{-1} for coulomb interactions (Table 1.1).

Table 1.1. Average Interaction Energies of Various Noncovalent Interactions Frequently Used in Supramolecular Chemistry

Entry	Type of interaction	Strength (kJ/mol)
1	Covalant	100-400
2	Coulomb	250
3	Hydrogen bond	10-65
4	Ion-dipole	50-200
5	Dipole-dipole	5-50
6	Cation-π	5-80
7	π-π	0-50
8	van der Waals forces	< 5
9	Hydrophobic effects	Difficult to assess
10	Metal-ligand	0-400

Even though, noncovalent interactions are very weak, the cooperative effect of several such interactions may lead to the formation of reversible, thermodynamically or kinetically stable supramolecular assemblies under a variety of conditions.

1.3. Noncovalent Interactions: *Importance of Hydrogen Bonding*

Among different noncovalent interactions mentioned above, hydrogen bonds are the most important glue to stick molecules together. Hydrogen bonds are the most crucial and favorite secondary interaction to construct supramolecular architectures due to their selectivity, tunable strength and directionality. Hydrogen bonds are attractive electrostatic interaction between a positively charged H-atom bonded to an electronegative element (donor: $D^{\delta-}$–$H^{\delta+}$), and a negatively charged atom with a lone pair of electrons (acceptor: $A^{\delta-}$). The strength of a single H-bond is related to the acidity of the hydrogen-bond donor group and the basicity of the hydrogen-bond acceptor group involved, which ranges from 10-65 kJ mol^{-1} for neutral molecules, to 40-190 kJ mol^{-1} for an ionic acid-base hydrogen-bond. Apart from the fundamental significance of H-bonds, they, in cooperation with other noncovalent forces can lead molecules to organize in different ways to form stable supramolecular architectures of definite shape and properties. Therefore, the study of H-bonds and its use in the creation of supramolecular architectures are of fundamental and technological importance, particularly in the area of advanced functional materials.

1.4. Multiple Hydrogen-Bond Interactions of Heteroaromatic Modules

Compounds that have more than one hydrogen-bond donor (D) and acceptor (A) groups are capable of forming multiple hydrogen-bonding interactions. Rigidity and well-defined geometry of heteroaromatic compounds make them special as multiple hydrogen-bonding modules featuring highly specific and directional binding properties. The specificity is undoubtedly epitomized by the base-pairing in DNA and RNA as genetic information storage event.[5] Triple hydrogen-bonding interaction between cytosine (DDA) and guanine (AAD) have been used to connect functional chromophores (Figure 1.1), as demonstrated by seminal works of Sessler et al.[6–9] Significant effort has been devoted to develop artificial multiple hydrogen-bonding modules by the groups of Zimmerman, Meijer and Lehn with the aim to create more specific artificial molecular recognition systems.[10,11] From the practical application view point, the primary importance of hydrogen-bonding modules may be their synthetic accessibility that can allow the conjugation with other functional molecules such as dyes. Triple hydrogen-bonding interaction between diaminopyridine DAD modules and imide-type ADA modules, first reported by Hamilton and van Engen,[12] have been widely used to noncovalently connect functional molecules because of their synthetic accessibility (Figure 1.1). Later, more versatile hydrogen-bonding modules have been reported by connecting DAD modules through a rigid spacer as in Figure 1.1c.[13,14]

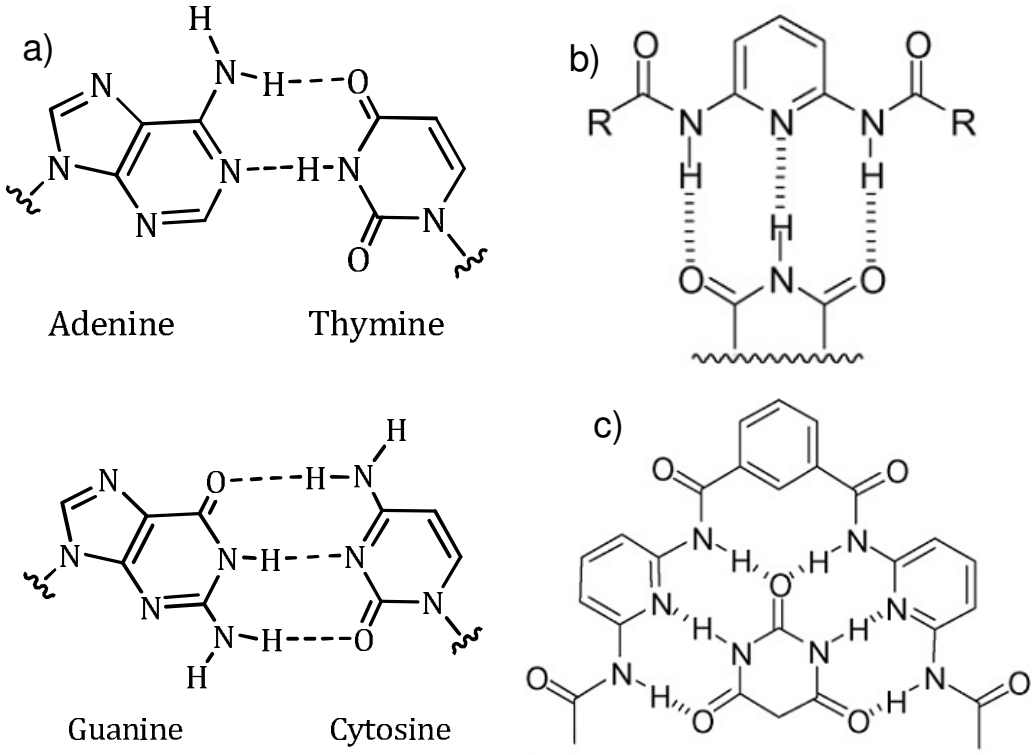

Figure 1.1. Examples of multiple hydrogen-bonding interactions between (a) guanine and cytosine modules; (b) acylated diaminopyridine and imide modules and (c) Hamilton-type receptor and barbituric acid module.

Covalently preorganized receptor, such as the Hamilton-type receptor (Figure 1.1c), promises more specific and stronger interaction with ditopic ADA modules such as barbituric and cyanuric acids. Complexation between ditopic *N*, *N*-disubstituted melamine type DAD module and barbiturate or cyanurate ADA modules provides different hydrogen-bonded networks, which have been extensively studied by Whitesides and Lehn.[15,16–18] Whitesides et al. have found a distinct substituent effect on the formation of extended hydrogen bonded networks.[19] The introduction of sterically demanding substituents to melamine (R in Figure 1.2) leads to the preferential formation of the cyclic hexamer (rosette)

over the competing linear tape like aggregates (tape). The mechanism of this substituent effect remains controversial.[20,21] A large number of functional assemblies have been constructed using these extended hydrogen bonded networks as supramolecular scaffolds. Among them, calixarene linked double rosette assemblies developed by Reinhoudt and coworkers are interesting due to supramolecular chirality, nanoscale assemblies, sensor applications, molecular capsule formation, and so forth.[22-27]

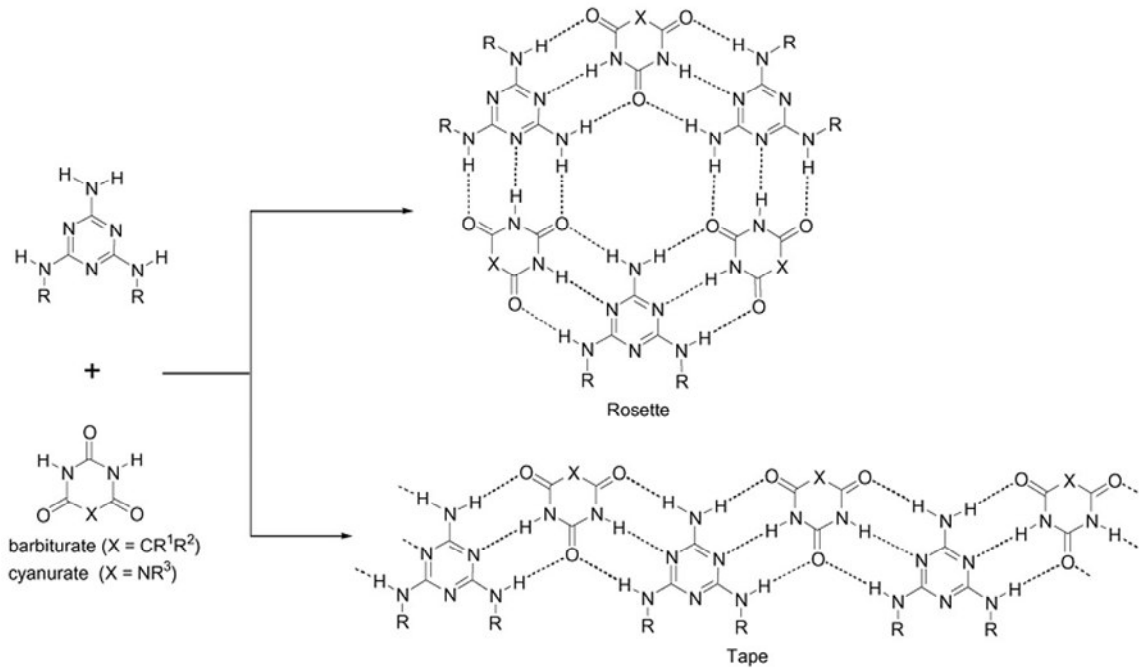

Figure 1.2. Supramolecular rosette and tape like architectures formed from melamine and barbiturate/cyanurate modules via triple hydrogen-bonding.

Quadruple hydrogen-bonding modules such as ureidotriazine (UTr) and ureidopyrimidinone (UPy) developed by the Meijer, Sijbesma and coworkers have attracted much attention because of their prominent properties such as high binding strength (K_{ass}) and synthetic accessibility (Figure 1.3).[28–32] Supramolecular

polymerization driven by the quadruple hydrogen-bonding of these modules promises high degree of polymerization even in solution state.

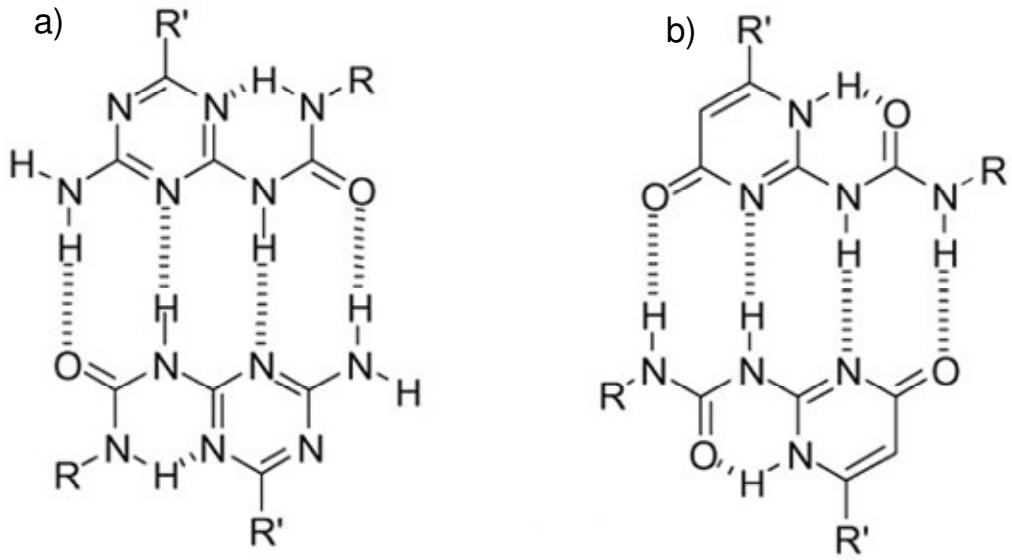

Figure 1.3. Quadruple hydrogen bonding in (a) ureidotriazine (UTr) and (b) ureidopyrimidinone derivatives (UPy).

1.5. Multiple Hydrogen-Bonding in π-Conjugated Molecules

Extended π-conjugated chromophores are attractive compounds for optoelectronic applications due to pronounced electronic, magnetic and photophysical properties.[33–36] Thus, numerous efforts have been devoted to construct supramolecular assemblies of π-conjugated chromophores.[37] The resulting self-assemblies could, not only be directly applied to functional materials but also of fundamental importance toward understanding the relationship between chromophore arrangements and functions. Directionality and rigidity of multiple hydrogen-bonding interactions fulfill the demand to spatially arrange functional

chromophores so that they are capable of achieving efficient energy/electron transfer properties.

Porphyrins are the most widely explored chromophoric building blocks for functional noncovalent assemblies.[38,39] Several research groups have extensively investigated the self-assembling properties of porphyrins. Research in this direction has utilized the complementary H-bonding interactions between melamine-cyanurates or barbiturates, because of their ability to form macrocyclic as well as tape like architectures. Lehn and coworkers have prepared hexameric porphyrin array **1** using the melamine-barbiturate rosette assembly as the supramolecular scaffold (Figure 1.4).[40] Drain and Nishide et al. have independently reported the formation of tetrameric porphyrin assemblies **2** [41,42] and **3** [43], respectively, using quadruple hydrogen-bonding modules (Figure 1.4b). When complexes were prepared by mixing free base and Zn^{2+} metallated porphyrin modules, energy transfer from the later to the former was observed. In a similar study, Meijer and Schenning have extensively studied multiple hydrogen bonding-mediated self-assembly of oligo(*p*-phenylenevinylene)s (OPVs) to explore the versatility of nanomaterials composed of self-assemblies of well-defined conjugated oligomers as alternatives of those composed of π-conjugated polymers in optoelectronic applications.[44]

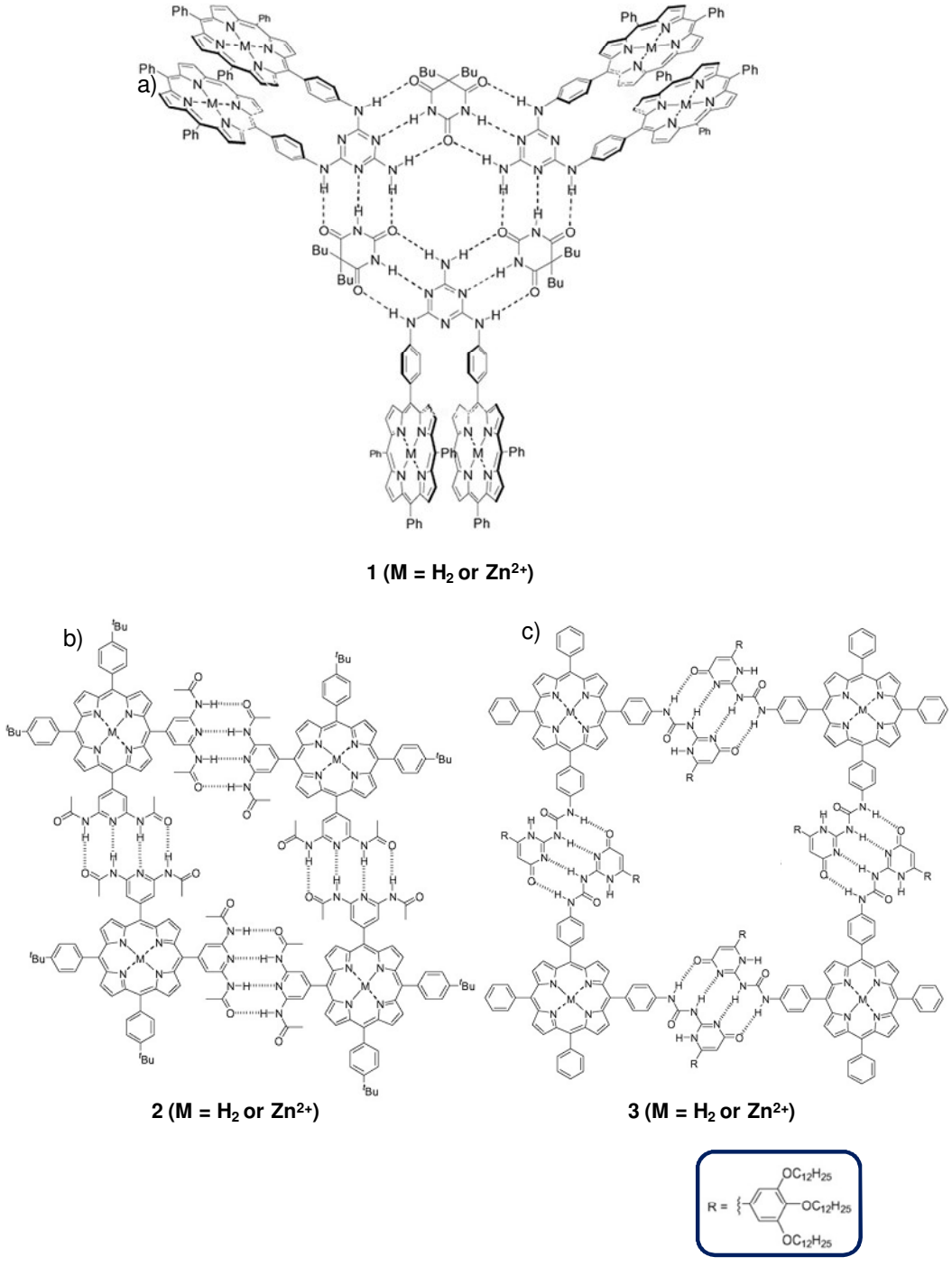

Figure 1.4. a) A hexameric porphyrin array **1** through H-bonded melamine-barbiturate rosette assembly; b) and c) Tetrameric porphyrin arrays **2** and **3** based on quadruple hydrogen-bonding interactions.

Schenning et al. have studied the self-assembly of OPVs which are functionalized with uriedotriazine quadruple H-bonding unit with the enantiomerically pure (*S*)-2-methylbutoxy side chains.[45] In chloroform, the monofunctional OPV derivative **4**, dimerizes through quadruple H-bonding with a dimerization constant of $K_{dim} = (2.1 \pm 0.3) \times 10^4$ L mol^{-1}. In dodecane, the H-bonded dimers self-assemble into left-handed helical stacks (Figure 1.5). Temperature and concentration dependent measurements have shown that the stability of the self-assembled stacks increases with conjugation length, due to the favorable π-π interactions. Detailed AFM studies have shown that, single fibers could be transferred only to inert substrates like graphite and silicium oxide. In the case of repulsive surfaces (mica and glass), clustering of the stacks occurs, whereas on attractive surfaces (gold), the stacks are destroyed (Figure 1.5b). These studies reveal the importance of inert substances for the better organisation of OPVs which is required for the fabrication of nanodevices.

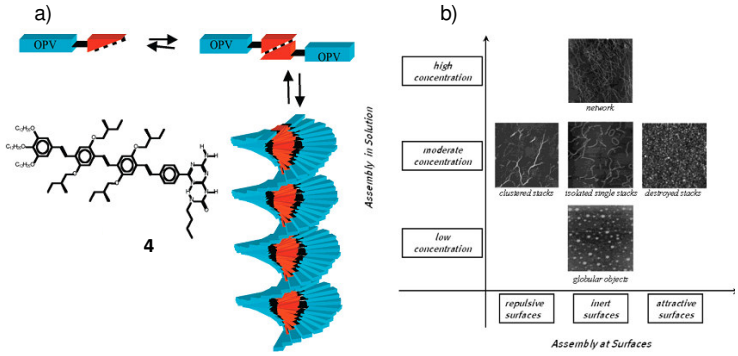

Figure 1.5 a) Schematic representation of the self-organization of **4** into helical stacks; b) Dependence of the morphology of **4** on solution concentration and on the surface nature.

The bifunctional OPV derivative **5** forms less organized frustrated polymeric stacks, due to the competition between favorable π-π interactions and restricted conformational freedom (Figure 1.6). More importantly, the length of these supramolecular polymers and its helicity could be controlled by the addition of monofunctional OPV derivatives as chain stoppers.

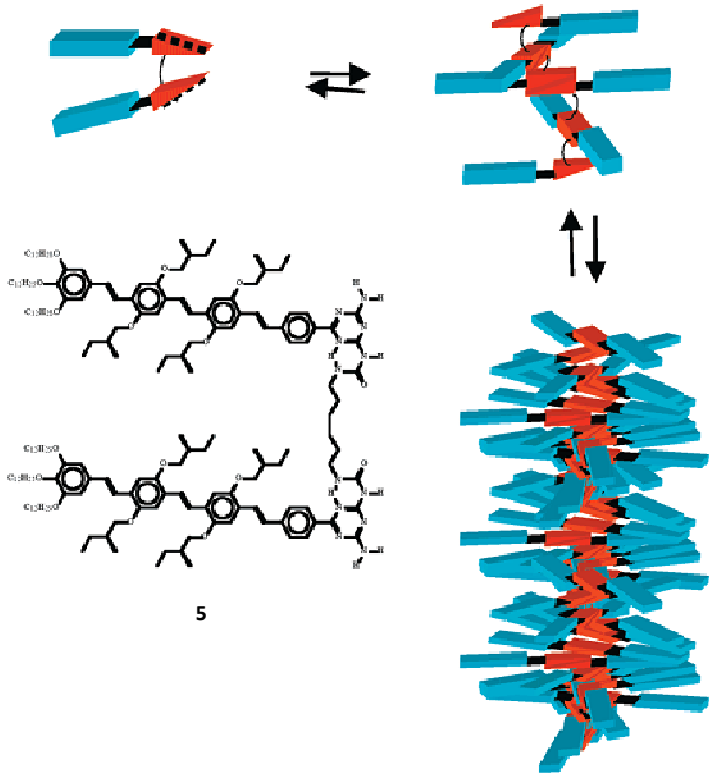

Figure 1.6. Schematic representation of the self-organization of **5** into frustrated polymeric stacks.

Beckers et al. have observed the preferential formation of a functional supramolecular heterodimer **6** between **5** and a C_{60} containing self-complementary ureidopyrimidinone moieties (Figure 1.7).[46] Formation of the heterodimer was confirmed by ^{1}H NMR studies and from the changes in the emission spectrum. During the mixing of the two components, the absorption bands remained unchanged, indicating a weak electronic interaction in the ground state. However,

considerable quenching of the OPV emission could be observed, indicating singlet energy transfer from the excited OPV to the C_{60}.

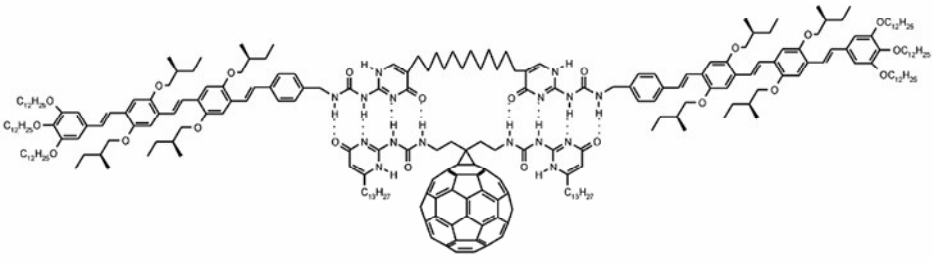

6

Figure 1.7. Quadruple hydrogen bonding in OPV-C_{60} heterodimer **6**.

Organized chromophore assemblies are crucial in electron and energy transfer processes of biological systems. Such assemblies are not only important for addressing fundamental questions in chemical biology but also of great interest to the design of photovoltaic devices. With this objective, Schenning et al. have designed a hydrogen-bonded OPV–perylene bisimide chiral assembly **7** (Figure 1.8a).[47] In this donor–acceptor–donor assembly, the acceptor perylene dye is placed in between two OPV donors through the complementary triple hydrogen-bond interaction of diaminotriazine and imide moieties. Optical and chiroptical studies have revealed the formation of helically organized chromophores in non-polar solvents (Figure 1.8b). This is confirmed by AFM images which showed the formation of helical rod like aggregates (Figure 1.8c). Electron transfer occurs from the OPV to perylene as evident from femtosecond pump-pulse spectroscopy measurements which revealed the formation of OPV radical cation at 1450 nm.

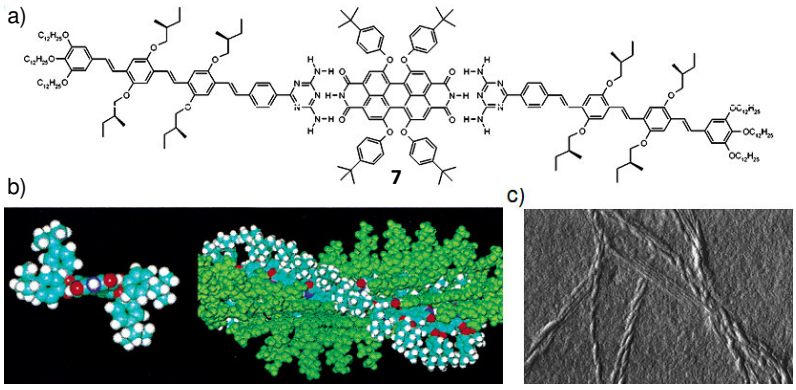

Figure 1.8. a) 2:1 Assembly of OPV and perylene bisimide, b) top view on one atropisomer of **7** (left) and possible helical arrangement for **7** (right; OPVs are shown in green color) and c) tapping mode AFM image (715 × 475 nm^2) of **7** on glass surface.

Recently, Iwaura et al. have synthesized a nucleotide appended OPV, {bis[2,5-bis(2-methoxyethoxy)-1,4-phenylene]bis(2,1-ethenediyl-1,4-phenylenemethylene)}bis(2′-deoxy-3′-thymidylicacid) (**8**).[48] Self-assembly of **8** and its binary self-assembly with a complementary single-stranded 20-meric oligodeoxyadenylic acid (**9**) in aqueous solutions has resulted in the formation of right-handed helical stacks (Figure 1.9a). Since oligodeoxyadenylic acids are known to form right-handed single helices in neutral aqueous solution, templating of **8** and **9** together induces a right-handed helical stack with the formation of A-T base pairs as in DNA double strands. Right-handed helices were obtained from the binary self-assembly of **8/9** (A:T = 1:1) with a thickness of 6.4 nm which correspond to the total width of **8** (3.9 nm) and adenylic acid monomers in the strands of **9** (two times 1.2 nm) ((Figure 1.9b). However, the helix obtained from the binary self-assembly of **8/9** (T:A = 2:1) resulted in the formation of a right-handed helix with

a width of 5.1 nm which is compatible with the sum of the lengths of **8** (3.9 nm) and a single strand of **9** (1.2 nm) (Figure 1.9c).

In another report, Meijer et al. have used single stranded DNA (ssDNA) building blocks to organize OPV molecules in a "bottom-up" self-assembly approach using complementary hydrogen-bonding interactions with the objective of constructing functional nanosized objects.[49] An oligothymine is used as the template to which a supramolecular stack of chromophores such as naphthalene, and OPV are hydrogen-bonded via the complementary diamino triazine unit (Figure 1.10). In solution at higher concentrations, **11** and **12** individually form weak aggregates as indicated by the blue-shift in absorption and a red-shifted, quenched photoluminescence.

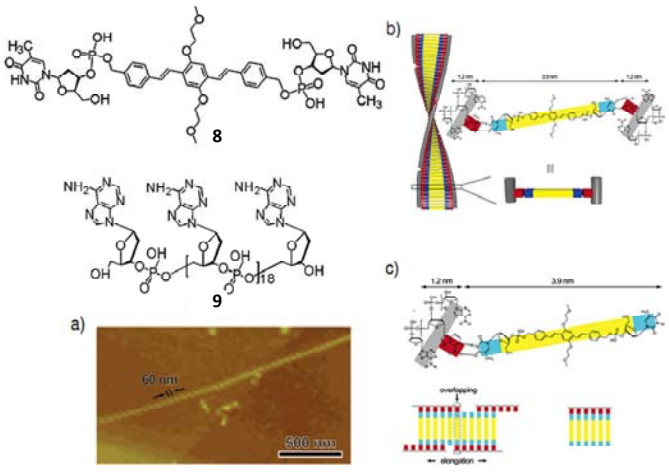

Figure 1.9. a) AFM image for the binary self-assembly of **8**/**9** (T: A = 1:1). Proposed structure for the binary self-assembly of b) **8**/**9** (T: A = 1:1) and c) **8**/**9** (T: A = 2:1). Possible elongation mechanism for the helical stacks self-assembled from **8**/**9** (T: A = 1:1) and **8**/**9** (T: A = 2:1) are also shown.

Interestingly, the co-assembly of **11** and **12** with **10** forms stable helical structures. The formation and the stability of the co-assemblies were monitored through temperature-dependent UV/Vis and CD spectroscopy measurements. Binding of chromophores to ssDNA occurs via hydrogen bonding and is stabilized by π-π interactions. This approach can, in principle, be applied to any functional molecule equipped with an appropriate hydrogen-bonding moiety to create uniform well-organized nanoscale objects that are potentially useful in the emerging field of supramolecular electronics.

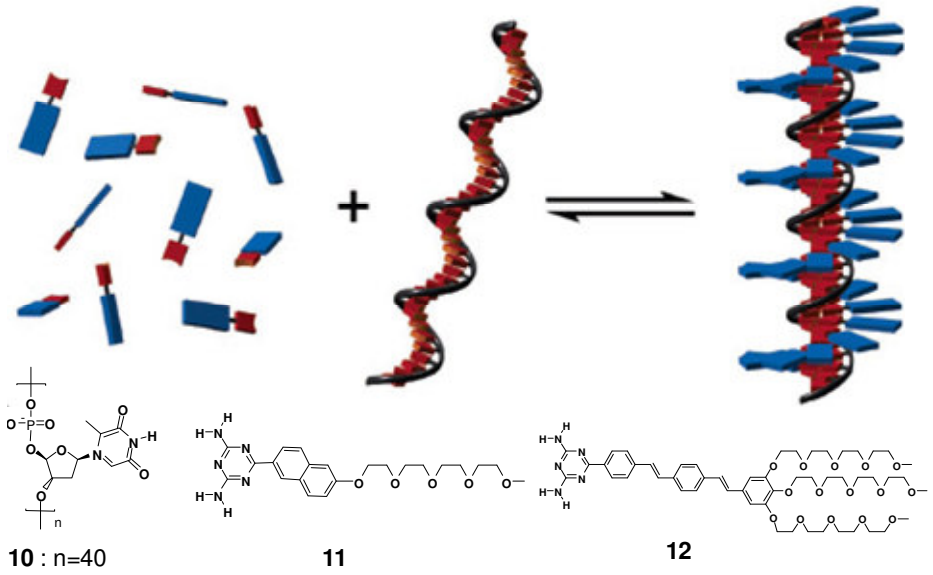

Figure 1.10. Schematic representation of ssDNA templated self-assembly of chromophores (black strand, ssDNA; blue bar, chromophores; red bar, hydrogen bonding unit).

Recently, an unprecedented dynamic self-assembly of an OPV, functionalized with barbituric acid as hydrogen-bonding head group, into nanorings and nanocoils in methylcyclohexane, has been reported.[50] Atomic force

microscopy (AFM) images of a methylcyclohexane solution of **13** when drop-casted or spin-coated on to a highly oriented pyrolytic graphite (HOPG) showed the formation of closed ring-shaped nanostructures (nanorings) under dilute conditions (2×10^{-5} M) (Figure1.11a). Open-ended nanofibers, which are the intermediate species between nanorings and nanorods, such as curved fibers, spirals, and double spirals with opposite rolling directions, were also found in the same sample as minor structures (10-20%).

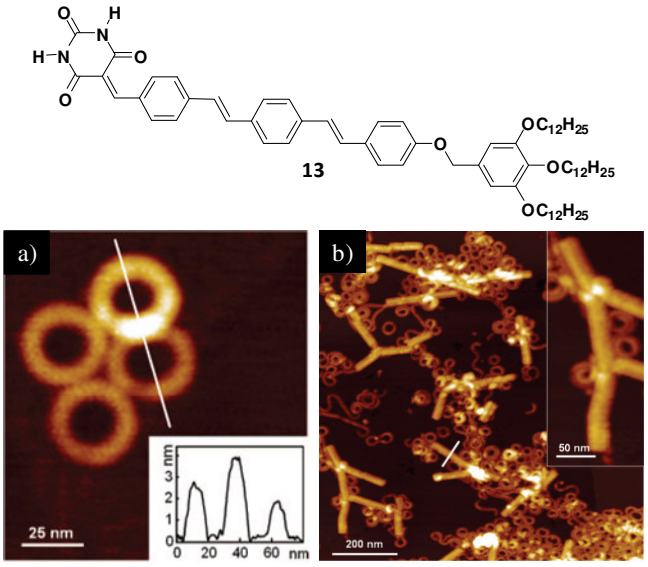

Figure 1.11. AFM height images of a sample prepared by drop casting of a) 2×10^{-5} M and b) 1×10^{-4} M methylcyclohexane solution of **13** on to HOPG (*Z* scale: 20 nm).

The formation of nanorings was further confirmed by transmission electron microscopy (TEM) images. A further increase in the concentration to 1×10^{-4} M resulted in the evolution of rod like nanostructures (nanorods) (Figure 1.11b). At lower concentrations, the translational and rotational offsets upon stacking of a

hexameric disk of **13** leads to a spontaneous curvature of columns whereas at moderate concentrations, the columnar stacks are isolated by solvation and behave as tape like nanofibers. At concentrations above 1×10^{-4} M, the columns further extend over 200 nm, which eventually leads to folding into nanorods, to minimize the surface free energy.

Meijer and coworkers have recently established the use of multiple H-bonded supramolecular polymers in energy transfer. Oligofluorenes, functionalized with UPy module at both ends as in **14** (Figure 1.12), self-aggregate to form supramolecular polymers whose main chains are composed of π-conjugated chromophores.[51] Mixing of mono-UPy-functionalized OPV **15** resulted in end-capping of the supramolecular polymers with OPV functional moieties, where light-energy harvested by the oligofluorene main chain is efficiently transferred to the terminal OPV moieties. When **15** was mixed with oligofluorenes lacking UPy modules, incomplete energy transfer was observed, confirming that the observed energy transfer is a result of the supramolecular polymerization driven by quadruple hydrogen-bonding.

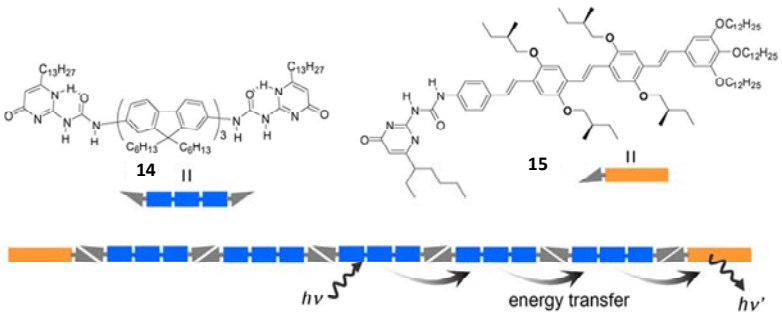

Figure 1.12. Schematic representation of energy transfer in the supramolecular polymers of UPy-functionalized oligofluorene **14,** end-capped with UPy functionalized OPV **15**.

In contrast to porphyrin and OPV derivatives, naphthalene bisimide (NBI) and perylene bisimide (PBI) chromophores, possess ADA hydrogen-bonding sites at both ends, and thus could be directly subjected to complexation with DAD hydrogen bonding modules. Kimizuka et.al. have examined the complexation of naphthalene bisimide with an alkylated melamine derivative (Figure 1.13).[52] The complex showed tubular nanostructures with 12–15 nm in diameter as observed by transmission and scanning electron microscopies. It is suggested that the observed nanostructures are constructed via either stacking of discrete dodecameric rosettes (**16**) or helical elongation of supramolecular polymers (**17**).

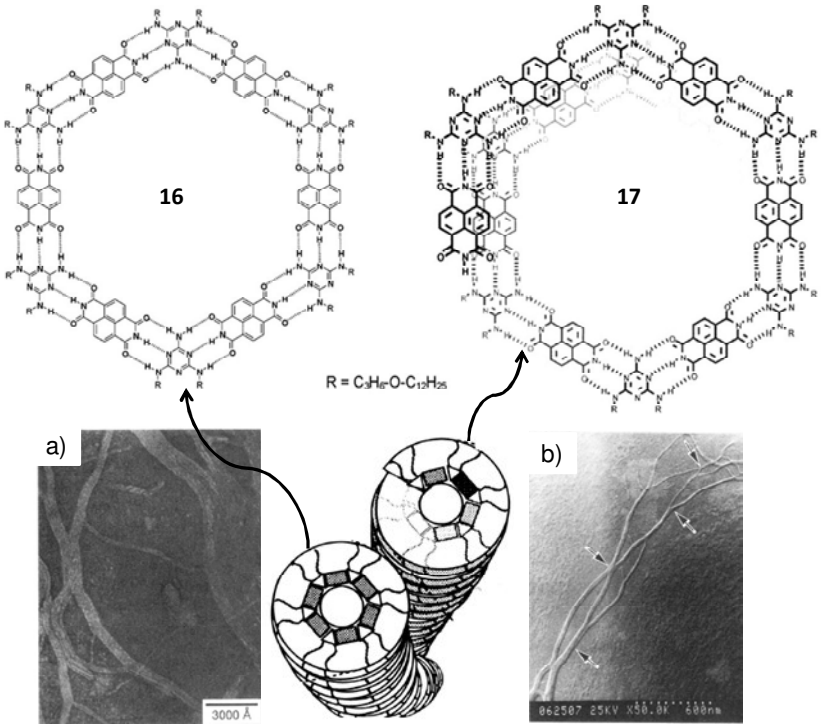

Figure 1.13. The macrocyclic architecture **16** and helically grown tubular structure **17** formed by NBI and alkylated melamine hydrogen-bonded complexes; (a) and (b) are SEM images.

Recently, it has been shown by scanning tunnelling microscopy (STM) that co-adsorption of perylene bisimide and melamine on Si(111) surface under ultrahigh-vacuum conditions provides two-dimensionally propagated supermacrocyclic architecture.[53] The large pores created by the honeycomb network can accommodate heptameric C_{60} clusters. Würthner et al. have extensively studied the hierarchical self-organization of perylene based complementary building blocks to nano- and mesoscopic superstructures, which are expected to show supramolecular functional properties such as light harvesting and long range vectorial transport of excitation energy within the superstructures.[54] Hierarchical organization of perylene bisimide (**18**) and the melamine (**19**) by multiple orthogonal intermolecular interactions leads to fluorescent mesoscopic structures as shown in Figure 1.14.

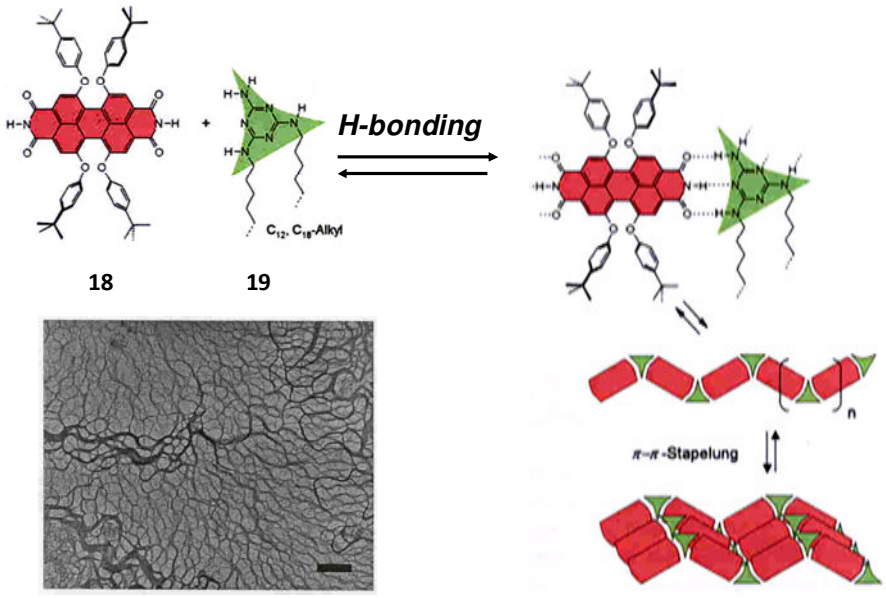

Figure 1.14. Formation of functional perylene superstructures by hierarchical self-organization.

The complementary H-bonding between perylene bisimides and the melamines initially form linear polymeric chains that subsequently aggregate to extended supramolecular systems as a result of the cooperative π-π stacking and alkyl chain interactions. The PBI derivative **20** is reported to be a good gelator of organic solvents such as limonene and ethyl acetate.[55] Also it can form gels even in hydrogen bond acceptor solvents such as THF, acetone, acetonitrile and hydrogen bond donor solvents such as ethanol. Gelation was observed at comparatively low concentrations (0.2-0.9 wt %) and hence is classified as a super gelator.

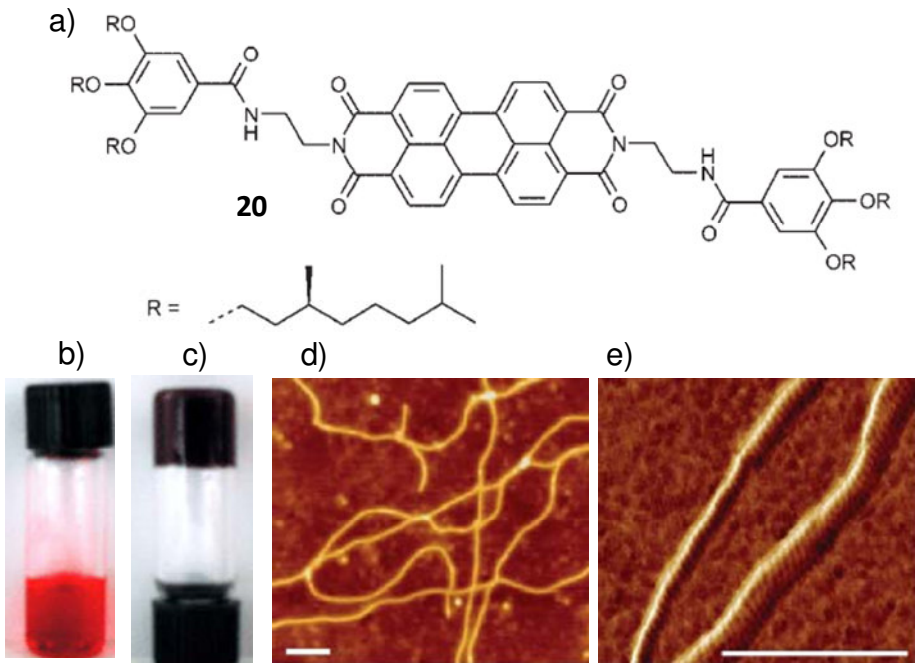

Figure 1.15. a) Molecular structure of the PBI organogelator **20.** b) Photograph of the original homogeneous solution of **20** at 60 ^{o}C. c) The corresponding gel upon cooling for 15 minutes. d) AFM height image of a film spin-coated from diluted gel solutions of **20** in methylcyclohexane (0.6 mM) onto HOPG. (e) AFM phase image on a silicon wafer, spin-coated from toluene.

1.6. Photoresponsive Supramolecular Assemblies

The incorporation of photoswitching molecules into molecular building blocks creates the possibility of photoresponsive self-assemblies in which the self-assembled architecture or self-assembling process can be controlled by external light stimulus. The primary requirement of a photoresponsive supramolecular system is the presence of large reversible changes in its molecular geometry or physical properties as a result of the photochemical reaction. Synthetic accessibility is also quite important. Among different photoswitching molecules, azobenzene has been used most widely by virtue of the large photoinduced changes in its molecular geometry and physical properties.

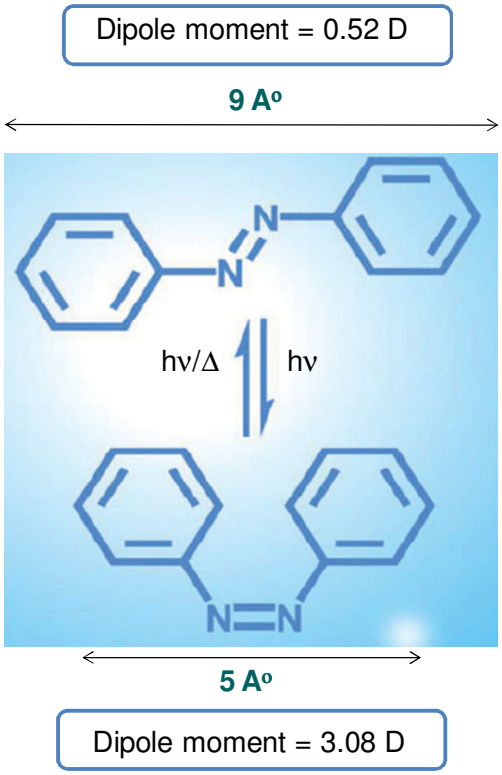

Figure 1.16. Conformational change of azobenzene on irradiation.

The *trans*-azobenzene with a molecular length of 9 A° upon irradiation with UV light will adopt a bent structure with 5 A° length with a change in dipole moment from 0.52 D to 3.08 D (Figure 1.16). The *cis*-isomer thus formed undergoes reversible change to the *trans* form upon irradiating with visible light or under dark by thermal energy. This phototransformation of azo chromophores has been extensively used for the preparation of a variety of smart materials such as liquid crystalline elastomers, photoimaging systems etc.[56] In addition, H-bonded complementary self-assembly modules linked with azo chromophores have been reported.[56d] For example, supramolecular assembly of an ammonium head group appended azobenzene-cyanuric acid and glutamate derivative of melamines have been reported which undergo complementary hydrogen bonding in water[57] and air water interfaces.[58] In water, helical structures were formed and the aggregation process could be controlled by photoisomerization of the azobenzene, resulting in the segregation of the two components.

Recently, Yagai et al. have reported the photoswitching properties of H-bonded assemblies between *trans*-azobenzene incorporated melamine **21**.[59] The azobenzene moieties of the rosette $\mathbf{21}_3 \cdot \mathbf{22}_3$ efficiently photoisomerize upon UV light irradiation, maintaining the rosette architectures as evidenced by ^{1}H NMR (Figure 1.17). It has been shown that the isomerization of azobenzene moieties has seemingly no impact on the self-assembly of the rosette. However, it is noticed that the UV irradiated solution does not produce any precipitates upon aging over 300 h (Figure 1.17c and d), the situation of which is considerably different from the solution without UV irradiation. This observation clearly demonstrates that the *cis*-azobenzene moieties suppress irreversible denaturation of the rosette into tape

like assemblies. It is believed that the *cis*-azobenzene moieties of **21** increase the solubility of the competing tape like oligomers, which must always be equilibrated with rosettes to a small extent, preventing their phase separation (precipitation) by open-ended polymerization. The modification of the azobenzene appended melamines as well as the barbiturates with sterically demanding substituents such as the tridodecyloxyphenyl (TDP) ''wedge'' might endow a more direct photoresponse with the self-assembly of a rosette.

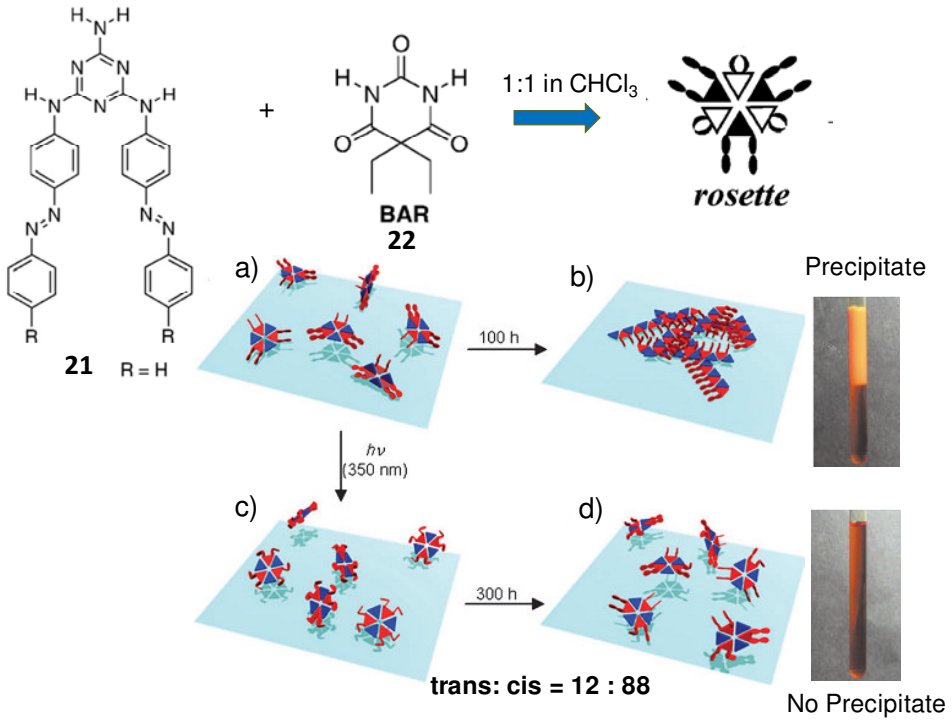

Figure 1.17. Schematic representation of the photoinduced stabilization of rosette $\mathbf{21}_3 \cdot \mathbf{22}_3$.

Incorporation of a bulky group on to the molecule **21** displayed low photoisomerization efficiency due to the steric crowding within the rosette. The *trans:cis* ratio in a photostationary state achieved in this case at the best conditions

is only 75: 25. It was found that the rosettes intrinsically lack the capability to organize into extended columnar superstructures even in the least aliphatic solvent such as cyclohexane, probably due to the bulky TDP wedge in the barbiturate component (BAR-TDP).[60]

The use of two distinct conformations of a photochromic molecules which are resulted by photoisomerization, as building blocks, provides extended supramolecular architectures that can be guided by light input. However, the construction of such systems appears to be extremely difficult because one of the two photoisomers may be flexible, and thereby unsuitable as building blocks for extended supramolecular architectures. One example of this type of photoresponsive self-assembly has been reported by Sleiman and coworkers. They found that the *trans* and the *cis* isomers of the azodibenzoic acid derivative **23** self-assembles into distinct higher-order structures (Figure 1.18).[61] Vapor pressure osmometry (VPO), NMR, single crystal and powder X-ray measurements and semi-empirical calculations have demonstrated that the *trans*-isomer forms linear tape like aggregates whereas the *cis*-isomer generates a discrete tetramer. Remarkably, hierarchically organized rod like superstructures have been visualized for the *cis*-isomer by using transmission electron microscopy, which was proposed to be constructed through extended π–π stacking of the tetrameric *cis*-isomers. This is a rare example where the bent conformation of *cis*-azobenzene is used as a building block of a well defined supramolecular edifice. As a result of the tetramerization (and further stacking of the resulting tetramers as suggested by a ^{1}H NMR spectral change), the thermal *cis* to *trans* isomerization was

significantly suppressed in CH_2Cl_2 when compared to the molecularly dissolved state in a hydrogen-bond competing solvent (DMSO).

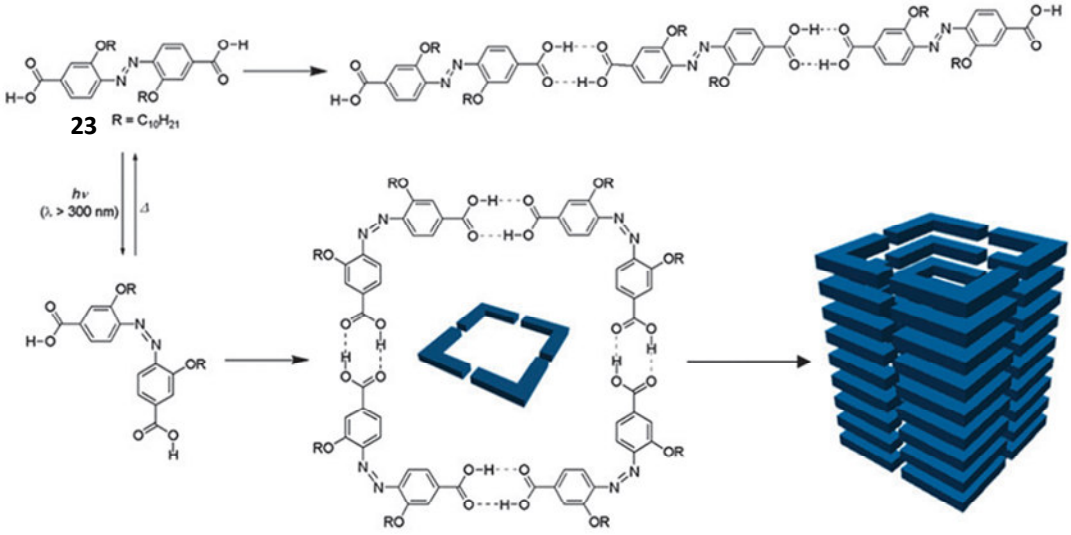

Figure 1.18. Photoresponsive self-assemblies of the azodibenzoic acid derivative **23**.

There is a growing interest in self-assembled helical nanoarchitectures because of their potential applications in liquid crystals, nonlinear optics, chiral sensing and as templates for inorganic materials.[62] As a new paradigm of photoresponsive self-assembly, it is possible to use azobenzene to introduce self-assembled nanofibers whose helical morphologies can be transformed by means of external light input. Manipulation of self-assembled helical nanostructures by external light input thus allows us to fabricate smart nanomaterials, chiroptical properties and functions of which could be controlled at will. One of such systems has been recently reported by Stupp et al. where helical nanostructures can be manipulated by light stimulus.[63] The amphiphile **24** (Figure 1.19a) possessing a terminal *trans*-azobenzene substituent self-organizes in cyclohexyl chloride to form super helical nanofibers (Figure1.19b). The helical pitch visualized by atomic

force microscopy is ca. 78 nm and uniform for all the nanofibers (Figure 1.19c and 1.19 d). Interestingly, irradiation of nanofibers dispersed in cyclohexyl chloride at 360 nm diminished the helical pitches to 40–70 nm (Figure 1.19e–g). This morphological change can be explained in terms of an increase in the torsional strain upon isomerization of *trans*-azobenzene into the less planar (sterically bulky) *cis*-isomer. The decrease in the helical pitch varied from nanofiber to nanofiber due to the inhomogeneous isomerization efficiency among nanofibers. In contrast, the helical pitch is uniform in each nanostructure, indicating that the photoinduced decrease in the helical pitch is a relaxation process throughout the entire nanostructure.

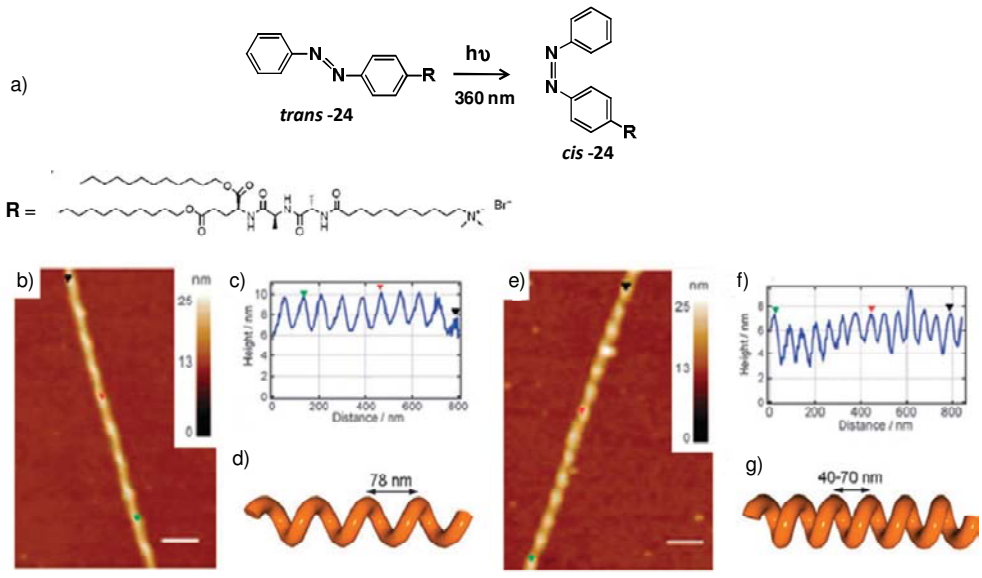

Figure 1.19. a) Photoisomerization of the azobenzene-functionalized amphiphile **24**. (b, e) AFM height images and (c, f) the corresponding height profiles and schematic representation of the helical morphologies for the photoinduced actuation of a helical nanofiber of **24** (b–d) before and (e–g) after irradiation of UV-light.

Recently Tour et al. have reported two new photoactive nanovehicles (nanoworms) based on OPEs substituted with azobenzene chromophores (Figure 1.20).[64] Incorporation of the azobenzene chassis allows a wormlike movement accompanying the rolling behaviour of the wheels. Two versions, the fullerene-wheeled and carborane-wheeled nanoworms were synthesized to examine the solution based photoisomerization yields of the chassis. It was surprising that no switching behaviour was observed from nanoworm **25**.

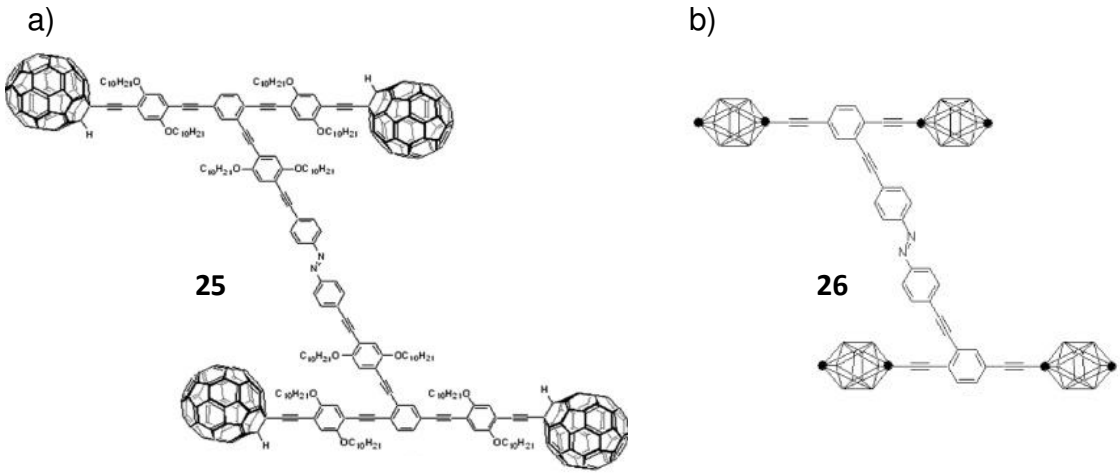

Figure 1.20. a) C_{60}-wheeled nanoworm **25**; Extended dodecyl substituted axles were added to ensure solubility. (b) *p*-Carborane wheeled nanoworm **26**. The *p*-carboranes have BH at every intersection except at the points denoted by black spheres, which represent C and CH positions, ipso and para, respectively.

Fullerenes attached via alkynes on the conjugated systems introduce a weak electronic interaction called periconjugation, where the fullerene-electrons communicate with the alkynyl π-electrons in a through-space *p*-orbital overlapping mechanism. This causes disruption in the electronic communication of the chromophore that has produced less conversion in systems with two fullerenes.[65,66]

Because of the small switching activity observed with **25**, another wheel system with carboranes was introduced in order to overcome the photoquenching effect. In this case, the *cis-trans* photoisomerization of the azobenzene chromophore potentially generate the worm-like motion on a surface (Figure 1.21). From the photoisomerization experiment, the highest concentration of the *cis*-isomer of **26** was obtained when the system was irradiated at 365 nm for 10 min. Switching of the *cis* to the *trans* isomer occurred photochemically when irradiated at >495 for 5 min (the temperature increase was <5 ° C) and thermally when heated at 40 ° C for 15 min.

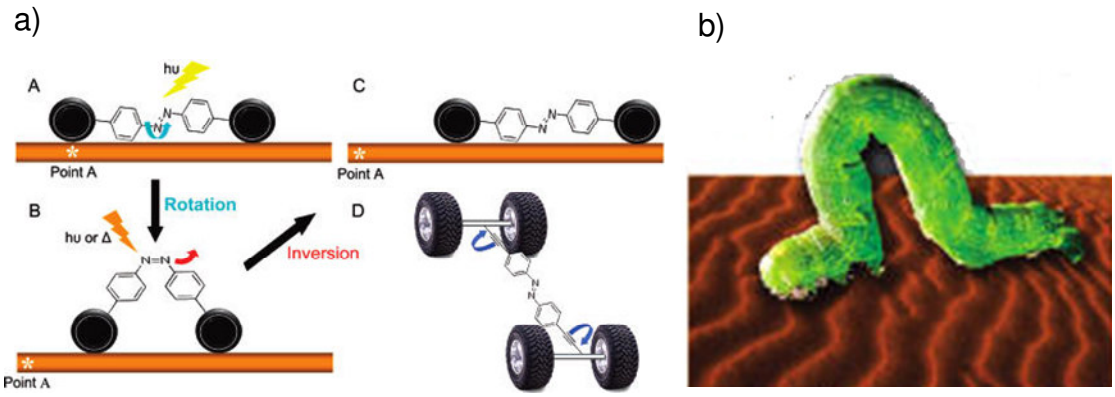

Figure 1.21. a) (A) Side view model of the nanoworm. The proposed photoactivated rotational pathway on a surface away from the reference point (noted by the star) by irradiating at 365 nm or 435 nm to convert A to B (*trans* to *cis* isomerization) by rotation. (B) Model of the nanoworm (*cis*) irradiated at >495 nm (or heated) to induce the inversion pathway to C which constitutes a *cis* to *trans* conversion, thus further propelling the nanoworm from the starred reference location. (C) The nanoworm again in the *trans* conformation, after completing the cycle of *trans* to *cis* to *trans* conversion, that is further displaced from the starred reference point. (D) Top view; rotation about the alkyne bonds is possible in order to achieve favourable conformations; b) Schematic representation of the nanoworm.

Armaroli et al. have recently reported the synthesis of π-conjugated chromophore **27** with an azobenzene core.[67] The compound **27** shows *trans–cis* isomerization upon irradiation with 365 nm UV light. Extensive investigation of the self-assembled monolayers (SAMs) of **27** at the solid/liquid interface were performed by means of scanning tunnelling microscopy (STM) on highly oriented pyrolytic graphite (HOPG) (Figure 1.22). The studies revealed that only the *trans* isomer can be physisorbed on the surface whereas the *cis* form, either produced under illumination in situ or prepared by irradiation of the solution prior to deposition (ex-situ), could be detected. For example, the only observable effect was the destabilization of the SAM, as shown by it's desorption after 2 h (Figure 1.22). STM investigations at the solid/liquid interface of **27** shed light into the behaviour of the azobenzene under these conditions. It was found that for compound **27**, only the *trans* isomer is capable of physisorbing at the HOPG surface, showing that the lack of planarity in the *cis* isomer constitutes a notable barrier to its interaction with the HOPG surface. These results are the basis to pursue further efforts in the functionalisation of azobenzene with a variety of chromophores and luminophores, which can be eventually anchored on surfaces and manipulated mechanically and photochemically.

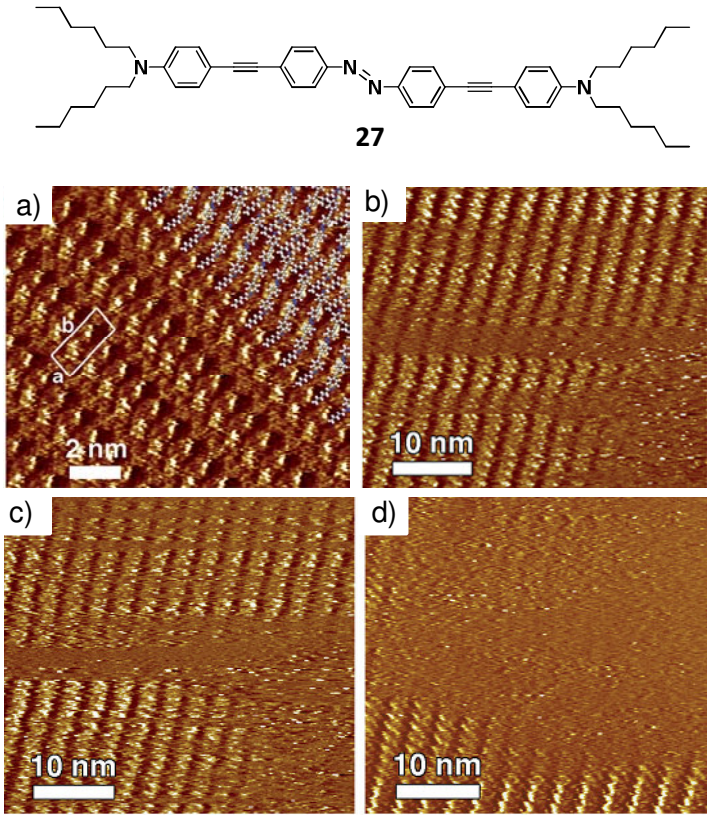

Figure 1.22. a) STM current image of the SAM formed by *trans*-**27** in 1-phenyloctane at the HOPG-solution interface. Tunnelling conditions: average tunnelling current (I_t) =10 pA, bias voltage (V_t) = 500 mV; STM image of the **27**-SAM after 100 min (b), 110 min (c) and 120 min (d) of irradiation.Tunnelling conditions: (I_t) =10 pA, (V_t) = 500 mV.

The photoresponsiveness of azobenzene can also be used for the creation of switchable assemblies of biologically relevant molecules such as peptides. In a recent report Ghadiri et al. have reported the synthesis and characterization of a novel peptide system **28** (Figure 1.23), in which E/Z isomerization of the azobenzene subunit results in photoswitchable hydrogen bonding.[68] This system allows the controlled conversion between inter- and intramolecularly assembled cylindrical structures both in solution and in thin films at the air–water interface.

The *trans* isomer of **28** forms linear and polydisperse hydrogen-bonded assemblies in chloroform. UV light irradiation of the solution of the linear species resulted in the switching to the intramolecularly hydrogen-bonded closed species with butterfly-like motion of the molecule, as evidenced by NMR studies. Interestingly, photogenerated closed species showed remarkable resistance of the *cis* to *trans* thermal isomerization, owing to the multiple intramolecular hydrogen-bonding interactions.

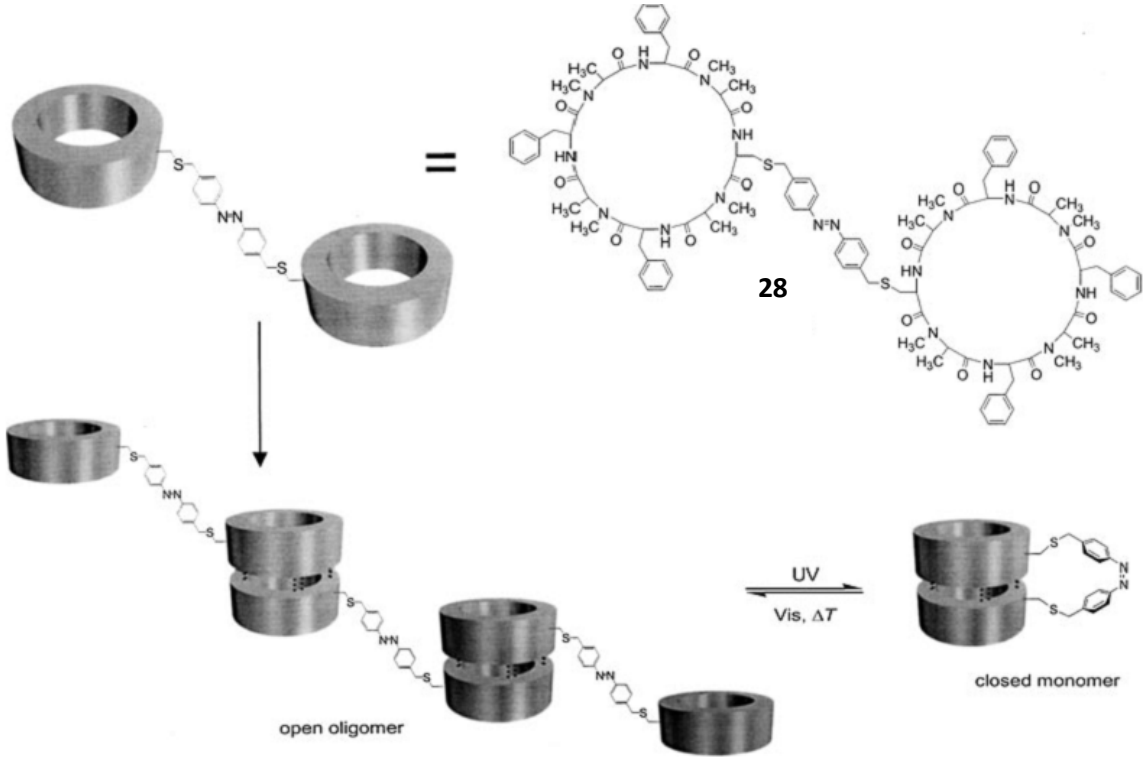

Figure 1.23. Schematic representation for the photoswitchable self-assembly of azobenzene/ cyclicoctapeptide **28**.

In a related example, Asanuma and Komiyama have established the photocontrolled self-assembly of DNA duplex[69a] and triplex[69b] using synthetic oligonucleotides featuring azobenzene side chains (**29**) (Figure 1.24). In the case

of the duplex system, they showed the drastic change of the melting temperature (T_m) of the duplex between the oligonucleotide 5'-AAA XAAAA-3' (X denotes the residue bearing azobenzene side chain) and the complementary strand 5'-TTT TTTTT-3', due to the *trans–cis* photoisomerization of the azobenzene moiety (T_m= 24.8 °C in *trans* and 15.9 °C in *cis*). It was suggested that the absence of sufficient aromatic stacking interaction between the *cis*-azobenzene with the adjacent DNA bases destabilizes the duplex. Based on this observation, phototriggered dissociation / reconstitution of the duplex were realized at the temperature between T_m (*trans*) and T_m (*cis*). Apart from this, there are several reports on the incorporation of photoresponsive molecules into DNA.[69c-g] This kind of photoresponsive bio-assemblies may have various technological applications.

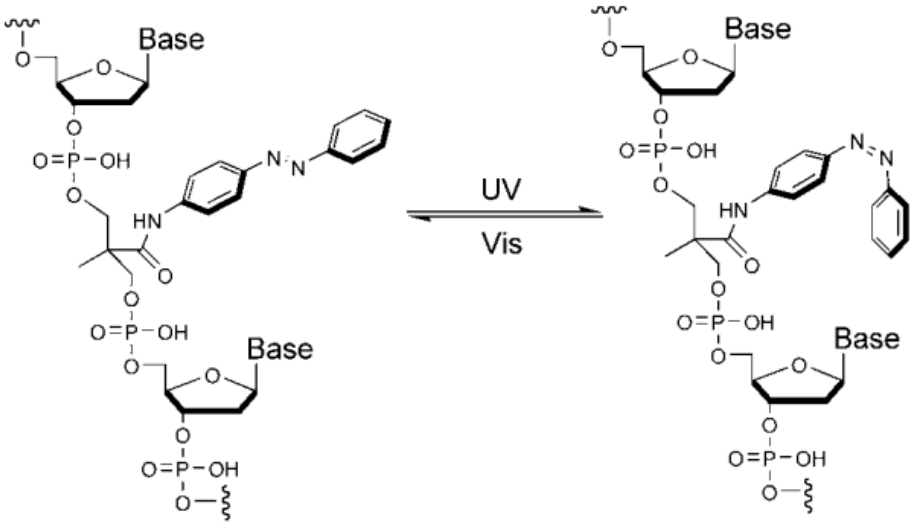

29

Figure 1.24. Photoisomerization of azobenzene incorporated DNA

Research on low-molecular-weight organogelators has increased enormously during the past decade.[70] Interestingly, the morphologies of organogels can be controlled reversibly in response to changes in external chemical, photochemical, or thermal stimuli. Azobenzene is one of the smartest molecules for this purpose. Kato and coworkers have reported a chiral azobenzene (**30**) containing a cyclic *syn*-carbonate moiety, that self-assembles via dipole-dipole interaction to form a photoswitchable organogelator (Figure 1.25).[71]

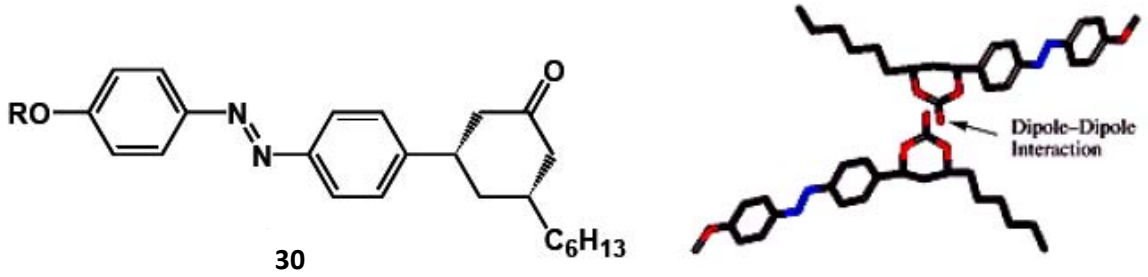

30

Figure 1.25. Structure and dipole-dipole assisted self-assembly of an azo containing organogelator **30**.

A new family of hydrogelators based on azobenzene-appended sugar bolaamphiphiles (**31-34**) has been reported jointly by Shinkai and Reinhoudt.[72] These bolaamphiphiles consist of two solvophilic amino phenyl sugar skeleton, such as *β*-D-glucopyranoside (**31**), *α*-D-glucopyranoside (**32**), *α*-D-galactopyranoside (**33**) or *α*-D-mannopyranoside (**34**), as chiral aggregate forming group and the solvophobic azobenzene moiety as a π-π stacking site. Compound **31** is found to be a 'super' hydrogelator, as it can form gels even at concentrations as low as 0.05 wt%, whereas compound **32** could gelate only 1:1 (v/v) DMSO-water solvent mixtures. On the other hand, **33** and **34** could not gelate any of the

solvents investigated. The chiral sugar derivatives **31** and **32** are found to form right-handed helical aggregates in 50 vol% DMSO, whereas **33** and **34** form left-handed helical aggregates as evident from the corresponding exciton coupled CD spectra. TEM studies have revealed right-handed helical fibrillar structures for the aggregates of **31** and **32**, reflecting the microscopic one-dimensional columnar orientation of the azobenzene chromophores. However **33** and **34** tend to aggregate into vesicular structures as a result of their two-dimensional aggregation mode, which prevent them from gelation (Figure 1.26).

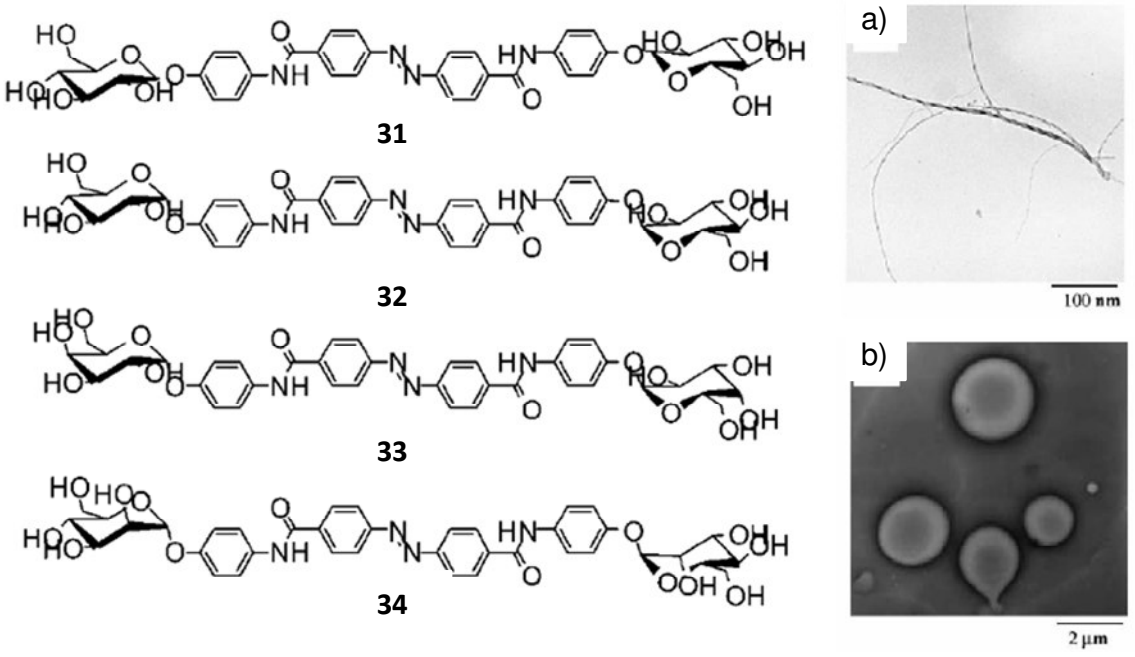

Figure 1.26. Structures of sugar-appended azobenzene organogelators and the TEM images of **32** (a) and **33** (b) in 1:1 (v/v) DMSO-water mixtures.

Feringa and coworkers have reported chiral recognition in hybrid gel assemblies of 1,2-bis(uriedocyclohexane) derivative **35** and the azobenzene incorporated derivative **36**.[73] Both (*R*)-**36** and (*S*)-**36** isomers showed concentration independent exciton coupled CD spectra corresponding to the azobenzene absorption. As a result of the intramolecular stacking of the azobenzene chromophores, the sign of the CD spectra depends on the absolute configuration of the molecule. Incorporation of (*R*)-**36** into a gel of (*S*)-**35** or (*R*)-**35** resulted in distinctly different chiral gels, in which the azobenzene chromophores are stacked in different orientations depending on the chirality of **35** (Figure 1.27). The CD spectrum of (*R*)-**36** in 1-butanol gel of (*S*)-**35** showed a slightly more intense bisignated CD signal at room temperature, indicating that the environment of (*R*)-**36** is less polar when it is incorporated into the (*S*)-**35** gel than in 1-butanol itself as shown in Figure 1.27b. However, incorporation of (*R*)-**36** in a gel of (*R*)-**35** results in a strong positive Cotton effect, which is not exciton coupled, indicating that the azobenzene groups are no longer stacked but incorporated between the closely packed alkyl chains of (*R*)-**35** as shown in Figure 1.27a. In both cases, intramolecular exciton coupled CD signal of (*R*)-**36** reappears upon melting of the gel. In addition, the more exposed "solvent like' environment of (*R*)-**36** in the (*S*)-**35** gel results in its slow isomerization when incorporated into the former gel.

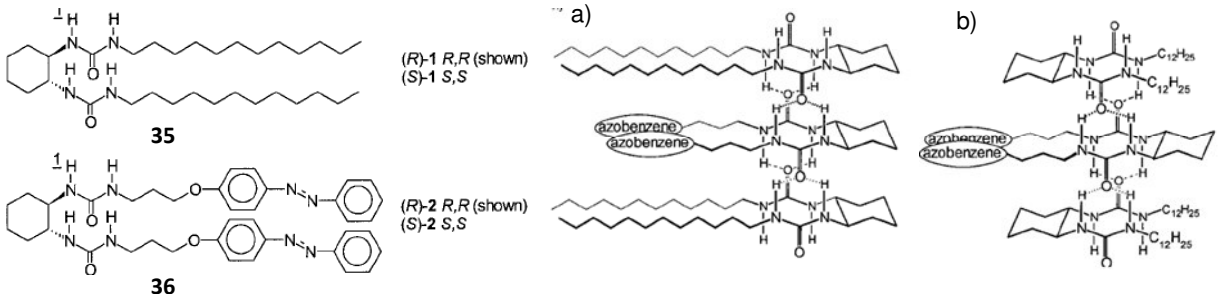

Figure 1.27. Structures of the 1,2-bis(uriedocyclohexane) derivatives. Schematic representation for the incorporation of (*R*)-**36** in a) an aggregate of (*R*)-**35** and b) an aggregate of (*S*)-**35** showing the different environments for the azobenzene groups.

van Esch and coworkers have studied the gelation behavior of the bisurea-appended azobenzene derived organogelators **37** and **38** (Figure 1.28).[74] 4,4'-Disubstituted derivative (**37**) is found to be a poor gelator, whereas the 2, 2'-disubstituted derivative (**38**) is an excellent gelator of a variety of organic solvents at concentrations as low as 0.2 mM. Interestingly, **38** showed remarkable polymorphism in their gel state leading to two different types of supramolecular aggregates, which differ in the stacking of chromophore moiety as well as in their H-bonding patterns, as evident from the differences in the UV/Vis absorption and IR spectra. This novel observation of polymorphism in organogels was found to depend on the solvent polarity and kinetic factors.

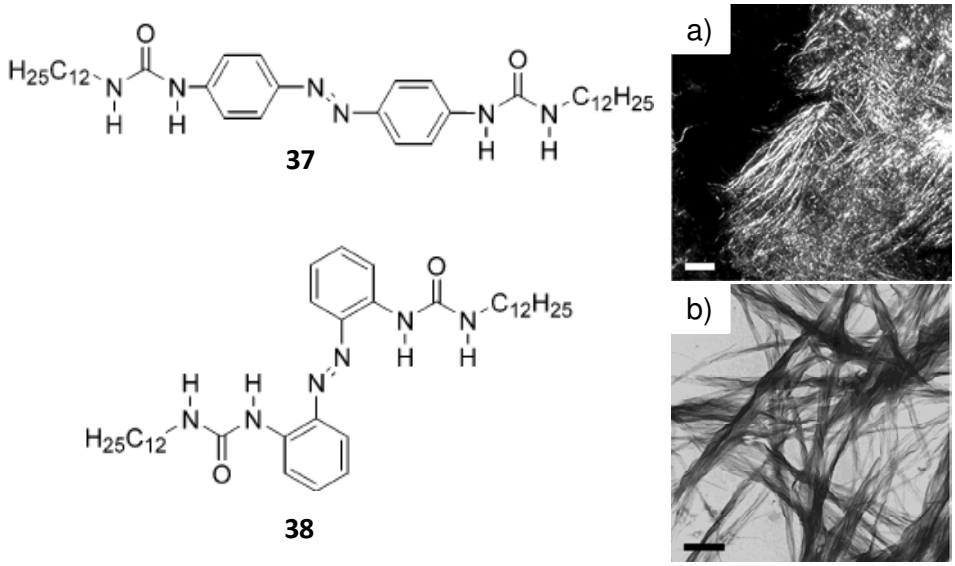

37

38

Figure 1.28. Bisurea-appended azobenzene derived organogelators **37** and **38**; a) Optical microscopy of a toluene gel of **37** and b) cryo electron microscopy of a toluene gel of **38** (1.6 mM, bar = 400 nm).

Recently, Huang and coworkers have reported that, the novel tripodal gelator **39**, (Figure 1. 29) functionalized by three urea and azobenzene moieties and tailed with three long alkyl chains, is capable of forming anisotropic bilayers which are hydrophilic along the plane but hydrophobic near the rim.[75] Compound **39** has the ability to gelate a wide variety of organic solvents, such as 1-butanol (*n*-BuOH), 1-methyl-2-pyrrolidone (NMP), chloroform, xylene, and *n*-hexane, at a critical gelation concentration range of 10-30 mg/mL. The related short chain compound **40** cannot gelate any of the above solvents. The most dramatic feature is that the xerogels formed by **39** display morphologies and surface properties that strongly depend on the nature of the gelling solvent. The xerogels from *n*-BuOH shows regular flakes of about 100-200 nm in size, connected by thin ribbons.

Cabbage-like topography and super hydrophobicity were observed in the xerogel formed from a low polar aromatic solvent such as xylene (Figure 1.29c). The wettability of a xerogel could be switched from hydrophobicity to hydrophilicity by applying a sol-gel process with different solvents.

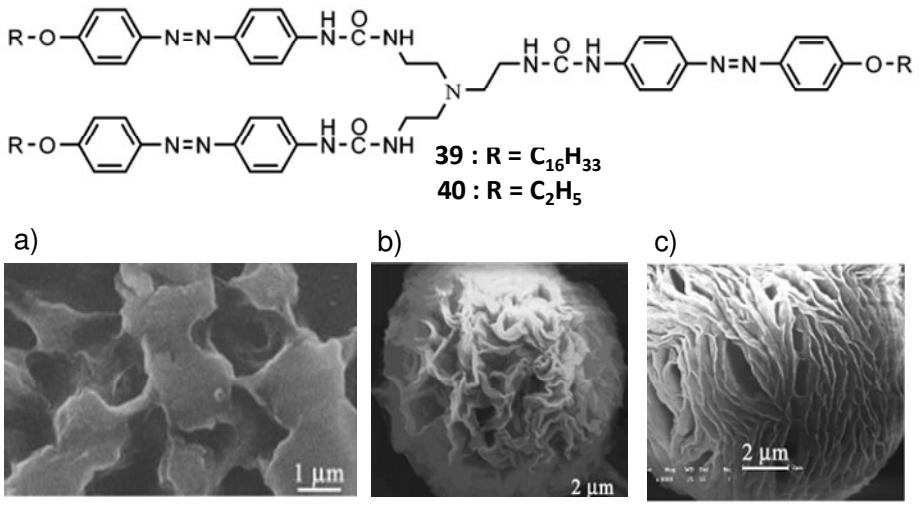

Figure 1.29. Structures of the tripodal gelator **39** and **40** (a) SEM images of the xerogels from *n*-BuOH (b) NMP (c) Xylene

Banerjee and coworkers have investigated low molecular weight (LMW) organic gelator, **41** (Figure 1.30), a chromophoric azobenzene based tetra amide moiety containing amino acid (isoleucine) residues.[76] It forms gels in various organic solvents including toluene, *o*-xylene, *m*-xylene and *p*-xylene using hydrogen bonds between amides, π-π interactions and van der Waal interactions to provide a nanofibrillar network. Morphological analysis revealed that the fibers obtained from a toluene gel are approximately 98 to 162 nm in width and several micrometers in length. However, in the case of *o*-xylene (88- 300 nm), *m*-xylene

(125-155 nm) and *p*-xylene (122-167 nm) gels, the fibers are denser in nature indicating the effect of solvent on the morphology.

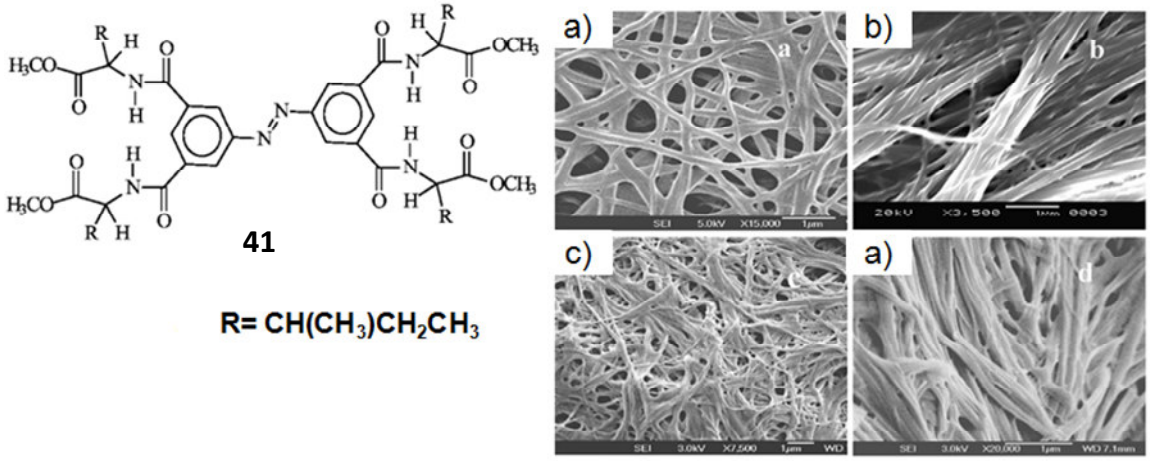

Figure 1.30. Structure of the gelator **41**. SEM images of the xerogels from a) *n*-BuOH; b) from NMP; c) from Xylene

Apart from the above mentioned reports, azobenzene is also utilized for controlling the morphology of polymers by introducing into the main chain or side chain. In a recent example, the reversible optical switching of self-assembly was achieved by the incorporation of azobenzene units into one of the polymeric building blocks with the aid of hydrogen bonding interactions between the polymeric pairs comprising poly(4-phenylazomaleinanil-*co*-4-vinylpyridine) (AzoMI-VPy) (**42)** and polybutadiene with a terminal carboxy group (CPB).[77] First, the AzoMI-VPy/CPB form "graftlike" interpolymer complexes in toluene due to the hydrogen-bonding interaction between carboxylic acid and pyridine. The complex is soluble in toluene when the azobenzene units of AzoMI-VPy are

in the *trans* conformation. Under UV irradiation, the azobenzene units transform into the polar *cis* conformation and thus facilitate the AzoMI-VPy chains to aggregate. However, macroscopic precipitation is inhibited by the soluble CPB chains surrounding the AzoMI-VPy aggregates through hydrogen-bonding interactions. Thus, core-shell micelles are formed with a volume of about 250 nm. Upon irradiation with visible light, the micelles are quickly disassociated into a transparent interpolymer complex, as the azobenzene *cis* form returns to the *trans* form. The UV light-induced micelles can be readily cross-linked by the pyridyl units reacting with 1,4-diiodobutene. The core cross-linked micelles respond to light irradiation with reversible and remarkable morphological changes. For example, visible light causes the formation of hollow spheres as a result of intense swelling of the core as the *cis*-azobenzene turns into the *trans* form, while UV light causes the hollow spheres to return to micelles as a result of isomerization in the opposite direction (Figure 1.31).

Recently, Grzybowski and coworkes have reported a conceptually different self-erasing material in which both the "writing" and self-erasure of color images are controlled by the dynamic aggregation of azobenzene linked photoresponsive metal nanoparticles (NPs) embedded in thin, flexible organogel films (Figure 1.32).[78]

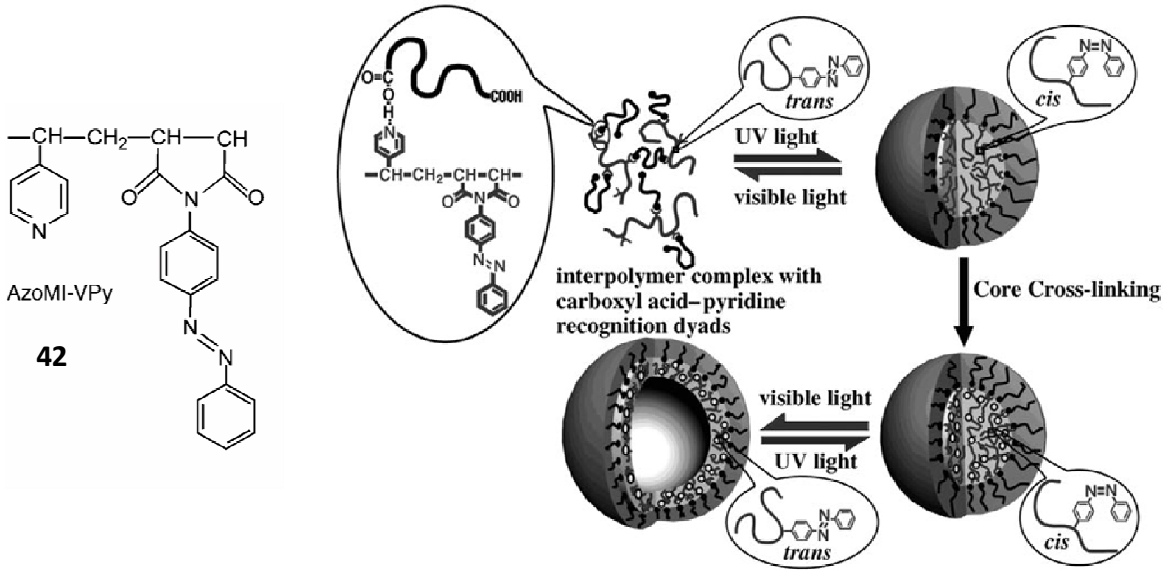

Figure 1.31. Illustration of the reversible photoinduced micellization and micelle-hollow sphere transition of hydrogen-bonded polymers.

When exposed to UV light, the *trans*-azobenzene groups attached to NPs isomerizes to *cis*-azobenzene with a large dipole moment increase. As a result, the NPs aggregate into supraspherical assemblies whose apparent color depends on the duration of UV irradiation. Since the supraspherical assemblies are metastable and fall apart spontaneously in the absence of UV irradiation, the images written onto the films gradually self-erase (Figures 1.32c). The erasure times can be controlled by the number of dipoles induced on the nanoparticles and can also be accelerated by exposure to visible light or by heating the material. Multiple images can be written on to the same film either concurrently or after erasure.

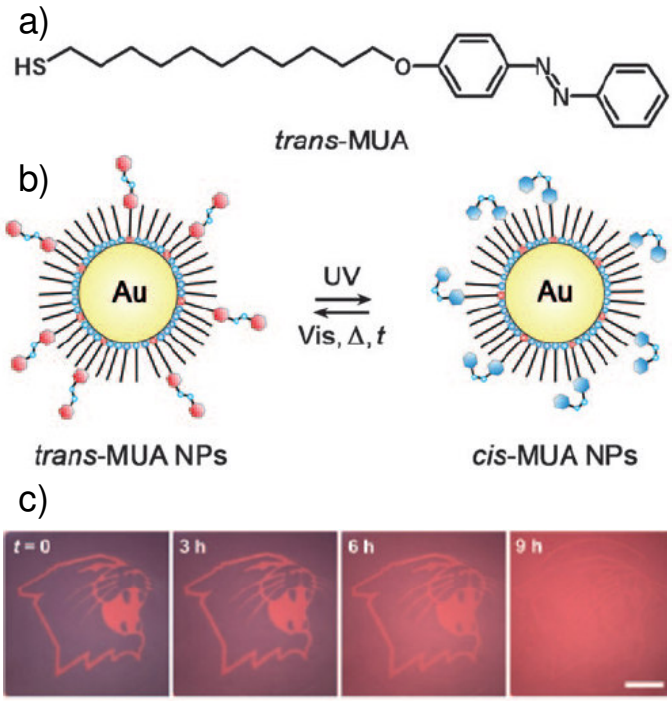

Figure 1.32. Reversible aggregation of photoactive nanoparticles. a) Structure of *trans*-4-(11-mercaptoundecanoxy) azobenzene (*trans*- MUA); b) UV irradiation of nanoparticles covered with a mixed monolayer and dodecylamine (DDA); c) Writing into self-erasable NP films created in AuNP films by exposure through a transparency photo mask. The image in the AuNP film self-erases in daylight within 9 h.

The present overview has covered most of the reports pertaining to multiple H-bonded assemblies and azobenzene derived photoresponsive self-assemblies. Even though a large number of such systems are known, there are still possibilities to design new and novel systems, where the physical properties and morphologies can be controlled.

1.7. Origin, Objectives and Approach to the Thesis

Multiple H-bonding interactions of melamines with their complementary partners have been extensively used for the creation of a variety of supramolecular

architectures of different shape and size. Similarly, a variety of photoresponsive supramolecular assemblies based on the photochromic azo chromophores have been reported. In addition, combinations of complementary multiple H-bonding systems and photochromic molecules to the creation of photoresponsive self-assembled have also been reported. However, self-assembly of π-conjugated molecules using melamine-cyanurate interactions or melamine-barbiturate interactions has not been studied in detail. Similar is the case of photoresponsive self-assemblies of π-conjugated molecules. The present thesis work has been designed in such a way, to address these issues. To be more precise, the main objective of the present thesis is the design, synthesis and study of π-conjugated molecules linked with complementary H-bonding moieties and photochromic azo groups.

In order to achieve the above objectives we have selected *p*-phenyleneethynylene (PE) as the π-conjugated module. PEs were selected because, these systems when properly functionalized undergo self-assembly resulting in supramolecular structures and organogels.[79,80] However, these self-assemblies are not very stable due to the weak π-π interaction of the PE moiety. Therefore, we thought that, it will be easy to photochemically modulate the self-assembling properties of PEs by integrating with azobenzene moieties. On the other hand, incorporation of multiple H-bonding groups with PEs may result in stable self-assemblies with defined morphologies.

In order to study the effect of azo chromophores, we have planned the synthesis of two isomeric PE molecules. Similarly, for the purpose of creating stable self-assemblies, a few PE derivatives were functionalized with melamines.

These molecules were synthesized, characterized and their self-assembly properties under different conditions were examined. The present thesis is a detailed and systematic investigation of the above molecules and their properties.

1.8. References

1. J.-M. Lehn, *Perspect. Supramol. Chem*. **1994**, *1*, 307.
2. J. Schenning, F. J. M. Hoeben, P. Jonkheijm, E. W. Meijer and A. P. H.J. Schenning, *Chem. Rev*, **2005**, *105*, 1491.
3. D. S. Lawrence, T. Jiang and M. Levett, *Chem. Rev*. **1995**, *95*, 2229.
4. L. Brunsveld, B. J. Folmer, E. W. Meijer and R. P. Sijbesma, *Chem. Rev*. **2001**, *101*, 4071.
5. J. D. Watson, F. H. C. Crick, *Nature,* **1953**, *171,* 4356.
6. A. Harriman, Y. Kubo, J. L. Sessler, *J. Am. Chem. Soc*.**1992**, *114*, 388.
7. A. Berman, E. S. Izraeli, H. Levanon, B. Wang, J.L. Sessler, *J. Am. Chem. Soc*. **1995**, *117*, 8252.
8. J. L. Sessler, B. Wang, A. Harriman, *J. Am. Chem. Soc*. **1995**, *117*, 704.
9. J. L. Sessler, J. Jayawickramarajah, *Chem. Commun*. **2005**, 1939.
10. S. C. Zimmerman, P. S. Corbin, *Struct. Bonding*, **2000**, *96*, 63.
11. R. P. Sijbesma, E. W. Meijer, *Chem. Commun*. **2003**, 5.
12. A. D. Hamilton, D. van Engen, *J. Am. Chem. Soc*. **198**7, *109*, 5035.
13. S. K. Chang, A. D. Hamilton, *J. Am. Chem. Soc*. **1988**, *110*,131.
14. P. Tecilla, R. P. Dixon, G. Slobodkin, D. S. Alavi, D. H. Waldeck, A. D. Hamilton, *J. Am. Chem. Soc*.**1990**, *112*, 9408.

15. G. M. Whitesides, E. E. Simanek, J. P. Mathias, C. T. Seto, D. Chin, M Mammen, D. M. Gordon, *Acc. Chem. Res*. **1995**, *28*, 37.

16. J.-M. Lehn, M. Mascal, A. DeCian, J. Fischer, *J. Chem. Soc. Chem Commun*. **1990**, 479.

17. J. A. Zerkowski, C. T. Seto, G. M. Whitesides, *J. Am. Chem. Soc.***1992**, 5473.

18. J. P. Mathias, E. E. Simanek, J. A. Zerkowski, C.T. Seto, G. M. Whitesides, *J. Am. Chem. Soc.***1994**, *116*, 4316.

19. J. P. Mathias, E. E. Simanek, G. M. Whitesides, *J. Am. Chem. Soc*. **1994** , *116,* 4326.

20. A.G. Bielejewska, C. E. Marjo, L. J. Prins, P. Timmerman, F. deJong, D. N. Reinhoudt, *J. Am. Chem. Soc*. **2001**, *123*, 7518.

21. I. Ghiviriga, D. C. Oniciu, *Chem. Commun*. **2002**, 2718.

22. R. H. Vreekamp, J. P. M. van Duynhoven, M. Hubert, W. Verboom, D. N. Reinhoudt, *Angew. Chem. Int. Ed. Engl*. **1996**, *35*, 1215.

23. L. J. Prins, J. Huskens, F. deJong, P.Timmerman, D. N. Reinhoudt, *Nature*, **1999**, *398*, 498.

24. H.-A. Klok, K. A. Jolliffe, C. L. Schauer, L. J. Prins, J. P. Spatz, M. Moller, P. Timmerman, D. N. Reinhoudt, *J. Am. Chem. Soc*. **1999**, *121*, 7154.

25. L. J. Prins, P. Timmerman, D. N. Reinhoudt, *J. Am. Chem. Soc*. **2001**, *123*, 10153.

26. T. Ishi, M. A. Mateos-Timoneda, P. Timmerman, M. Crego-Calama, D. N. Reinhoudt, S. Shinkai, *Angew. Chem. Int. Ed*. **2003**, *42*, 2300.

27. J. M. C. A. Kerckhoffs, M. G. J. ten Cate, M.A. M. -Timoneda, F. W. B. van Leeuwen, B. S. Ruel, A. L. Spek, H. Kooijman, M. C. Calama, D.N. Reinhoudt, *J. Am. Chem. Soc*. **2005**, *127*, 12697.

28. R. P. Sijbesma, F. H. Beijer, L. Brunsveld, B. J. B. Folmer, J. H. K. K. Hirschberg, R. F. M. Lange, J. K. L. Lowe, E.W. Meijer, *Science*, **1997**, *278,* 1601.

29. J. H. K. K. Hirschberg, L. Brunsveld, A. Ramzi, J. A. J. M. Vekemans, R. P. Sijbesma, E.W. Meijer, *Nature,* **2000***, 407*, 167.

30. L. Brunsveld, B. J. B. Folmer, R. P. Sijbesma, E.W. Meijer, *Chem. Rev*. **2001**, *101*, 4071.

31. A.T. ten Cate, R. P. Sijbesma, *Macromol. Rapid. Commun*. **2002**, *23*, 1094.

32. H. M. Keizer, R. P. Sijbesma, E. W. Meijer, *Eur. J. Org. Chem*. **2004**, 2553.

33. M. D. Watson, A. Fechtenkotter, K. Müllen, *Chem. Rev*. **2001**, *101*, 1267

34. A. J. Berresheim, M. Muller, K. Müllen, *Chem. Rev*. **1999**, *99*, 1747.

35. J. A. A.W. Elemans, R. van Hameren, R. J. M. Nolte, A. E. Rowan, *Adv. Mater*. **2006**, *18*,1251

36. F. Würthner, *Chem. Commun*, **2004**, 1564.

37. F. J. M. Hoeben, P. Jonkheijm, E.W. Meijer, A. P. H. J. Schenning, *Chem. Rev*. **2005**, *105*, 1491.

38. A. Satake, Y. Kobuke, *Tetrahedron,* **2005***, 6*, 13.

39. M. D. Ward, *Chem. Soc. Rev.***1997***, 26*,365.

40. C. M. Drain, R. Fischer, E. G. Nolen, J. -M. Lehn, *J. Chem. Soc. Chem. Commun*. **1993**, 243.

41. C. M. Drain, K. C. Russell, J. -M. Lehn, *Chem. Commun.* **1996**, 337.

42. C. M. Drain, X. Shi, T. Milic, F. Nifiatis, *Chem. Commun*. **2001**, 287.

43. H. Ohkawa, A. Takayama, S. Nakajima, H. Nishide, *Org. Lett*. **2006**, *8*, 2225.

44. A. P. H. J. Schenning, E. W. Meijer, *Chem. Commun*. **2005**, 3245.

45. A. P. H. J. Schenning, P. Jonkheijm, E. Peeters, E. W. Meijer, *J. Am. Chem. Soc.* **2001**, *123*, 409.

46. E. H. A. Beckers, A. P. H. J. Schenning, P. A. van Hal, A. El-ghayoury, L. Sánchez, J. C. Hummelen, E. W. Meijer, R. A. J. Janssen, *Chem. Commun.* **2002**, 2888.

47. A. P. H. J. Schenning, J. van Herrikhuyzen, P. Jonkheijm, Z. Chen, F. Würthner, E. W. Meijer, *J. Am. Chem. Soc.* **2002**, *124*, 10252.

48. R. Iwaura, F. J. M. Hoeben, M. Masuda, A. P. H. J. Schenning, E. W. Meijer, T. Shimizu, *J. Am. Chem. Soc.* **2006**, *128*, 13298.

49. a) M. Surin, P. G. A. Janssen, R. Lazzaroni, P. Leclére, E. W. Meijer, A. P. H. J. Schenning, *Adv. Mater.* **2008**, *20*, 1126; b) P. G. A. Janssen, J. Vandenbergh, J. L. J. van Dongen, E. W. Meijer, A. P. H. J. Schenning, *J. Am. Chem. Soc.* **2007**, *129*, 6078.

50. a) S. Yagai, S. Kubota, H. Saito, K. Unoike, T. Karatsu, A. Kitamura, A. Ajayaghosh, M. Kanesato, Y. Kikkawa, *J. Am. Chem. Soc.* **2009**, *131*, 5408.

51. S.P. Dudek, M. Pouderoijen, R. Abbel, A.P.H.J. Schenning, E.W. Meijer, *J. Am. Chem. Soc*. **2005**, *127*, 11763.

52. N. Kimizuka, T. Kawasaki, K. Hirata, T. Kunitake, *J. Am. Chem. Soc*. **1995**, *117,* 6360.

53. A. Theobald, N. S. Oxtoby, M. A. Phillips, N. R. Champness, P. H. Beton, *Nature*, **2003**, *424*,1029.

54. a) F. Würthner, C. Thalacker, A. Sautter, *Adv. Mater*. **1999**, *11* 754; b) F.Würthner, C. Thalacker, A. Sautter, W. Schärtl, W. Ibach, O. Hollricher *Chem. Eur*. **2000**, *16*, 3871; c) C. Thalacker, A. Miura, S. DeFeyter, F. C. DeSchryver, F. Würthner, *Org.Biomol. Chem*. **2005**, *3*, 414.

55. S.Yagai, S. Hamamura, H. Wang, V. Stepanenko, T. Seki, K.Unoike, Y. Kikkawa, T. Karatsu, A. Kitamura, F. Würthner, *Org. Biomol. Chem.***, 2009,** *7***,** 3926.

56. a) A. Ikegami, M. Suda, T. Watanabe, Y. Einaga, *Angew. Chem. Int. Ed*. **2009**, *48*, DOI: 10.1002/anie.200904548); b) M. Yamada, M. Kondo, J.-ichi Mamiya, Y. Yu, M. Kinoshita, C. J. Barrett, T. Ikeda, *Angew. Chem. Int. Ed*. **2008**, *47*, 4986; c) S. Yagai, A. Kitamura, *Chem. Soc. Rev***. 2008**, *37*, 1520.

57. a) T. Kawasaki, M. Tokuhiro, N. kimizuka, T. Kunitake, *J. Am. Chem. Soc*. **2001**, *123*, 6792; b) N. Kimizuka, T. Kawasaki, K. Harata, T. kunitake, *J. Am. Chem. Soc*. **1998**, *120*, 4094.

58. K.Ariga, T. Kunitake, *Acc. Chem. Res*. **1998**, *31*, 371.

59. S. Yagai, T. Karatsu, A. Kitamura, *Chem. Commun*. **2003**, 1844.

60. S. Yagai, T. Nakajima, T. Karatsu, K. Saitow, A. Kitamura, *J. Am. Chem. Soc*., **2004**, *126*, 11500.

61. F. Rakotondradany, M. A. Whitehead, A.-M. Lebuis and H. F. Sleiman, *Chem.–Eur. J*. **2003**, *9*, 4771.

62. *Materials-Chirality, Topics in Stereochemistry* , ed. M. M. Green, R. J. M. Nolte, and E. W. Meijer, *Wiley Interscienc*e, *New Jersey*, **2003**, *24.*

63. L.-s. Li, H. Jiang, B. W. Messmore, S. R. Bull and S. I. Stupp, *Angew. Chem. Int. Ed*. **2007**, *46*, 5873.

64. T. Sasaki, J. M. Tour, *org. lett.* **2008**, *10*, 897.

65. Y. Shirai, T. Sasaki, J. M. Guerrero, B. -C. Yu, P. Hodge, J. M. Tour, *ACS Nano,* **2008**, *2*, 97.

66. J.–F. Morin, Y. Shirai, J. M. Tour, *Org. Lett.* **2006**, *8*, 1713.

67. J. Zeitouny, C. Aurisicchio, D. Bonifazi, R. De. Zorzi, S. Geremia, M. Bonini, C. –A. Palma, P. Samorí, A. Listorti, A. Belbakra, N. Armaroli, *J. Mater. Chem.* **200**9, *19*, 4715.

68. M. S. Vollmer, T. D. Clark, C. Steinem, M. R. Ghadiri, *Angew. Chem*. **1999**, *111*, 1703; *Angew. Chem. Int. Ed*. **1999**, *38*, 1598.

69. a) H. Asanuma, T. Ito, T. Yoshida, X. Liang, M. Komiyama, *Angew. Chem.* **1999**, *111*, 2547; *Angew. Chem. Int. Ed*. **1999**, *38*, 2393; b) X. Liang, H. Asan uma, M. Komiyama, *J. Am. Chem. Soc*. **2002**, *124*, 1877; c) R. L. Letsinger, T. Wu, *J. Am. Chem. Soc*. **1995**, *117*, 7323; d) F. D. Lewis, X. Liu, J. *Am. Chem. Soc*. **1999**, *121*, 11928; e) F. D. Lewis, Y. Wu and X. Liu, *J. Am. Chem. Soc.* **2002**, *124*,12165; f) F. D. Lewis, L.

Zhang, X. Liu, X. Zuo, D. M. Tiede, H. Long and G. C. Schatz, *J. Am. Chem. Soc*. **2005**, *127*, 14445.

70. (a) P. Terech, R. G. Weiss, *Chem. Rev*. 1997, *97*, 3133; b) J. H. van Esch, B. L. Feringa, *Angew. Chem. Int. Ed*. **2000**, *39*, 2263; c) D. J. Abdallah, R. G. Weiss, *Adv. Mater*. **2000**, *12*,123.

71. J.-i. Mamiya, K. Kanie, T. Hiyama, T. Ikeda, T. Kato, *Chem. Comm*. **2002**, 1870.

72. a) H. Kobayashi, A. Friggeri, K. Koumoto, M. Amaike, S. Shinkai, D. N. Reinhoudt, *Org. Lett.* **2002**, *4*, 1423; b) H. Kobayashi, K. Koumaoto, J. H. Jung, S. Shinkai, *J. Chem. Soc., Perkin Trans. 2*, **2002**, 1930.

73. M. de Loos, J. van Esch, R. M. Kellogg, B. L. Feringa, *Angew. Chem. Int. Ed*. **2001**, *40*, 613.

74. S. van der Laan, B. L. Feringa, R. M. Kellogg, J. v. Esch, *Langmuir*, **2002**, *18*, 7136.

75. Y. Zhou, T. Yi, T. Li, Z. Zhou, F. Li, W. Huang, C. Huang, *Chem. Mater*. **2006**, *18*, 2974.

76. G. Palui, A. Banerjee, *J. Phys. Chem. B*. **2008**, *112*, 10107.

77. X. Liu, M. Jiang, *Angew. Chem. Int. Ed*. **2006**, *45*, 3846.

78. R. Klajn, P. J. Wesson, K. J. M. Bishop, B. A. Grzybowski, *Angew. Chem. Int . Ed.* **2009**, *48*, 7035.

79. a) A. Ajayaghosh; S. J. George, *J. Am. Chem. Soc.* **2001**, *123*, 5148; b) S. J. George, A. Ajayaghosh, *Chem. Eur. J*. **2005**, *11*, 3217; c) A. Ajayaghosh, R. Varghese, S. J. George, C. Vijayakumar, *Angew. Chem., Int. Ed*. **2006**, *45*, 1141; d) S. S. Babu, V. K. Praveen, S. Prasanthkumar,

A. Ajayaghosh, *Chem. Eur. J*. **2008**, *14*, 9577; e) S. Srinivasan, S.S. Babu, V. K. Praveen, A. Ajayaghosh *Angew. Chem. Int. Ed*. **2008**, *47*, 5746; f) A. Ajayaghosh, V. K. Praveen, *Acc. Chem. Res*. **2007**, *40*,644.

80. a) A. Ajayaghosh, R. Varghese, V. K. Praveen, S. Mahesh, *Angew. Chem*. **2006**, *118*, 3339; Angew. *Chem. Int. Ed*. **2006**, *45*, 3261; b) A. Ajayaghosh, R. Varghese, S. Mahesh, V. K. Praveen, *Angew. Chem.* **2006**, *118*, 7893; *Angew. Chem. Int. Ed*. **2006**, *45*, 7729; c) S.Yagai, S. Mahesh, Y. Kikkawa, K. Unoike, T. Karatsu, A. Kitamura, A. Ajayaghosh, *Angew. Chem. Int. Ed*. **2008**, *47*, 4691; d) S. Mahesh, R, Thirumalai, S. Yagai, A. Kitamura, A. Ajayaghosh, *Chem. Commnu.* **2009**, 5925.

Chapter 2

Photoisomerization Triggered Morphogenesis of Flakes and Rods from Self-assembled Photochromic Isomers

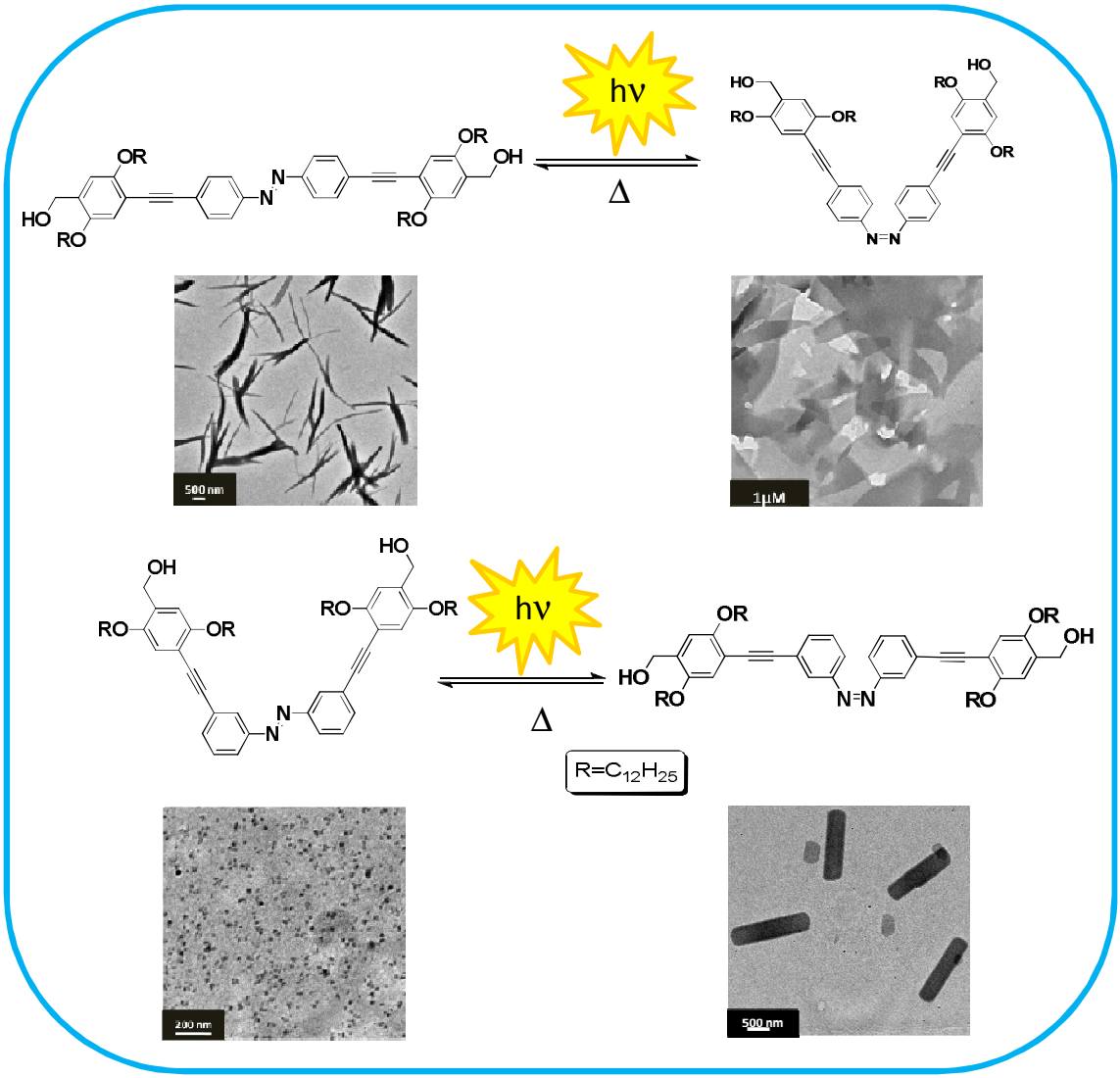

2.1. Abstract

The objective of the present study is to investigate the effect of a photoisomerizable azobenzene moiety on the self-assembly and the morphological properties of H-bonded π-conjugated molecules. For this purpose, two isomeric phenyleneethynylenes, ***p-AZO-PE*** *and* ***m-AZO-PE****, having an azobenzene moiety on the conjugated backbone have been designed, synthesized and characterized. The para isomer showed a broad absorption around 400 nm, whereas the meta isomer exhibited two absorption bands at 290 nm and 335 nm, indicating that the chromophores are not conjugated in the latter isomer. The aggregation behavior of these molecules in cyclohexane was monitored by variable temperature UV/Vis spectroscopy. Photoirradiation of solutions of* ***p-AZO-PE*** *and* ***m-AZO-PE*** *showed change in their absorption spectra which indicate trans to cis photoisomerization of the azo moiety. The para isomer,* ***p*****-AZO-PE**, *in cyclohexane showed irregular rod like morphology before irradiation which transformed into 2-D flakes after irradiation. The meta substituted isomer,* ***m*****-AZO-PE**, *formed nanoparticles which upon irradiation, transformed into rods. The mechanism of the morphogenesis of flakes and rods are rationalized based on a photoinduced surface polarity change of the initially formed morphology which facilitated their hierarchical association as a result of the trans to cis isomerization of the azobenzene chromophores.*

2.2. Introduction

The "bottom-up" molecular self-assembly approach is currently recognized as one of the powerful methods to create new organic materials with controlled physical and chemical properties.[1] Chemists are often inspired by the beauty and complexity of biological systems and strive for a deeper understanding of the processes involved, to copy them to artificial systems. Beyond the scientific curiosity of creating aesthetic architectures, the ultimate goal of these studies is to control the size, shape and properties of molecular self-assemblies within a specific length scale and their modulation at will. Towards this end, self-assemblies that respond to external stimuluii such as electrical, chemical, or optical signals are of importance. Arguably light represents perhaps the most attractive external stimulus to control physical properties of molecules and materials. Nature sets the best examples and make use of light-responsive pathways to regulate biological systems. Natural phenomena such as photosynthesis, vision, and photomorphogensis are important processes that alter biological functions in response to light. These biological processes are based on the interaction of light with suitable chromophores that induce change in properties such as volume or polarity changes. Among various photochromic molecules azobenzene has received much attention due to its reversible *E-Z* photoisomerization that proceeds with large change in the geometry and dipole moment of the chromophore.[2] Hence, photoisomerization of azobenzene derivatives has been extensively used to control conformation,[3] catalytic activity,[4] molecular motion,[5] degree of π-conjugation,[6] binding affinity,[7] and sol-gel transformation.[8] In some of these cases, photoisomerization of

azobenzene could be specifically applied to impart shape memory and photomechanical effects leading to smart materials.[9]

Azobenzene has been widely used for the creation of photoresponsive gels. A new class of gelator containing substituted azobenzene as the aromatic part has been studied extensively by Shinkai and coworkers.[10] In their first report, two types of gelators,with either a natural (*S*)-configuration (**1**) or the inverted (*R*)-configuration (**2**) at position 3 of the steroidal part have been reported. Among them, the gelators bearing a *p*-alkoxyazobenzene moiety are found to be the most efficient and they can specifically gelate either nonpolar (*S* derivatives, **1**) or polar solvents (*R* derivatives, **2**). It is possible to 'read-out' the sol-gel phase transition as well as the chirality of the supramolecular stacks using CD spectroscopy. For example, **1** showed a positive exciton coupling and **2** showed a negative exciton coupled band, characteristic of the clockwise and anticlockwise orientation of the azobenzene dipoles in the gel state, respectively. This is supported by the observation of right-handed and left-handed helical fibers through SEM pictures. In this case, the sol-gel transition could be controlled by the *cis*-to-*trans* isomerization of azobenzene, leading to photoresponsive organogels (Figure 2.1b).

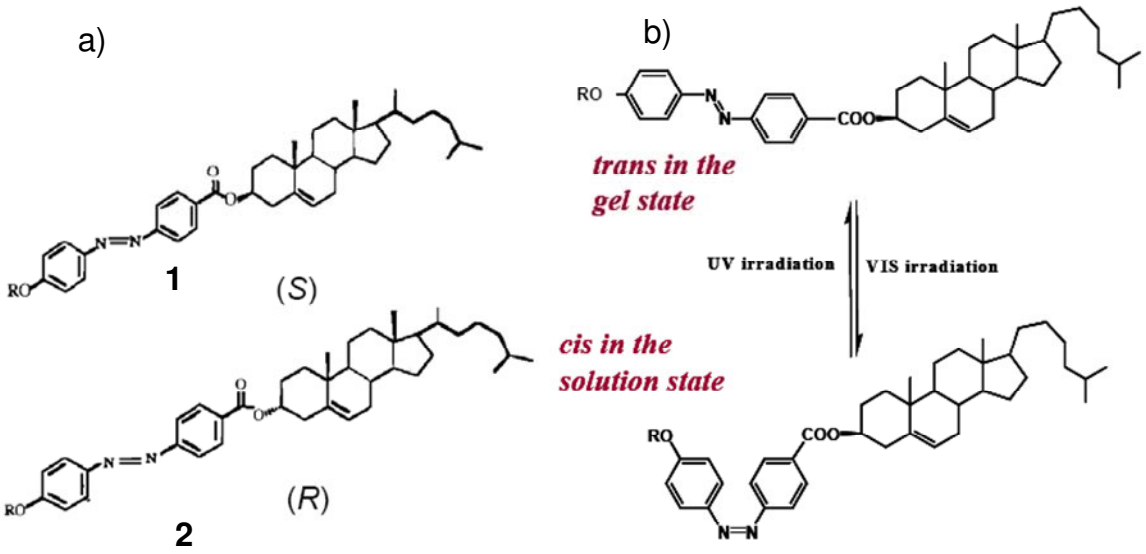

Figure 2.1. a) Structures of azobenzene-appended gelators and b) *trans*-to-*cis* isomerization of **1**.

In a recent report Tamaoki and coworkers have studied the gelation of azobenzene derivatives **3** and **4,** *meta* substituted with two urethane linked cholesteryl esters that exhibit gel-sol phase transitions upon photoirradiation (Figure 2.2).[11] The molecule **3** (m = 4, = 1), **4** (m = 3, n = 2) and **5** (m = 4, = 2), form gels in cyclohexane. When the cyclohexane gels were irradiated with 365 nm light, a gel to sol transition was observed as a result of the *trans*-to-*cis* isomerization of the central azobenzene unit. An FTIR spectroscopic investigation of the cyclohexane gel of the compound **4** indicated that these gels are formed by H-bonding between the amide and the carbonyl groups of the urethane units. During the sol-gel phase transition, H-bonds, which are partly responsible for stabilizing the gels, are broken or reformed.

Figure 2.2. Structures of the photoismerizable azobenzene derivatives (Top). Images of (a) cyclohexane gel of *trans*-**4** (1.0 wt %), (b) after irradiation with 365-nm light, and (c) after irradiation with 436-nm light.

Azobenzene photoisomerization has been widely utilized for the preparation of photoresponsive host–guest complexes. The photoresponsive self-assemblies of water-soluble polymer **6** reported by Harada et al.[12] is unique because the photochromic molecule is used as a 'photoresponsive key' (Figure 2.3a). They have utilized phototunable binding affinities of azobenzene dicarboxylic acid (**7**) with α-cyclodextrin (α-CD). Similar to unsubtituted azobenzene, *trans*-**7** shows higher binding affinity to α-CD when compared to the *cis*-isomer. Poly (acrylic acid) (**6**) modified by dodecyl groups self-assembles in water through solvophobic interaction between the aliphatic side chains (Figure 2.3b), affording hydrogels. When α-CD is added to the gels, gel-to-sol conversion is observed because α-CDs capture the dodecyl groups, disrupting their solvophobic interactions (Figure 2.3b and Figure 2.3c). Remarkably, the addition of *trans*-**7** to this binary mixture converts the solution to the original gel state since

trans-**7** can predominantly complexes with α-CD, thus rendering the dodecyl chains free (Figure 2.3c and Figure 2.3d). This ternary mixture including **6**, **7** and α-CD is therefore capable of photoswitching between gel and solution states owing to the phototunable binding affinity between **7** and α-CD. Indeed, irradiation of the gel of the ternary mixture with UV light resulted in a gel-to-sol conversion as a result of lower binding affinity of the photogenerated *cis*-**7** to α-CD than that of dodecyl group (Figure 2.3d and Figure 2.3e). Subsequent irradiation of the photogenerated solution with visible light again induced gelation due to preferential complexation of α-CD with *trans*-**7** (Figure 2.3e and Figure 2.3d). This system might be categorized as a unique photoresponsive self-assembly driven by a ‘‘photoresponsive key’’.

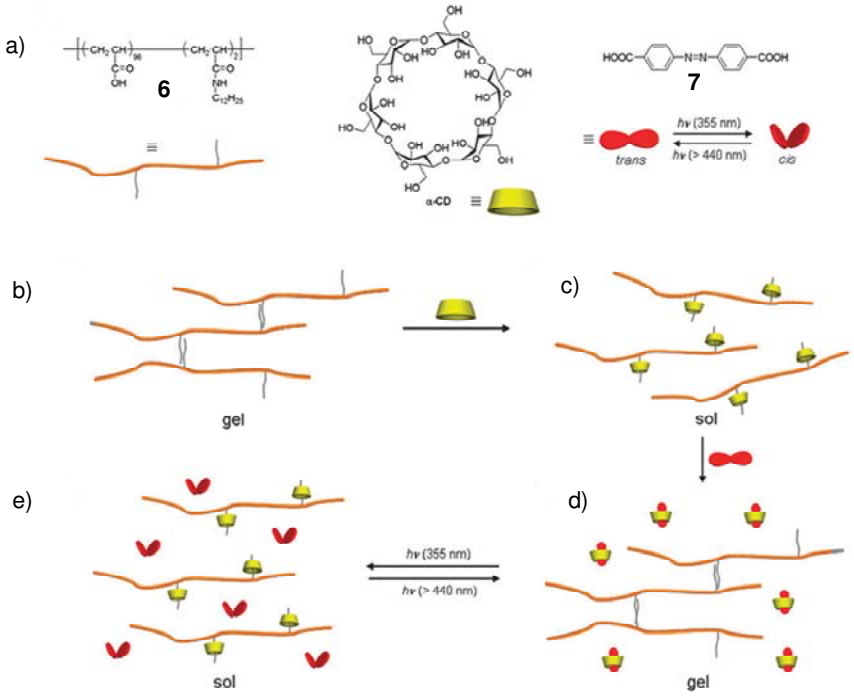

Figure 2.3. (a) Cartoon representations of the interaction of polymer **6** with α-CD and azo compound **7.** (b-e) Representation of different stages of the self assembly of the aqueous polymer controlled by the photoresponsive complexation between **7** and α-CD.

There are several reports on azobenzene based compounds, in particular hybrid materials with fullerenes[13] or OPEs[14–17]. Photoisomerization of azo chromophores has also been utilized for the preparation of elastomers which undergo photoinduced mechanical changes.[18] In addition, photoswitching of the self-assembly of azo-linked amphiphilic systems has been reported. Recently Armaroli et al. have reported the photoisomerization induced changes in the molecular self-assembly of π-conjugated molecules on HOPG surface.[18b] Detailed STM analysis has revealed that only the *trans* isomer is capable of physisorbing at the HOPG surface, showing that the lack of planarity in the *cis* isomer constitutes a notable barrier to its interaction with the HOPG surface. Thus azo chromophore has been extensively utilized for a variety of applications.

In the present work, we explore the well known *E-Z* isomerization of azobenzene in combination with a linear π-system, in view of the latter's inherent optoelectronic properties and propensity for self-assembly.[19-21] To be specific, we have chosen a *p*-phenyleneethynylene (PE) backbone, due to their ability to form diverse architectures.[22] For this purpose, we have designed and synthesized two classes of molecules, with different substitution pattern. Chart 2.1 shows the *para* substituted azobenzene incorporated OPEs, ***p*-AZO-PE** and the corresponding *meta* substituted derivative ***m*-AZO-PE**. The incorporation of photochromic azobenzene on the π-conjugated backbone allows control of morphology as well as the self-assembling properties of these molecules by the photoisomerization of the azobenzene unit.

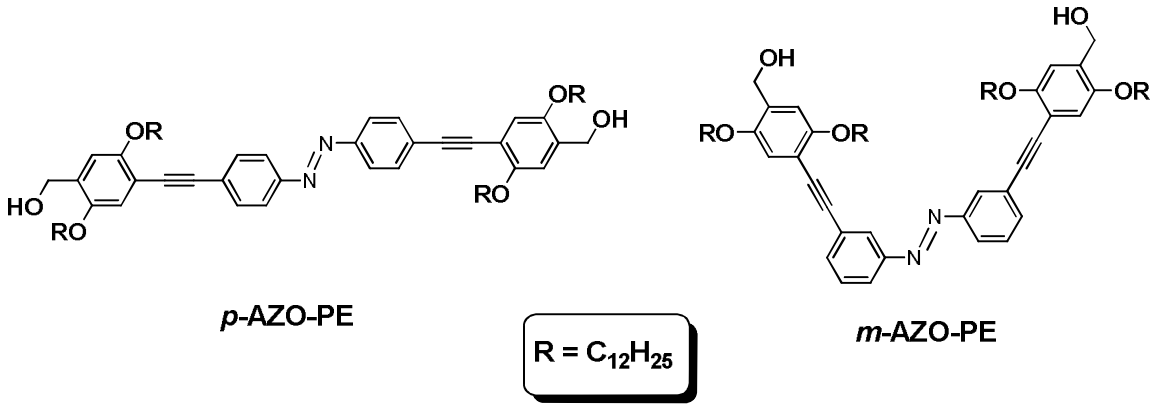

Chart 2.1

2.3. Results and Discussion

2.3.1. Synthesis of the Azo-linked PEs

Synthesis of ***p*-AZO-PE** and ***m*-AZO-PE** is achieved by multistep reactions involving several intermediate products. For the synthesis of ***p*-AZO-PE**, the bisethynyl derivative **11** was prepared starting from 4-iodoaniline (Scheme 2.1), which was first treated with a mixture of $KMnO_4/CuSO_4$ in dichloromethane at room temperature to give the compound **9**. Reaction of **9** with two equivalents of trimethylsilylacetylene in diisopropylamine using $[Pd(PPh_3)_2(Cl_2)_2]$ / CuI as the catalyst gave the corresponding silyl protected derivative (**10**) in 71% yield. Deprotection of **10** using potassium hydroxide (KOH) in a mixture of THF and methanol gave the corresponding bisethynyl derivative, **11** in 76% yield.

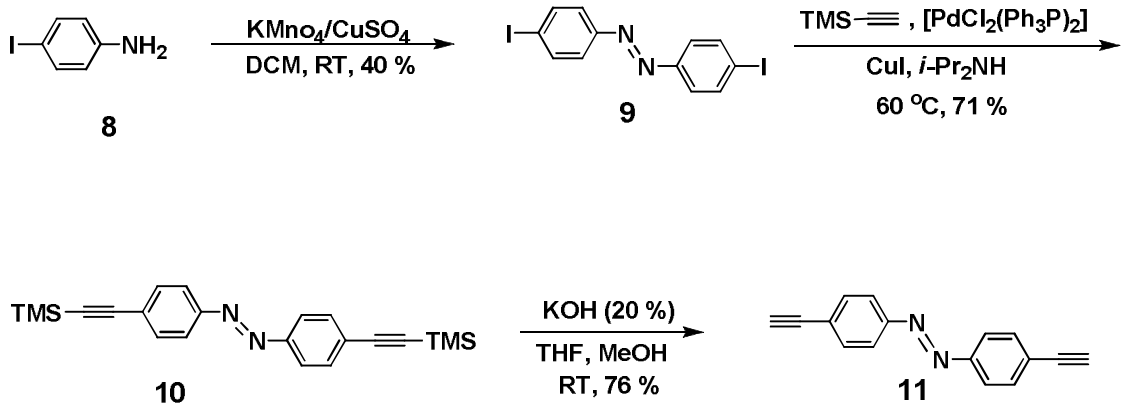

Scheme 2.1

For the synthesis of ***m*-AZO-PE**, the bisethynyl derivative **15** was prepared by starting from 3-iodoaniline (Scheme 2.2). 3-Iodoaniline was first treated with a mixture of $KMnO_4/CuSO_4$ in dichloromethane at room temperature to give the azo compound **13**. Reaction of **13** with two equivalents of TMS-acetylene in diisopropylamine using $[Pd(PPh_3)_2(Cl_2)_2]$/CuI as the catalyst gave the corresponding silyl protected derivative (**14**) in 75% yield. Deprotection of **14** using potassium hydroxide (KOH) in a mixture of THF and methanol gave the corresponding bisethynyl derivative, **15** in 80% yield. The compounds **11** and **15** were characterized by ^{1}H NMR, ^{13}C NMR and mass spectral analyses.

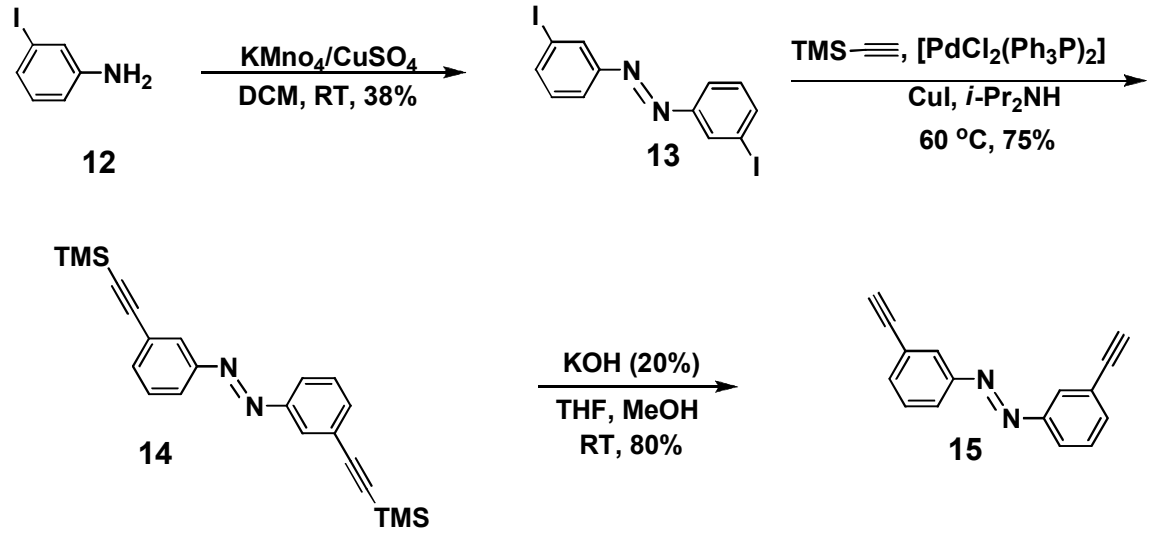

Scheme 2.2

The required intermediate, 1-bromo-4-formyl-2,5-bis(dodecyloxy)benzene (**21**) for the synthesis of ***p*-AZO-PE** and ***m*-AZO-PE** was synthesized starting from methyl hydroquinone which was first alkylated using dodecyl bromide in DMF using NaOH which resulted in the corresponding alkylated derivative (**17**) in 73% yield. Reaction of **17** with *N*-bromosuccinimide (NBS) in CCl_4 using azobis-(isobutyro) nitrile (AIBN) as the radical initiator gave the corresponding bromomethylated derivative which was subsequently brominated using NBS in tetrahydrofuran (THF), to give the corresponding dibromo derivative (**18**) in 60% yield. Reaction of **18** with potassium acetate and tetrabutyl ammonium bromide (TBAB) in a mixture of chloroform and acetonitrile gave the corresponding acetylated derivative (**19**) which was subsequently hydrolyzed using KOH in methanol and THF, to give the corresponding alcohol (**20**) in 60% yield. Controlled oxidation of **20** using pyridinium chlorochromate (PCC) in dichloromethane gave the corresponding aldehyde **21** in 63% yield (Scheme 2.3).

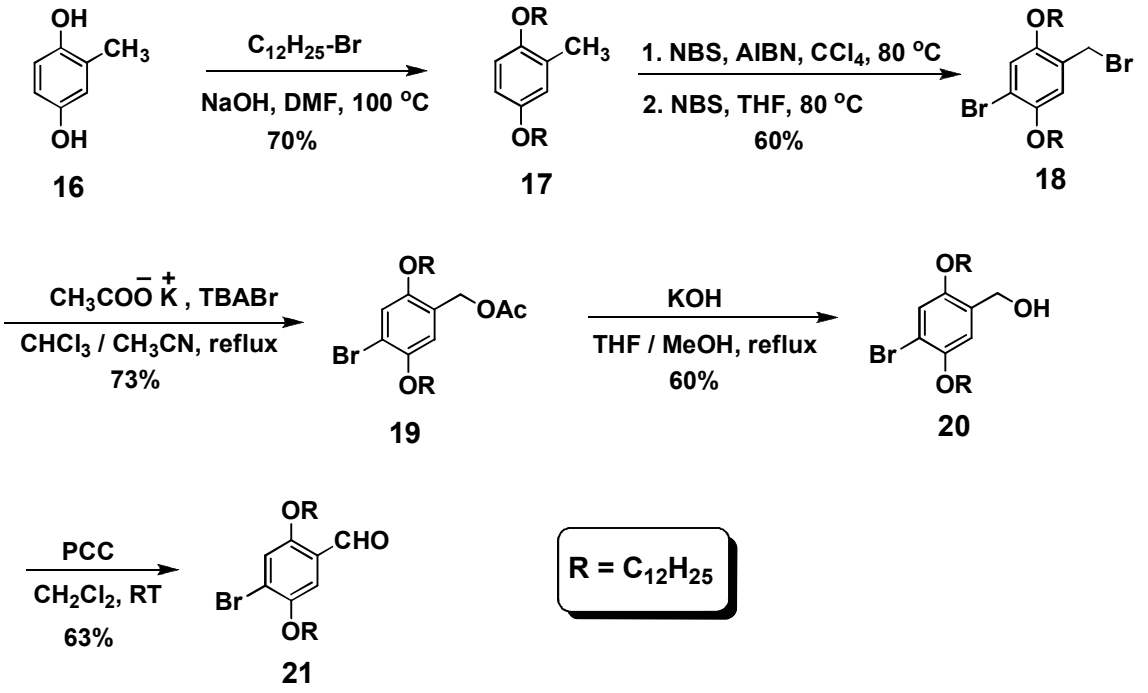

Scheme 2.3

***p*-AZO-PE** was synthesized by the Sonogashira-Hagihara cross coupling reaction between the bisethynyl derivative (**11**) and two equivalents of 1-bromo-4-formyl-2,5-bis(dodecyloxy)benzene (**21**) in a mixture of toluene and diisopropylamine using [$Pd(PPh_3)_4$]/CuI as the catalyst. The corresponding bisaldehyde thus obtained (45% yield) was subsequently reduced using sodium borohydride in a mixture of methanol and dichloromethane at room temperature (Scheme 2.4). The crude product obtained was purified by column chromatography (silica gel 100-200 mesh using 50% $CHCl_3$/hexane as eluent) to get ***p*-AZO-PE** in 95% yield. The same procedure was adopted for the synthesis of the ***m*-AZO-PE** using the corresponding 3, 3' bisethynyl derivative (Scheme 2.5). After purification by column chromatography (silica gel 100-200 mesh using

50% $CHCl_3$/hexane as eluent) the pure product was obtained in 87% yield. Both products were characterized by ^{1}H-NMR, ^{13}C-NMR and MS-FAB spectroscopic techniques.

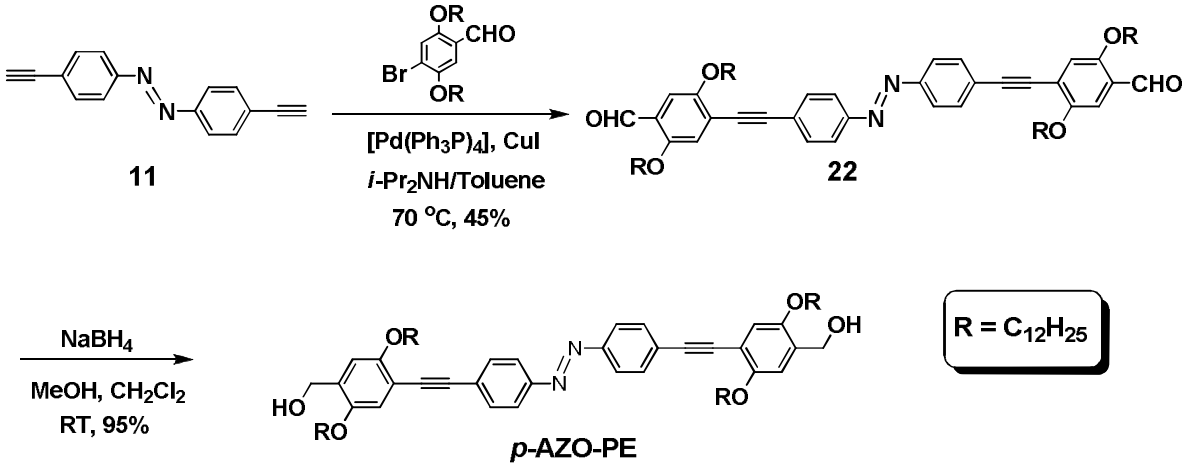

Scheme 2.4

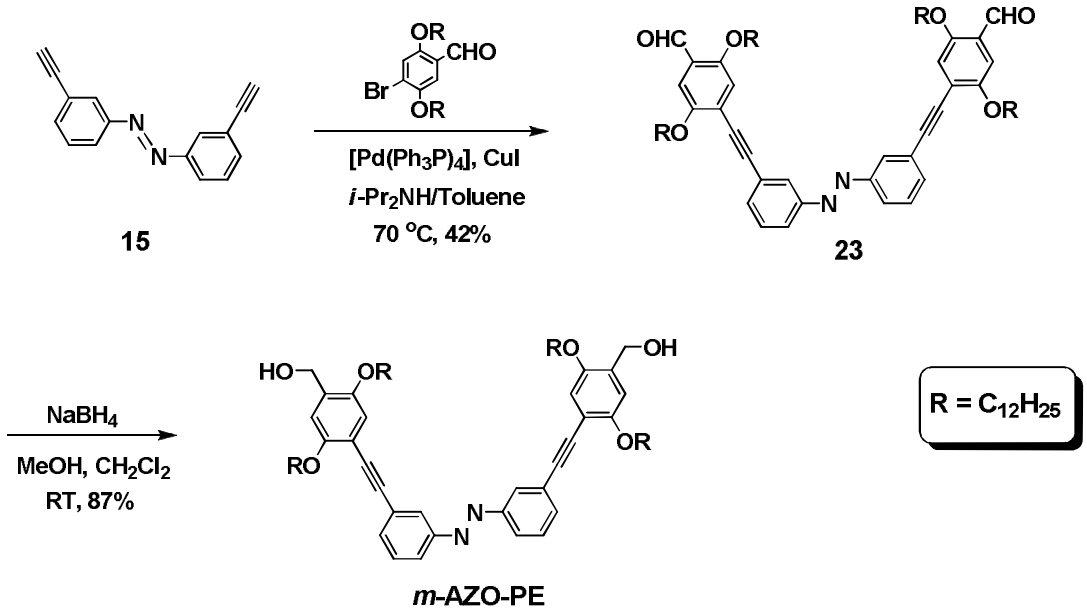

Scheme 2.5

2.3.2. Aggregation Properties of *p*-AZO-PE and *m*-AZO-PE

The absorption spectra of ***p*-AZO-PE** and ***m*-AZO-PE** are compared in Figure 2.4. Absorption spectrum of ***p*-AZO-PE** in cyclohexane (1×10^{-5} M) shows a maximum around 405 nm corresponding to π-π* transition. In the case of ***m*-AZO-PE**, the absorption spectrum in cyclohexane (1×10^{-5} M) exhibited two maxima around 280 nm corresponding to the phenyleneethynylene backbone and 330 nm corresponding to π-π* transition (Figure 2.4). The absorption corresponding to the π-π* transition is considerably shifted from 330 nm to 405 on moving from ***m*-AZO-PE** to ***p*-AZO-PE** ($\Delta\lambda$ = 75 nm). This observation reveals that ***p*-AZO-PE** and ***m*-AZO-PE** differ considerably in their electronic properties and the 3, 3' substitution of the PE moiety to the azo group is not through-conjugated in the latter case.

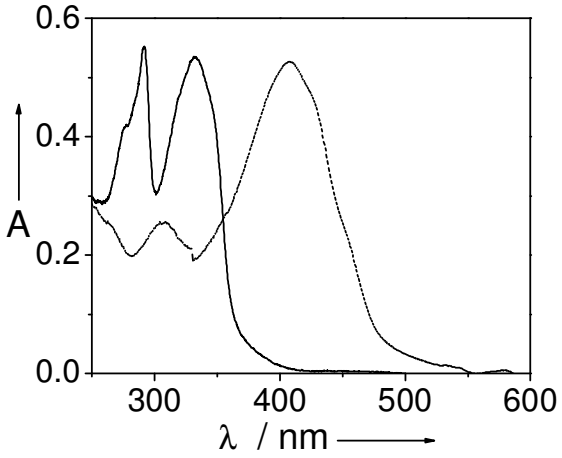

Figure 2.4. a) UV/Vis spectra of ***p*-AZO-PE** (……..) and ***m*-AZO-PE** (solid line) in cyclohexane (1×10^{-5} M) at 25°.

In order to get more insight into the aggregation behavior of ***p*-AZO-PE** and ***m*-AZO-PE** in solution, detailed UV/Vis spectral studies were carried out in different solvents. The UV/Vis absorption spectra of the ***p*-AZO-PE** and ***m*-AZO-PE** in cyclohexane and chloroform are shown in Figure 2.5a, and Figure 2.5b, respectively. While the absorption maxima of both compounds are nearly identical in chloroform and in cyclohexane, the intensities of the absorptions are considerably different. For example, the absorption spectrum of ***p*-AZO-PE** in cyclohexane (1×10^{-5} M) after heating and cooling of the solution to 25 °C showed considerable decrease in the intensity of the absorption band at 422 nm (ε = 16,370 $M^{-1}cm^{-1}$) when compared to that in chloroform (ε = 54,150 $M^{-1}cm^{-1}$), indicating the probable aggregation of the PE moiety (Figure 2.5a). When the temperature is increased to 60 °C, the intensity of the absorption band at 422 nm is increased with an ε value of 48,896 $M^{-1}cm^{-1}$(Figure 2.6a).

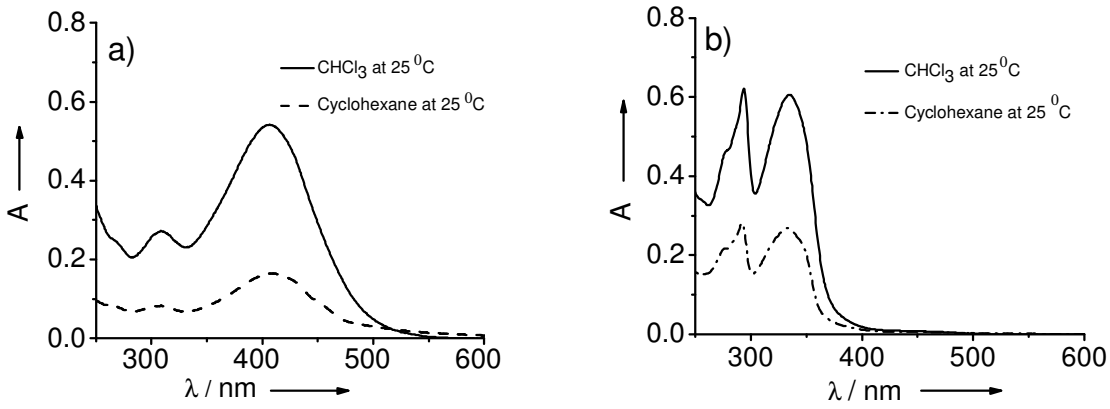

Figure 2.5. a) Absorption spectra of ***p*-AZO-PE** (1×10^{-5} M) and (b) ***m*-AZO-PE** (1×10^{-5} M) in chloroform at 25 °C and cyclohexane at 25 °C.

A similar trend is observed in the case of ***m*-AZO-PE** in cyclohexane (1×10^{-5} M) in which the ε value is as low as 26,855 $M^{-1}cm^{-1}$ when compared to that in chloroform (60,655 $M^{-1}cm^{-1}$) (Figure 2.5b). The increase in the ε value with increase in temperature in both cases indicates the breaking of the aggregate resulting in isotropic solutions (Figure 2.6a and 2.6b). However, the melting transition temperatures of these aggregates differ considerably on moving from ***m*-AZO-PE** to ***p*-AZO-PE**.

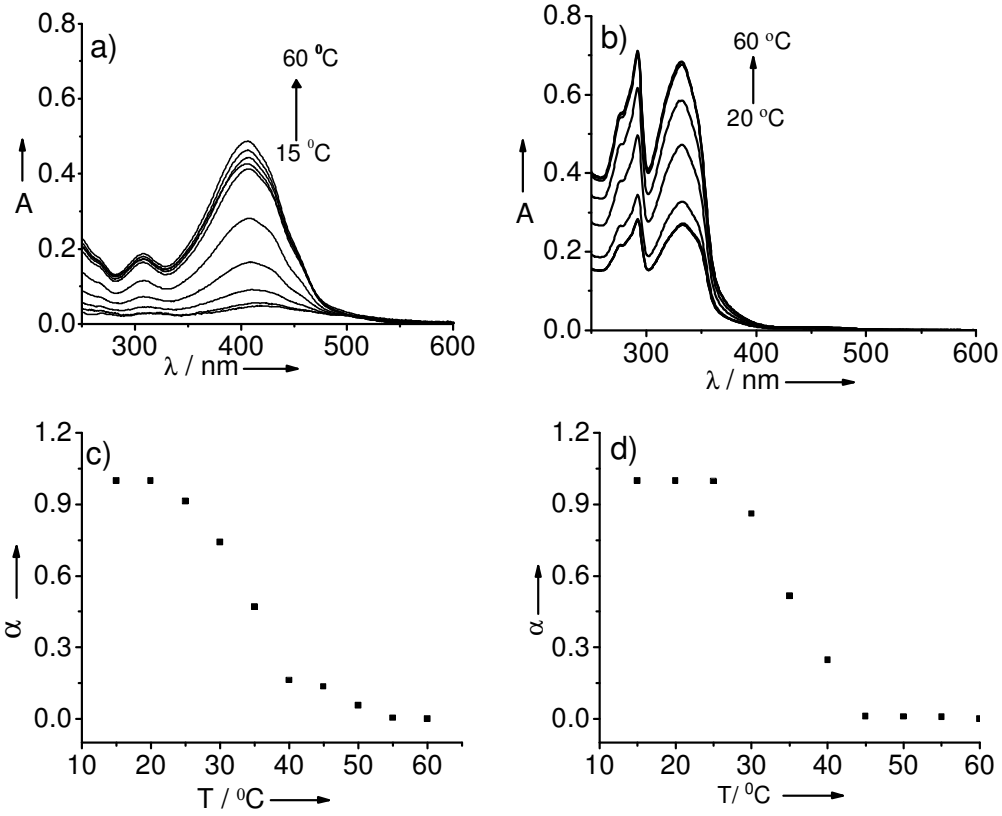

Figure 2.6. Temperature dependent absorption spectral changes in cyclohexane (a) ***p*-AZO-PE** and (b) ***m*-AZO-PE** (*c* =1 × 10^{-5} M). Plots of the fraction of aggregates (α) obtained from absorption versus temperature for (c) ***p*-AZO-PE** and (d) ***m*-AZO-PE** in cyclohexane (c =1 × 10^{-5} M). The fraction of aggregated species (α) were calculated from ε at the absorption maximum, according to the equation $(\varepsilon_{monomer} - \varepsilon) / (\varepsilon_{monomer} - \varepsilon_{aggregate})$, where $\varepsilon_{aggregate}$ and $\varepsilon_{monomer}$ were taken from fully aggregated and completely monomeric spectra at 60 °C in cyclohexane.

The aggregates of ***m*-AZO-PE** exhibited a melting transition temperature (T_m) of 34 °C whereas ***p*-AZO-PE** showed a T_m of 39 °C (Figure 2.6c and 2.6d.). These results reveal that both derivatives are able to form self-assembled species in cyclohexane and undergo melting upon increasing the temperature in a cooperative fashion as indicated by the sigmoidal transition. The observed 5 °C difference between the aggregates of ***p*-AZO-PE** and ***m*-AZO-PE** indicates that the former forms much stable aggregates when compared to that of the latter.

2.3.3. Photoisomerization Studies of *p*-AZO-PE and *m*-AZO-PE

The facile *trans-cis* photoisomerization and reverse *cis-trans* thermal or photochemical isomerization are attractive features of the azobenzene chromophore which can be followed by UV/Vis spectroscopy. The *trans* to *cis* isomerization of the ***p*-AZO-PEs** can be induced by irradiating the solution with light of wavelength corresponding to the absorption maximum, which results in the decrease of absorbance of the π-π* transition. We could not observe any change in the n-π* transition which may be due to the extended conjugation of the azo chromophore with PE moiety. Irradiation of the ***p*-AZO-PE** in cyclohexane (*c* = 1×10^{-5} M) at 400 nm using a band pass filter ($\lambda_{band\ pass}$ = 400 nm, LOT-Oriel 200 W high-pressure Hg Lamp) for 10 minutes resulted in a decrease in the absorbance of the π-π* transition band (350-450 nm) with the concomitant increase in the absorbance at 300 nm through an isosbestic point at 364 nm (Figure 2.7a). A photostationary state (PS) is attained within this period indicating the conversion of ***p*-AZO-PE**$_{trans}$ to ***p*-AZO-PE**$_{cis}$ as monitored by the UV/Vis absorption spectroscopy. The content of the *cis* isomer at the PS was found to be

ca. 40% as calculated by the equation $(A_o-A_{ps(400)})/ A_o$, where A_o and $A_{ps(400)}$ are the absorbance at 400 nm of the unirradiated solution and of the solution at the photostationary state.[23]

In the case of ***m*-AZO-PE** (Figure 2.7b), when irradiated at 350 nm in cyclohexane ($c = 2.5 \times 10^{-5}$ M) using a band pass filter ($\lambda_{band\ pass}$ = 350 nm, LOT-Oriel 200 W high-pressure Hg Lamp), a slow decrease in the intensity of the absorption maximum at 350 nm is noticed with the formation of a weak band at 450 nm (Figure 2.7b, inset). These changes are typical of the *E-Z* isomerization of the azobenzene moiety, resulting in the conversion of ***m*-AZO-PE**$_{trans}$ to ***m*-AZO-PE**$_{cis}$. The content of the *cis* isomer at the photostationary state was found to be ca. 17% as calculated (*vide supra*). The weak change in the absorption spectra and the low percentage conversion of the *trans* to *cis* derivatives could be due to the competing absorption of the phenyleneethynylene moiety [24] and also due to the steric effect of the long alkyl chains in the aggregated state.[25]

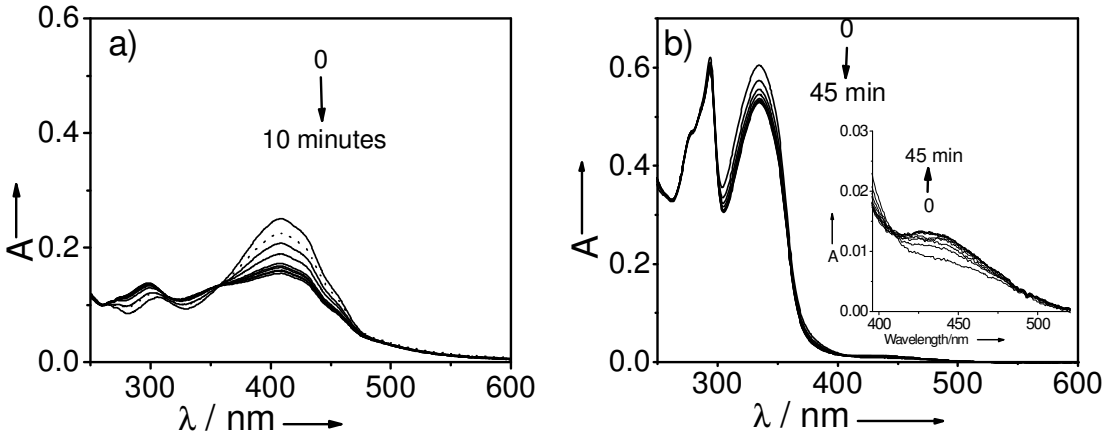

Figure 2.7. a) UV/Vis absorption spectral changes of ***p*-AZO-PE** in cyclohexane (1×10^{-5} M) with irradiation (λ = 400 nm) at 25 °C and b) ***m*-AZO-PE** in cyclohexane (2.5×10^{-5} M) upon irradiation (λ = 350 nm) at 25 °C.The inset of the Figure b shows zoomed spectra in the region of 400-550 nm.

Another possible reason for the low *trans* to *cis* photoconversion could be due to the aggregation of ***p*-AZO-PE** and ***m*-AZO-PE** in cyclohexane. The photoinduced changes may be occurring mainly on the surface of the aggregates.

2.3.4. Dynamic Light Scattering (DLS) Analysis

Dynamic light scattering (DLS) experiments were performed on ***p*-AZO-PE** as well as ***m*-AZO-PE** in cyclohexane solution to further investigate its aggregation behavior in solution. A solution of ***p*-AZO-PE** ($c = 1 \times 10^{-4}$ M) showed the presence of aggregates with hydrodynamic radii (R_H) of 500 nm before irradiation (Figure 2.8a). However, upon irradiation with UV light (400 nm) using a band pass filter for 10 minutes resulted in a photostationary state (PSS) indicating the rapid conversion to ***p*-AZO-PE**$_{cis}$. Interestingly, the photoirradiated solution of ***p*-AZO-PE** showed an increase in the hydrodynamic radii due to the formation of aggregates with average size of 1μm (Figure 2.8b).

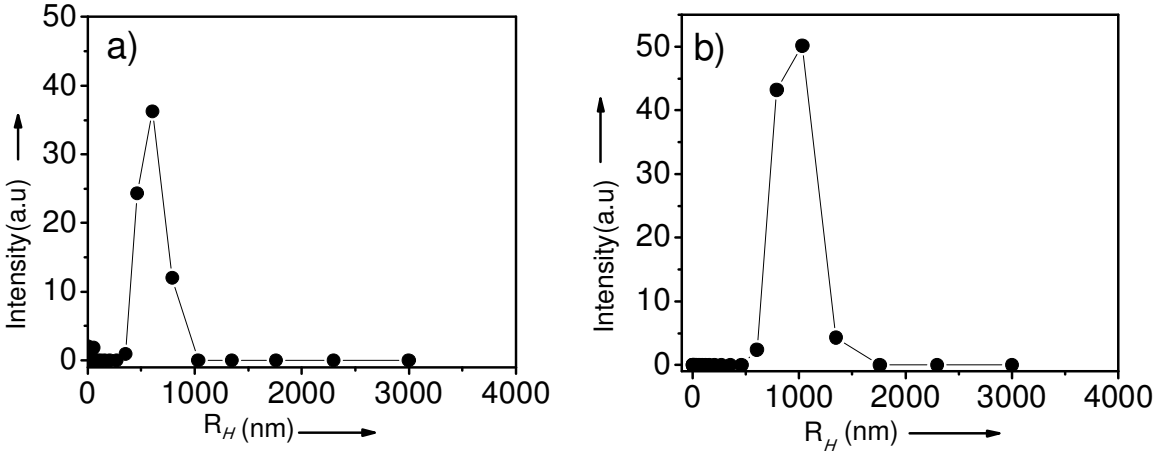

Figure 2.8. The intensity weighted distribution of particles obtained from DLS measurements of ***p*-AZO-PE** from cyclohexane at a concentration of 1×10^{-5} M at 25 °C; a) ***p*-AZO-PE** before irradiation and b) after 10 minutes irradiation at 400 nm.

In the case of ***m*-AZO-PE** ($c = 1 \times 10^{-4}$ M) in cyclohexane, aggregates with hydrodynamic radii (R_H) of around 40 nm were observed before irradiation (Figure 2.9a). Irradiation at 350 nm using a band pass filter for 1 h, resulted in a photostationary state (PSS) indicating the rapid conversion to ***m*-AZO-PE**$_{cis}$. After irradiation, an increase in the hydrodynamic radii is observed for the aggregates with average size of 300-400 nm (Figure 2.9b) with significant deviation of the plot, indicating a change in the morphology of the aggregates. Even though these values are not quantitative, the trend observed in the case of both molecules before and after irradiation indicates the possible difference in the size of the aggregates formed at different experimental conditions.

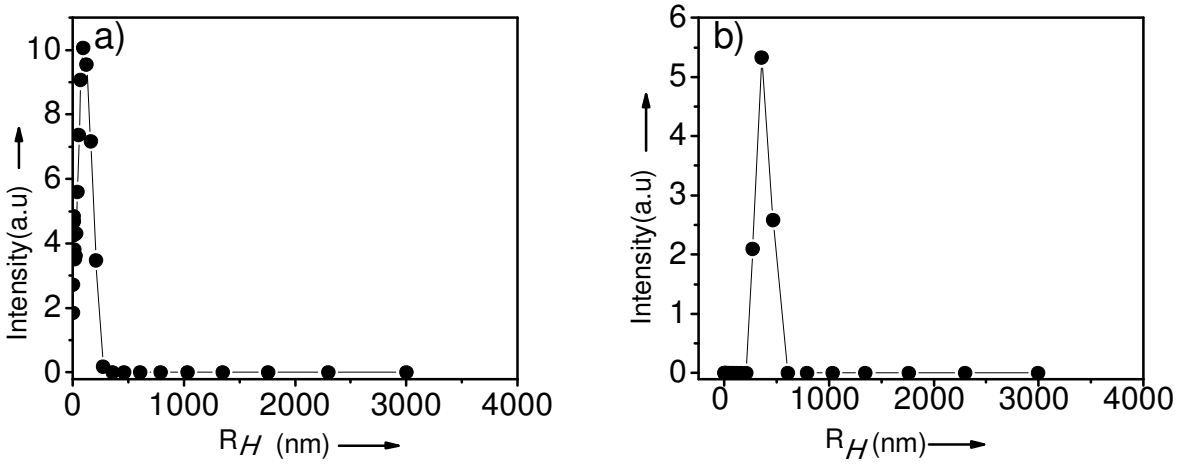

Figure 2.9. The intensity weighted distribution of the aggregates obtained from DLS measurements of ***m*-AZO-PE** in cyclohexane at a concentration of 1×10^{-5} M at 25 °C; a) ***m*-AZO-PE** before irradiation; b) after 10 minutes of irradiation with UV light of 350 nm.

2.3.5. Microscopic Analysis

Detailed Transmission Electron Microscopy (TEM), analysis was carried out on ***p*-AZO-PE** as well as on ***m*-AZO-PE** in cyclohexane and chloroform at

different concentrations. The TEM images have provided insight into the supramolecular morphology of the aggregates formed in solution and the effect of photoisomerization on the morphology of these aggregates. Samples were casted on to TEM grids before and after irradiation from cyclohexane. TEM image of ***p*-AZO-PE** in cyclohexane (1×10^{-4} M) showed the presence of rods of irregular shape with a length of around 3-5μm and width of nearly 200-400 nm (Figure 2.10a). This observation reveals that the ***p*-AZO-PE**$_{trans}$ favors π-π stacking leading to aggregation to form rods. Interestingly, the TEM images of the aggregates after irradiation with 400 nm light for about 30 min revealed that the initially formed morphology has transformed into 2D flake like structures (Figure 2.10c). This morphology change is a time dependent phenomenon as evident from Figure 2.10b and Figure 2.10c. The TEM image of ***m*-AZO-PE** in cyclohexane (1×10^{-4} M) showed the formation of particles with ca. 20 nm in size, which is consistent (Figure 2.10d) with the size observed in the DLS analysis before irradiation. Surprisingly, the TEM images obtained after irradiation revealed the complete transformation of the nanoparticles to shape controlled supramolecular rods having diameter ca. 200-400 nm and length of nearly 500 nm - 2 μm (Figure 2.10f). While, the widths are comparable among different rods, the length significantly varies indicating a pseudo 1D hierarchical growth process. This time dependent growth is further clarified by the TEM analysis of the samples after intervals of irradiation which revealed (Figure 2.10e and 2.10f) a longitudinal growth of the rods with almost uniform diameter.

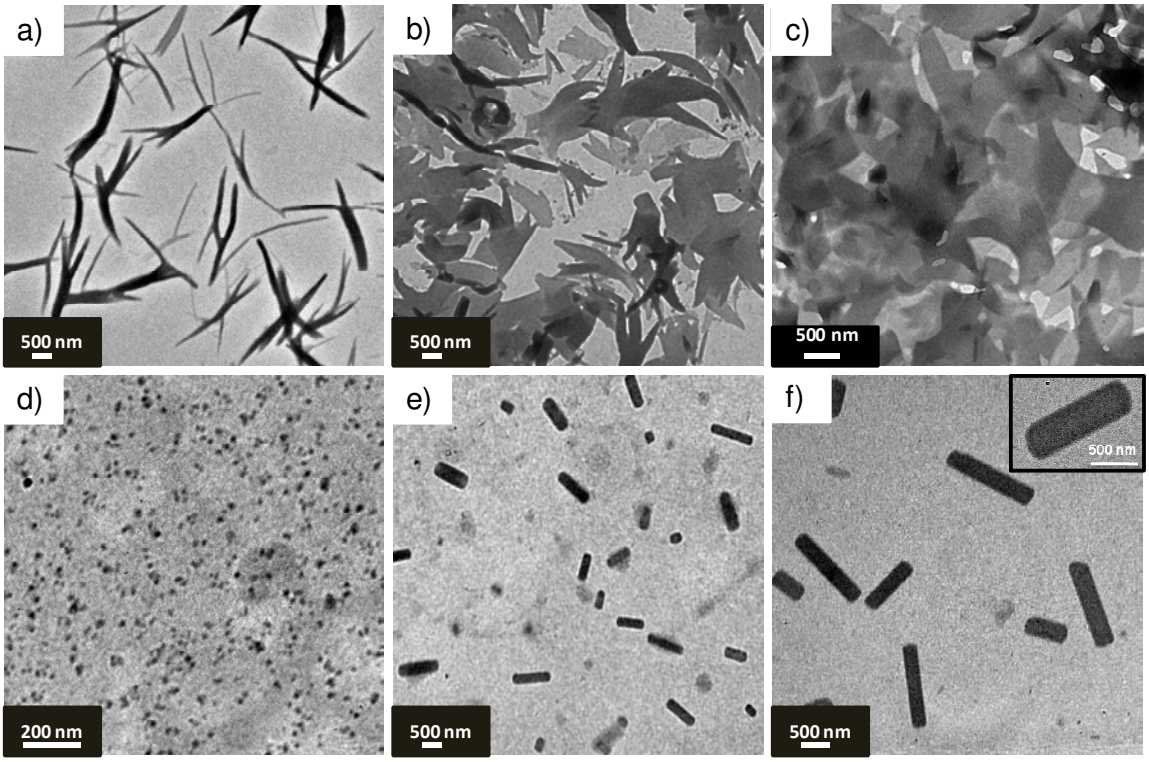

Figure 2.10. Light triggered morphogenesis of self-assembled ***p*-AZO-PE** and ***m*-AZO-PE**. TEM images of ***p*-AZO-PE** (1 x 10^{-4} M) in cyclohexane; (a) Before irradiation; (b) Transformation of nanorods to flakes upon irradiation with 400 nm light for 10 minutes; (c) Complete transformation of nanorods to flakes upon irradiation with 400 nm light for 30 minutes; (d) TEM images of ***m*-AZO-PE** before irradiation; (e) Transformation of nanoparticles to rods upon irradiation with 350 nm light for 10 minutes; (f) TEM image after irradiation with 350 nm of light for 1 h.

An interesting feature of the flakes and rod structures is the time dependent reversibility of the morphology. The flakes of ***p*-AZO-PE** after keeping for several weeks showed the reversal of the morphology to the original structure which goes back again to flakes on irradiation. For example, Figure 2.11a is the TEM image of the flakes of ***p*-AZO-PE** after keeping for 15 days. In this case, disintegration of the flakes to smaller size and the formation of the initial rod like structures could be seen. After keeping for several weeks, a complete transformation of the flakes

to rods was observed (Figure 2.11b). The same solution containing the reverted rods was again irradiated and the morphology was examined by TEM analysis. Figure 2.11c represents the TEM image after the irradiation of the solution which reveals that the flakes are regenerated.

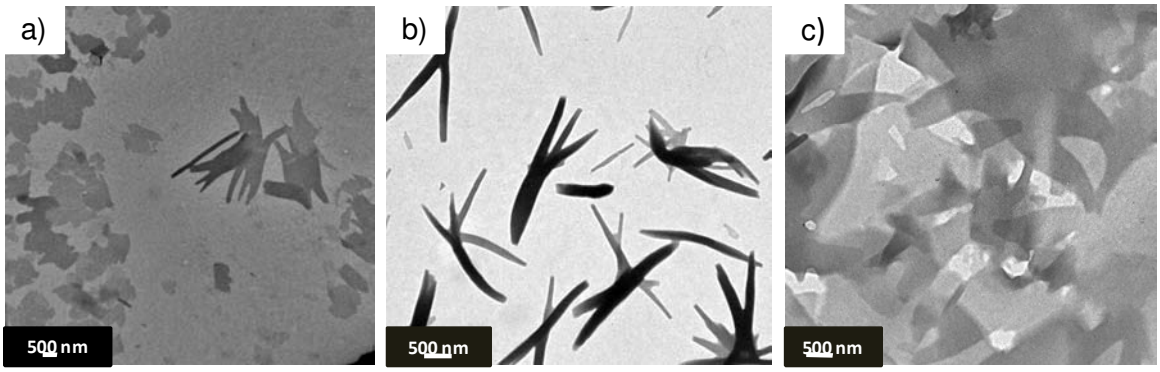

Figure 2.11. Reversible change (in dark) of the self-assembled ***p*-AZO-PE** (1 x 10^{-4} M) in cyclohexane; (a) TEM image after 15 days showing partial transformation of flakes to rods; (b) TEM image after 30 days showing complete reversal of flakes to rods; (c) TEM image showing the reappearance of flakes after irradiation with 400 nm.

Similarly, the TEM images of the rods of ***m*-AZO-PE** after keeping in dark for 15 days exhibited a decrease in the size (Figure 2.12a). Upon keeping the solution for one month, complete transformation of the rods into nanoparticles was observed (Figure 2.12b). The TEM images of the same sample after irradiation with 350 nm light revealed the reformation of rods (Figure 2.12c), thus indicating the reversibility of the structures.

The effect of temperature on the stability of the rods was studied by heating the photoirradiated solution above 60 $^{\circ}$C. The rods instantly transformed into particles by heating which is clear from the TEM image (Figure 2.13a). The

same sample after cooling to room temperature followed by irradiation with 350 nm light showed the regeneration of rods as evident from the TEM image (Figure 2.13b). These experiments convincingly indicate that the rod formation is a time and temperature dependent reversible process.

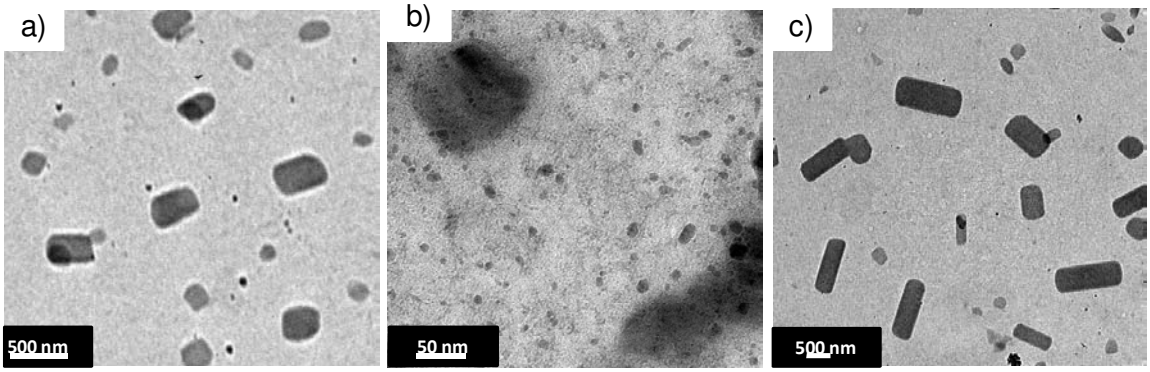

Figure 2.12. Reversible change (in dark) of the self-assembled rods of ***m*-AZO-PE** (1 x 10^{-4} M) in cyclohexane. (a) TEM image after 15 days; (b) TEM image after 30 days and (c) Regeneration of the rods upon irradiation with 350 nm light.

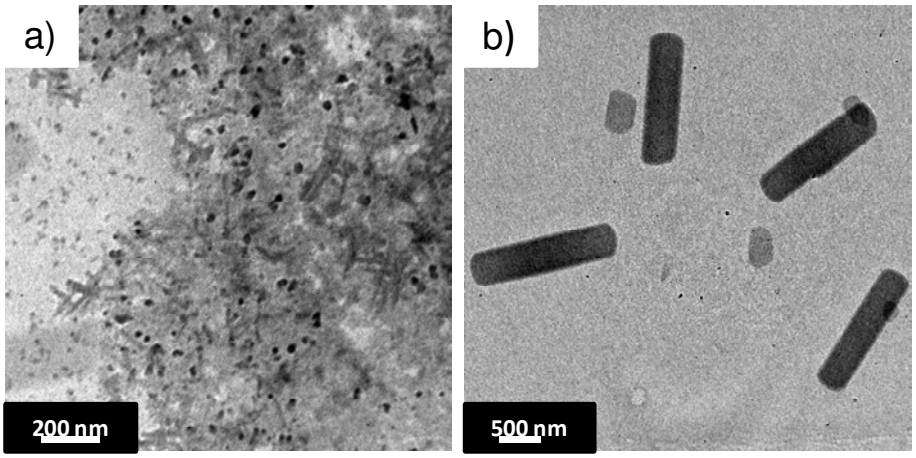

Figure 2.13. (a) Transformation of rods to nanoparticles after heating above 60 °C; (b) Regeneration of rods upon irradiation with 350 nm light.

The nature of the solvent and the initial shape of the aggregates seems to be important in the photoinduced morphology evolution. For example, both molecules do not strongly aggregate in chloroform as indicated by their respective absorption spectra. The TEM images of the molecules from chloroform before and after irradiation showed ill-defined morphologies even though the molecules exhibit a tendency to aggregate (Figure 2.14). Higher polarity of chloroform when comapared to that of cyclohexane may discourage the molecules from the initial self-assembly and its transformation to the final morphology after irradiation. The above observations unveil a unique property of ***p*-AZO-PE** and ***m*-AZO-PE** to organize into discrete shape and size before and after irradiation in cyclohexane at micromolar concentrations. Accordingly, a unique stacking property might be evolved in this case, for which the azobenzene segment and the linking to the PE moiety play important roles. The light triggered formation of the supramolecular rods of the short ***m*-AZO-PE** is particularly interesting considering the fact that such well-defined organic nano- and micro-sized rods resembling metallic nanorods (gold and silver) with controlled aspect ratio are difficult to prepare. Therefore, the light triggered structural evolution to supramolecular rods as observed here is attractive when compared to the direct self-assembly approach using organic as well as inorganic molecules.

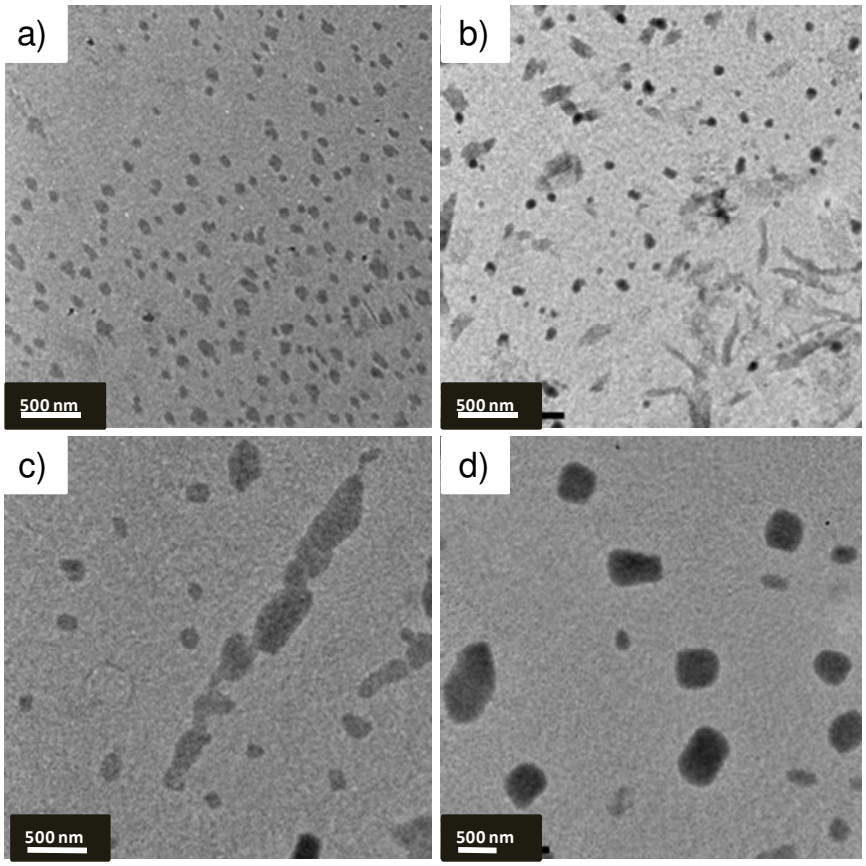

Figure 2.14. Light triggered chages of ***p*-AZO-PE** and ***m*-AZO-PE** in chloroform (1 x 10^{-4}M) ; TEM images of ***p*-AZO-PE** (a) before irradiation and (b) after irradiation with 400 nm light for 10 minutes. TEM images of ***m*-AZO-PE** (1 x 10^{-4}M) in chloroform; (c) before irradiation and (d) after irradiation with 350 nm light for 10 minutes.

2.3.6. X-ray Diffraction (XRD) Studies

Powder X-ray diffraction (XRD) is a useful technique to gather information on molecular packing in self-assemblies. Figure 2.15 shows the XRD pattern of ***p*-AZO-PE** before and after irradiation. The X-ray diffractograms show diffraction patterns characteristics of the long range ordering of the molecules with sharp reflections having *d*-spacing of 40.1, 24.7, 12.74, 4.6, 4.1 and 3.7 A°. The peak at 40.07 A° in the small angle region may corresponds to the interchain lamellar

packing distance which is slightly higher than the calculated molecular width (34.5 A°) in which the alkyl chains are in a fully extended conformation. Another strong peak at the small angle region corresponding to a d-spacing of 24.07 A° is observed which is close to the calculated length of the molecule (24.7 A°). In addition to these peaks in the small angle region, broad diffraction peaks with d-spacing of 4.6 and 4.07 A° were observed in the wide angle region corresponding to the packing of the alkyl chains in the assembly of ***p*-AZO-PE**. Another signal with d-spacing of 3.7 A° was also observed in the wide angle region corresponding to the π-π stacking. From these diffraction peaks in the XRD, it can be concluded that ***p*-AZO-PE** self-assembles in a lamellar fashion. In the lamellar phase, ***p*-AZO-PE** adopts a planar structure in which aryl rings are almost coplanar and the alkyl chains are laterally extended between the interchain packing.

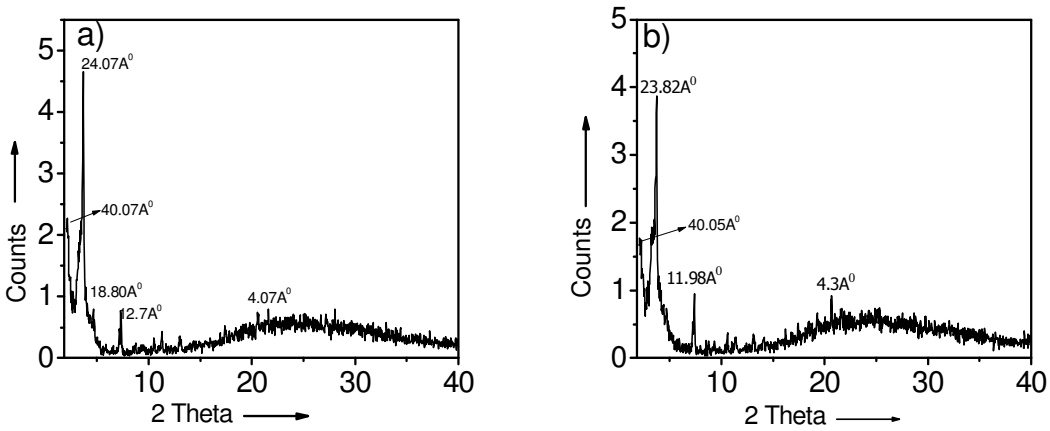

Figure 2.15. The XRD pattern of ***p*-AZO-PE** from cyclohexane at a concentration of 8×10^{-3} M at 25 °C; a) ***p*-AZO-PE** before irradiation, b) ***p*-AZO-PE** after 10 minutes with UV light of 400 nm

The XRD pattern of ***p*-AZO-PE** after irradiation is shown in Figure 2.15b. A comparison of XRD data before and after UV light irradiation did not show

significant difference in the differaction pattern. The values corresponding to the d-spacing of 40.05, 23.82, 11.98 and 4.3 A° are almost similar to those values before irradiation. This observation indicates that no major change has occurred to the initial packing of the molecules even after the irradiation. If significant amount of the *cis*-isomer would have formed upon irradiation, the XRD patterns would have considerably changed. Therefore, it is reasonable to believe that the molecular packing before and after irradiation remains almost same.

The XRD pattern in the case of ***m*-AZO-PE** is shown in Figure 2.16. The strong peak at 31.90 A° in the small angle region nearly matches with the calculated molecular width (32 A°) in which the alkyl chains are in an extended conformation. The wide angle area was very broad and weak with no characteristic diffractions, indicating weak π-interaction in the molecule. These data indicate a weak lamellar type interaction. In contrast to ***p*-AZO-PE**, XRD data of ***m*-AZO-PE** before and after UV light irradiation showed significant difference, indicating that UV light irradiation leads to considerable changes in the molecular packing. XRD after irradiation shows diffraction patterns characteristics of the long range ordering of the molecules with sharp reflections having *d*-spacing of 24.9, 17.9, 9.07, 4.8, 4.3, and 3.8 A°. While the peak at 24.98 A° corresponds to the molecular length, the new peaks at 17.92 A° indicates ca. half the width of the molecule when the alky chains are extended which indicates an interdigitated arrangement of the molecules.

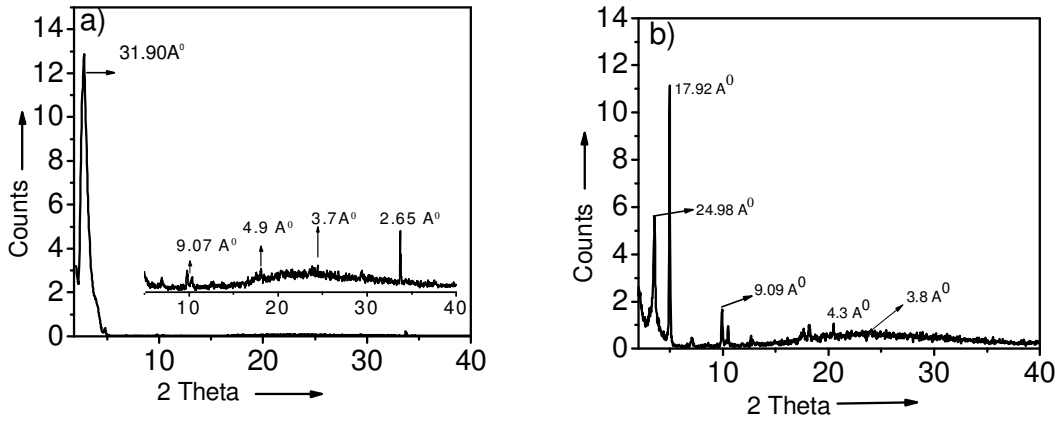

Figure 2.16. The XRD pattern of ***m*-AZO-PE** from cyclohexane at a concentration of 8 × 10^{-3} M at 25 °C; a) ***m*-AZO-PE** before irradiation, b) ***m*-AZO-PE** after 60 minutes with UV light of 350 nm.

Since the XRD data of ***m*-AZO-PE** after irradiation (Figure 2.16b) showed diffraction patterns characteristics of the long range ordering of the molecules with sharp reflections, we have carried out the high resolution TEM measurements to see the presence of any lattice planes. However, the TEM images indicates no sign of any higher order arrangements thereby ruling out the possibility of molecular level ordering in the rods (Figure 2.17b and 2.17c).

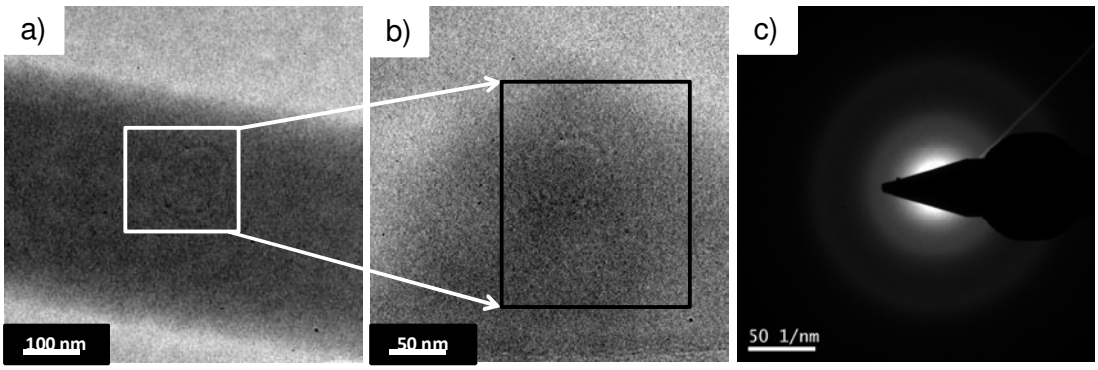

Figure 2.17. (a) High resolution TEM image of the rods (200 KV); (b) Zoomed portion from image (a); (c) Diffraction pattern corresponding to image b.

2.4. Mechanism of Photomorphogenesis

The observed complete transformation of the initial morphology upon irradiation cannot be explained based on the molecular level *E-Z* isomerization effect as evident from the low isomerization yields observed by the absorption spectral changes in Figure 2.7. Normally, for a complete transformation of a given morphology of a photochromic building block to another, significant change should occur at the molecular level which is not the case with the present system. Moreover, in the case of self-assembly and gelation of azo-linked molecules, *trans-cis* isomerization has been known to disrupt the self-assembly and induce gel to sol transition. However, in our case, we have noticed the formation of well defined and larger self-assembly as a result of photoirradiation. Therefore, we had to invoke a macroscopic mechanism associated with a time dependent light triggered process as shown in Figure 2.18. The resulted morphology evolution is corroborated to a photoinduced dipole moment change associated with *E-Z* isomerization occurring at the surface of the initially formed aggregates. For example, during the *trans* to *cis* isomerization of azobenzene, the dipole moment increases from 0.52 D to 3.08 D. The involvement of the polarity difference in the morphology change is strongly supported by recent reports pertaining to agglomeration of azobenzene linked gold nanoparticles initiated by a photoinduced *cis-trans* isomerization[9a] as well as the conductivity modulation of a passivated ultra thin Nb film functionalized with a self-assembled azobenzene monolayer.[9b] In both cases, the observed phenomena are attributed to the change in the surface dipoles as a result of *trans* to *cis* isomerization.

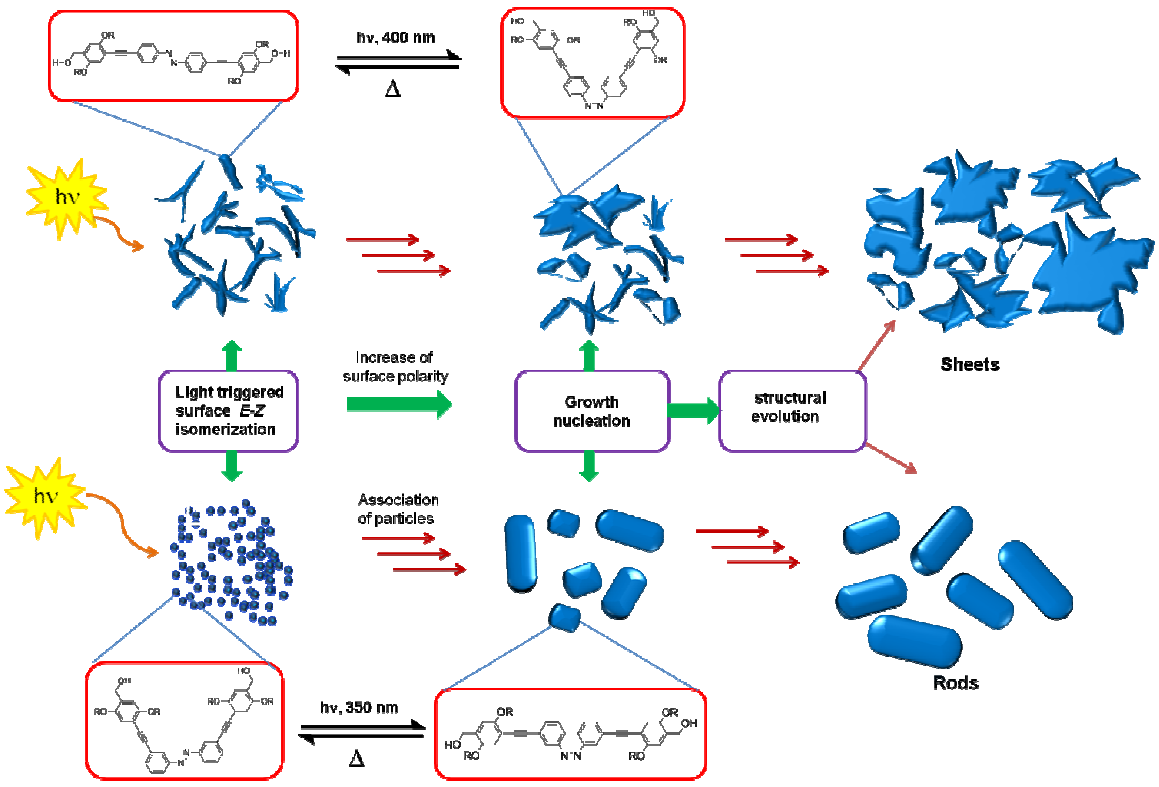

Figure 2.18. Schematic representation of the steps involved in the photomorphogenesis leading to flakes and rods in ***p*-AZO-PE** and ***m*-AZOPE** respectively.

Apparently, the initial morphology of the aggregates has tremendous influence on deciding the light induced morphology transition. In cyclohexane, ***m*-AZO-PE** self-assembles to form short irregular tapes whereas ***m*-AZO-PE** forms nanoparticles. Upon irradiation in cyclohexane, the initially formed morphology restricts the *trans-cis* isomerization only on the surface of the aggregates. Therefore, majority of the molecules within the aggregates remain in *trans* form. Since the dipole moment of the *cis* isomers are higher than the *trans* isomers, the net polarity on the surface of the initially formed structures will increase. This

increase in the surface polarity will nucleate and propagate the agglomeration of the self-assemblies in cyclohexane, resulting in hierarchical structures of different morphologies which are decided by the initial shape of the aggregates. Thus, the short, irregularly shaped aggregates of ***p*-AZO-PE** self-associate to form irregular 2D flakes as observed in the TEM images whereas the initially formed nanoparticles of ***m*-AZO-PE** transform into well-defined supramolecular rods. If at all, can be compared, the major difference between the photomorphogenesis in biology and in the artificial system described here is in the secondary growth process. More precisely, while a complex, phytochrome triggered enzymatic change is responsible for the cell growth in the former, a simple photochrome triggered polarity assisted interparticle association is the reason for the hierarchical growth of the self-assembly in the latter.

2.5. Conclusions

In conclusion, described here is an example for light triggered morphogenesis of supramolecular architectures and has not been reported elswhere. A complete transition of an initial morphology to another defined structure could be achieved by the photoinduced isomerization and the resultant local dipole moment change at the surface. The formation of the supramolecular rods is remarkable since organic nanorods, hierarchically constructed from small molecular building blocks via irradiation, with uniform size and aspect ratio is rare. In addition, the two isomeric forms of the molecules described here have resulted in two different kinds of initial and final architectures, thus higlighting the importance of the structure of the molecules

in the morphology evolution. Thus, yet another intriguing property of the versatile azobenzene chromophore is revealed which may open up further interest and application of *E-Z* photoisomerization process.

2.6. Experimental Section

2.6.1. Synthesis and Characterization

General

All reactions were performed under an atmosphere of nitrogen unless stated otherwise. All commercially available reagents and solvents were of reagent grade and used without further purification. Silica gel plates were 250 μm thick, 60 F_{254} grade from Merck. Silica gel was grade 60N (Spherical, Neutral, 60-210 mesh) from SD fine chemicals, India. Melting points were determined with a Mel-Temp-II melting point apparatus and are uncorrected. ^{1}H and ^{13}C NMR spectra were measured on a 300 MHz Bruker Avance DPX spectrometer using TMS as internal standard. Mass Spectral analysis was done on a JEOL JMS600 instrument. Yields, melting points, and spectral details of each product are given below.

General procedure for the coupling of terminal alkyne with an aryl halide utilizing a palladium-copper cross-coupling (Sonogashira protocol)

To an oven-dried screw cap tube or a round bottom flask equipped with a magnetic stir bar was added the aryl halide, bis(triphenylphosphine)palladium (II) dichloride (1-10 mol % based on the aryl halide), and copper (I) iodide (1-10 mol % based on the aryl halide). The vessel was then sealed with rubber septum, evacuated and backfilled with nitrogen three times. Triethylamine or *N*, *N*-diisopropylethylamine (Hünig's base) was added followed by THF to serve as the

co-solvent. After stirring for 5 minutes at room temperature, the terminal alkyne was added and the reaction mixture was stirred at 60 °C until complete reaction was noted by TLC. The vessel was cooled to room temperature and the reaction mixture was passed through a short column of celite (CH_2Cl_2 as eluent). The fractions obtained were evaporated under reduced pressure. The crude product was further purified by flash or column chromatography (silica gel) using hexane or ethyl acetate as eluent.

General procedure for the deprotection of a trimethylsilyl (TMS)-protected alkyne.

To a round bottom flask equipped with a magnetic stir bar was added the TMS-protected alkyne and THF, followed by KOH in methanol (2 N). The reaction vessel was sealed with a rubber septum and then filled with nitrogen. The reaction was allowed to go to completion for around 3 h and the solvent was removed under vacuum. The solid obtained was dissolved in water. The product was extracted with chloroform and the organic layer was washed three times with brine, and two times with water. The extracts were combined and dried over anhydrous sodium sulphate. The solvent was removed under reduced pressure. The crude product obtained was further purified by column chromatography using hexane or ethyl acetate as eluent.

(E)-1,2-Bis(4-iodophenyl)diazene (9): Iodoaniline (5 g, 23 mmol) was dissolved in 100 mL dry dichloromethane under argon atmosphere. To this, a binary ground mixture of $KMnO_4$ and $CuSO_4.5H_2O$ was added and the

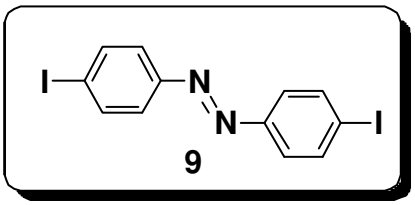

9

reaction mixture was stirred at room temperature for 3 days. After the completion of the reaction, the crude mixture was filtered through celite. The collected fractions were concentrated under reduced pressure. The crude product was purified by chromatography using hexane as eluent to give an orange solid with 40% yield. m. p. 246-248 °C; ^{1}H NMR (300 MHz, $CDCl_3$, TMS) δ: 7.87-7.85 (d, 4H, J = 8 Hz, aromatic), 7.65-7.62 (d, 4H, J = 8 Hz, aromatic) ppm; HRMS-FAB: calculated: $C_{12}H_8I_2N_2$: 433.88, found: 434.77

(E)-1,2-Bis(4-((trimethylsilyl)ethynyl)phenyl)diazene (10): To a solution of **9**

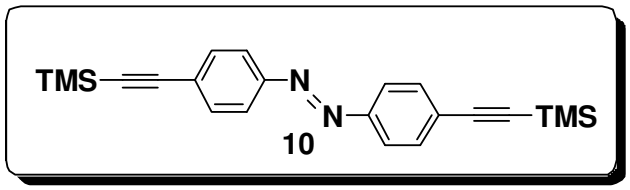

10

(1g, 2.3 mmol) in Et_3N, CuI (0.050 g, 0.256 mmol) and $PdP(Ph_3)_2Cl_2$ (0.160 g, 0.2279 mmol) were added and stirred for 5 minutes. To this mixture, TMS acetylene (0.9 mL, 6.322 mmol) was added drop wise and stirred under reflux for 15 h with ice water circulation. The reaction mixture was then passed through a celite column. The filtrate was concentrated and purified by column chromatography using hexane as eluent to give an orange product in 71% yield. m. p. 176-178 °C, ^{1}H NMR (300 MHz, $CDCl_3$, TMS) δ: 7.87-7.85 (d, 4H, J = 8 Hz, aromatic), 7.65-7.62 (d, 4H, J = 8 Hz, aromatic), 0.24 (t, 18H) ppm; HRMS-FAB: calculated: $C_{22}H_{26}N_2Si_2$: 374.16, found: 374.6.

(E)-1,2-Bis(4-ethynylphenyl)diazene (11): To a solution of **10** (0.985 g, 2.634 mmol) in THF, 2.5 mL of 20% KOH in methanol was added and stirred for 3 h. The solvent was removed under reduced pressure followed by the addition of distilled water (50 mL). The organic layer was collected, dried over anhydrous sodium sulphate, concentrated and purified by column chromatography using hexane as eluent to obtain the product in 76% yield. m. p. 85-87 °C, ^{1}H NMR (300 MHz, $CDCl_3$, TMS) δ *:* 7.87-7.86 (d, 4H, *J* = 8 Hz , aromatic) 7.65-7.62 (d, 4H, *J* = 8 Hz, aromatic) 3.23 (s, 2H,) ppm; HRMS-FAB: calculated: $C_{16}H_{10}N_2$: 230.08, found: 230.26

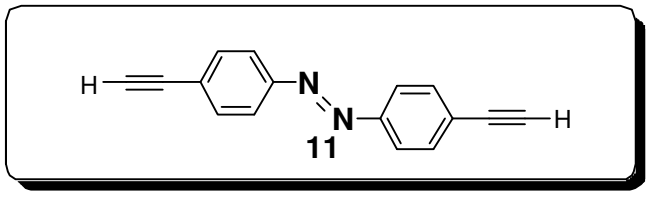

(E)-1,2-Bis(3-iodophenyl)diazene (13): *m*-Iodoaniline (**12**) (2 g, 9.17 mmol) was dissolved in 100 mL dry dichloromethane under argon atmosphere. To this, a binary ground mixture of $KMnO_4$ (5 g, 31.65 mmol) and $CuSO_4.5H_2O$ (3.6 g, 14.4 mmol) were added and the reaction mixture was stirred at room temperature for 3 days. After completion of the reaction, the crude mixture was filtered through celite. The collected fractions were concentrated under reduced pressure. The crude product was purified by column chromatography using hexane as eluent to give an orange solid in 38% yield. m. p. 243-245 °C; ^{1}H NMR (300 MHz, $CDCl_3$) δ : 8.241(s, 2H, aromatic), 7.92-7.89 (d,

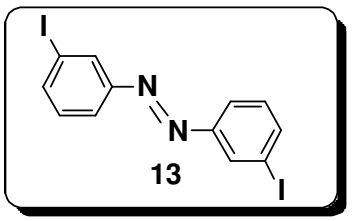

2H, aromatic), 7.83-7.80 (d, 2H, aromatic), 7.30-7.262 (t, 2H, aromatic) ppm; HRMS-FAB: calculated: $C_{12}H_8I_2N_2$: 433.88, found: 434.01.

(E)-1,2-Bis(3-((trimethylsilyl)ethynyl)phenyl)diazene (14): To a solution of **13**

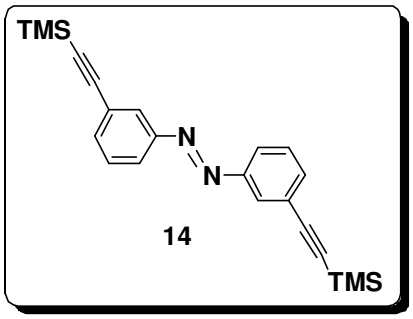

14

(0.500 g, 1.15 mmol) in Et_3N, CuI (0.0025 g, 0.0128 mmol), and $PdP(Ph_3)_2Cl_2$ (0.080 g, 0.114 mmol) were added and stirred for 5 minutes. To this mixture, TMS acetylene (0.715 mL, 5.04 mmol) was added drop wise and stirred at reflux for 15 h with ice water circulation. The reaction mixture was then passed through celite. The filtrate was concentrated and purified by column chromatography using hexane as eluent to yield the product in 75%. m. p. 167-169 °C; ^{1}H NMR (300 MHz, $CDCl_3$) δ: 8.011 (s, 2H, aromatic), 7.88-7.86 (d, 2H, aromatic), 7.58-7.55 (d, 2H, aromatic), 7.48-7.43 (t, 2H, aromatic), 0.24 (t, 18H) ppm; HRMS-FAB: calculated: $C_{22}H_{26}N_2Si_2$: 374.16, found: 374.63.

(E)-1,2-Bis(3-ethynylphenyl)diazene (15): To a solution of **14** (0.190 g, 0 .0508

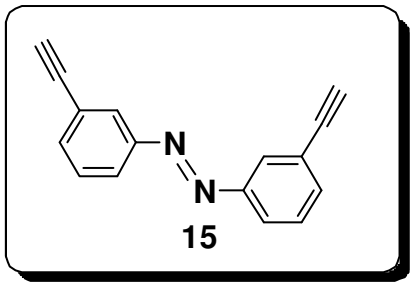

15

mmol) in THF, 2.5 mL of 20% KOH in methanol was added and stirred for 3 h. Subsequently, the solvent was removed under reduced pressure followed by the addition of distilled water (40 mL) and the organic layer was collected, dried over anhydrous sodium sulphate, concentrated and purified by column chromatography using hexane eluent to yield the product in 80%. m.p. 87-89 °C; ^{1}H NMR (300 MHz, $CDCl_3$) δ: 8.011 (s, 2H,

aromatic), 7.92-7.90 (d, 2H, aromatic), 7.62-7.59 (d, 2H, aromatic), 7.51-7.46 (t, 2H, aromatic), 3.15 (s, 2H, CH) ppm; HRMS-FAB: $C_{16}H_{10}N_2$: calculated: 230.08: found: 230.63.

1,4-Bis(dodecyloxy)-2-methylbenzene (17): A suspension of powdered KOH (5.04 g, 90 mmol) and DMF (100 mL) was stirred at room temperature for 30 min. Methylhydroquinone (5.01 g, 40.4 mmol) in DMF (50 mL) was added drop wise. To the stirred mixture, bromododecane (22.4 g, 90 mmol) in DMF (50 mL) was added. After stirring for 24 h under refluxing, the brownish residue was poured into water (500 mL) and extracted with chloroform. The combined organic layer was washed with water, brine, and dried over anhydrous sodium sulfate and purified using column chromatography with hexane as the eluent to give **17** as a white powder in 70% yield. m. p. 50-51 °C; ^{1}H NMR (300 MHz, $CDCl_3$, TMS) δ: 6.81(m, 3H, aromatic), 3.87-3.90 (t, 4H, -OCH_2), 2.20 (s, 3H, -CH_3), 1.26-1.78 (m, 40H, -CH_2), 0.86-0.90 (t, 6H, -CH_3) ppm; HRMS-FAB: calculated: $C_{31}H_{56}O_2$: 460.43, found: 460.77.

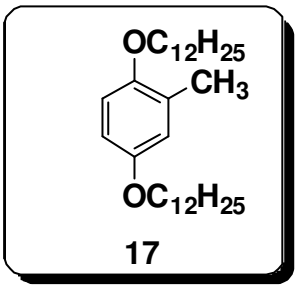

17

1-Bromo-4-(bromomethyl)-2,5-bis(dodecyloxy)benzene (18): *N*-bromosuccinimide (NBS) (1.42 g, 8.02 mmol) and AIBN (0.328 g, 2 mmol) were added to a solution of **17** (3 g, 6.5 mmol) in dry CCl_4 (30 mL) under an atmosphere of argon. After the reaction mixture was stirred for 1 h under refluxing, it was subsequently allowed to cool to room temperature followed by filtration. After evaporation of the solvent, hexane (50 mL) was added to the

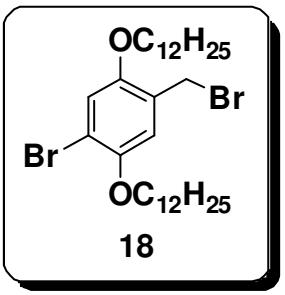

18

residue and the resulting suspension was filtered and evaporated to dryness. The residue obtained was dissolved in dry THF (50 mL), NBS (1.4 g, 7.86 mmol) was added and the reaction mixture was stirred at reflux for 1 h. After evaporation of the solvent, hexane (50 mL) was added. The solution was filtered and the solvent was removed under vacuum. Crystallization of the residue from ethanol gave **18** in 60% yield. m.p. 55-56 °C; ^{1}H NMR (300 MHz, $CDCl_3$, TMS): δ: 7.04 (s, 1H, aromatic), 6.89 (s, 1H, aromatic), 4.50 (s, 2H, -CH_2Br), 3.94-3.98 (t, 4H, -OCH_2), 1.26-1.95 (m, 40H, -CH_2) 0.85-0.89 (t, 6H, -CH_3) ppm; ^{13}C NMR (75 MHz, $CDCl_3$) δ:15.53, 22.62, 28.28, 29.35, 29.37, 34.95, 68.71, 113.25, 117.41, 125.36, 156.36 ppm; HRMS-FAB: calculated: $C_{31}H_{54}Br_2O_2$: 616.25, found: 618.59.

4-Bromo-2,5-bis(dodecyloxy)benzyl acetate (19): A solution of **18** (6.4 g, 10.4 mmol), potassium acetate (3.07 g, 31.3 mmol) and tetrabutylammonium bromide (0.5 mg, 0.0155 mmol) in a mixture of 100 mL of acetonitrile and 50 mL of chloroform, was refluxed for 14 h. The resulting solution was then poured in water and extracted with chloroform. The extracts were collected, washed with water and dried over anhydrous sodium sulfate to give the acetyl derivative **19** in 73% yield. m. p. 53-55 °C; ^{1}H NMR (300 MHz, $CDCl_3$, TMS): δ: 6.90 (s, 1H, aromatic), 6.77 (s, 1H, aromatic), 5.13 (s, 2H, -OCH_2), 3.88-3.99 (m, 4H, -CH_2), 2.11 (s, 3H, -CH3), 1.27-1.82 (m, 40H, -CH_2), 0.86-0.90 (t, 6H, -CH_3), ppm; ^{13}C NMR (75 MHz, $CDCl_3$) δ: 14.24, 25.65, 29.36, 34.58, 35.53, 58.38, 66.96, 108.54, 112.32, 127.58, 131.36, 141.02, 156.65 ppm; HRMS-FAB: calculated: $C_{33}H_{57}BrO_4$: 596.34, found: 595.98.

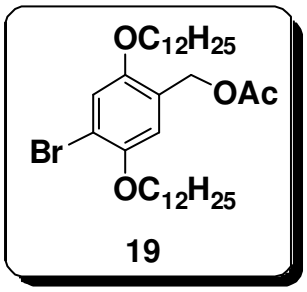

19

4-Bromo-2,5-bis(dodecyloxy)phenyl)methanol (20): To a suspension of $LiAlH_4$ (1.13 g, 29.73 mmol) in dry THF was added drop wise a solution of **19** (4.472 g, 7.5 mmol) in dry THF. Then the mixture was stirred at room temperature for 2 h. The excess $LiAlH_4$ was then quenched by the addition of ethyl acetate at 0 °C. The resulting suspension was poured into water and extracted with chloroform. The extracts were combined and washed with water. Removal of the solvent gave **20** in 60% yields. m. p. 75-77 °C; ^{1}H NMR (300 MHz, $CDCl_3$, TMS) δ: 6.90 (s, 1H, aromatic), 6.77 (s, 1H, aromatic), 4.66 (s, 2H, -CH_2OH), 3.88-3.99 (m, 4H, -OCH_2), 2.11 (s, 3H, -CH3), 1.27-1.82 (m, 40H, -CH_2), 0.86-0.90 (t, 6H, -CH_3) ppm; ^{13}C NMR (75 MHz, $CDCl_3$) δ: 13.96, 28.70, 29.49, 29.82, 35.45, 58.37, 67.19, 108.54, 113.27, 128.54, 132.56, 140.29, 157.12 ppm; HRMS-FAB: calculated: $C_{33}H_{55}BrO_3$: 554.33, found: 554.86.

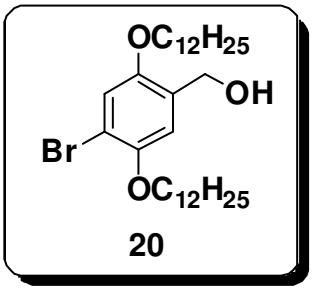

4-Bromo-2,5-bis(docyloxy)benzaldehyde (21): A suspension of **20** (2.48 g, 4.47 mmol) and pyridinium chlorochromate (0.426 g, 1.97 mmol) in 200 mL of dichloromethane was stirred at room temperature for 2 h. The reaction mixture was then directly transferred on to the top of a short silica column and eluted with chloroform. The solvent was removed under vacuum and the crude product was subsequently purified using column chromatography using hexane as the eluent to give **21** in 63% yield. m. p. 69-70 °C; ^{1}H NMR (300 MHz, $CDCl_3$, TMS) δ : 10.40 (s, 1H, -CHO), 7.30 (s, 1H, aromatic), 7.22 (s, 1H, aromatic), 3.98-4.03 (m, 4H, -OCH_2), 0.85-0.89 (t, 6H, -CH_3), 1.23-1.83 (m, 40H,

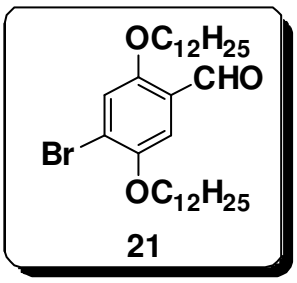

-CH_2) ppm; ^{13}C NMR (75 MHz, $CDCl_3$) δ : 14.09, 22.67, 25.93, 29.03, 29.29, 29.56, 31.90, 69.51, 69.88, 110.70, 118.51, 120.98, 124.33, 188.91 ppm; HRMS-FAB: calculated: $C_{31}H_{53}BrO_3$: 552.32, found: 551.88.

(E)-(4,4'-(4,4'-(Diazene-1,2-diyl)bis(4,1-phenylene))bis(ethyne-2,1-diyl)bis(2,5-bis(dodecyloxy)-4,1-phenylene))dimethanol (*p*-AZO-PE): Diethynyl derivative

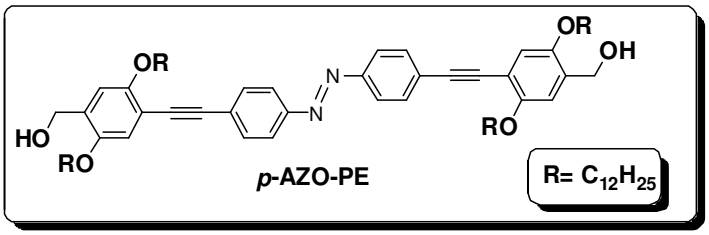

11 (0.250 g, 1.08 mmol)bromo-2,5-bis(dodecyloxy)benzaldehyde (**21**) (1.19 g, 2.16 mmol) were added to solution of diisopropylamine (30 mL) and toluene (30 mL) and degassed for 30 minutes. The catalysts, CuI (0.0025 g, 0.01282 mmol), and $PdP(Ph_3)_2Cl_2$ (0.080 g, 0.1139 mmol) were then added and the reaction mixture was heated to 80 ºC for 24 h. After cooling to room temperature, the reaction mixture was added drop wise into vigorously stirred methanol. The precipitate was collected and purified by column chromatography (silica gel 100-200 mesh using 10% $CHCl_3$/hexane as solvent). The bisaldehyde obtained was then subsequently reduced to the corresponding alcohol derivative by using $NaBH_4$ in a mixture of methanol and dichloromethane at room temperature. The reaction mixture was extracted with water and then added to methanol. The precipitate was collected and then purified by column chromatography (silica gel 100-200 mesh using 50% $CHCl_3$/hexane as eluent to ***p*-AZO-PE** in 95% yield. m. p. 86-87 °C; ^{1}H NMR (300 MHZ, $CDCl_3$) δ : 7.93-7.90 (d, J = 8.5 Hz, 4H), 7.68-7.65 (d, J = 9 Hz, 4H), 6.91 (s, 2H), 6.92 (s, 2H), 4.71 (s, 4H), 4.07-3.98 (m, 8H), 2.35 (m, 2H), 1.87-1.78 (m, 9H), 1.27-1.24 (m,

69H), 0.88-0.83 (m, 14H) ppm; ^{13}C NMR (125 MHz, $CDCl_3$, TMS) δ :14.11, 22.69, 26.15, 29.37, 29.48, 29.66, 31.93, 62.07, 68.77, 69.92, 89.04, 93.23, 100.01, 112.00, 113.66, 115.57, 123.02, 131.52, 132.33, 150.43, 151.76, 154.39 ppm; MALDI-TOF: $[M]^+$ calcd for $C_{78}H_{118}N_2O_6$, 1178.90; found: 1178.97.

(E)-(4,4'-(3,3'-(diazene-1,2-diyl)bis(3,1-phenylene))bis(ethyne-2,1-diyl)bis(2,5bis(dodecyloxy)-4,1-phenylene))dimethanol (*m*-AZO-PE): The ***m*-AZO-PE** was obtained by the reaction of the diethynyl derivative (**15**) and bromo-2, 5-bis(dodecyloxy) benzaldehyde (**21**) using a similar procedure described for ***p*-AZO-PE**. The crude product obtained was then purified by column chromatography (silica gel 100-200 mesh using 50% $CHCl_3$/hexane as eluent to yield ***m*-AZO-PE** in 87% yield. m. p. 93-94 °C; ^{1}H NMR (300 MHZ, $CDCl_3$) δ: 8.01(s, 2H), 7.91-7.88 (d, J = 9 Hz, 2H), 7.66-7.63 (d, J = 9 Hz, 2H), 7.53-7.47 (m, 2H), 7.07 (s, 2H), 6.95-6.89 (s, 2H), 5.29 (s, H), 4.70 (s, 4H), 4.07-4.01 (m, 8H), 1.85-1.81 (m, 9H), 1.37-1.27 (m, 71H), 0.88-0.86 (m,16H) ppm; ^{13}C NMR (75 MHz, $CDCl_3$, TMS) δ :14.09, 22.67, 26.13, 27.52, 29.33, 29.45, 29.61 29.66, 30.17, 31.42, 31.90, 62.06, 68.67, 69.92, 86.93, 92.54, 106.27, 112.12, 113.67, 115.54, 122.89, 124.75, 125.68, 129.04, 131.23, 133.96, 150.37, 152.36, 154.26 ppm; MALDI-TOF: $[M]^+$ calcd for $C_{78}H_{118}N_2O_6$, 1178.90; found: 1179.19.

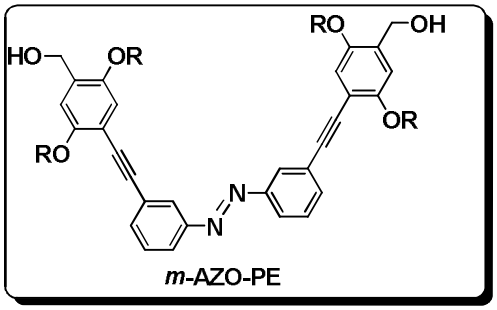

2.6.2. Description of Experimental Techniques

Photoirradiation

Irradiation experiments were performed on degassed solutions (Ar for 5 min) of ***p*-AZO-PE** or ***m*-AZO-PE** in cyclohexane using Oriel optical bench with a 200 W high pressure mercury lamp. For ***p*-AZO-PE** band pass filter $\lambda_{band\ pass}$ = 400 nm, was used. A band pass filter (λ_{max} = 365 nm) was used for irradiation experiments of ***m*-AZO-PE**. The *trans-cis* isomerization was monitored through change in UV/ Vis spectroscopy.

Sample Preparation for Microscopy Measurements

A required concentration of ***p*-AZO-PE** or ***m*-AZO-PE** (1×10^{-4} M) was prepared in cyclohexane by sonication and warming the solution and allowed to cool for few hours followed by drop casting this solution on a carbon coated grid (400 mesh). For the morphology transition experiments, about 500 μL of the solution was then placed in a 1mM cuvette and irradiated with appropriate wavelengths (i.e 400 nm for the ***p*-AZO-PE** and 350 nm for ***m*-AZO-PE**) by monitoring the absorbance changes. Small amounts were withdrawn from this solution in different time intervals (e.g : 10 minutes, 20 minutes) and drop casted on the TEM grid.

Transmission Electron Microscopy (TEM)

TEM measurements were performed on a JEOL-JEM0310 microscope with an accelerating voltage of 80 kV. Samples were prepared by drop casting the ***p*-AZO-PE** or ***m*-AZO-PE** solution (before and after irradiation) from cyclohexane

on carbon coated copper grids and the TEM pictures were obtained without staining.

X-ray Diffraction (XRD)

Solutions (before and after irradiation) of ***p*-AZO-PE** and ***m*-AZO-PE** (8 mM) were coated on a glass plate and the solvent was slowly evaporated. X-ray diffractograms of the dried films were recorded on a Phillips diffractometer using Ni filtered Cu Kα radiation.

Electronic Spectral Measurements

Electronic absorption spectra were recorded on a Shimadzu UV-3101 PC NIR scanning spectrophotometer and the emission spectra were recorded on a SPEX-Flourolog F112X spectrofluorimeter. Temperature dependent studies were carried out with a thermostat directly attached to the wall of the cuvette holder.

Dynamic Light Scattering (DLS)

Dynamic light scattering measurements were performed on Beckman Coulter N5 with an Ar laser operating at 514.5 nm with 300 mW laser power. Sample solutions were filtered (0.2 μm, Millipore) before measurements and put into cylindrical quartz cuvette. The temperature was kept at 25° C and the scattering angle was set to 90° C. During the measurements, dry nitrogen gas was passed around the index matching vat, including the cuvette, to avoid condensation. The data acquisition was performed using multiple-tau digital correlator (ALV5000E). The average hydrodynamic radii were calculated from Stork-Einstein equation ($R_h = kBT/(6\pi\eta D)$).

2.7. References

1. a) J. M. Lehn, *Supramolecular Chemistry*, Winheim, Germany, **1995**, (b) J. W. Steed, J. L. Atwood, *Supramolecular Chemistry*, Wiley Chichester, **2000**.
2. a) V. Balzani, A. Credi, M. Venturi, *Molecular Devices and Machines*: *A Journey into the Nanoworld*, Wiley-VCH, Weinheim, **2003**; b) V. Balzani, A. Credi, F. C. Raymo, J. F. Stoddart, *Angew.Chem*. **2000**, *112*, 3484; *Angew. Chem. Int. Ed*. **2000**, *39*, 3348; c) Special Issue: "Molecular Machines"; *Acc.Chem. Res*. **2001**, *34*, 409.
3. a) O. Pieroni, A. Fissi, N. Angelini, F. Lenci, *Acc.Chem. Re*s. **2001**, *34*, 9. b) D. G. Flint, J. R. Kumita, O. S. Smart, G. A. Woolley, *Chem. Biol*. **2002**, *9*, 391; c) M. S Vollmer, T. D. Clark, C. Steinem, M. R. Ghadiri, *Angew. Chem*. **1999**, *111*, 1703; *Angew. Chem. Int. Ed*. **1999**, *38*, 1598.
4. a) F. Würthner, J. Rebek, *Angew Chem*. **1995**, *107*, 503; *Angew. Chem. Int. Ed. Engl*. **1995**, *34*, 446; b) R. Cacciapaglia, S. Di Stefano, L. Mandolini, *J. Am. Chem.Soc.* **2003**, *125*, 2224.
5. a) T. Hugel, N. B. Holland, A. Cattani, L. Moroder, M. Seitz, H. E. Gaub, *Science* **2002**, *296*, 1103; b) T. Muraoka, K. Kinbara, Y. Kobayashi, T. Aida, *J. Am. Chem. Soc*.**2003**, *125*, 5612; c) K. Ichimura, S.-K. Oh, M. Nakagawa, *Science,* **2000**, *288*, 1624.
6. a) B. Jousselme, P. Blanchard, N. Gallego-Planas, J. Delaunay, M. Allain, P. Richomme, E. Levillain, J. Roncali, *J. Am. Chem. Soc.* **2003**, *125*, 2888; b) B. Jousselme, P. Blanchard, N. Gallego-

Planas, E. Levillain, J. Delaunay, M. Allain, P. Richomme, J. Roncali, *Chem. Eur. J*. **2003**, *9*, 5297.

7. a) C. A. Hunter, M. Togrul, S. Tomas, *Chem.Commun*. **2004**, 108; b) I. A. Banerjee, L. Yu, H. Matsui, *J. Am. Chem. Soc*. **2003**, *125*, 9542.

8. a) K. Murata, M. Aoki, T. Nishi, A. Ikeda, S. Shinkai, *J. Chem. Soc. Chem. Commun.* **1991**, 1715; b) K. Murata, M. Aoki, T. Suzuki, T. Harada, H. Kawabata, T. Komori, F. Ohseto, K. Ueda, S. Shinkai, *J. Am. Chem. Soc*. **1994**, *116*, 6664; c) M. de Loos, J. H. van Esch, R. M. Kellogg, B. L. Feringa, *Angew. Chem.* **2001**, *113*, 633; *Angew. Chem. Int. Ed*. **2001**, *40*, 613; d) S. van der Laan, B. L. Feringa, R. M. Kellogg, J. H. van Esch, *Langmuir* **2002**, *18*, 7136.

9. a) R. Klajn, P. J. Wesson, K. J. M. Bishop, B. A. Grzybowski, *Angew. Chem. Int . Ed.* **2009**, *48*, 7035; b) A. Ikegami, M. Suda, T. Watanabe, Y. Einaga, *Angew. Chem. Int . Ed.* **2009**, *48,* (DOI:10.1002/anie.200904548).

10. K. Murata, M. Aoki, T. Suzuki, T. Harada, H Kawabata, T. Komri, F. Ohrseto, K. Ueda, S. Shinkai, *J. Am. Chem. Soc*. **1994**, *116*, 6664.

11. N. Koumura, M. Kudo, N. Tamaoki, *Langmuir*, **2004**, *20*, 9897.

12. I. Tomatsu, A. Hashidzume, A. Harada, *Macromolecule*s, **2005**, *38*, 5223.

13. M. Prato, Fullerene Materials. *Top. Curr. Chem.* **1999**, *199*, 173.

14. T. Konishi, A. Ikeda, S. Shinkai, *Tetrahedron* **2005,** *61,* 4881.

15. J. L. Segura, N. Martín, D. M. Guldi, *Chem. Soc. Rev.* **2005,** *34,* 31.

16. U. H. F. Bunz, *Chem. Rev.* **2000**, *100*, 1605.

17. a) T. Sasaki, J. M. Tour, *Org. Lett.* **2008**, *10*, 897; b)Y. Shirai, T. Sasaki, J. M. Guerrero, B. -C. Yu, P. Hodge, J. M. Tour, *ACS Nano*, **2008**, *2*, 97; b) J. –F. Morin, Y. Shirai, J. M. Tour, *Org. Lett.* **2006**, *8*, 1713.

18. a) M. Yamada, M. Kondo, J.-ichi Mamiya, Y. Yu, M. Kinoshita, C. J. Barrett, T. Ikeda, *Angew. Chem. Int. Ed.* **2008**, *47*, 4986; b) J. Zeitouny, C. Aurisicchio, D. Bonifazi, R. De. Zorzi, S. Geremia, M. Bonini, C. A. Palma, P. Samorí, A. Listorti, A. Belbakra, N. Armaroli, *J. Mater. Chem.* **200**9, *19*, 4715.

19. a) P. Samorí, V. Francke, K. Müllen, J. P. Rabe, *Chem. Eur. J.* **1999**, *5*, 2312; b) U. H. F. Bunz, *Chem. Rev.* **2000**, *100*, 1605; c) U. H. F. Bunz, *Acc. Chem. Res.* **2001**, *34*, 998; d) S. Zahn, T. M. Swager, *Angew. Chem.* **2002**, *114*, 4399; *Angew. Chem. Int. Ed.* **2002**, *41*, 4225; e) S. Sivakova, S. J. Rowan, *Chem. Commun.* **2003**, 2428; f) J. Xu, C.-Z. Zhou, L. H. Yang, N. T. S. Chung, Z.-K. Chen, *Langmuir* **2004**, *20*, 950.

20. (a) A. Ajayaghosh; S. J. George, *J. Am. Chem. Soc.* **2001**, *123*, 5148; (b) S.J. George, A. Ajayaghosh, *Chem. Eur. J.* **2005**, *11*, 3217; (c) A. Ajayaghosh, S. J. George, V. K. Praveen, *Angew. Chem. Int. Ed.* **2003**, *42*, 332; (d) A. Ajayaghosh, R. Varghese, S. J. George, C. Vijayakumar, *Angew. Chem, Int. Ed.* **2006**, *45*, 1141.

21. a) Y. Shirai, T. Sasaki, J. M. Guerrero, B-C. Yu, P. Hodge, J. M. Tour, *ACS Nano,* **2008**, *2*, 97; b) T. Sasaki, J. M. Tour, *Org. Lett.* **2008**, *10*, 897; c) A. Khan, C. Kaiser, S. Hecht, *Angew. Chem. Int. Ed.* **2006**, *45*, 1878; d) A. Khan, S. Hecht, *Chem. Eur. J.* **2006**, *12*, 4764; e) A. Izumi, R. Nomura,

T. Masuda, *Macromolecules* **2001**, *34*, 4342; f) M. Teraguchi, T. Masuda, *Macromolecules* **2000**, *33*, 240.

22. a) A. Ajayaghosh, R. Varghese, V. K. Praveen, S. Mahesh, *Angew. Chem*. **2006**, *118*, 3339; *Angew. Chem. Int. Ed*. **2006**, *45*, 3261; b) A. Ajayaghosh, R. Varghese, S. Mahesh, V. K. Praveen, *Angew. Chem.* **2006**, *118*, 7893; *Angew. Chem. Int. Ed.* **2006**, *45*, 7729; c) S. Sivakova, J. Wu, C. J. Campo, P. T. Mather, S. J. Rowan, *Chem. Eur. J*. **2006**, *12*, 446.

23. a) A. Khan, C. Kaiser, S. Hecht, *Angew. Chem. Int. Ed*. **2006**, *45*, 1878; b) D. G. Koehler, D. Liu, S. De Feyter, V. Enkelmann, T. Weil, C. Engels, C. Samyn, K. Müllen, F. C. De Schryver, *Macromolecules* **2003**, *36*, 578.

24. a) T. Sasaki, J. M. Tour, *Org. Lett*. **2008**, *10*, 897; b) A. Khan, S. Hecht, *Chem. Eur. J*. **2006**, *12*, 4764.

25. a) Y. Shirai, T. Sasaki, J. M. Guerrero, B.-C. Yu, P. Hodge, J. M. Tour, *ACS Nano*, **2008**, *2*, 97; b) J.–F. Morin, Y. Shirai, J. M. Tour, *Org. Lett*. **2006**, *8*, 1713.

Chapter 3

Toroidal Nanoobjects from Rosette Assemblies of Melamine-Linked Oligo (*p*-phenyleneethynylene)s and Cyanurates

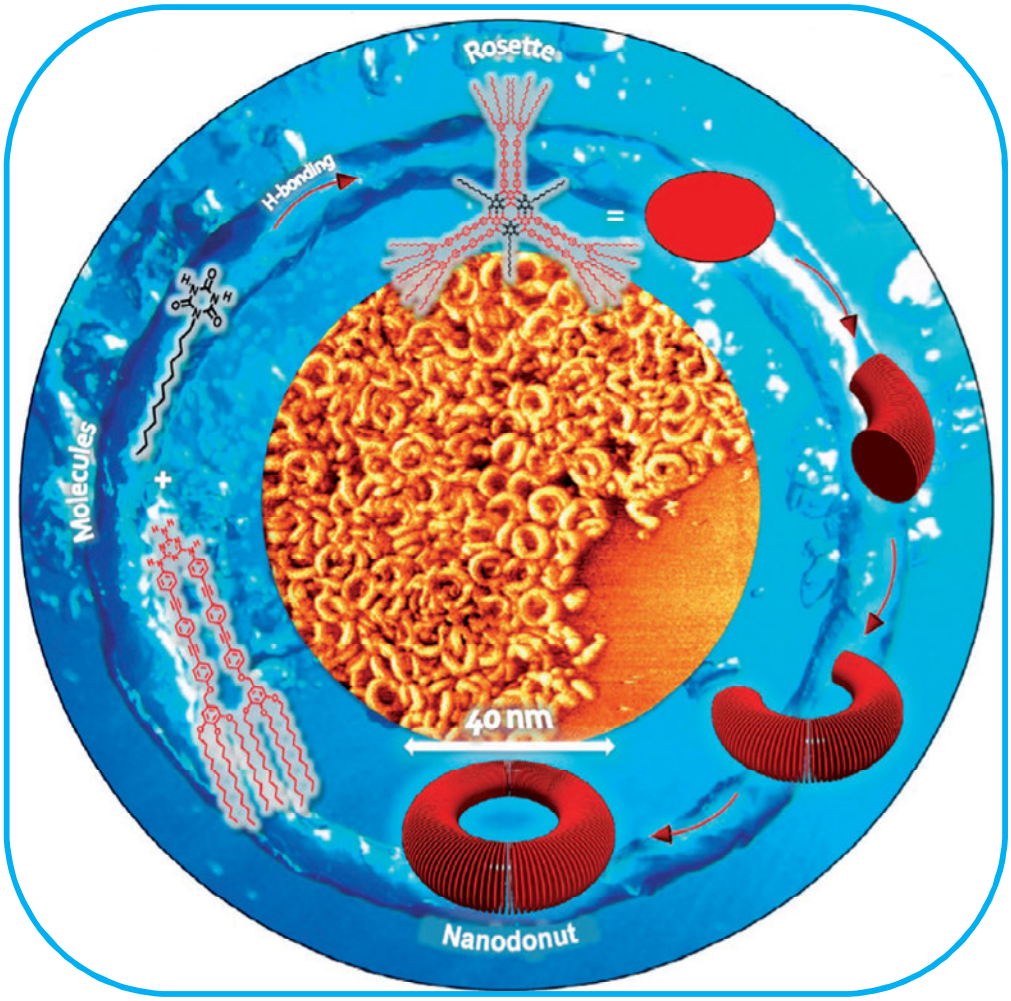

3.1. Abstract

*Co-assembly of an OPE-melamine derivative **12** with a cyanurate **13** resulting in discrete H-bonded rosettes (**12**$_3$·**13**$_3$) is described. The formation of the co-assembly was confirmed by dynamic light scattering (DLS) studies. In $CHCl_3$ (1×10^{-3} M), a narrow size distribution centered at 8 nm, is observed which is in good agreement with the diameter of the rosette estimated from the molecular modeling. In decane (1×10^{-5} to 5×10^{-4} M), formation of large aggregated species with average hydrodynamic diameter of 50 nm is found by DLS analysis, indicating the formation of nanoobjects hierarchically organized from rosettes. AFM and TEM analyses show an unprecedented self-organization of H-bonded rosette assemblies of the oligo(p-phenyleneethynylene) (OPE) attached melamine **12** and the cyanurate **13** in aliphatic solvents, leading to the formation of toroidal objects of nanometer dimension. When the concentration of **12** and **13** is increased (10 mM), stable gels with macroporous morphology are obtained.*

3.2. Introduction

Control of size and shape of self-assembled molecular architectures has been a topic of significant interest.[1,2] Spontaneous organizations of small molecular building blocks into complex superstructures via concerted action of various noncovalent interactions is abundant in Nature. The precision, elegance, complexity and functions of these structures pose significant challenge to scientists. The quest to translate the salient features of Nature's self-assembly

principles has lead to the design of a variety of artificial objects useful in the field of advanced materials research.[3] In this context, the fabrication of well-defined, discrete nanoobjects of photonically and electronically active molecular components with controlled size, shape and functions is of paramount importance.[4] One of the main focus on this area is the self-assembly of linear π-conjugated molecules due to their inherent optical and electronic properties which are vulnerable to intermolecular interactions.[5] Such interactions can be controlled by directional multiple H-bonding modules, leading to supramolecular objects of various dimensionalities.[6] Among various multiple H-bonding modules, the complementary interaction between melamines and cyanurates has been of great value for chemists to the design of rosette (macrocyclic) and tape like (linear or crinkled) architectures.[7] The most challenging task is the utilization of these directional noncovalent interactions for the programmed self-assembly of chromophoric systems. Organized chromophore assemblies are crucial in electron and energy transfer processes as observed in photosythetic systems.

In a recent report, Jonkheijm et al. have described the self-assembly of OPVs **1** and **2** to rosettes and nanotubes.[8] The OPV trimer and tetramer (**1** and **2**) were functionalized with a diaminotriazine H-bonding motif and a tridodecyloxy wedge as end groups and further substituted with enantiomerically pure (*S*)-2-methylbutoxy side chains on the OPV backbone. STM images showed the formation of chiral hexameric rosette structures which are lying flat on the surface with the diaminotriazine moieties pointing to the center, forming a H-bonded cavity (Figure 3.1a). The rosettes are ordered in rows, which form a hexagonal two-dimensional crystal lattice with alkyl chains interdigitating with adjacent

rosettes. The cavity of the rosette has an estimated diameter of approximately 0.7 nm. Small angle neutron scattering (SANS) and AFM studies revealed the formation of tubules of 7 nm in diameter and 180 nm in length (Figure 3.1b).

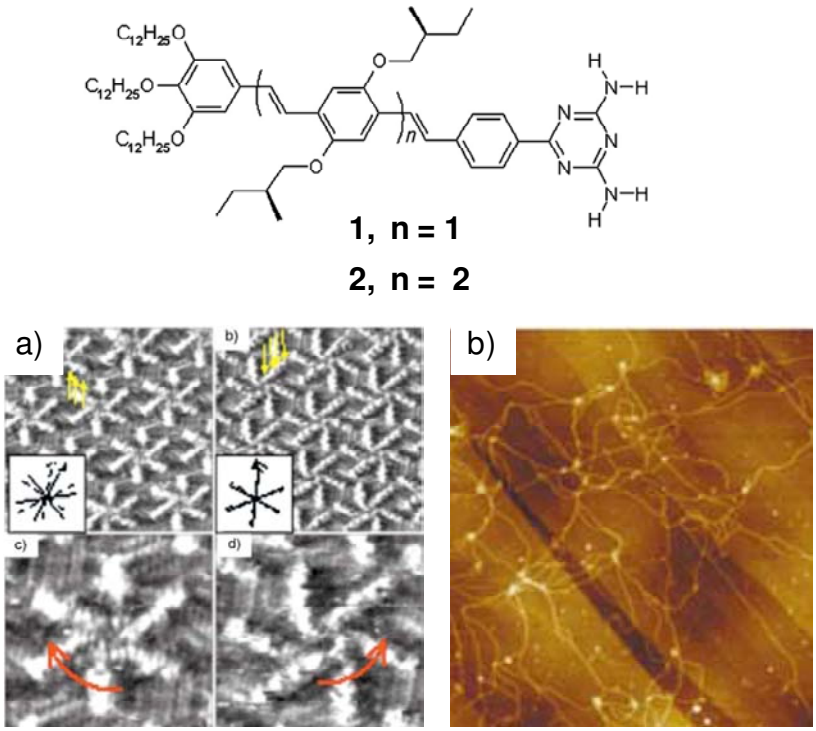

Figure 3.1. a) STM images (14.4 × 14.4 nm^2) of the chiral hexameric OPV rosettes and b) AFM image (6.3 × 6.3 μm^2) of the OPV rosette nanotubes derived from the self-assembly of **1**.

Yagai and co-workers have reported the formation of rosettes from melamine substituted azobenzene and dodecyl cyanurate (dCA), affording columnar assemblies, stable in apolar solvents.[9] Under high concentration (4 mM), solvent molecules were confined in the fibrous networks composed of bundled rosette columns, giving organogels (Figure 3.2). The *trans-cis* photoisomerization of the azobenzene moieties occurred even in the hierarchically organized state, showing a *cis* content of ca. 45% under the best conditions. The morphological

change of rosette, accompanying the isomerization of azobenzene moieties, impairs its stacking ability, which was demonstrated by the photoinduced gel-to-sol transition (Figure 3.2b). The resulting solution could be reconverted to the gel state upon irradiation with visible light and subsequent aging. Thus, by varying the number of the bulky tridodecyloxyphenyl (TDP) wedges, different types of photoresponses, such as photoinduced stabilization, phototriggered formation, and eventually photoregulatable stacking have been achieved for the H-bonded macrocycles.

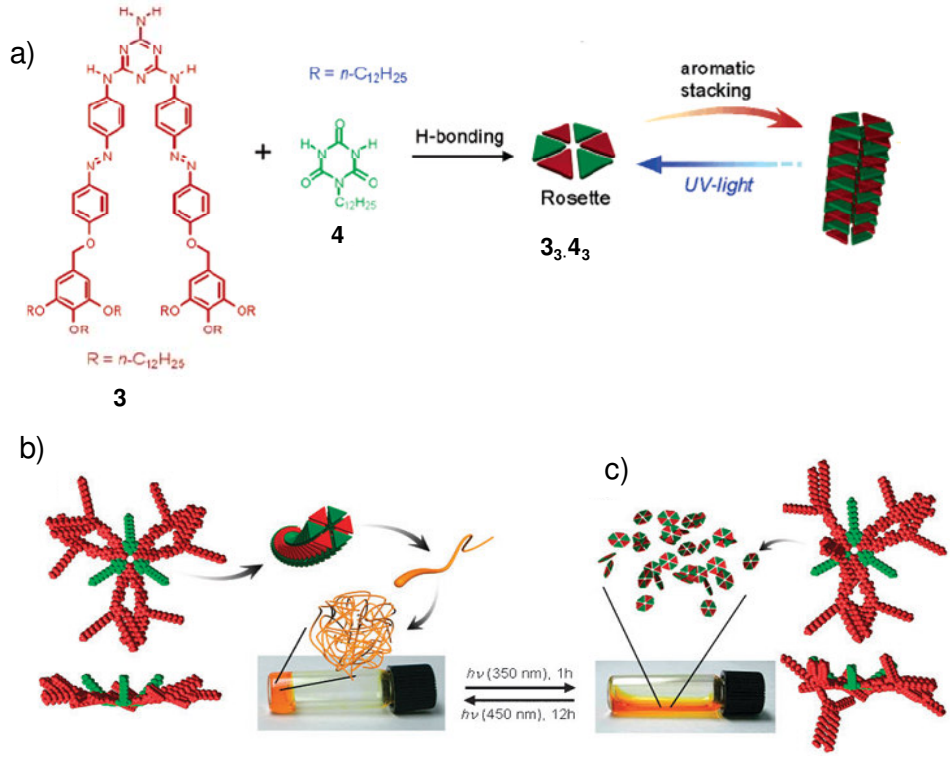

Figure 3.2. (a) Aggregation of the melamine-azobenzene conjugate **3** with the barbiturate **4**. (b) Hierarchical organization of supramolecular rosette $\mathbf{3}_3\cdot\mathbf{4}_3$ in cyclohexane. (c) Photoresponsive dissociation of the rosette $\mathbf{3}_3\cdot\mathbf{4}_3$ possessing one *cis*-azobenzene moiety, leading to gel-sol transition.

Among various self-assembling motifs, the particularly attractive one is disk-shaped molecules that form columnar superstructures via aromatic π-π stacking interactions.[10-11] They are of potential applicability to one-dimensional mass transporting[10a-c] and as optoelectronic nanomaterials.[10d] However, superstructures hierarchically organized from cyclic or linear supramolecular assemblies reported so far is limited to extended architectures.[12-13] In this chapter, we reveal an unprecedented self-organization of H-bonded rosette assemblies of oligo(*p*-phenyleneethynylene) (OPE)[14] attached melamine **12** and a cyanurate **13** in aliphatic solvents, leading to the formation of toroidal objects of nanometer dimension.[15-17]

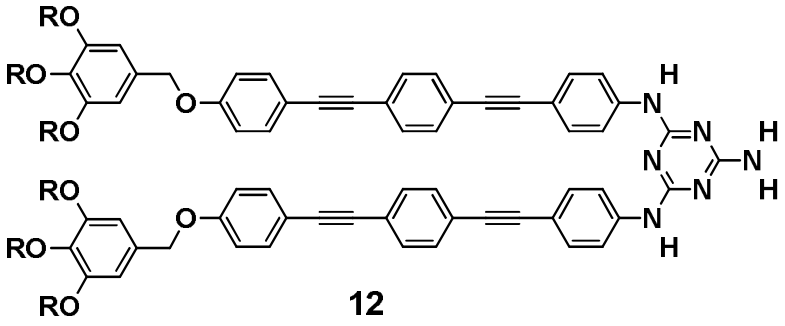

12

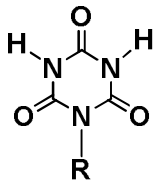

13

$R = C_{12}H_{25}$

3.3. Results and Discussion

3.3.1. Synthesis of the OPE derivative 12

The melamine-linked OPE derivative **12** was prepared by Sonogashira coupling[18]of *N*, *N*′-di(*p*-iodophenyl)-triaminotriazine (**11**) with 3,4,5-trido-decyloxybenzyloxy-substituted ethynyltolane (**10**). For this purpose, the compound **10** was prepared starting from the, 4,5-tri(*n*-dodecan-1-yloxy)benzyl

chloride (**5**). 4,5-Tri(*n*-dodecan-1-yloxy)benzyl chloride was first treated with 4-iodophenol and K_2CO_3 in in *N*,*N*-dimethylformide, at 120 °C to give the compound **6**. Reaction of **6** with one equivalent of trimethylsilylacetylene (TMS-acetylene) in diisopropylamine using $[Pd(PPh_3)_2(Cl_2)_2]$/CuI as the catalyst gave the corresponding silyl protected derivative (**7**) in 93% yield. Deprotection of **7** using KOH in a mixture of THF and methanol gave the corresponding ethynyl derivative, **8** in 87% yield. The ethynyl derivative (**8**) was further reacted with 1-iodo-4-(trimethylsilylethynyl)benzene in diisopropylamine using $[Pd(PPh_3)_2(Cl_2)_2]$ / CuI as the catalyst to give the corresponding silyl protected derivative (**9**) in 78% yield (Scheme 3.1). Deprotection of **9** using 20% KOH in a mixture of THF and methanol gave the corresponding ethynyl derivative, **10** in 87% yield. Synthesis of **12** was achieved by a controlled Sonogashira-Hagihara cross coupling reaction of the ethynyl derivative, **10** with one equivalents of *N*, *N*'-(*p*-iodophenyl)-triaminotriazine[18b](**11**) in a mixture of diisopropylamine and tetrahydrofuran (THF) using $[Pd(PPh_3)_2(Cl_2)_2]$ / CuI as catalyst at 70 °C, resulting in 25% yield. The cynurate **13** was prepared as per the procedures reported in the literature.[19] All the molecules were purified by column chromatography using silica gel (100-200 mesh) and characterized by ^{1}H-NMR, ^{13}C-NMR and MS-FAB spectroscopic techniques.

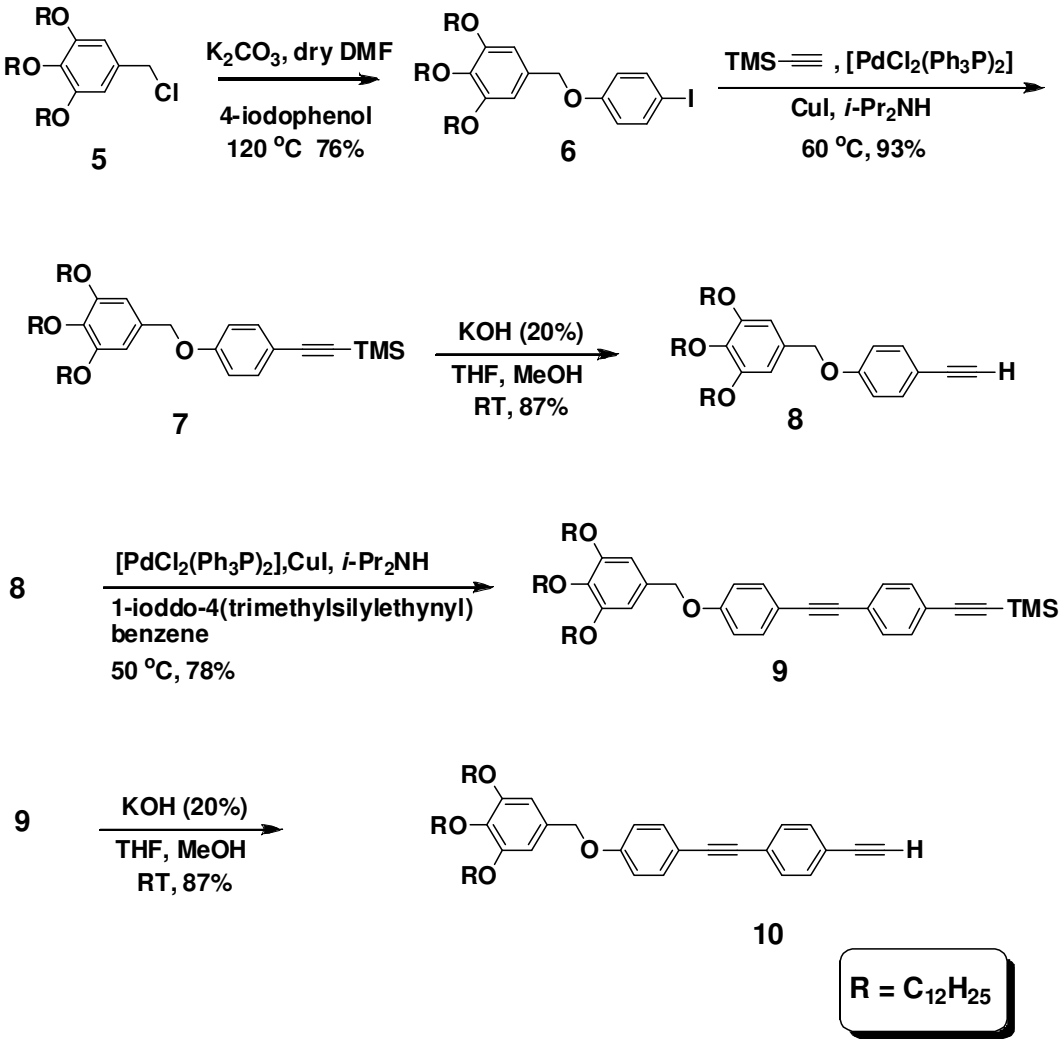

Scheme 3.1

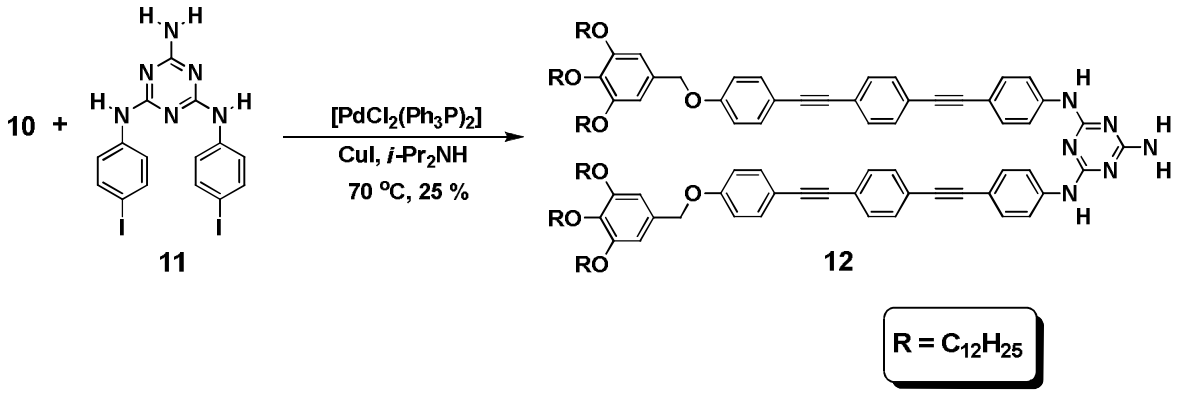

Scheme 3.2

3.3.2. Characterization of the H-Bonded Rosettes

A combination of *N*, *N'*-disubstituted melamine and barbiturate (or isocyanurate) is one of the most promising supramolecular building blocks for the creation of cyclic assemblies. These complementary triple H-bonded assemblies provide three different kinds of supramolecular architectures, such as discrete cyclic hexamers (rosettes) and two polymeric tape like assemblies (linear and crinkled tapes). The pioneering studies by Whitesides and co-workers have demonstrated that introduction of bulky substituents (*e.g.*, 4-*tert*-butylphenyl) into a melamine results in the preferential formation of rosettes.

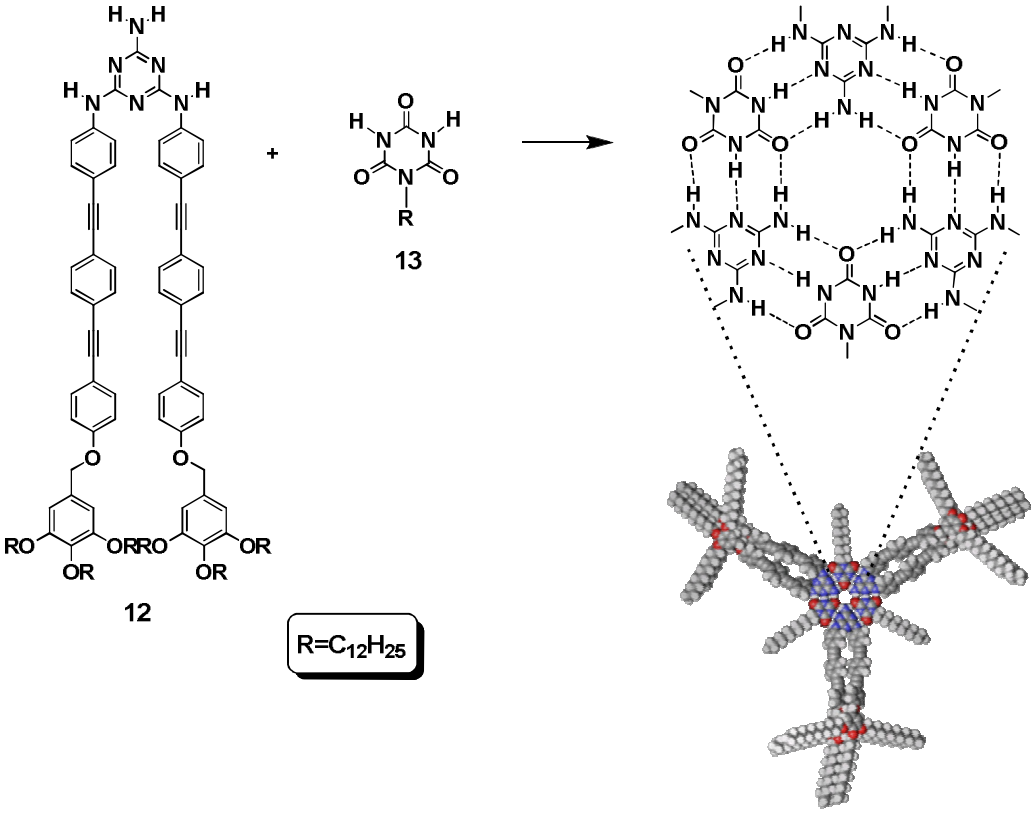

Figure 3.3. Self-assembly of melamine-linked OPE, **12** and cyanurate **13**.

The co-assembly between melamine (**12**) and the dodecyl cyanurate (**13**) results in the formation of discrete rosette ($\mathbf{12}_3 \cdot \mathbf{13}_3$) as shown in Figure 3.3. The formation of H-bonded rosette was confirmed by ^{1}H-NMR as well as DLS measurements. Figure 3.4 a and 3.4 b show the result of the ^{1}H NMR titration experiment of **12** (5 mM) with **13** in $CDCl_3$ at 25 °C. The ^{1}H NMR spectrum of an equimolar mixture of **12** and **13** ([**12**] = [**13**] = 5×10^{-3} M) in $CDCl_3$ showed resonance peaks of the H-bonded imide protons of **13** at δ = 14.3 ppm (red circles) and the secondary amino protons of **12** at δ = 9.58 ppm (blue circles) which are characteristic of the formation of well-defined rosette assembly.

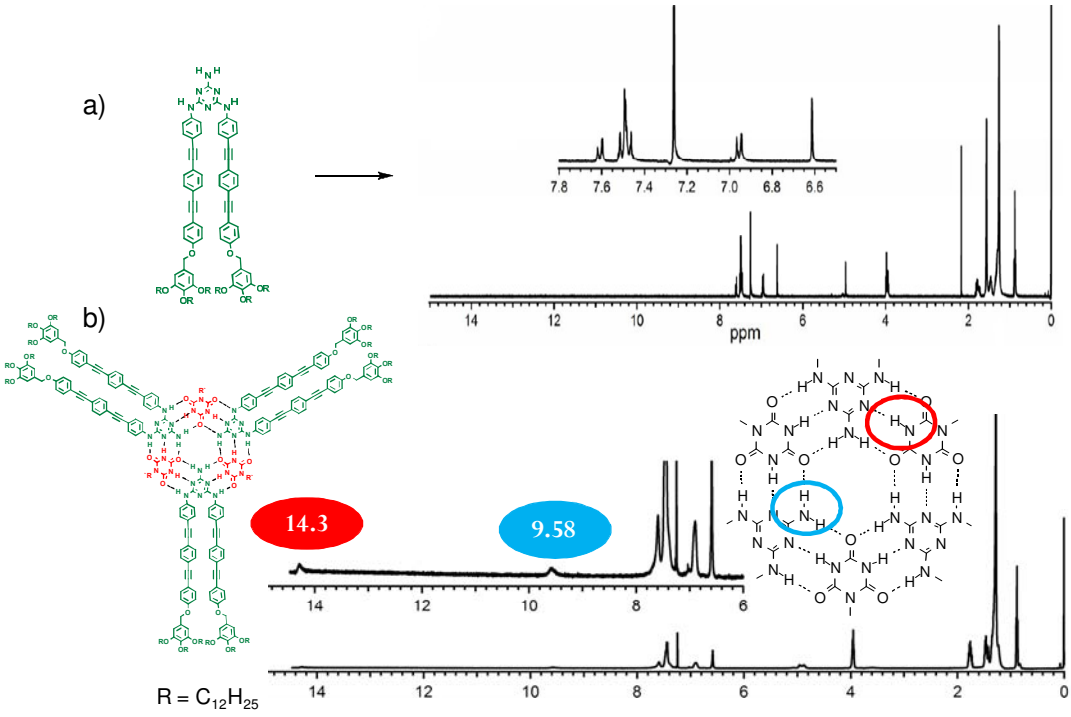

Figure 3.4. ^{1}H NMR spectra of a) **12** in $CDCl_3$, and b) equimolar mixture of **12** and **13** in $CDCl_3$ (*c* = 5.0×10^{-3} M). Insets show the magnified spectra.

To further establish the formation of the rosette ($\mathbf{12}_3\cdot\mathbf{13}_3$), dynamic light scattering (DLS) studies were carried out. DLS measurements of ($\mathbf{12}_3\cdot\mathbf{13}_3$) in $CHCl_3$ ($c = 1 \times 10^{-3}$ M) shows a narrow size distribution centered at 8 nm (Figure 3.5b). The diameter of the rosette is also estimated from the molecular modeling (Figure 3.5a). The size of the aggregated species (R_h) obtained from DLS agrees with the calculated R_h (8 nm) for ($\mathbf{12}_3\cdot\mathbf{13}_3$) based on molecular modeling, thus supporting the formation of a rosette between **12** and **13**.

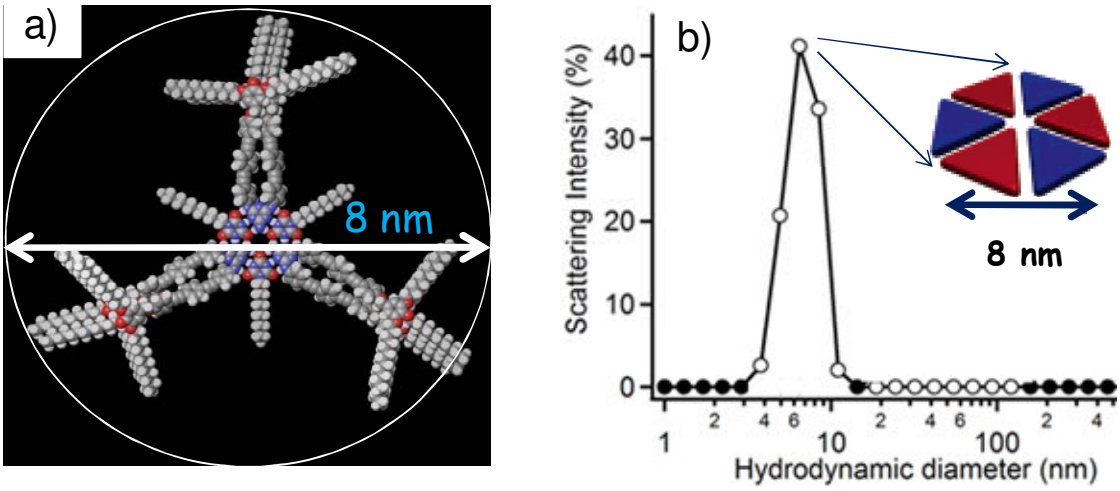

Figure 3.5. a) Molecular-modeled structure of the rosette $\mathbf{12}_3\cdot\mathbf{13}_3$; The gyration diameter of the rosette is approximately 8 nm; b) DLS profile in chloroform (c =1 x 10^{-3} M).

3.3.3. Optical Properties and Hierarchical Organization of the Co-assembly

In order to get more insight into the aggregation of **12** and **13** in solution, detailed electronic spectral studies were carried out in different solvents. For example, the UV/Vis absorption spectra of a 1:1 mixture of **12** and **13** in $CHCl_3$ ($c = 1 \times 10^{-2}$ M) showed a maximum at λ = 334 nm, which is slightly blue-shifted

(Figure 3.6) from that of **12** in $CHCl_3$ (λ_{max} = 339 nm). This observation indicates relatively strong interaction between OPE segments upon conformational fixation of **12** to form H-bonded rosette assembly with **13**.[14] The emission of the OPE co-assembly showed a red-shift of ca. 30 nm (λ_{em} = 407 nm) when compared to that of the monomer (λ_{em}= 378 nm).

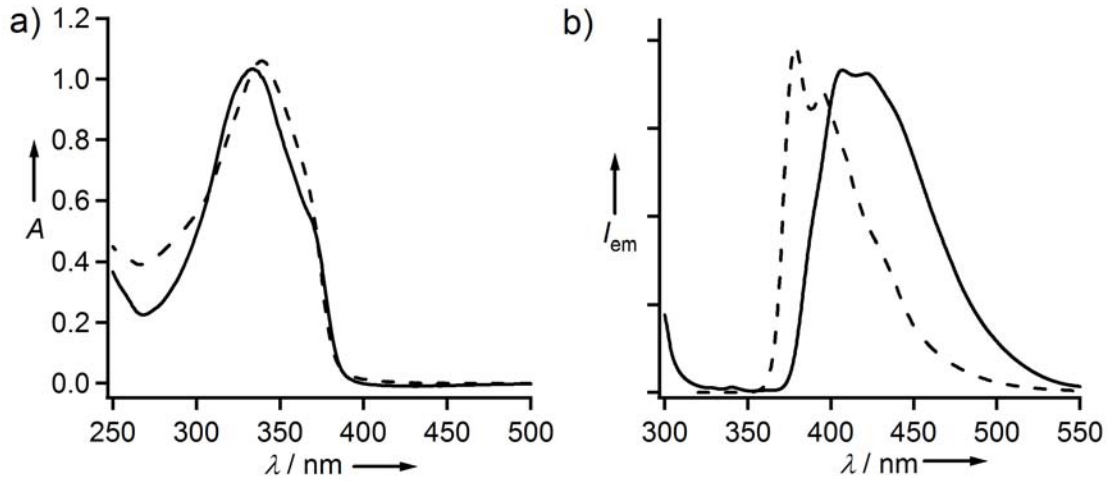

Figure 3.6. a) Absorption and b) fluorescence spectra of **12** in the presence of one equivalent of **13** (solid curves, c = 1.0 × 10^{-2} M, 0.01 mm quartz cuvette) and **12** alone (dashed curves, c = 1.0 × 10^{-5} M, 1 cm quartz cuvette) in chloroform. Excitation wavelength of the emission spectra is 300 nm. Fluorescence spectra of the mixture were measured by front face illumination setup using 1 mm cuvette.

Figure 3.7 represents the comparison of absorption and emission in decane and in chloroform. Upon changing the solvent from chloroform to decane, the spectral properties of the 1:1 mixture of **12** and **13** (c = 1 × 10^{-5} M) exhibited a further interaction of the OPE segments. The absorption maximum emerged at 324 nm whereas the fluorescence maximum appeared at 436 nm, which are blue- and red-shifted from the respective values in $CHCl_3$ (c = 1 × 10^{5} M, Figure 3.7). This,

observation indicates the extended aggregation of OPE segments upon hierarchical organization of the rosette.

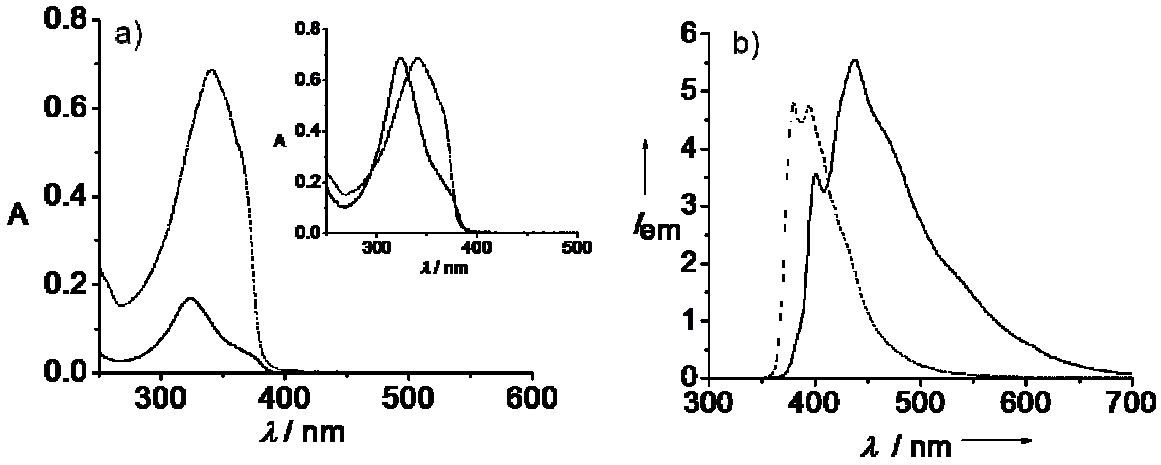

Figure 3.7. Comparison of a) absorption and b) fluorescence spectra of **12** in the presence of one equivalent of **13** (dashed curves, c = 1.0 × 10^{-5} M) in $CHCl_3$ and (solid curves, c = 1.0 × 10^{-5} M) in decane. (λ_{ex} = 300 nm). The inset of the Figure a represents the normalized spectra.

Effect of temperature on the absorption and emission spectra are shown in Figure 3.8. Both spectra showed marginal changes upon heating the solution up to 70 °C. Accordingly, the rosette-rosette interaction as well as the H-bonding interaction within rosettes are significantly high which may render the hierarchically organized assemblies considerably stable (Figure 3.8). This is due to the presence of 18 H-bonds formed between the complementary H-bonding melamines and the cyanurate upon the formation of the rosette assembly.

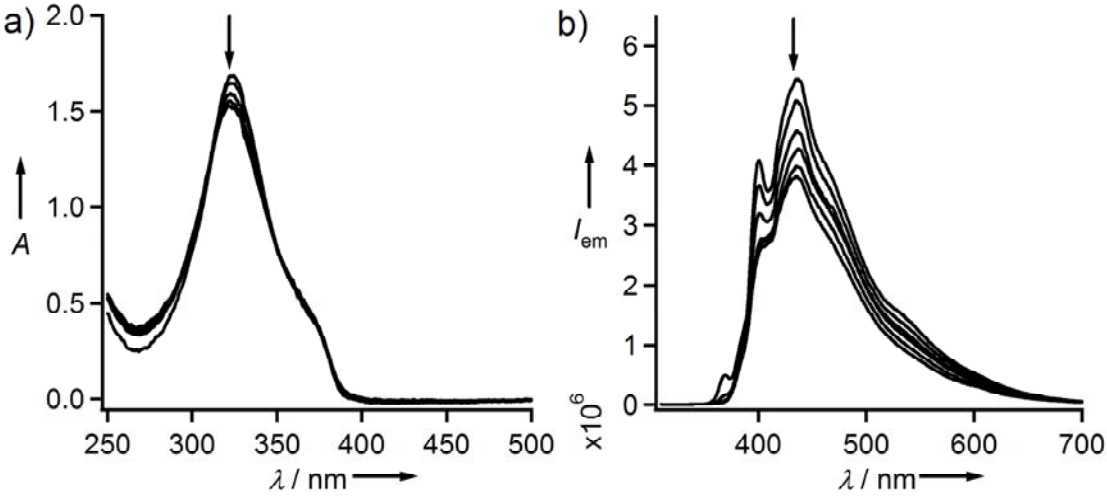

Figure 3.8. Temperature-dependent (20−70 °C) absorption (a) and emission spectra (b) of **12** (*c* = 1.0 × 10^{-5} M) in the presence of one equivalent of **13** in decane. (λ_{ex} = 300nm), Arrows indicate the changes upon increasing temperature.

DLS experiments of the solution of equimolar mixtures of **12** and **13** in chloroform and decane are shown in Figure 3.9. In chloroform at high concentrations, rosette is formed as evident from the NMR analysis. DLS data also support this observation. In chloroform, aggregates of ca. 8 nm corresponding to the rosette assemblies are obtained. However, in decane ([**12**] = [**13**] = 1 × 10^{-5} to 5 × 10^{-4} M), large aggregates with average hydrodynamic diameter of 50 nm are obtained, indicating the formation of nanoobjects hierarchically organized from rosettes. Such nanoobjects have a discrete shape, since the hydrodynamic diameter does not change in the above concentration regime.

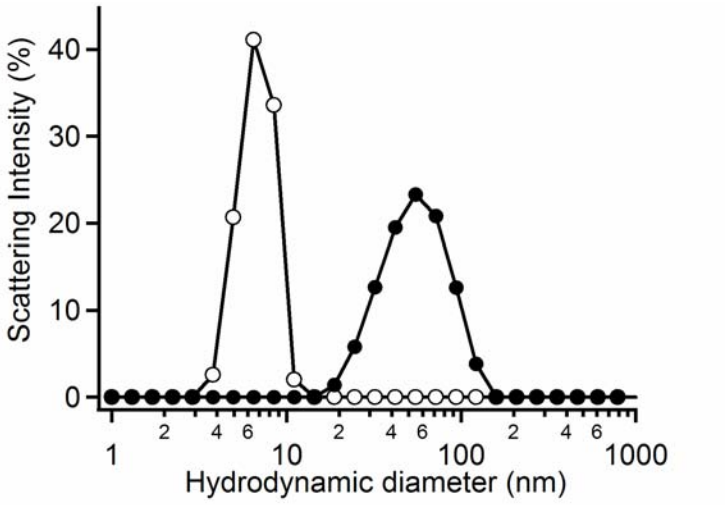

Figure 3.9. Dynamic light scattering analysis of an equimolar mixture of **12** and **13** in $CHCl_3$ (open circles, c = 1 x 10^{-3} M) and in decane (closed circles, c = 5 × 10^{-5} M).

3.3.4. Morphological Investigation by AFM and TEM

Detailed Atomic Force Microscopy (AFM) and Transmission Electron Microscopy (TEM), analyses were carried out on the rosette $\mathbf{12}_3 \cdot \mathbf{13}_3$ in decane at different concentrations. The AFM images of a decane solution (c = 5 × 10^{-5} M), spin-coated (3000 rpm) on to freshly cleaved highly oriented pyrolytic graphite (HOPG), displayed a large number of toroidal nanoobjects (Figure 3.10). These toroidal objects have an average size of 40 nm. Detailed AFM investigation of these toroids shows that the outer diameters (Figure 3.11c) are uniform at around 40 nm, which is in line with the hydrodynamic diameter (D_h) detected by DLS. The average cross-sectional diameter (a) is 20 nm whereas the height (a') is 3.2 ± 0.3 nm.

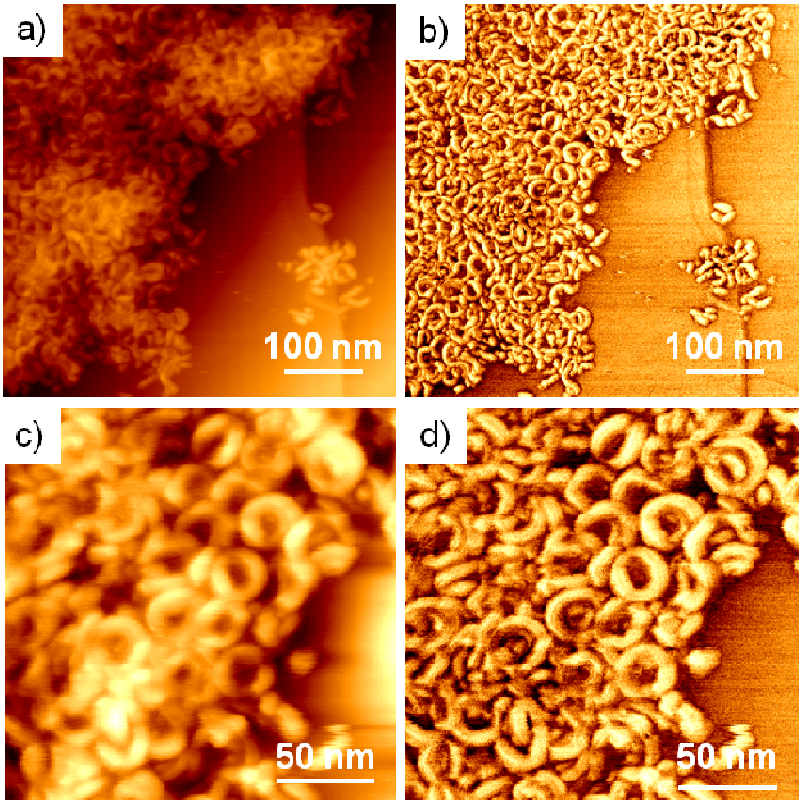

Figure 3.10. AFM height (a, c) and phase (b, d) images representing toroidal nanostructures of **12** and **13** from decane ($\mathbf{12}_3{\cdot}\mathbf{13}_3$, c= 5 × 10^{-5}M), spin coated (3000 rpm) on to HOPG: A_{sp}/A_0 = 0.7).

The actual cross-sectional diameter of toroids was estimated to be 8 ± 2 nm after subtracting the tip broadening parameters.[20] This value matches with the gyration diameter of a molecular-model of the rosette, implying that toroids are formed by the stacking of the individual rosettes. The discrepancy between the height and width of rosette obtained by AFM analysis might be caused by the deformation of the aliphatic chains by the local force exerted by the AFM tip. The body-to-body distance (*b*) given by cross-sectional analysis is 21±2 nm (Figure 3.11b), leading to the circumference of the toroids to be ca. 67 nm. Assuming that the periodic distance of rosettes is in the range of 3.5-5 Å, inclination between the

adjacent rosette disks are roughly calculated to be 191-134 and 1.9°-2.7°, respectively.

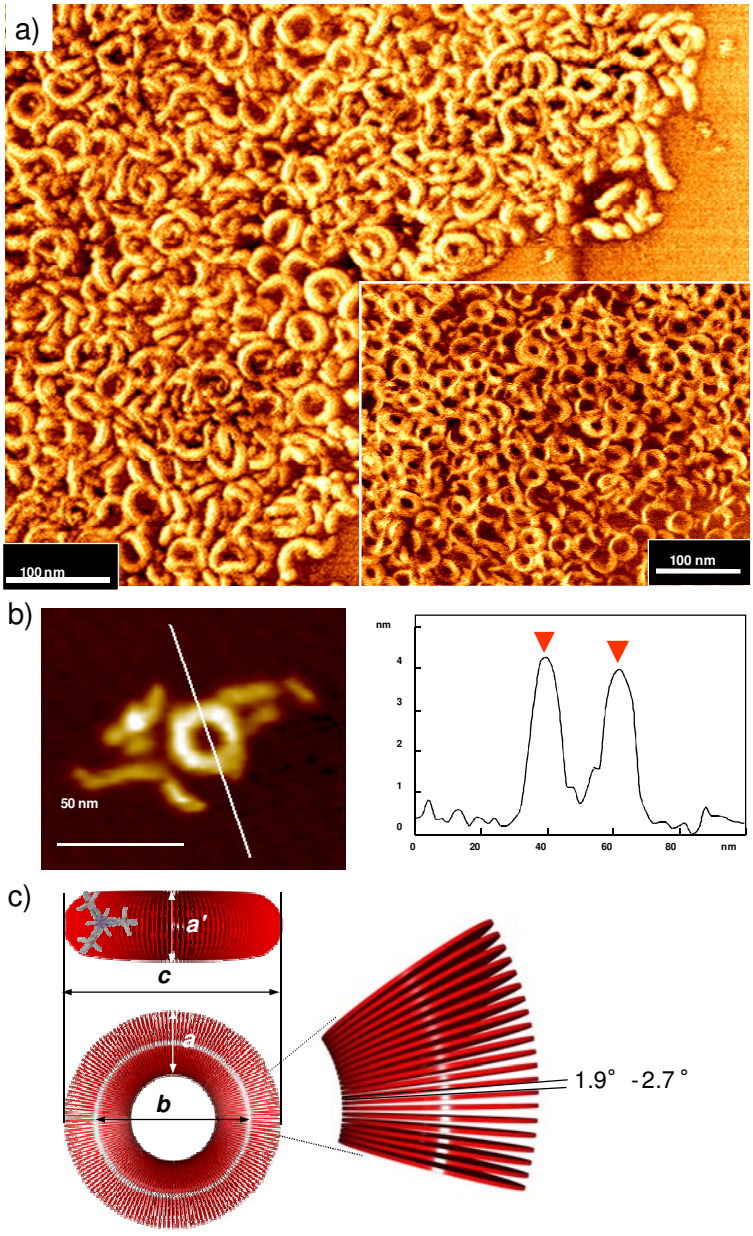

Figure 3.11. AFM phase image of an equimolar mixture of **12** and **13** spin-coated from decane solution (c = 5 x 10^{-5} M) on HOPG. Inset is the image obtained by low tapping force. b) Cross-sectional analysis of isolated toroid. c) Schematic illustration of the toroidal organization of rosettes (red disk).

In the AFM image of the self-assemblies (Figure 3.11), short worm-like and 'opened' objects are also visualized, which might be due to the deformation of the toroids by AFM tip force. Imaging with lower tapping force thus allowed almost all the nanoobjects to retain the toroidal shape (inset in Figure 3.11a). This observation indicates that the toroids are fragile in nature upon AFM imaging due to the soft nature of the material. This is clear from the repeated scan of the images as shown in the Figure 3.12c. During the first scan, a toroid can be clearly seen. However, the third and fifth scan indicates the breaking of the toroids due to the tapping force of the AFM tip. The fragile nature of toroids is more pronounced in isolated areas than in crowded areas, making visualization of "isolated toroids" by the AFM difficult. Spontaneous formation of the toroidal nanostructures on different substrates was confirmed by AFM measurements on HOPG, mica and silicon substrates (Figure 3.12a and 3.12b), all showing the same nanostructures.

The toroidal nature of the supramolecular assembly of $\mathbf{12}_3 \cdot \mathbf{13}_3$ was further confirmed by transmission electron microscopy (TEM) measurements. Figure 3.13 shows the TEM image of a dip-coated sample from a decane solution at a concentration of 5×10^{-5} M after negatively staining by vapor of RuO_4. Isolated toroids are clearly seen with size around 40 nm, which is in good agreement with those found in the AFM images. The cross-sectional diameter ("*a*" in Figure 3.11c) is approximately 10 nm, close to the diameter of the rosette calculated from the molecular modeling (8 nm). These results highlight the stability of toroids

which remain intact with staining, and subsequent vacuum drying and non-contact imaging processes. Furthermore, DLS and AFM analyses showed no evidence of morphological transformation in decane dispersions while keeping for over a year, or heating to 60 °C, which implies that, the toroids is a thermodynamically stable product.

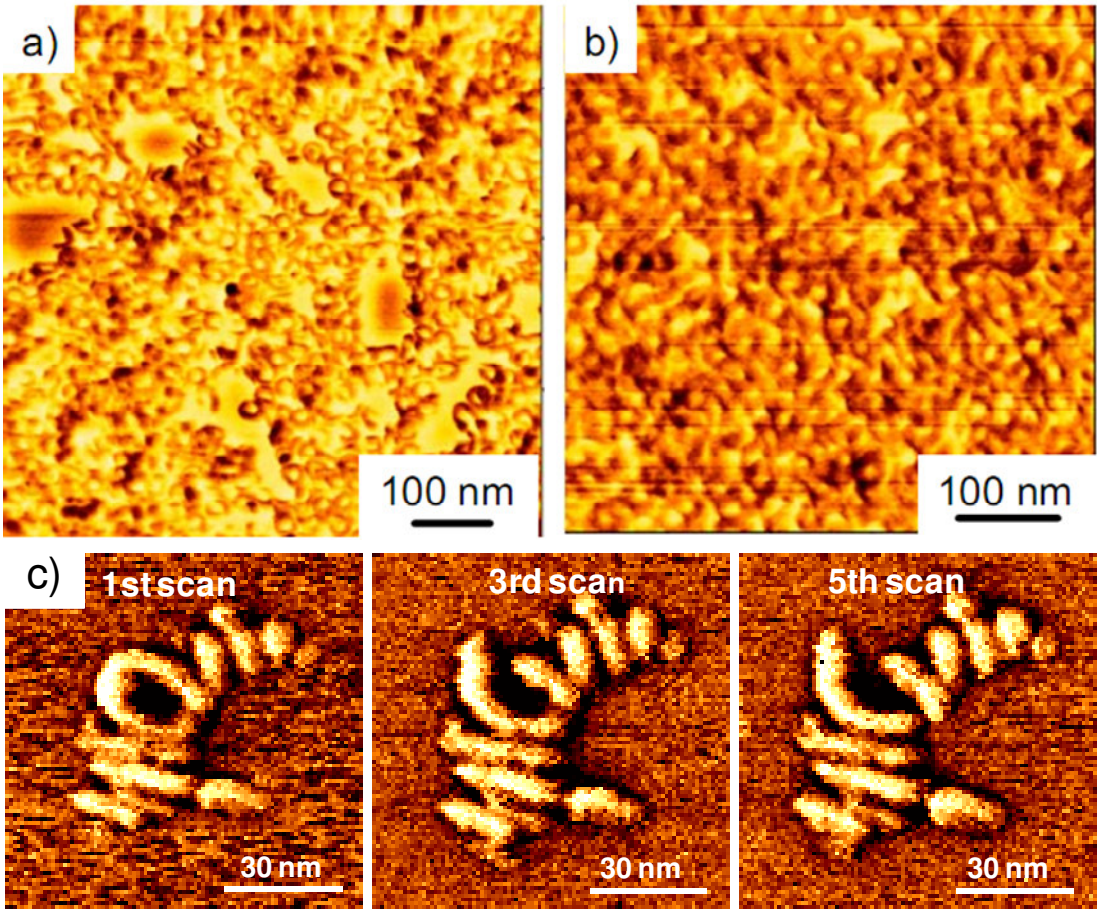

Figure 3.12. AFM phase images of toroidal nanostructures cast from decane solution of (5.0×10^{-5} M) on (a) mica and (b) silicon substrate. (c) Deformation of an isolated toroid by multiple AFM scans (Tapping force: A_{sp}/A_0=0.3).

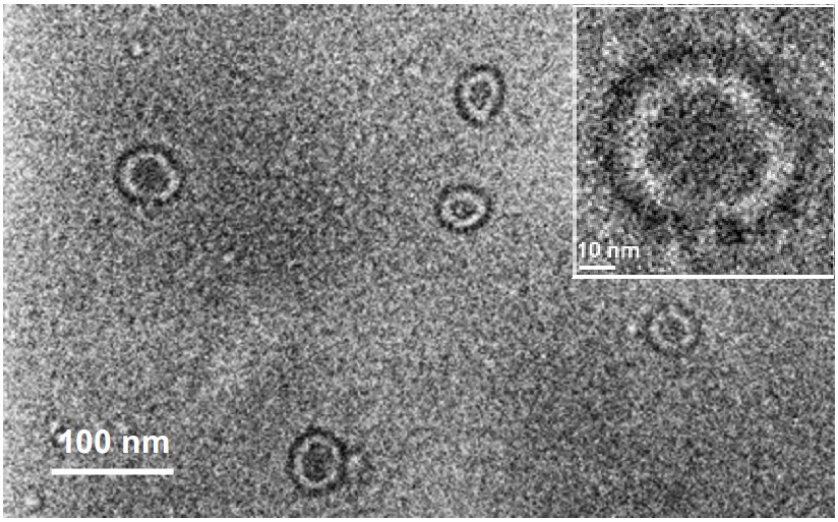

Figure 3.13. TEM image of an equimolar mixture of **12** and **13** from decane on a carbon coated grid (c = 5 × 10^{-5} M). The inset shows a zoomed image of the toroid. The sample is stained by RuO_4.

The above observations unveil a unique property of the rosette $\mathbf{12}_3 \cdot \mathbf{13}_3$ hierarchically organizing into discrete toroidal nanostructures in decane. However, the end-to-end binding of a short columnar nanostructure with persistent length of 67 nm (average circumference of toroids, Figure 3.11c) seems to be energetically disfavoured because of the stiffness of such columns consisting of stacked disk-shaped supramolecules. Molecular modeling of the rosette reveals the fact that the two of the OPEs with the bulky end groups are in a plane and the other one is out of the plane (Figure 3.5). The uneven twisted arrangements of the six OPE segments in the rosette may not favour a perfect face-to-face stacking of the individual rosette to form an extended columnar assembly. Thus, inter-rosette attractive force on the OPE segments of the undulated H-bonded cores, leads to a stack of the rosette disks with one side closer and the other side slightly distant, resulting in a curvature during the packing of the rosette (Figure 3.11c).

3.3.5. Gel Formation by the H-Bonded Rosette ($12_3 \cdot 13_3$)

As already explained toroidal organization of the rosettes could be attributed to the head-to-end interaction of short columnar structures, the curvature of which is strictly regulated by the biased stacking between the rosette disks with a specific angle (2.7°). Increasing the concentrations to millimolar regime in decane resulted in the formation of a viscous solution, and finally gelation of the solvent was observed at 1×10^{-2} M (inset, Figure 3.14a). The formation of gels strongly suggests that the rosette $\mathbf{12}_3 \cdot \mathbf{13}_3$ self-organize into hierarchical structures which may entangle and immobilize solvent molecules. AFM height image of the dried gel on HOPG showed porous nanostructures (Figure 3.14 a). A 3D AFM image shown in the Figure 3.14b clearly indicates the porous nature of the self-assembly in the gel state. The sizes of the pores are found to be ca. 30 nm.

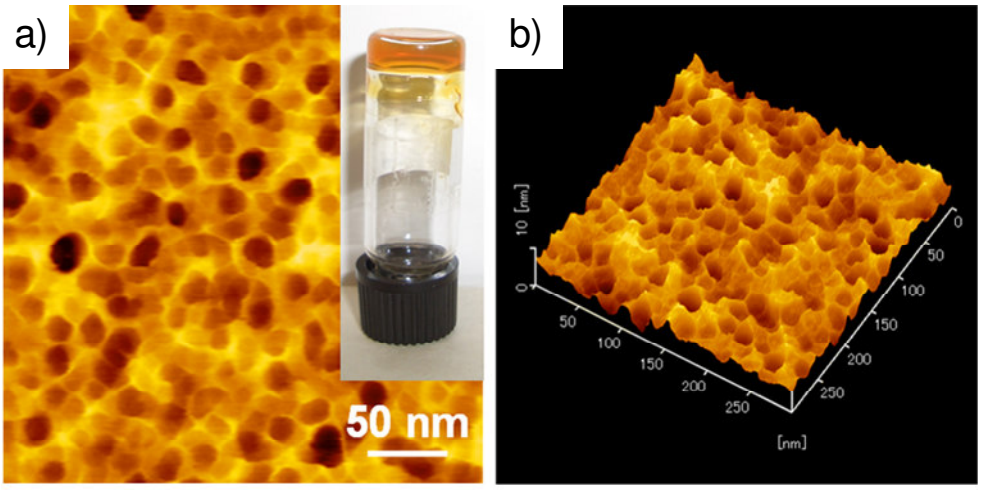

Figure 3.14. a) AFM height image of a dried decane gel formed by an equimolar mixture of **12** and **13** ($c = 1 \times 10^{-2}$ M). Inset shows a photograph of the gel; b) A 3D presentation of the AFM height image of the dried gel.

It is interesting to note that organogels are mainly formed through extended fibrous assembly whereas organogels having porous morphology are rare.[22] In the present case, the AFM images do not show the formation of entangled fibers. Thus, the present system is unique in the sense that at low concentration nanotoroids are formed whereas at higher concentration, the toroids further aggregate to form porous organogels.

3.4. Conclusions

The results shown here are remarkable since toroidal nanoobjects, hierarchically constructed from small molecular building blocks via discrete cyclic supramolecules, are rare. The present method allows the preparation of nanometer-sized toroids (donut-shaped objects) via hierarchical self-assembly of rosettes. This is in contrast to the previously reported toroidal nanostructures that are directly formed from building blocks such as amphiphilic polymers,[15a,c,f] dumbbell-shaped molecules,[15b,d,g], proteins[15], DNA or biopolymers.[16] The present assembly is novel since π-electronic segments are spatially arranged in closed circular structures, which is reminiscent of the light harvesting photosynthetic systems where the circular arrays of chlorophyll pigments are crucial for efficient excitation energy migration.[21] Thus, intriguing applications such as the creation of artificial light harvesting nanodevices with ring-shaped morphology might be possible based on the present system.

3.5. Experimental Section

General

All reactions were performed under an atmosphere of nitrogen unless stated otherwise. All commercially available reagents and solvents were of reagent grade and used without further purification. Silica gel plates were 250 μm thick, 60 F_{254} grade from Merck. Silica gel was grade 60N (Spherical, Neutral, 60-210 mesh) from Kanto chemicals, Japan. ^{1}H NMR spectra were recorded on JEOL LA400 or LA500 spectrometer and chemical shifts were reported in ppm (δ) with the signal of TMS as internal standard. Variable temperature ^{1}H NMR spectra were recorded on JEOL LA500 spectrometer. MALDI-TOF MS spectra were obtained on a Voyager DE Pro (Applied Biosystems) using α-cyano-4-hydroxy cinnamic acid as the matrix. UV/Vis spectra were recorded on a JASCO V660 spectrophotometer. Fluorescence spectra were obtained on SPEX-Fluorolog F112X spectrofluorimeter. Polarized optical and fluorescence microscopic observations were carried out using an Olympus BX51 optical microscopy. Powder X-ray diffraction analysis was carried out with a Rigaku Rint-2200 X-ray diffractometer with monochromated $Cu_{K\alpha}$ radiation and temperature controlled heating stage. Molecular modeling was performed on Macro Model version 9.0 (AMBER force field).

3.5.1. Synthesis and Characterization

Details of the general procedure for the coupling of terminal alkyne and for the deprotection of a trimethylsilyl (TMS)-protected alkyne are described in the experimental section (section 2.6.1) of Chapter 2. Preparation, yield, melting

point, and spectral details of the molecules used in the present study are given below.

Synthesis of 1,2,3-tris(dodecyloxy)-5-((4-iodophenoxy)methyl)benzene (6): To a solution of 4-iodophenol (4.89 g, 22.09 mmol) in dry DMF and K_2CO_3 (10.15 g, 73.6 mmol), was added the compound **5** (10 g, 14.72 mmol). The reaction mixture was heated to 120 °C for 12 h. After the completion of the reaction, the mixture was poured into ice-cold water and the precipitate formed was filtered. The residue was then dissolved in chloroform, washed two times with brine and three times with water. The organic fractions were extracted, combined and dried over anhydrous sodium sulphate. The solvent was removed under reduced pressure. The brown solid thus obtained was purified by column chromatography (hexane as the eluent) to give **6** as a white solid in 76.8% yield. m. p. 34-35 °C; ^{1}H NMR (400 MHz, $CDCl_3$, TMS) δ: 7.55-7.53 (d, J = 8 Hz, 2H), 6.74-6.72 (d, J = 8 Hz, 2H), 6.58 (s, 2H), 4.89 (s, 2H), 3.97-3.92 (m, 6H), 1.80 (m, 6H), 1.47 (m, 6H), 1.30 (m, 48H), 0.89 (t, 9H) ppm; ^{13}C NMR (75 MHz, $CDCl_3$, TMS) δ: 14.09, 22.68, 26.08, 29.35, 29.40, 29.63, 29.68, 30.32, 31.91, 69.18, 70.50, 73.44, 106.14, 117.31,131.37, 138.22, 153.34,153.14 ppm ; HRMS-FAB: $[M]^+$ calcd for $C_{49}H_{83}IO_4$, 862.53; found: 862.81

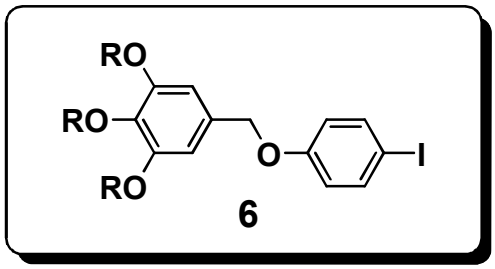

Synthesis of trimethyl((4-(3,4,5-tris(dodecyloxy)benzyloxy) phenyl) ethynyl) Silane (7): To a solution of **6** (3 g, 3.476 mmol) in dry triethylamine (50 mL), CuI (0.033 g, 0.174 mmol), $Pd(PPh_3)_2Cl_2$ (0.1220 g, 0.174 mmol) were added followed by dry THF (50 mL) as the co-solvent. The mixture was cooled in an ice bath and

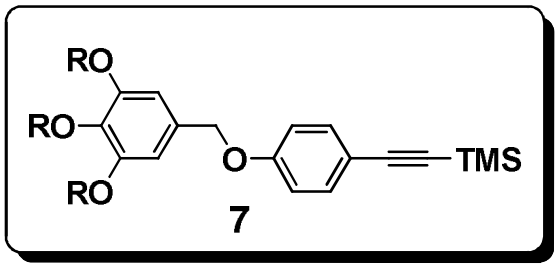

7

(trimethylsilyl) acetylene (0.6237 mL, 4.52 mmol) was added slowly. The reaction mixture was subsequently stirred at room temperature for 30 minutes and the temperature was raised to 50 °C for 12 h. After the completion of the reaction, the mixture was passed through a short celite column using dichloromethane as the eluent. The fractions were combined and the solvent was removed under reduced pressure. The crude product obtained was further purified by column chromatography (EtOAc/Hexane = 1:9) to give **7** in 93% yield. m. p. 53-55 °C; ^{1}H NMR (400 MHz, $CDCl_3$, TMS) δ: 7.42-7.40 (d, J = 8 Hz, 2H), 6.89-6.87 (d, J = 8 Hz, 2H), 6.59 (s, 2H), 4.93 (s, 2H), 3.97-3.92 (m, 6H), 1.80 (m, 6H), 1.48 (m, 6H), 1.27 (m, 48H), 0.86 (t, 9H), 0.23 (s, 9H) ppm; ^{13}C NMR (75 MHz, $CDCl_3$, TMS) δ: 0.039, 14.09, 22.67, 26.08, 29.40, 29.63, 29.68, 29.74, 30.32, 31.92, 69.17, 70.39, 73.43, 106.15, 114.71, 115.56, 133.45, 153.32 ppm ; HRMS-FAB: $[M]^+$ calcd for $C_{54}H_{92}O_4Si$, 832.68; found: 833.01

Synthesis of 1,2,3-tris(dodecyloxy)-5-((4-ethynylphenoxy)methyl)benzene (8): To a solution of **7** (2.65 g, 3.19 mmol) in dry THF (50 mL), 2 N KOH in methanol

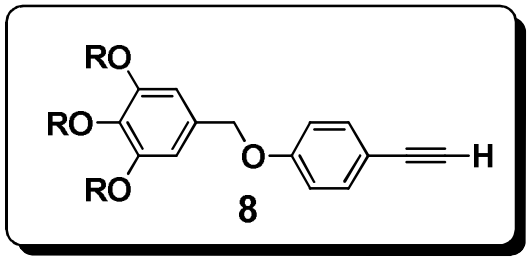

8

was added and stirred at room temperature for 3 h. After completion of the reaction, the solvent was removed under reduced pressure. The solid obtained was dissolved in water. The mixture was then extracted with chloroform, washed two times with brine followed by two times with distilled water. The organic layer was combined and dried over anhydrous sodium sulphate. The

solvent was removed under reduced pressure to get the crude product, which was further purified by column chromatography (EtOAc/Hex = 1:9) to give the compound **8** as a brown solid (2.10 g, yield 87%); m. p. 72-75 °C; ^{1}H NMR (400 MHz, $CDCl_3$, TMS) δ: 7.43-7.41 (d, J = 8 Hz, 2H), 6.92-6.90 (d, J = 8 Hz, 2H), 6.59 (s, 2H), 4.93 (s, 2H), 3.98-3.92 (m, 6H), 3.1 (s, 1H), 1.81 (m, 6H), 1.47 (m, 6H) 1.26 (m, 48H), 0.87 (t, 9H) ppm; ^{13}C NMR (75 MHz, $CDCl_3$, TMS) δ: 14.08, 22.67, 26.09, 29.12, 29.35, 29.40, 29.63, 29.69, 30.33, 31.92, 69.18, 70.43, 73.43, 106.18, 114.84, 114.47, 131.37, 133.58, 138.13, 153.34, 159.14 ppm; HRMS-FAB: $[M]^+$ calcd for $C_{51}H_{84}O_4$, 760.64; found: 760.80

Synthesis of trimethyl((4-((4-(3,4,5-tris(dodecyloxy)benzyloxy)phenyl) ethynyl)phenyl)ethynyl)silane (9): To a solution of **8** (1.10 g, 1.5 mmol) in triethylamine (50 mL), $Pd(PPh_3)_2Cl_2$ (0.055 g, 0.0788 mmol), CuI (0.03 g, 0.1577 mmol) were added followed by THF (15 mL) as the co-solvent. 1-Ioddo-4(trimethylsilylethynyl)benzene (0.473 g, 1.577 mmol) was then added and the reaction mixture was kept at ambient temperature (50 °C) for 12 h. After completion of the reaction, the mixture was passed through short celite column using CH_2Cl_2 as the eluent. The fractions were collected and the solvent was removed under reduced pressure. The crude product obtained was further purified by column chromatography (EtOAc/Hexane = 1:9) to give the compound **9** in 78% yield. m. p. 66-67 °C; ^{1}H NMR (400MHz, $CDCl_3$, TMS) δ: 7.46-7.44 (d, J = 8 Hz, 2H), 7.42 (s, 4H), 6.95-6.93 (d, J = 8 Hz, 2H), 6.60 (s, 2H),

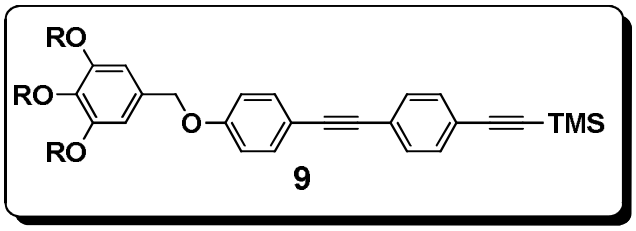

9

4.96 (s, 2H), 3.98-3.92 (m, 6H), 1.80 (m, 6H), 1.48 (m, 6H), 1.26 (m, 48H), 0.86 (t, 9H), 0.24 (t, 9H) ppm; ^{13}C NMR (75 MHz, $CDCl_3$, TMS) δ: 0.08, 14.09, 22.68, 26.10, 29.36, 29.41, 29.65, 29.70, 30.34, 31.93, 69.19, 70.47, 73.45, 104.73, 106.20, 114.97, 131.19, 131.40, 131.86, 133.09,153.35, 159.14 ppm ; HRMS-FAB: $[M]^+$ calcd for $C_{62}H_{96}O_4Si$, 932.71; found: 933.91

Synthesis of 1,2,3-tris(dodecyloxy)-5-((4-((4-ethynylphenyl)ethynyl)phenoxy) methyl)benzene (10): To a solution of **9** (0.50 g, 0.5356 mmol) in dry THF, 2 N KOH in methanol was added and stirred at room temperature for 2 h. After completion of the reaction, the solvent was removed under vacuum and the solid obtained was dissolved in water. It was then extracted with chloroform, washed two times with brine followed by two times with distilled water. The organic layer was combined, dried over anhydrous sodium sulphate. The solvent was removed under reduced pressure to give the crude product, which was further purified by column chromatography (EtOAc/Hex = 1:9) to give **10** as a pale yellow solid (0.407 g, yield 87%), m. p. 75-77 °C; ^{1}H NMR (400 MHZ, $CDCl_3$, TMS) δ: 7.43 (m, 6H), 6.92-6.89 (d, J = 9 Hz, 2H), 6.55 (s, 2H), 4.94 (s,2H) 3.97-3.92 (m, 6H), 3.1 (s, 1H), 1.80 (m, 6H), 1.48 (m, 6H), 1.26 (m, 48H), 0.87 (t, 9H) ppm; ^{13}C NMR (75 MHz, $CDCl_3$, TMS) δ : 14.04, 22.63, 26.04,26.08, 29.30, 29.36, 29.59, 29.64, 29.68, 29.69, 30.28, 31.87, 69.13, 70.41, 73.39, 83.29, 87.68, 91.37, 106.13, 114.91, 115.26, 121.46, 124.06, 131.22, 131.33, 131.97, 133.06, 133.96, 138.07, 153.29, 158.99 ppm ; HRMS-FAB: $[M]^+$ calcd for $C_{59}H_{88}O_4$, 860.67 ; found: 861.14

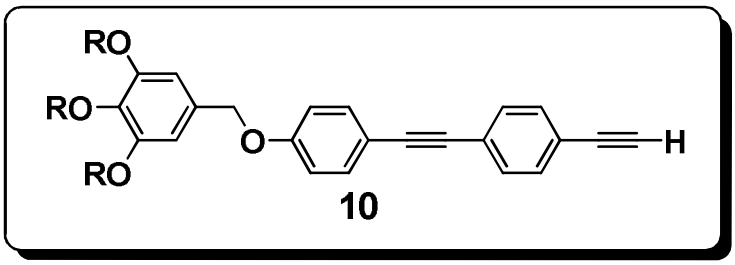

10

Synthesis of N^2, N^4-bis (4-((4-((4-(3,4,5-tris(dodecyloxy)benzyloxy)phenyl) ethynyl)phenyl)ethynyl)phenyl)-1,3,5-triazine-2,4,6-triamine (12): To a solution of **10** (0.10 g, 0.1162 mmol) in dry triethylamine (50 mL), THF (50 mL) was added followed by **11** (0.03, 0.057 mol). The reaction mixture was purged with nitrogen for 30 minutes. The flask was then filled with nitrogen after adding Pd $(PPh_3)_2Cl_2$ (3.9 mg, 0.00566 mmol), and CuI (0.5 mg, 0.00566 mmol) and stirred at ambient temperature (50 °C) for 24 h. After completion of the reaction, the content was passed through a celite column using dichloromethane as the eluent. The fractions were collected and the solvent was removed under reduced pressure. The crude product obtained was further purified by column chromatography (EtOAc/Hex = 3:7) to give the compound **12** as a solid (0.60 g, yield 25.8%) m.p.: 214 °C; ^{1}H NMR (500 MHz, $CDCl_3$) δ: 7.61-7.59 (d, J = 8 Hz, 4H), 7.51-7.46 (m, 16H), 6.96-6.94 (d, 4H), 6.93 (br-s, 2H), 6.61 (s, 4H), 5.02 (br-s, 2H), 4.95 (s, 4H), 3.99-3.95 (m, 12H), 1.81-1.70 (m, 12H), 1.40-1.50 (m, 12H), 1.40-1.20 (m, 96H), 0.85 (m, 18H) ppm; ^{13}C NMR (75 MHz, $CDCl_3$, TMS) δ: 10.94, 14.09, 21.02, 22.68, 22.96, 23.74, 24.77, 26.11, 28.91, 29.08, 29.38, 29.68, 30.35, 31.91, 38.72, 60.39, 68.15, 69.14, 106.13, 107.09, 111.26, 114.11, 114.92, 115.36, 128.51, 128.67, 128.79, 130.86, 131.36, 131.59, 132.14, 132.21, 132.36, 132.56, 133.12, 153.32, 167.76 ppm; MS (MALDI-TOF): $[M]^+$ calcd for $C_{133}H_{186}N_6O_8$,1996.94; found: 1996.28

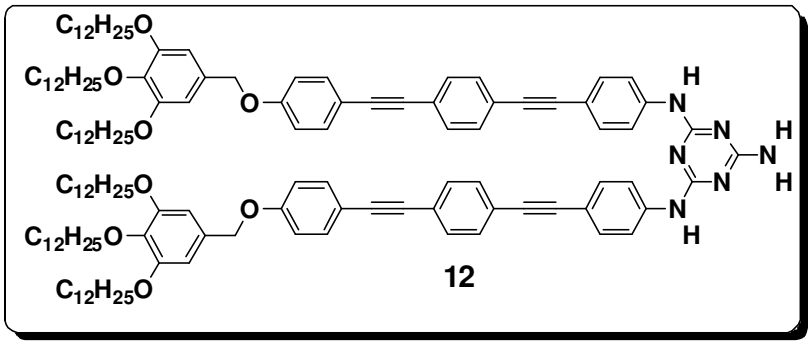

3.5.2. Description of Experimental Techniques

Details of the instrumentation are described in the experimental section (section 2.6.2) of Chapter 2.

Sample Preparation for Microscopic and Spectroscopic Analyses

Decane solutions of toroidal assemblies were prepared by mixing chloroform solution of **12** and chloroform/methanol mixed solution of **13** with a 1:1 molar stoichiometry and the solvent was evaporated thoroughly. The resulting solid was dissolved in decane by gentle heating to give decane solutions of the toroidal assemblies. In another method, compounds **12** and **13** were taken in a 1:1 molar ratio in a screw capped vial and dissolved in a mixture of chloroform and methanol (1:1) ($c = 1 \times 10^{-2}$ M in 1 mL) by sonication followed by heating. It was then flushed with nitrogen gas to remove the solvent and further dried in vacuum for 36 h. The residue was then dissolved in decane and diluted to different concentrations for different microscopic and spectroscopic analyses such as DLS (1×10^{-4} M - 5×10^{-5} M), AFM (5×10^{-5} M) and for UV/ Vis and fluorescence measurements (1×10^{-4} M - 5×10^{-5} M). For all AFM analysis, only the aged solution (thermodynamically equilibrated solution) was used.

Atomic Force Microscopy (AFM)

AFM images of the toroids were acquired under ambient conditions using Digital Instruments, Multimode Nanoscope IIIa (Veeco Instruments, Santa Barbara, CA) in tapping mode with different set points. Silicon cantilevers (OMCL-AC160TS-C2) with a spring constant of 42 N/m and frequency of 300 kHz (nominal value, Olympus, Japan) were used for the AFM observations in air.

The scan rate was varied from 1 to 2 Hz. Variations of the tapping force can be achieved by changing the driving amplitude (A_0) and set-point amplitude (A_{sp}) ratio. Simultaneous registration was performed for height and phase images. The samples were prepared by spin coating (3000 rpm) from equimolar mixture of **12** and **13** (c = 5 × 10^{-5} M) on a freshly cleaved highly oriented pyrolytic graphite (HOPG.). The samples were dried under vacuum for 24 h after spin coating. In all AFM images, the apparent diameter of the toroids was corrected for the AFM tip broadening effect by subtracting the broadening factor from the apparent diameter. The tip broadening was calculated according to the equation 1 where 'R'is the radius of the tip and 'h' is the mean height of the toroids.

$$2\Delta = 2[h\,(2R-h)]^{1/2} \qquad (1)$$

Radius of the tip (OLYMPUS OMCL-AC series cantilevers, Model: OMCL-AC160TS-C2) is 6.8 nm. The calculated tip broadening factor 2Δ was 11.54 ± 0.3. The average height of the toroids formed from a solution of concentration 5 × 10^{-5} M was 3.2 ± 0.3. The actual diameter obtained after subtracting from the observed diameter was 8.46 nm.

Transmission Electron Microscopy (TEM)

The samples were prepared by dipping the carbon coated copper grids (400 mesh) to an equimolar mixture of **12** and **13** in decane (c = 5 ×10^{-5} M). TEM images were obtained after staining with RuO_4 vapors followed by drying the sample in vacuum for 24 h. The samples were stained by placing the TEM grids above the aqueous solution of RuO_4 for 15-30 minutes in a closed chamber.

3.6. References

1. a) J.-M. Lehn, *Supramolecular Chemistry, Concepts and Perspectives* VCH, Weinheim, **1995**; b) J. W. Steed, J. L. Atwood, *Supramolecular Chemistry,* Wiley, Chichester, **2000**.
2. a) F. J. M. Hoeben, P. Jonkheijm, E. W. Meijer, A. P. H. J. Schenning, *Chem. Rev*. **2005**, *105*, 1491; b) A. P. H. J. Schenning, E. W. Meijer, *Chem. Commun.* **2005**, 3245; c) A. C. Grimsdale, K. Müllen, *Angew. Chem. Int. Ed.* **2005**, *44*, 5592.
3. M. Lee, B.-K. Cho, W.-C. Zin, *Chem. Rev.* **2001**, *101*, 3869.
4. a) F. J. M. Hoeben, P. Jonkheijm, E. W. Meijer, A. P. H. J. Schenning, *Chem. Rev.* **2005**, *105*, 1491; b) A. P. H. J. Schenning, E. W. Meijer, *Chem. Commun*. **2005**, 3245; c) J. Wu, W. Pisula, K. Müllen, *Chem. Rev.* **2007**, *107*, 718; d) A. Ajayaghosh, S. J. George, A. P. H. J. Schenning, *Top. Curr. Chem*. **2005**, *258*, 83.
5. a) A. Ajayaghosh, V. K. Praveen, *Acc. Chem. Res*. **2007**, *40*, 644; b) A. Ajayaghosh, V. K. Praveen, C. Vijayakumar, *Chem. Soc. Rev*, **2008**, *37*,109.
6. a) Supramolecular Dye Chemistry: *Top. Curr. Chem.* **2005**, *258* (Ed.: F. Würthner), whole volume; b) S. Yagai, J. *Photochem. Photobio. C: Photochem. Rev*. **2006**, *7*, 164.
7. a) J.-M. Lehn, M. Mascal, A. Decian, J. Fischer, *J. Chem. Soc., Chem. Commun.* **1990**, 479; b) D. S. Lawrence, T. Jiang, M. Levett, *Chem. Rev.* **1995**, *95*, 2229; c) G. M. Whitesides, E. E. Simanek, J. P. Mathias, C. T. Seto, D. N. Chin, M. Mammen, D. M. Gorden, *Acc. Chem.*

Res. **1995**, *28*, 37; d) A. Ranganathan, V. R. Pedireddi, C. N. R. Rao, *J. Am. Chem. Soc*. **1999**, *121*, 1752; e) L. J. Prins, D. N. Reinhoudt, P. Timmerman, *Angew. Chem*. **2001**, *113*, 2446; *Angew. Chem. Int. Ed*. **2001**, *40*, 2382; f) D. C. Sherrington, K. A. Taskinen, *Chem. Soc. Rev*. **2001**, *30*, 83.

8. P. Jonkheijm, A. Miura, M. Zdanowska, F. J. M. Hoeben, S. De Feyter, A. P. H. J. Schenning, F. C. De Schryver, E. W. Meijer, *Angew. Chem.* **2004**, *116*, 76; *Angew. Chem. Int. Ed.* **2004**, *43*, 74.

9. S. Yagai, T. Nakajima, K. Kishikawa, S. Kohmoto, T. Karatsu, A. Kitamura, *J. Am. Chem. Soc.* **2005**, *127*, 11134.

10. (a) M. Yoshio, T. Mukai, H. Ohno, T. Kato, *J. Am. Chem. Soc*. **2004**, *126*, 994; (b) U. Beggin, G. Zipp, A. Mourran, P. Walther, M. Möller, *Adv. Mater*. **2000**, *12*, 513; (c) H.-K. Lee, H. Lee, Y. H. Ko, Y. J. Chang, N.-K. Oh, W.-C. Zin, K. Kim, *Angew. Chem., Int. Ed*. **2001**, *40*, 2669; (d) V. Percec et al. *Nature* **2002**, *419*, 384; (e) V . Percec, W.-D Cho,G. Ungar, D. J. P. Yeardley, *J. Am. Chem. Soc*. **2001**, *123*, 1302; (f) R. Kleppinger, C. P Lillya, C. J Yang, *J.Am. Chem. Soc*. **1997**, *119*, 4097; (g) M. Suárez, J.-M Lehn, S. Zimmerman, A. Skoulios, B. J.Heinrich, *J. Am. Chem. Soc.* **1998**, *120*, 9526.

11. (a) N. Kimizuka, T. Kawasaki, K. Hirata, T. Kunitake, *J. Am. Chem. Soc.* **1995**, *117*, 6360; (b) N. Kimizuka, S. Fujikawa, H. Kuwahara, Kunitake, A. Marsh,J. -M. Lehn, *J. Chem. Soc., Chem. Commun*. **1995**, 2103; (c) W. Yang, X. Chai, Y. Tian, S. Chen, Y. Cao, X. Lu,Y. Jiang, T. Li, *Chem. Eur. J.* **1999**, *5*, 1144; (d) H.-A. Klok, K. A. Jolliffe, C. L.

Schauer, L. J. Prins, J. P. Spatz, M. Möller, P. Timmerman, D. N. Reinhoudt, *J. Am. Chem. Soc*. **1999**, *121*, 7154; (e) L. Brunsveld, H. Zhang, M. Glasbeek, J. A. J. M. Vekemans, E. W. Meijer, *J. Am. Chem. Soc*. **2000**, *122*, 6175; (f) M. Enomoto,A. Kishimura, T. Aida, *J. Am. Chem. Soc*. **2001**, *123*, 5608; (g) H. Fenniri, B.-L Deng, A. E. Ribbe, *J. Am. Chem. Soc*. **2002**, *124*,11064.

12. a) N. Kimizuka, T. Kawasaki, K. Hirata, T. Kunitake, *J. Am. Chem. Soc*. **1995**, *117*, 6360; b) W. Yang, X. Chai, L. Chi, X. Liu, Y. Cao, R. Lu, Y. Jiang, X. Tang, H. Fuchs, T. Li, *Chem. Eur. J*. **1999**, *5*, 1144; c) H.-A. Klok, K. A. Jolliffe, C. L. Schauer, L. J. Prins, J. P. Spatz, M. Möller, P. Timmerman, D. N. Reinhoudt, *J. Am. Chem. Soc*. **1999**, *121*, 7154; d) H. Fenniri, P. Mathivanan, K. L. Vidale, D. M. Sherman, K. Hallenga, K. V. Wood, J. G. Stowell, *J. Am. Chem. Soc*. **2001**, *123*, 3854; e) P. Jonkheijm, A. Miura, M. Zdanowska, F. J. M. Hoeben, S. De Feyter, A. P. H. J. Schenning, F. C. De Schryver, E. W. Meijer, *Angew. Chem*. **2004**, *116*, 76; *Angew. Chem. Int. Ed*. **2004**, *43*, 74; f) S. Yagai, T. Nakajima, K. Kishikawa, S. Kohmoto, T. Karatsu, A. Kitamura, *J. Am. Chem. Soc*. **2005**, *127*, 11134; g) T. Kato, T. Matsuoka, M. Nishii, Y. Kamikawa, K. Kanie, T. Nishimura, E. Yashima, S. Ujiie, *Angew. Chem*. **2004**, *116*, 2003; *Angew. Chem. Int. Ed*. **2004**, *43*, 1969; h) H. M. Keizer, R. P. Sijbesma, *Chem. Soc. Rev*. **2005**, *34*, 226.

13. Kimizuka et al. suggested the helical organization of a rosette type assembly into a coil-like nanostructure: N. Kimizuka, S. Fujikawa, H.

Kuwahara, T. Kunitake, A. Marsh, J.-M. Lehn, *J. Chem. Soc., Chem. Commun.* **1995**, 2103.

14. For OPE-based nanostructures, see: a) P. Samorí, V. Francke, K. Müllen, J. P. Rabe, *Chem. Eur. J*. **1999**, *5*, 2312; b) U. H. F. Bunz, *Chem. Rev*. **2000**, *100*, 1605; c) U. H. F. Bunz, *Acc. Chem. Res*. **2001**, *34*, 998; d) S. Zahn, T. M. Swager, *Angew. Chem.* **2002**, *114*, 4399; *Angew. Chem. Int. Ed*. **2002**, *41*, 4225; e) S. Sivakova, S. J. Rowan, *Chem. Commun*, **2003**, 2428; f) J. Xu, C.-Z. Zhou, L. H. Yang, N. T. S. Chung, Z.-K. Chen, Langmuir **2004**, *20*, 950; g) A. Ajayaghosh, R. Varghese, V. K. Praveen, S. Mahesh, *Angew. Chem*. 2006, *118*, 3339; *Angew. Chem. Int. Ed*. **2006**, *45*, 3261; h) A. Ajayaghosh, R. Varghese, S. Mahesh, V. K. Praveen, *Angew. Chem*. **2006**, *118*, 7893; *Angew. Chem. Int. Ed.* **2006**, *45*, 7729; i) S. Sivakova, J. Wu, C. J. Campo, P. T. Mather, S. J. Rowan, *Chem. Eur. J*. **2006**, *12*, 446.

15. For toroidal nanostructures, see: a) D. J. Pochan, Z. Chen, H. Cui, K. Hales, K. Qi, K. L. Wooley, *Science* **2004**, *306*, 94; b) W.-Y. Yang, J. -H. Ahn, Y.-S. Yoo, N. -K. Oh, M. Lee, *Nature Mater*. **2005**, *4*, 399; c) Z. Chen, H. Cui, K. Hales, Z. Li, K. Qi, D. J. Pochan, K. L. Wooley, *J. Am. Chem. Soc*. **2005**, *127*, 8592; d) J.-K. Kim, E. Lee, Z. Huang, M. Lee, *J. Am. Chem. Soc.* **2006**, *128*, 14022; e) J. C. T. Carlson, S. S. Jena, M. Flenniken, T. Chou, R. A. Siegel, C. R. Wagner, *J. Am. Chem. Soc*. **2006**, *128*, 7630; f) Z. Nie, D. Fava, E. Kumacheva, S. Zou, G. C. Walker, M. Rubinstain, *Nature Mater.* **2007**, *6*, 609; g) E. Lee, Y.-H. Jeong, J.-K. Kim, M. Lee, *Macromolecules* **2007**, *40*, 8355.

16. For toroidal structure of biopolymers, see: a) A. Ohira, S.-Y. Kim, M. Fujiki, Y. Kawakami, M. Naito, G. Kwak, A. Saxena. *Chem. Commun.* **2006**, 2705; DNA based toroidal structures, see: b) C. Böttcher, C. Endisch, J.-H. Fuhrhop. C. Catterall. M. Eation, *J. Am .Chem. Soc*. **1998**, *120*, 12; c) R. Golan, L.I. Pietrasantha, W. Hsieh, H.G. Hansma, *Biochemistry*, **1999**, *38*, 14069; d) D. Rasched, D. Ackermann, T. L. Schimidt, P. Broekmann, A. Heckel, M. Famulok, *Angew. Chem*. **2008**, *120*, 981; *Angew. Chem. Int. Ed*. **2008**, *47*, 967.

17. For substrate assisted formation of ring like structures, see: a) A. P. H. J. Schenning, F. B. G. Benneker, H. P. M. Geurts, X. Y. Liu, R. J. M. Nolte, *J. Am .Chem. Soc*. **1996**, *118*, 8549; b) H. A. M. Biemans, A. E. Rowan, A. Verhoeven, P. Vanoppen, L. Latterini, J. Foekema, A. P. H. J. Schenning, E. W. Meijer, F. C. de Schryver, R. J. M. Nolte, *J. Am .Chem. Soc*. **1998**, *120*, 11054; c) S. Masuo, H. Yoshikawa, T. Asahi, H. Masuhara, T. Sato, D.-L. Jiang, T. Aida. *J. Phys. Chem. B* **2001**, *105*, 2885; d) F. Balzer, J. Beermann, S. I. Bozhevolnyi, A. C. Simonsen, H.-G. Rubahn, *Nano Lett*. **2003**, *3*, 1311; e) M. C. Lensen, K. Takazawa, J. A. A. W. Elemans, C. R. L. P. N. Jeukens, P. C. M. Christianen, J. C. Maan, A. E. Rowan, R. J. M. Nolte, *Chem. Eur. J*. **2004**, *10*, 831.

18. K. Sonogashira, Y. Tohda, N. Hagihara, *Tetrahedron Lett*. **1975**, *16*, 4467; b) C.T. Seto, G. M. Whitesides, *J. Am .Chem. Soc*. **1993**, *115*, 905.

19. F.J. M. Hoben, M. J. Pouderoijen, A. P. H. Schenning, E. W. Meijer, *Org. Biomol. Chem,* **2006,** *4,* 4460.

20. Tip broadening effect was estimated as reported in: a) H.-J. Butt, R. Guckenberger, J. P. Rabe, *Ultramicroscopy*, **1992**, *46*, 375; b) P. Samorí, V. Francke, T. Mangel, K. Müllen, J. P. Rabe, *Opt. Mater.* **1998**, *9*, 390.

21. a) T. Pullerits, V. Sundström, *Acc. Chem. Res*. **1996**, *29*, 381; b) X. Hu, A. Damjanovic, T. Ritz, K. Schulten, *Proc. Nat. Acad. Sci. USA* **1998**, *95*, 5935.

22. a) S. S. Babu, S. Mahesh, K. K. Kartha, A. Ajayaghosh, *Chem. Asian J*. **2009**, *4*, 824; b) S. Malik, D. Roizard, J. M. Guenet, *Macromolecules,* **2006**, *39*, 5957 ; c) C. Daniel, D. Alfano, V. Venditto, S. Cardea, E. Reverchon, D. Larobina, G. Mensitieri, G. Guerra, *Adv. Mater*. **2005**, *17*, 1515; d) L. A. Connal, R. Vestberg, P. A. Gurr, C. J. Hawker, G. G. Qiao, *Langmuir,* **2008**, *24*, 556 ; e) H. Ejima, T. Iwata , N. Yoshie, *Macromolecules* **2008**, *41*, 9846 ; f) L. Song, R. K. Bly, J. N. Wilson, S. Bakbak, J. O. Park, M. Srinivasarao, U. H . F. Bunz, *Adv. Mater.* **2004** , *16*, 115.

Chapter 4

Role of Complementary H-Bonding Interaction of a Cyanurate in the Self-assembly and Gelation of a Bismelamine Linked Tri(*p*-phenyleneethynylene)

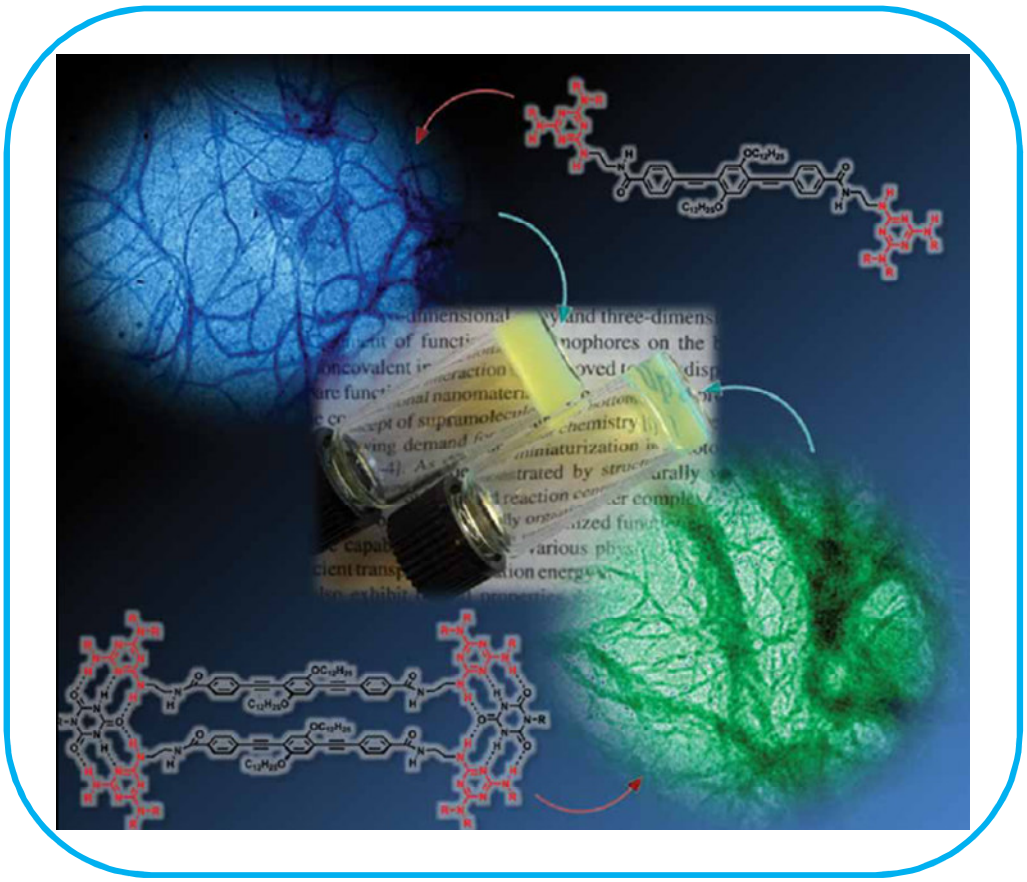

4.1. Abstract

*The objective of this study is to investigate the effect of the complementary H-bonding interaction of a cyanurate on the self-assembly, gelation and the morphological characteristics of a bismelamine-functionalized tri(p-phenyleneethynylene) (**BM-TPE**). The aggregation behavior of this molecule in methylcyclohexane was monitored by variable temperature fluorescence measurements. In methylcyclohexane, **BM-TPE** (1×10^{-5} M) showed an emission maximum at 407 nm. The absence of significant solvent dependence on the emission maximum suggests that this compound exists as monomeric species at low concentration. When aliquots of the ditopic cyanurate (**dCA**) was added to the solution of **BM-TPE**, considerable shift in the emission is noticed which indicated the electronic interaction between the π-conjugated molecules as a result of the H-bonding interaction. In the absence of **dCA**, **BM-TPE** self-assembles to form opaque and weak gels in aliphatic solvents which turned to transparent and stable upon addition of **dCA**, affording supramolecular nanostructures with distinct physical properties. TEM and AFM analyses of the self-assemblies exhibited considerable variations in the morphology of **BM-TPE** in the absence and presence of **dCA**.*

4.2. Introduction

Complex superstructures of organized biopolymers are created by the interplay of complementary H-bonding interactions. While nature uses amide H-bonding in protein organization, complementary double and triple H-bonding interaction between heteroaromatic components are used in transferring genetic

information of nucleic acids.[1] Thus, multiple H-bonding interactions are vital in deciding the structure and properties of supramolecular architectures.[2] In recent years, complementary H-bonding between heterocyclic compounds have been exploited to regulate the structure and properties of functional chromophores.[3,4] Due to strong propensity for π-stacking, linear π-conjugated systems when functionalized with H-bonding moieties are known to form diverse supramolecular architectures.[5,6] Recently, various research groups have been exploring the use of *p*-phenyleneethynylene systems (PE) for the creation of a variety of supramolecular architectures.[7,8] Multiple H-bonding interactions between heterocyclic compounds have been widely used to regulate the spatial arrangements of chromophoric units on the molecular scale.

Recenly, Yagai and coworkers have used this strategy for the fabrication of well-defined nanoobjects composed of extended π-electronic molecules.[9] They have synthesized a perylene bisimide (PBI) anchored to a melamine H-bonding unit (**1**) (Figure 4.1a), and its supramolecular polymerization upon binding with *N*-dodecylcyanurate (**CA**) have been examined. The perylene derivative **1** could self-aggregate from a variety of solvents. However in the presence of complementary H-bonding component such as *N*-dodecylcyanurate (**CA**), the compound **1** resulted in the formation of supramolecular polymers where the PBI chromophores are uniformly arranged within the main chain.

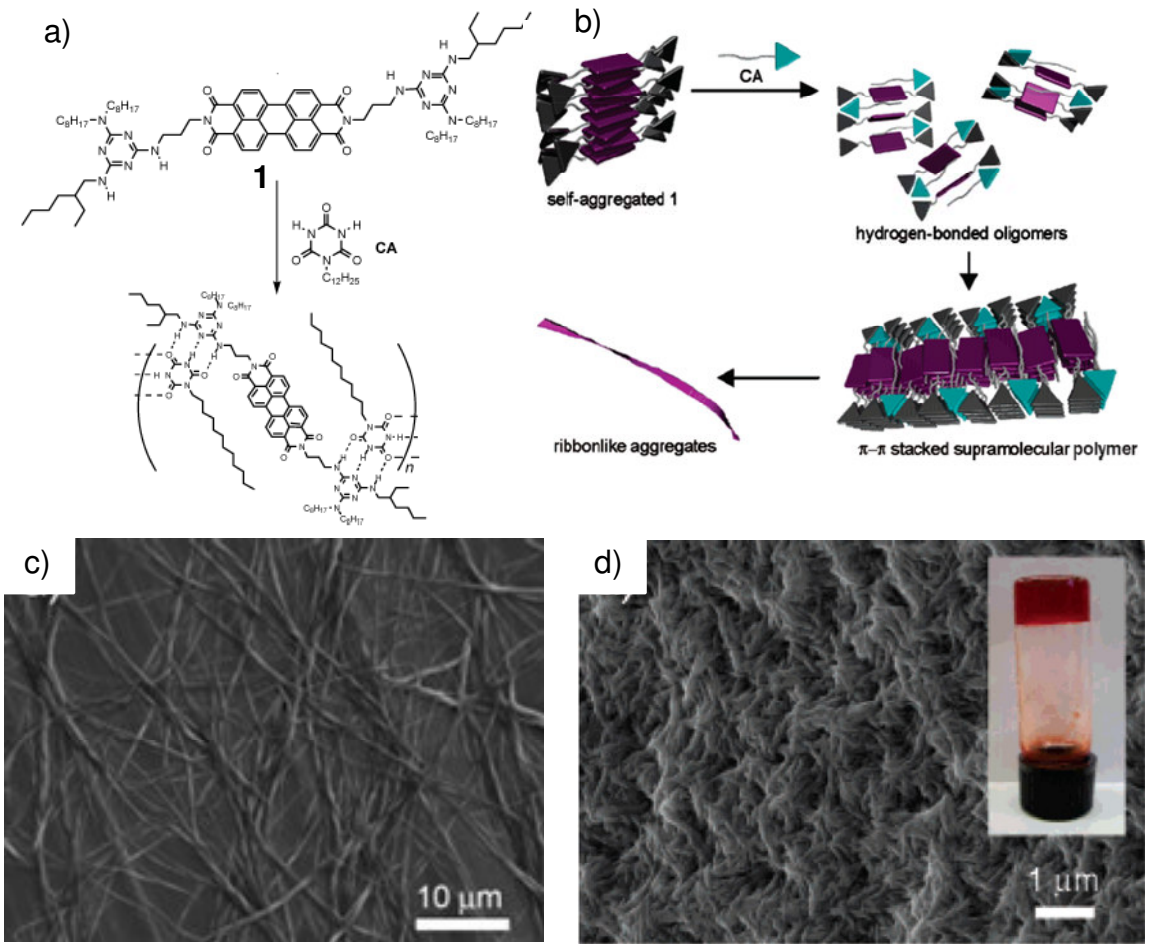

Figure 4.1. a) Scheme for supramolecular polymer formation by the triple H-bonding interaction between melamine linked PBI (**1**) and cyanuric acid (CA). b) Schematic representation of the aggregation of **1** and **CA** in methylcyclohexane (MCH). c) FE-SEM of the filamentous precipitates of $\mathbf{1}_n\cdot\mathbf{CA}_n$ formed from MCH. d) FE-SEM images of the dried decane gel of $\mathbf{1}_n\cdot\mathbf{CA}_n$ in the heavily entangled region. Inset in Figure d shows a photograph of a decane gel (2 mM).

It has recently been reported that supramolecular structures of H-bonded species which are formed at the lowest level of the organization hierarchy could be controlled by the length of the alkyl linker moieties of the building blocks.[10] In this study, two different molecules, **2** and **3** where a perylene bisimide core and two melamine moieties, linked through ethylene and trimethylene linkers, were

examined. Despite a marginal structural difference in the length of alkyl linkers, the aggregation of **2** and **3** with **dCA** has generated remarkably distinct supramolecular species as revealed by various spectroscopic and microscopic observations.

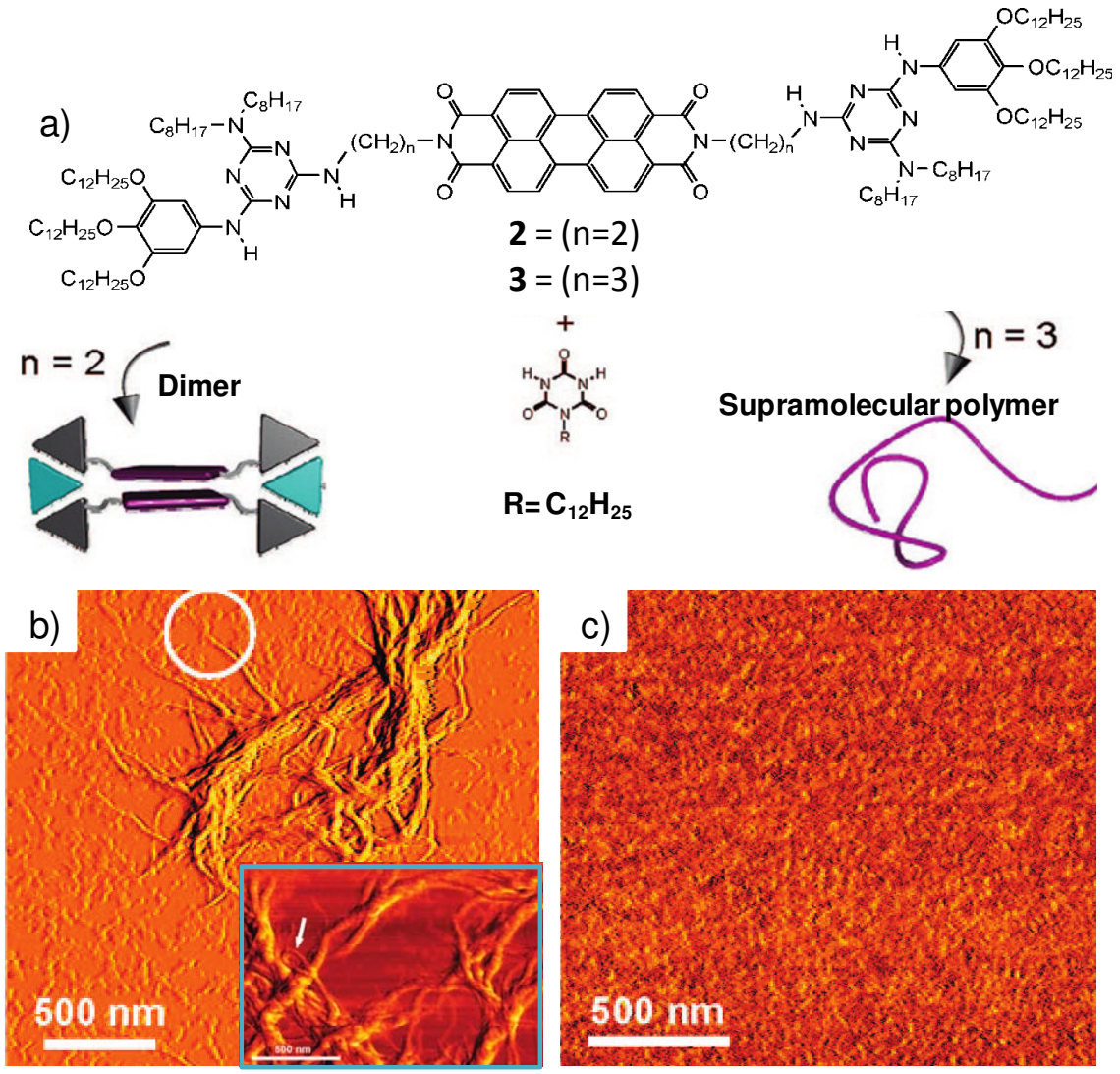

Figure 4.2. a) Structures of the melamine-linked perylene bisimide **2**, and **3**, and the cyanurate **dCA**. b) AFM Phase images of **3**·**dCA** spin-coated from MCH solution (5×10^{-5} M). Inset in Figure b shows a magnified image. c) AFM phase images of **2**·**dCA** spin-coated from MCH solution (5×10^{-3} M).

UV/Vis spectral studies have revealed that both **2** and **3** self-assemble in nonpolar organic solvents through π-π stacking interaction between perylene cores, giving self-aggregates with nearly identical thermal stabilities. Upon addition of one equivalent of the cyanurate **dCA**, the stabilities of the resulting aggregates were dramatically changed, suggesting the formation of different types of H-bonded supramolecular species. Dynamic light scattering and atomic force microscopic studies have revealed that the system featuring ethylene linker moieties (**2**) generates a discrete dimer of **2**, supported by two cyanurate molecules, whereas the system featuring trimethylene linker moieties (**3)** affords extended supramolecular polymers hierarchically organizing into nanoscopic fibers. These results demonstrate that it is possible to obtain distinct supramolecular species by just changing the number of carbon atoms of the linker moieties of individual components.

Multiple H-bonding interactions between heterocyclic compounds have been widely used to regulate the spatial arrangements of chromophoric units on the molecular scale. Yagai and coworkers have used this strategy for the organization of oligo(*p*-phenylenevinylene)*s* (OPVs), using complementary H-bonds between melamine functionalised OPV and cyanurates.[11] The OPV(**4**) capped on one end with a monotopic DAD-type triple H-bonding melamine module showed distinct optical properties as well as self-organization behavior upon complexation with the complementary cyanurates **CA**, **dCA** and **ddCA** (Figure 4.3). Complexation of **4** with **CA**, **dCA**, and **ddCA** produced supramolecular species with different numbers of OPV segments (Figure 4.3), leading to distinct hierarchical organization.

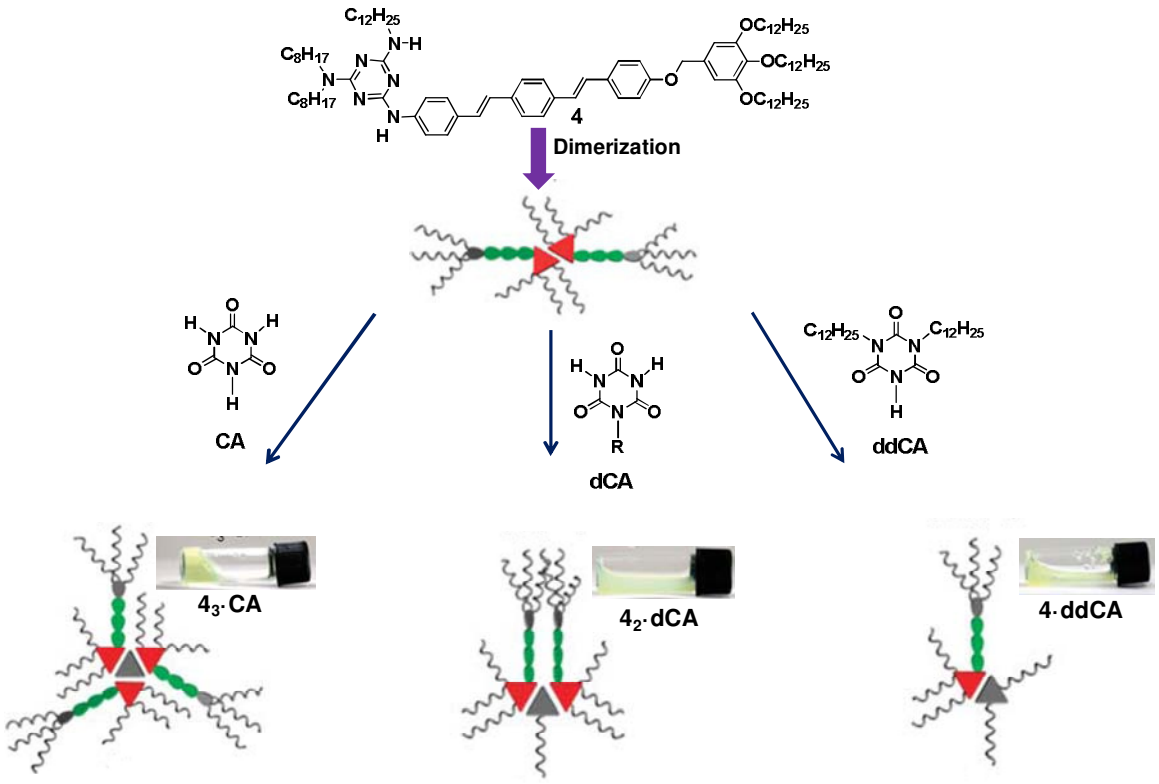

Figure 4.3. Schematic representation of the complexation of **4** with different cyanurates and photographs of the corresponding gels formed.

Because of the predictable shapes of the H-bonded species, resulted from the directional multiple H-bonding interactions, this strategy has been used as a reasonable noncovalent glue for the "bottom-up" creation of optically and electronically active functional materials. From the above examples, it can be seen that by using OPV as a functional chromophore segment, it is possible to modulate the self organization process and optical properties of individual building blocks. The main objective of the present study is to investigate the role of multiple H-bonding groups and their complementary H-bonding partner to the self-assembly of *p*-phenyleneethynylenes. The reason for this study is that the π-stacking in OPEs are weaker than in OPVs and hence the former forms relatively weaker gels.

Hence the presence of multiple H-bonding groups may allow the formation of stronger and extended assemblies and may facilitate the π-stacking between the π-conjugated backbones. For this purpose, a *p*-phenyleneethynylene derivative (**BM-TPE**) tethered to two melamine units has been synthesized. Introduction of the TPE moiety confers molecular rigidity required for regular molecular packing and may facilitate π-stacking interactions. The two amide functionalities may also enhance the interchain association by H-bonding interaction.

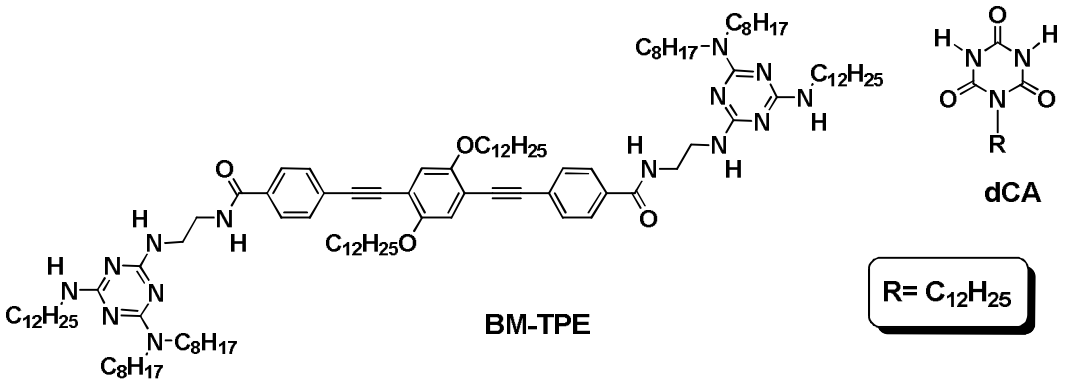

4.3. Results and Discussion

4.3.1. Synthesis

The bismelamine compound, **BM-TPE** was synthesized by the reaction of the bisacid, [4,4'-(2,5-bis(dodecyloxy)-1,4-phenylene)bis(ethyne-2,1-diyl)dibenzoic acid] with two equivalents of N^2-(2-aminoethyl)-N^4-dodecyl-N^6,N^6-dioctyl-1,3,5-triazine-2,4,6-triamine (**14**) using amide cross-coupling reaction in the presence of *N*-ethyl-*N*′-(3-dimethylaminopropyl)-carbodiimide (WSC). Synthesis of **9** was achieved by starting from the hydroquinone (**5**), which was first alkylated using

dodecyl bromide in DMF in the presence of NaOH as a base to give **6**. Reaction of **6** with iodine and potassium iodate in a mixture of acetic acid, water and sulphuric acid in the ratio of 90:7:3 by volume gave the corresponding diiodo derivative (**7**) in 60% yield. The reaction between **7** and two equivalents of trimethylsilylacetylene (TMS-acetylene) in diisopropylamine using $[Pd(PPh_3)_2(Cl_2)_2]$/CuI as the catalyst gave the corresponding silyl protected derivative (**8**) in 75% yield. Deprotection of **8** using KOH in a mixture of THF and methanol gave the corresponding bisethynyl derivative, **9** in 80% yield (Scheme 4.1.)

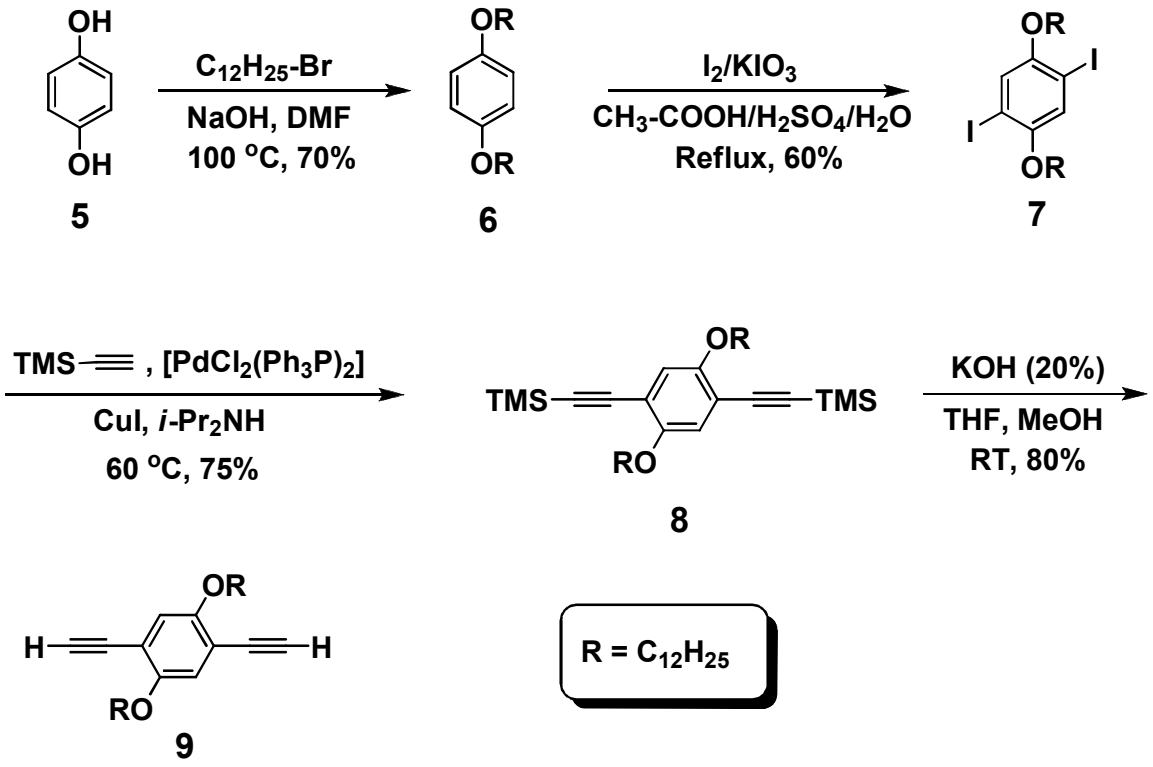

Scheme 4.1

Compound **11** was synthesized by Sonogashira-Hagihara cross coupling reaction[12] between the bisethynyl derivative **9** and two equivalents of 4-iodobenzoate in a mixture of toluene and diisopropylamine using $[Pd(PPh_3)_2Cl_2]$ /

CuI as the catalyst. The bisester thus obtained was subsequently hydrolyzed using KOH in a mixture of methanol and THF at reflux conditions to give the compound **11**, in 63% yield (Scheme 4.2).

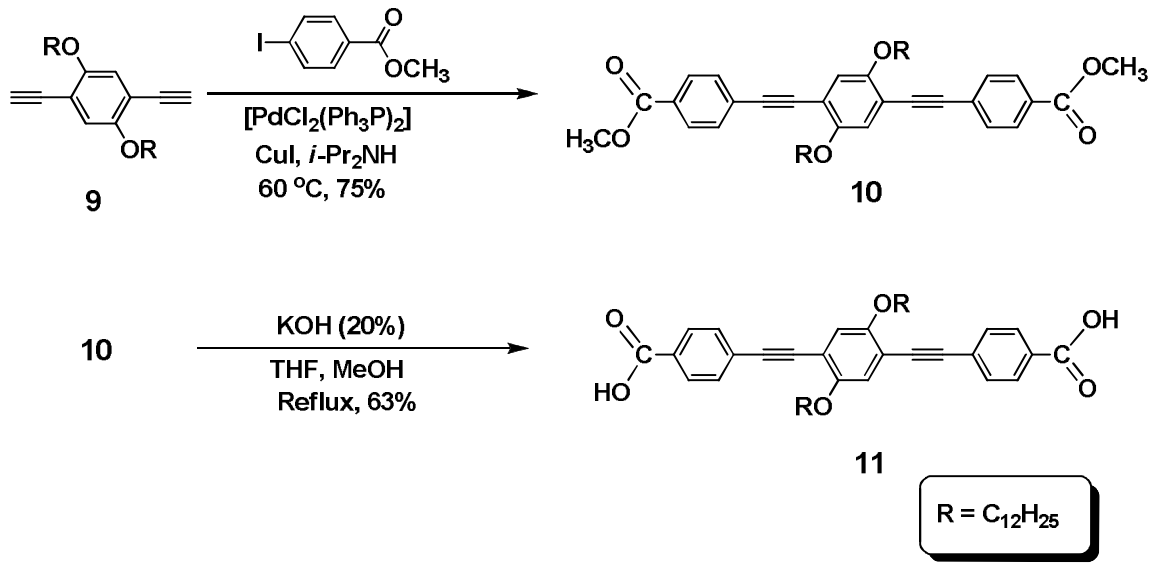

Scheme 4.2

The compound N^2-(2-aminoethyl)-N^4-dodecyl-N^6, N^6-dioctyl-1,3,5-triazine-2,4,6-triamine (**14**) was synthesized as shown in Scheme 4.3. For this purpose, the molecule **13** was synthesized from trichlorotriazine (**12**) which was first alkylated using dodecyl amine in presence of DIPEA (*N*, *N*-Diisopropylethylamine) at ice cold temperature followed by reaction with octylamine. The compound **13** was obtained in 78% yield. The reaction between **13** and one equivalent of ethylenediamine, and DIPEA gave the compound **14** in 80% yield.

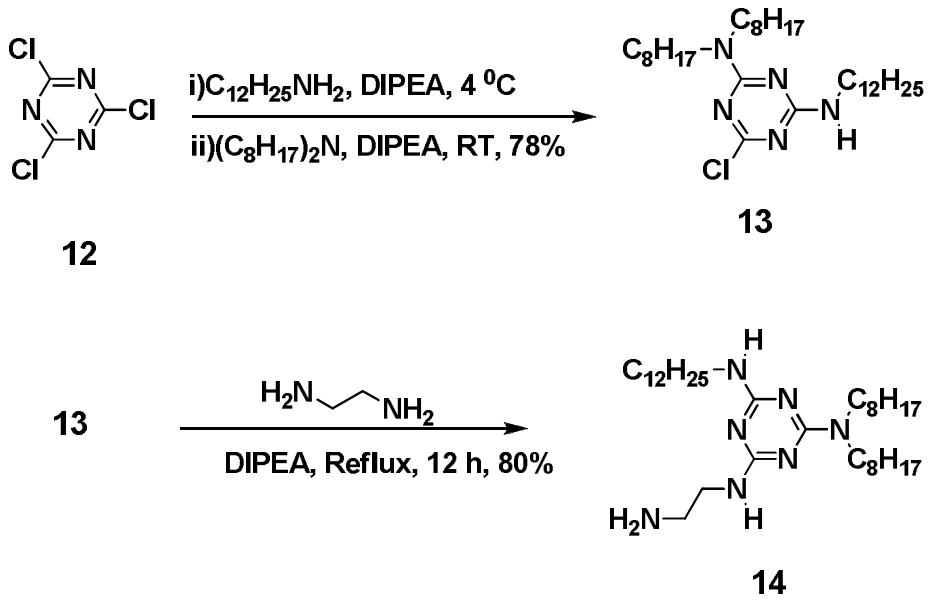

Scheme 4.3

The bismelamine compound, **BM-TPE** was synthesized by the coupling reaction between the bisacid (**11**) and two equivalents of N^2-(2-aminoethyl)-N^4-dodecyl-N^6, N^6-dioctyl-1,3,5-triazine-2,4,6-triamine (**14**) using *N*-ethyl-*N*′-(3-dimethylaminopropyl)-carbodiimide (WSC) in dry DCM in cold condition (5 °C) followed by stirring the reaction mixture at room temperature for 8 h. The crude product was purified by column chromatography (EtOAc: Hexane), to give **BM-TPE** in 30% yield (Scheme 4.4).

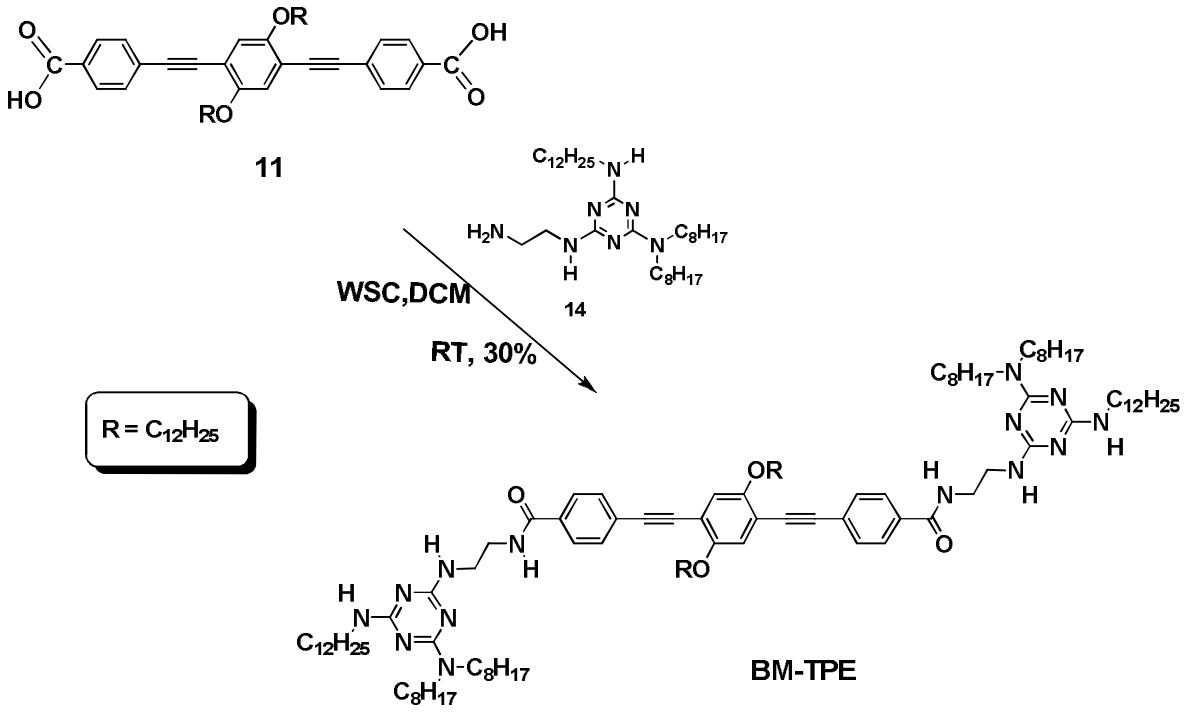

Scheme 4.4

Self-aggregates of melamine as well as its co-aggregates with complementary DAD·ADA type triple H-bonds provide different kinds of supramolecular architectures. It has already been demonstrated that the two distinct supramolecular species of perylene bisimide, i.e., supramolecular polymer and discrete dimer, can be constructed by mixing melamine appended perylene bisimide (MPBIs) and cyanurates.[13] In a similar fashion, it is expected that the melamine appended OPEs are likely leads to the generation of different types of supramolecular species through triple H-bonded assemblies. For example self-aggregation of **BM-TPE** may lead to the formation of supramolecular polymers through H-bonded interactions. However, in the presence of the complementary **dCA**, **BM-TPE** may form a 2:2 dimeric H-bonded complex (Scheme 4.5). In

order to verify this hypothesis, detailed studies on the absorption and emission properties of **BM-TPE** in the absence and in the presence of **dCA** were carried out.

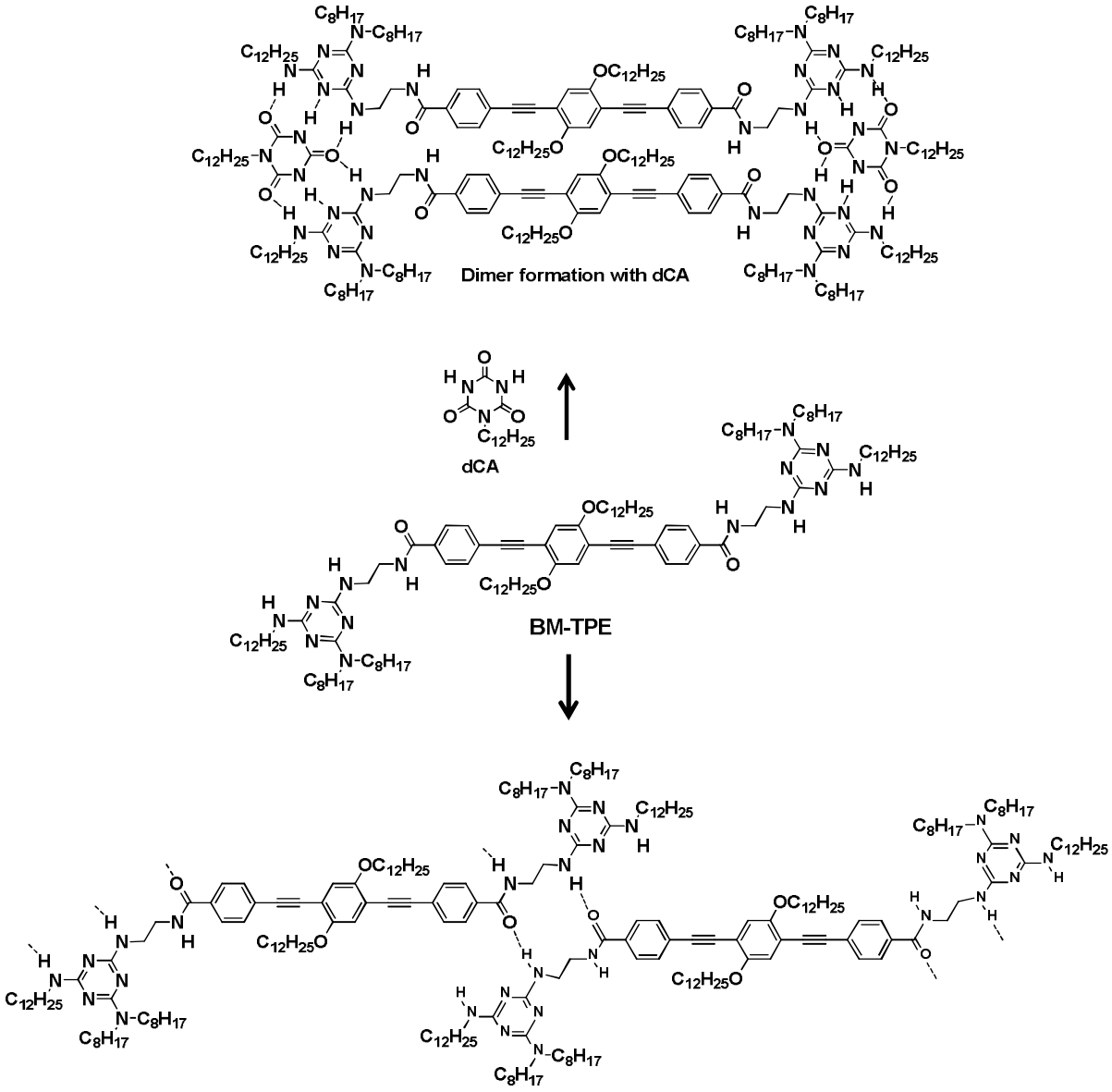

Scheme 4.5

4.3.2. Absorption and Emission Studies of BM-TPE

The UV/Vis absorption spectra of **BM-TPE** in methylcyclohexane and chloroform are shown in Figure 4.4a. The absorption spectrum of **BM-TPE** in chloroform (1×10^{-5} M) showed a broad band with two maxima at 310 nm and 377 nm. In methylcyclohexane (1×10^{-5} M), after heating and cooling to 25 °C, the molecule showed an almost similar spectrum with λ_{max} at 313 nm and 372 nm (Figure 4.4a). The emission spectrum in chloroform (1×10^{-5} M) at 25 °C showed a broad band with two maxima at 408 nm and 430 nm. In methylcyclohexane (1×10^{-5} M) at 25 °C, the emission spectrum was slightly red-shifted (Figure 4.4b). Since the absorption and emission spectra in methylcyclohexane and chloroform are almost identical except with some minor changes, it can be considered that **BM-TPE** did not form aggregates in these solvents. This is confirmed by the temperature dependent studies which revealed only minor changes to the absorption and emission spectra (Figure 4.4c and 4.4d). However, upon moving to a higher concentration (>2mM), **BM-TPE** formed gels in methylcyclohexane which indicate hierarchical self-assembly of the molecule.

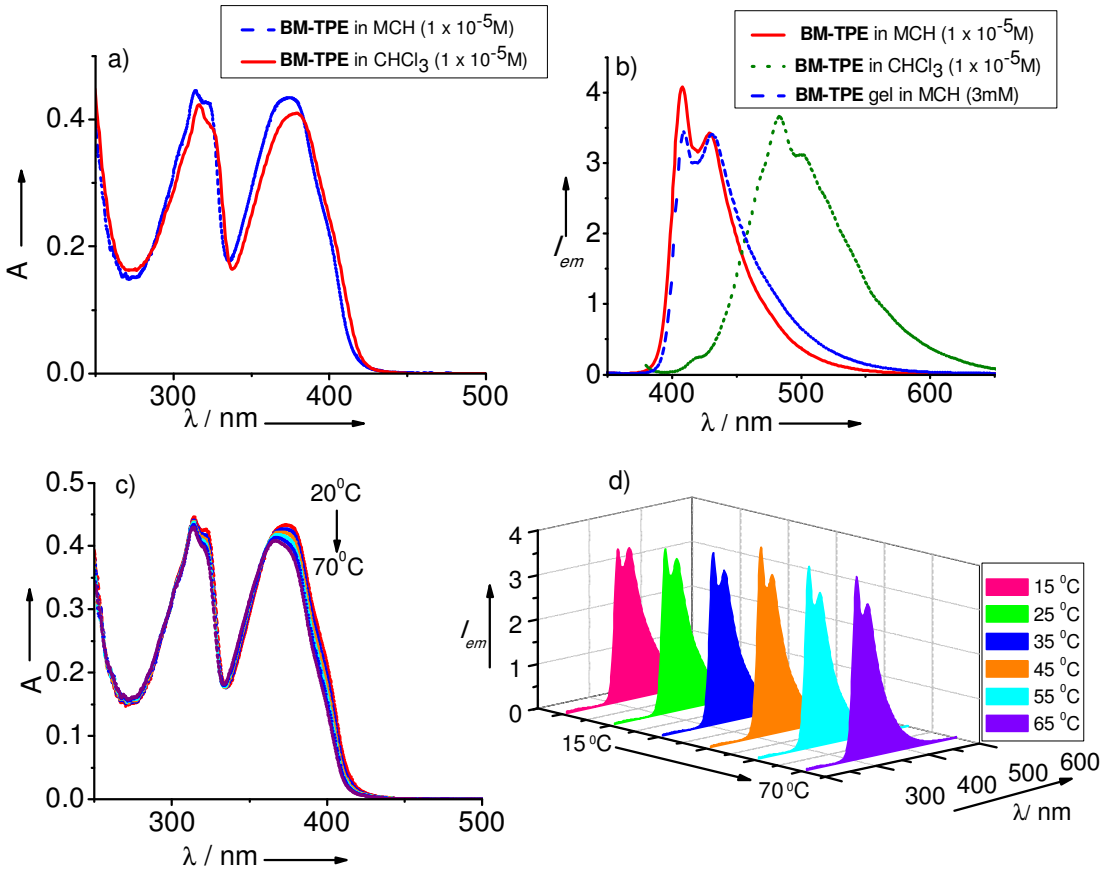

Figure 4.4. a) Absorption and b) fluorescence spectra of **BM-TPE** in $CHCl_3$ (Red curve, c = 1.0 × 10^{-5} M) and in methylcyclohexane (Blue curve, c = 1.0 ×10^{-5} M). c) Variable temperature absorption and d) fluorescence spectra of **BM-TPE** in methylcyclohexane (1 × 10^{-5} M, λ_{ex} = 370 nm).

4.3.3. Absorption and Emission Properties of the Co-assembly of BM-TPE and dCA

In order to get more insight into the aggregation behaviour of **BM-TPE**, detailed electronic spectral studies were carried out in presence of **dCA** in different solvents. For example, the UV/Vis absorption spectrum of the **BM-TPE·dCA** in methylcyclohexane (c = 1 × 10^{-5} M) showed a maximum at 367 nm,

which is 8 nm blue-shifted (Figure 4.5a) from that of **BM-TPE** in $CHCl_3$ (λ_{max} = 375 nm). This observation indicates the possibility of H-type excitonic interaction between the TPE segments. This situation could probably arise due to the conformational fixation of **BM-TPE** through H-bonded assembly with **dCA**. The emission of a 1:1 mixture of **BM-TPE** and **dCA** in methylcyclohexane (1×10^{-5} M) showed significant quenching with a red-shift of ca. 20 nm when compared to that of the monomer (λ_{em} = 430 → 448 nm), which is in good agreement with the H-type excitonic coupling (Figure 4.5b).

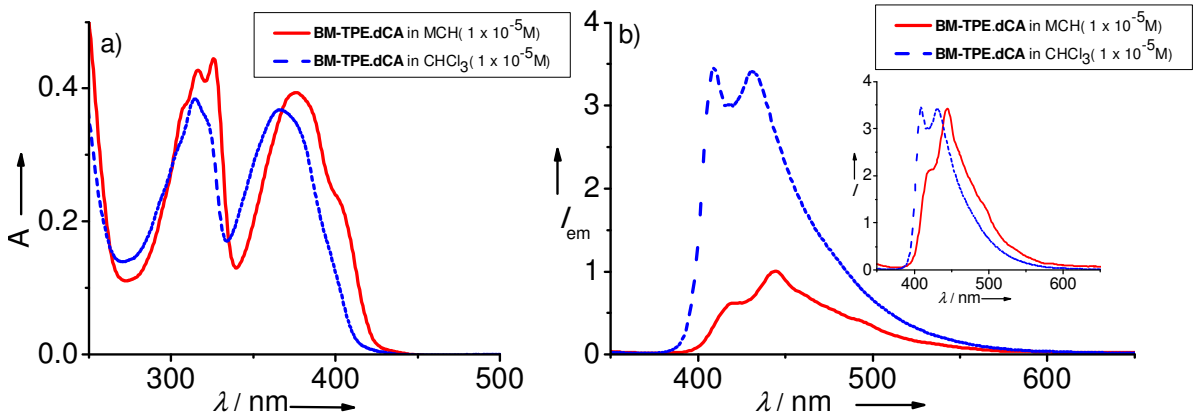

Figure 4.5. Absorption spectra of **BM-TPE·dCA** in $CHCl_3$ and in methylcyclohexane (c = 1.0 × 10^{-5} M). b) Fluorescence spectra of **BM-TPE·dCA** in methylcyclohexane and **BM-TPE·dCA** in $CHCl_3$ (c = 1.0 × 10^{-5} M). Inset in Figure b shows the normalized emission spectra of **BM-TPE·dCA**.

Figure 4.6a shows the fluorescence change upon titration of **BM-TPE** with **dCA** in methylcyclohexane. When aliquots of the ditopic **dCA** were added to the solution of **BM-TPE** at a concentration of 1×10^{-5} M, the emission was gradually quenched and red-shifted. These observations are diagnostic of the electronic

interaction between the π-conjugated molecules, possibly through the formation of a discrete dimer held together by two **dCA** molecules through 12 H-bonds in addition to π-π stacking interaction between TPE cores. In Figure 4.6b, a plot of the variation of the intensity of the emission of **BM-TPE** with increasing amounts of **dCA** is shown. Quenching of the emission gets saturated when one equivalent of **dCA** was added.

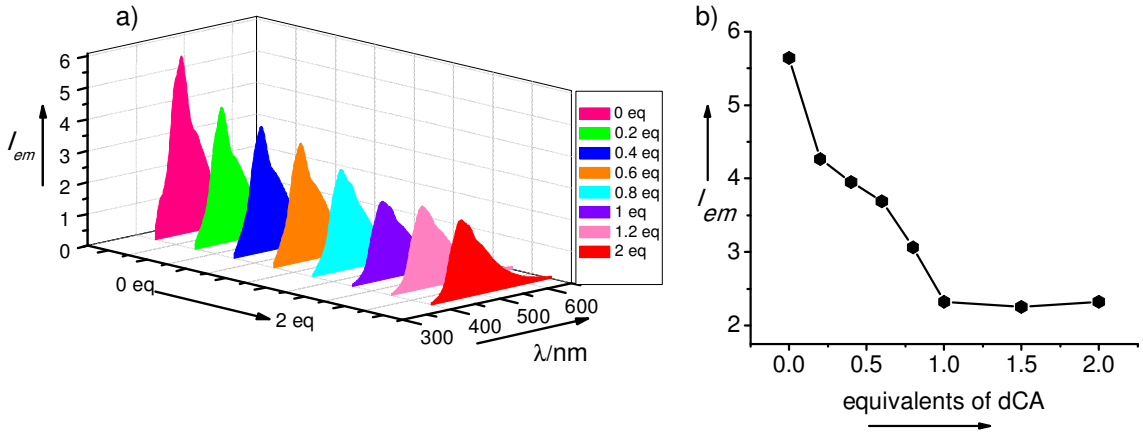

Figure 4.6. a) Change in the fluorescence intensity of **BM-TPE** (c =1 × 10^{-5} M) with different aliquots of **dCA** (c = 1 × 10^{-5} M). b) The corresponding plot of the fluorescence intensity variation.

In order to understand the stability of the dimer formed from **BM-TPE·dCA** complex, temperature dependent emission measurements were carried out. The emission intensity is initially found to be decreased upon increasing the temperature to 45 ^{o}C, whereas above 45 ^{o}C, the emission intensity is enhanced (Figure 4.7a and 4.7b). Interestingly, in the case of the self-assembly of **BM-TPE** alone, the fluorescence of the molecule did not vary much under similar experimental conditions. This is clear from the plots of the fluorescence intensities

of **BM-TPE·dCA** in the absence and presence of **dCA** at different temperatures (Figure 4.4d and 4.7b).

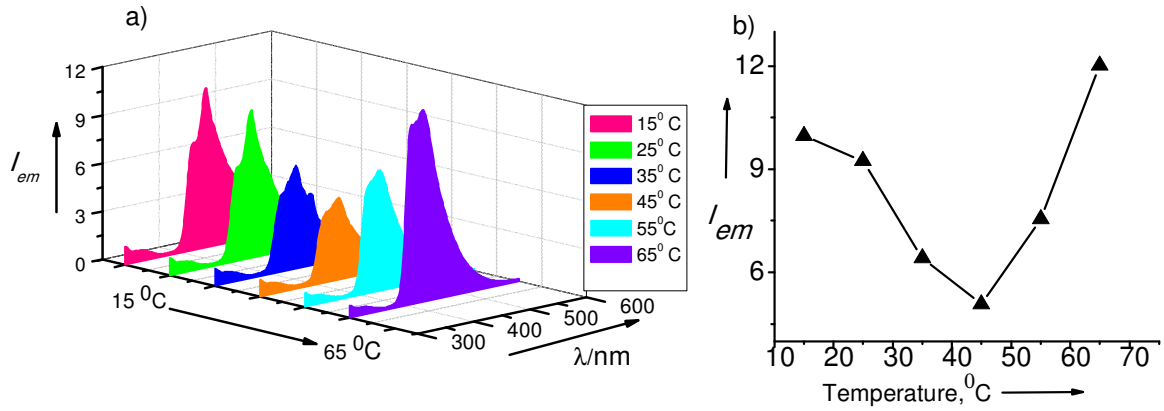

Figure 4.7. a) Variable temperature emission spectra of 1:1 complex of **BM-TPE·dCA** at 1 × 10^{-5} M. b) Plot of the fluorescence intensity changes with temperature for 1:1 complex of **BM-TPE·dCA**.

4.3.4. Optical Properties of BM-TPE and BM-TPE·dCA Gels

Hierarchical self-assembly of **BM-TPE** at higher concentrations resulted in blue emitting gels in aliphatic solvents such as hexane and methylcyclohexane. In order to get more insight into the gelation of **BM-TPE** at higher concentration in the absence and presence of **dCA**, detailed absorption and emission studies were carried out in methylcyclohexane. For example, the emission spectrum of the **BM-TPE ·dCA** gel in methylcyclohexane (c = 3 × 10^{-3} M) showed a maximum at λ = 462 nm, which is 20 nm blue-shifted (Figure 4.8a) from that of **BM-TPE** in methylcyclohexane (λ_{max} = 482 nm). This observation indicates H-type excitonic interaction between OPE segments upon conformational fixation of **BM-TPE** to form H-bonded assembly with **dCA**. The aggregate stability and the cooperative nature of the self-assembly process of **BM-TPE** and **BM-TPE·dCA** gels in

methylcyclohexane were studied by the temperature dependent fluorescence spectral changes.

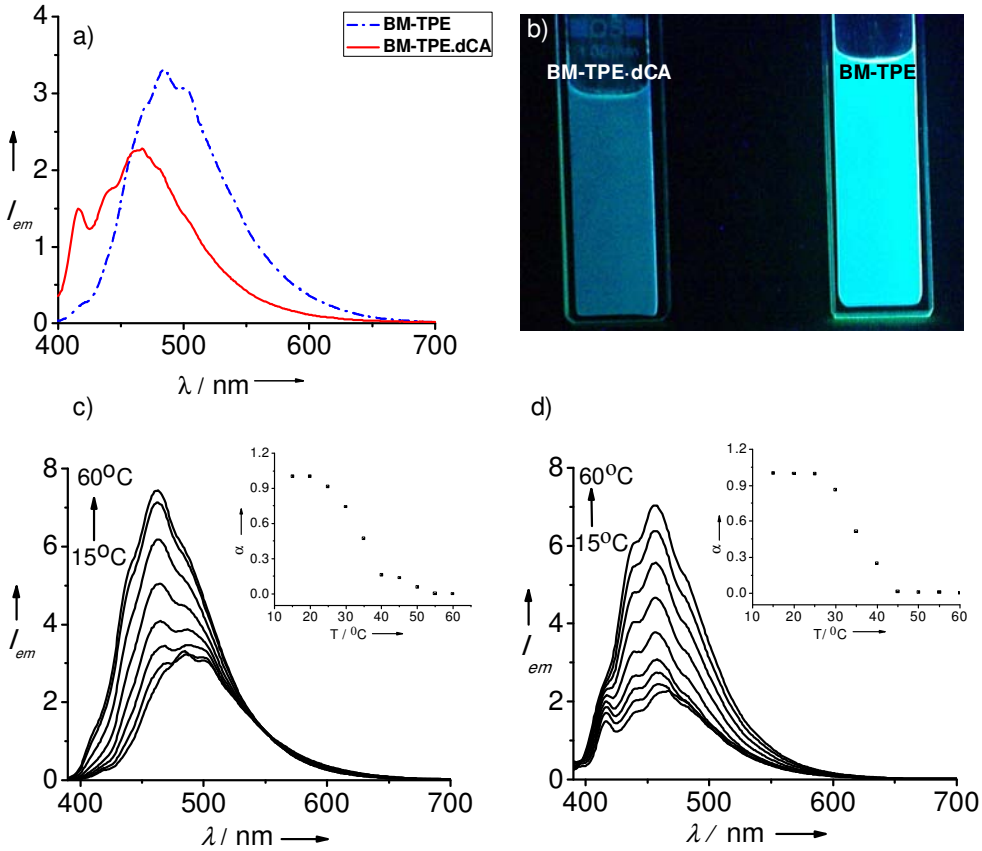

Figure 4.8. a) Emission spectra of **BM-TPE** and **BM-TPE·dCA** in methylcyclohexane (c = 3.0 × 10^{-3} M). b) Photographs of **BM-TPE** and **BM-TPE·dCA** gel in methylcyclohexane under UV (365 nm) illumination**.** c) Variable temperature emission spectra of **BM-TPE** at 3 × 10^{-3} M. d) Variable temperature emission spectra of 1:1 complex of **BM-TPE·dCA** at 3 × 10^{-3} M. Insets of Figure c and d show the plots of fraction of aggregates(α) versus temperature.

Both, **BM-TPE** and **BM-TPE·dCA** showed an increase in intensity at the emission maximum on increasing the temperature (Figure 4.8c and 4.8d). This emission changes in methylcyclohexane are due to the disruption of the self-

assembled species to the molecularly dissolved species with increase in temperature. Plots of the fraction of aggregated species (α) versus the temperature was drawn from the data obtained from the temperature dependent fluorescence (Figure 4.8c and 4.8d insets) experiments. The sigmoidal nature of the plots reveal the cooperative noncovalent interactions during the self-assembly and disassembly processes in **BM-TPE** and **BM-TPE·dCA** co-assembly. Moreover, these plots indicate better aggregate stability for **BM-TPE·dCA** co-assembly (38 °C) than that of the **BM-TPE** alone (34 °C).

In order to get more information on the gelation ability of **BM-TPE** and **BM-TPE·dCA** co-assembly, detailed gelation studies were carried out in methylcyclohexane. The critical gelator concentration (CGC) of **BM-TPE** in cyclohexane is 3 mM. The gel is turbid which indicates the tendency of the aggregates to precipitate or to form aggregates of large size which may scatter light (Figure 4.9a). In this case, the gel melting temperature (T_{gel}) at the CGC is found to be 38 ^{o}C which gradually increased with concentration. Remarkably, in the case of a 1:1 mixture of **BM-TPE·dCA**, a transparent gel is formed in aliphatic solvents (Figure 4.9a). The CGC of **BM-TPE·dCA** in methylcyclohexane is 2 mM which is less than that of **BM-TPE** alone. In this case, the T_{gel} is found to be 42 ^{o}C which is 4 ^{o}C higher than that of **BM-TPE** alone indicating that the **BM-TPE ·dCA** gel is stabilized by the complementary H-bonding interaction with **dCA**. A comparison of the plots of T_{gel} against concentration is shown in Figure 4.9b. The enhanced stability of the **BM-**

TPE·dCA gel is rationalized by the synergistic effect of the complementary H-bonding with cyanurates as well as the π-stacking of the TPE moieties.

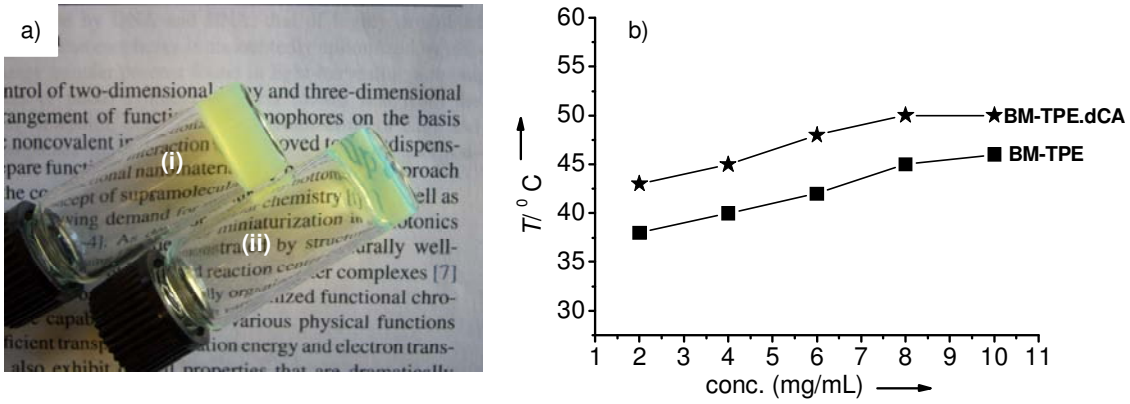

Figure 4.9. a) Photograph of the gels in methylcyclohexane in the absence (i) and in the presence (ii) of **dCA**. b) Plot of the gel melting temperature of **BM-TPE** and **BM-TPE·dCA** at different concentrations.

4.3.5. IR Spectral Studies of BM-TPE and BM-TPE·dCA Gels

Infrared spectroscopy is a useful tool for predicting the H-bond formation between donor and acceptor molecules. The formation of H-bonds causes a shift of the fundamental X-H stretching vibration and occurs as a consequence of the lengthening of the X-H bond. Since the **BM-TPE** contains the amide units, FT-IR data in the solution as well as in the gel state may give important information about the extent of involvement of the amide functional groups in the self-assembly process.[14] As the N-H and C=O groups are directly involved in the H-bonding, the relative shift in the IR values can be directly related to the involvement of the H-bonding in the self-assembly process. The FT-IR measurements of the gels have confirmed the contribution of the amide groups to the formation of the fibrous structures. A gel of **BM-TPE** in methylcyclohexane (3

mM) exhibited IR bands corresponding to the carbonyl and the N–H stretchings of the free amide groups at 1633 and 3288 cm^{-1}, respectively. In the case of **BM-TPE·dCA** gel, the former band is shifted to 1712 cm^{-1} and the latter band is completely disappeared from the original position (Figure 4.10 a and b). It can be assumed that the latter band is embedded in a broad band at around 3310 cm^{-1} involving the NH stretching of **dCA**.

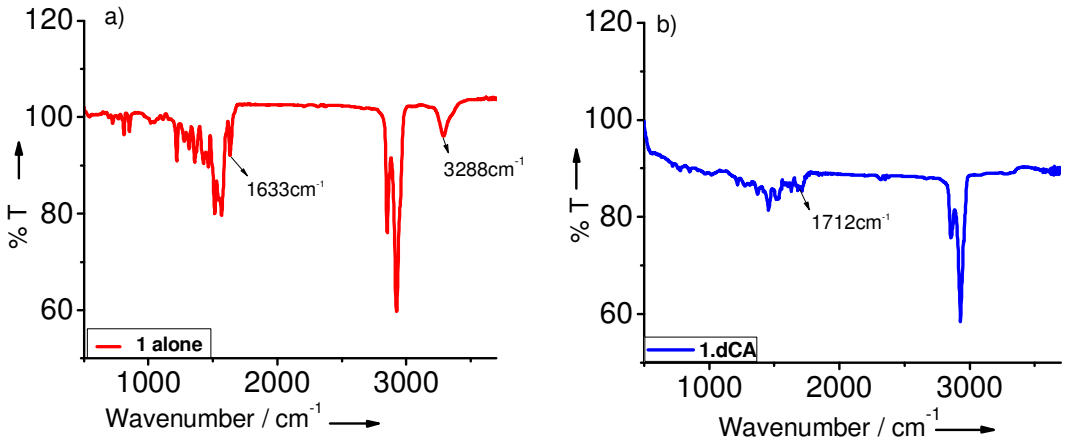

Figure 4.10. a) FT-IR spectra of **BM-TPE** and (b) **BM-TPE·dCA**.

4.3.6. Microscopic Analysis

Detailed Atomic Force Microscopy (AFM) and Transmission Electron Microscopy (TEM) studies were carried out on **BM-TPE** as well as on the co-assembly of **BM-TPE·dCA** obtained from methylcyclohexane. These studies have provided more insight into the supramolecular morphology of the aggregates formed in solution. TEM images of a drop casted dilute solution of **BM-TPE** is shown in Figure 4.11a. This image reveals the presence of fibrous network structures. The average width of fibers is ca. 100 nm. These fibers must have

originated from the bundling of the one-dimensional polymeric chains of **BM-TPE** which is formed by the amide-amide H-bonding and π-stacking. This observation is further confirmed by the AFM images of the diluted **BM-TPE** gels in methylcyclohexane which shows bundles of fibers (Figure 4.12a). The size of the smallest fiber is approximately around 40±5 nm.

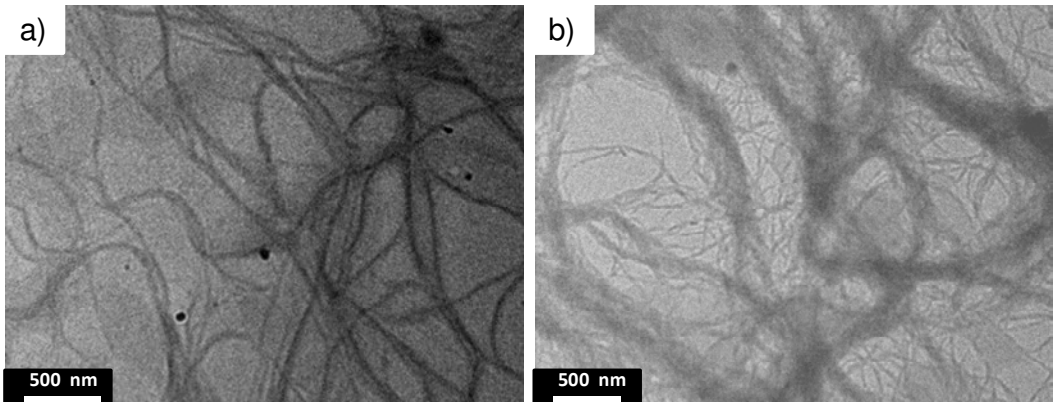

Figure 4.11. TEM images of **BM-TPE** in the absence (a) and (b) presence of **dCA**.

The TEM images of a dilute solution of **BM-TPE·dCA** showed thinner fibers of 20±5 nm in width (Figure 4.11b). In presence of solvent in the gel state, these thin fibers may be uniformly dispersed. As a result, the gel is optically transparent which is in sharp contrast to the gel of **BM-TPE** alone. When drop casted on a TEM grid, these thin and short fibers may entangle and agglomerate as can be seen in the TEM image. The AFM images in this case convincingly showed the formation of very short fibers with a length of ca. 200-250 nm and width of ca. 50 ± 5 nm (Figure 4.12b). These structures are significantly different from the long and thick fiberes formed by the self-assembly of **BM-**TPE alone (Figure 4.12 a).

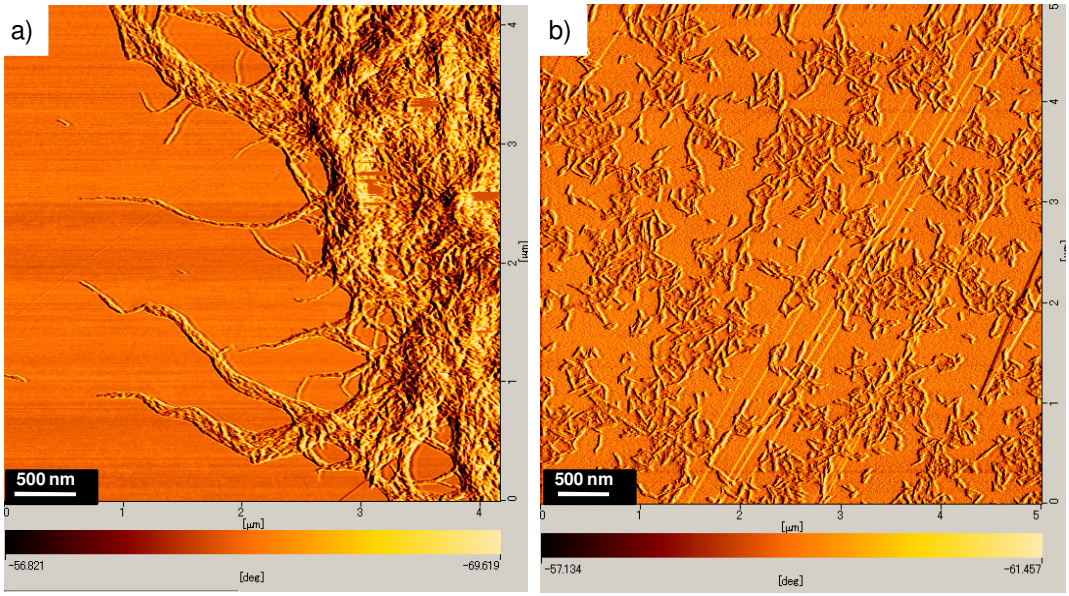

Figure 4.12. AFM images of **BM-TPE** in the absence (a) and (b) in the presence of **dCA**.

The above observations unveil a unique property of **BM-TPE** and **BM-TPE·dCA**, hierarchically organizing into discrete nanostructures in methylcyclohexane. The observed changes in the fluorescence emission, gelation properties and morphological features of **BM-TPE** in the absence and presence of **dCA** could be explained in analogy to a previous study on the self-assembly of perylene bisimide.[13] In the case of **BM-TPE·dCA**, the formation of a 2:2 dimer is invoked during the initial stage of the self-assembly as proposed in Scheme 4.5. In this dimer, **BM-TPE** is strongly bonded in an H-type fashion through twelve H-bonds. These dimers may further self-assemble to form heirarchical structures in a J-type fashion through amide H-bonding. The variable temperature fluorescence changes, thus could be explained by the selective breakage of the interaggregate J-type amide-amide H-bonding upon increasing the temperature up to 45 ^{o}C, thereby forming the H-type dimer with more favourable π-overlap which reduces the

fluorescence intensity. The H-dimers subsequently dissociate into individual components upon further increase of temperature (45–90 ^{o}C), resulting in a strong fluorescence from the molecularly dissolved TPE chromophores. In the case of **BM-TPE** alone, initially, a linear supramolecular polymeric assembly could be favoured, through the amide-amide H-bonding as suggested in Scheme 4.5. In such a situation, interchromophore interaction is minimum as indicated by the variable temperature fluorescence studies which did not show any considerable variation. At higher concentration, these noncovalent polymer chains may undergo further aggregation leading to the gelation of the solvents. A cartoon representation of the different self-assembly processes of **BM-TPE** in the absence and presence of **dCA** is shown in Figure 4.13.

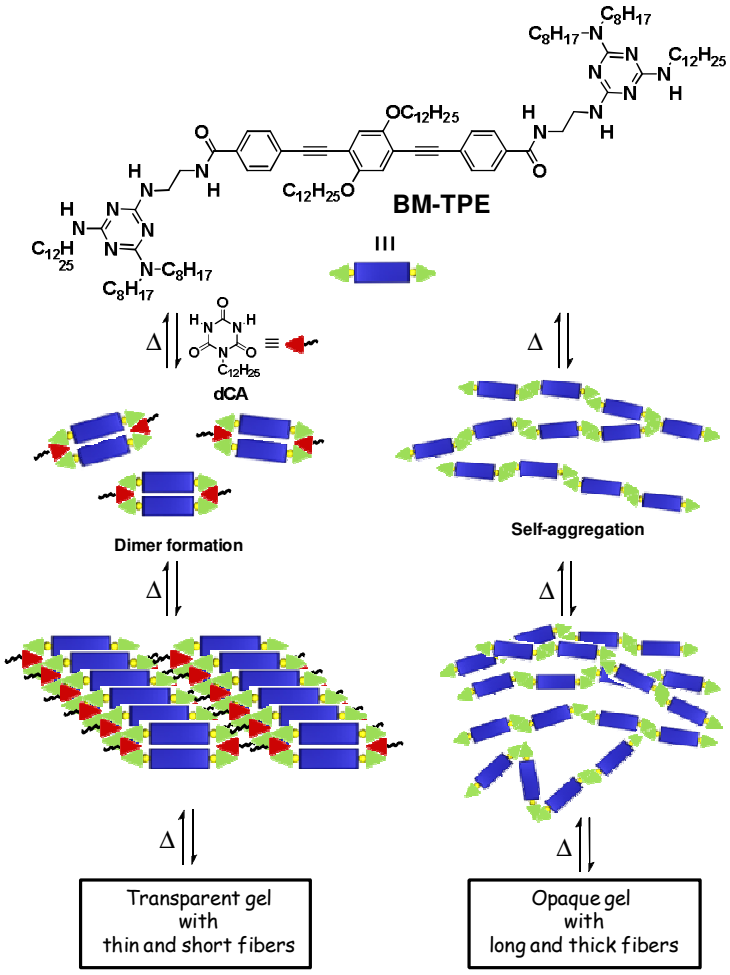

Figure 4.13. Cartoon representations of the different self-assembly processes of **BM-TPE** in the absence and presence of **dCA**

4.4. Conclusions

Melamine-functionalized tri(*p*-phenyleneethynylene) **BM-TPE** self-assembles to form opaque and weak gels in aliphatic solvents which turned transparent and stable upon addition of a cyanurate, affording supramolecular nanostructures with distinct physical properties. We have demonstrated the role of a cyanurate in the self-assembly of a melamine linked TPE thereby modifying the physical properties and morphological features of the resultant supramolecular gels. The fluorescence changes of the TPE moiety and the difference in the morphology and physical properties of the gels indicate that the molecule **BM-TPE** self-assembles to form 1D supramolecular polymers in the absence of **dCA** whereas in the presence of **dCA**, H-type dimers are formed during the initial stages of the self-assembly. This strategy can be applied to other functional chromophores to diversify their self-assembly pattern, morphology, optical and electronic properties

4.5. Experimental Section

General

All reactions were performed under an atmosphere of nitrogen unless stated otherwise. All commercially available reagents and solvents were of reagent grade and used without further purification. Silica gel plates were 250 μm thick, 60 F_{254} grade from Merck. Silica gel used was grade 60N (Spherical, Neutral, 60-210 mesh) from Kanto chemicals, Japan. ^{1}H NMR spectra were recorded on JEOL LA400 or LA500 spectrometer and chemical shifts were reported in ppm (δ) with the signal of TMS as internal standard. MALDI-TOF mass spectra were recorded

on a Voyager DE Pro (Applied Biosystems) using α-cyano-4-hydroxy cinnamic acid as the matrix. UV/Vis spectra were obtained on a JASCO V660 spectrophotometer. Fluorescence spectra were recorded on SPEX-Fluorolog F112X spectrofluorimeter.

4.5.1. Synthesis and Characterization

Details of general procedures for the coupling of terminal alkyne and for the deprotection of the TMS-protected alkyne are described in the experimental section of Chapter 2 (section 2.6.1). Preparation, yield, melting point, and spectral details of each product are given below:

1,4-Bis(dodecyloxy)benzene (6): A suspension of powdered KOH (1.4 g, 25 mmol) and DMF (50 mL) was stirred at room temperature for 30 min. Hydroquinone (1.1 g, 10 mmol) in DMF (20 mL) was added drop wise. To the stirred mixture, bromododecane (6.25 g, 25 mmol) in DMF (25 mL) was added. After stirring for 24 h under refluxing, the brownish residue obtained was poured into water (500 mL) and extracted with chloroform. The combined organic layer was washed with water, brine, and dried over anhydrous sodium sulfate and purified using column chromatography with hexane as the eluent giving **6** as a white powder in 70% yield. m. p. 70-71 °C; ^{1}H NMR (300 MHz, $CDCl_3$, TMS) δ: 0.86-0.90 (t, 6H, -CH_3), 1.26-1.79 (m, 40H, -CH_2), 3.87-3.91 (t, 4H, -OCH_2), 6.81(s, 4H, aromatic) ppm; ^{13}C NMR (75 MHz, $CDCl_3$): δ = 14.04, 22.44, 22.65, 25.62, 29.75, 29.63, 31.83, 68.01, 116.36, 129.16, 130.09, 135.36, 156.36 ppm. MS-FAB: calculated: $C_{30}H_{54}O_2$: 446.41, found: 446.25.

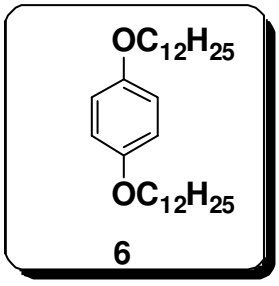

1,4-Bis(dodecyloxy)-2,5-diiodobenzene (7): To a solution of 1,4-bis(dodecyloxy)benzene (10 g, 22.4 mmol) in 225 mL of acetic acid, 20 mL of water, and 5 mL of concentrated H_2SO_4, were added KIO_3 (2.5 g, 11.7 mmol) and I_2 (7.12 g, 59.05 mmol). The reaction mixture was stirred at 80 °C for 24 h and then cooled to room temperature. Aqueous sodium thiosulfate (20%) was added until the brown color of iodine had disappeared. The mixture was poured into ice water and the white precipitate obtained was filtered. It was subsequently dissolved in chloroform and extracted with aqueous Na_2CO_3 (500 mL). The combined organic layer after washing with water and brine was dried over $MgSO_4$. The solvent was evaporated under reduced pressure and purified by column chromatography using hexane as the eluent to give **7** as white powder in 60% yield. m. p. 64-66 °C; ^{1}H NMR (300 MHz, $CDCl_3$, TMS): δ = 0.86-0.90 (t, 6H, -CH_3), 1.26-1.81 (m, 40H, -CH_2), 3.90-3.94 (t, 4H, -OCH_2), 7.17(s, 2H, aromatic) ppm; ^{13}C NMR (75 MHz, $CDCl_3$) δ: 14.44, 22.98, 26.34, 29.46, 29.87, 32.21, 68.81, 70.35, 86.57, 96.43, 113.27, 115.60, 121.89, 153.14 ppm; MS-FAB: calculated: $C_{30}H_{52}I_2O_2$: 698.21, found: 698.20.

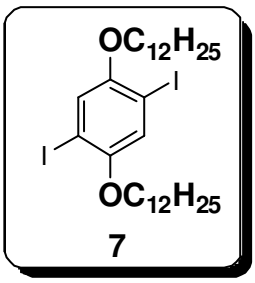

7

1,4-Bis[(trimethylsilyl)ethynyl]-2,5-bis(dodecyloxy)benzene (8): To a solution of 1,4-bis(dodecyloxy)-2,5-diiodobenzene (3 g, 4.3 mmol), was added CuI (0.0817 g, 0.43 mmol), $Pd(PPh_3)_2Cl_2$ (0.30 g, 0.43 mmol) in 30 mL of diisopropylamine, and (tri-methylsilyl)-acetylene (1.22 mL, 8.6 mmol). The reaction mixture was stirred under refluxing for 1 h. After cooling, dichloromethane (50 mL) was added, and the white

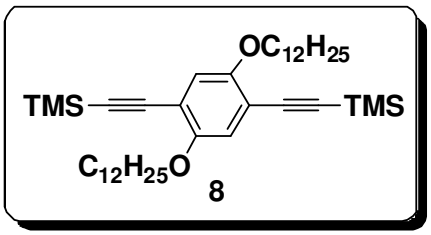

8

ammonium iodide which precipitated was filtered off. The solution was passed through a short silica gel column using toluene as the eluent. After evaporation of the solvent under reduced pressure, the crude product was column chromatographed using hexane as the eluent to give **8** as brown crystals in 75% yield. m. p. 74-75 °C; ^{1}H NMR (300 MHz, $CDCl_3$, TMS) δ: 0.25 (s, 18H, -$SiCH_3$), 0.85-0.87 (t, 6H, -CH_3), 1.25-1.82 (m, 40H, -CH_2), 3.90-3.95 (t, 4H, -OCH_2), 6.87 (s, 2H, aromatic) ppm; ^{13}C NMR (75 MHz, $CDCl_3$): δ = 19.74, 22.71, 22.89, 24.60, 28.23, 29.23, 114.20, 117.35, 153.94 ppm; MS-FAB: calculated: $C_{40}H_{70}O_2Si_2$: 638.49, found: 638.83.

1,4-Bis(ethynyl)-2,5-bis(dodecyloxy)benzene (9): Methanol (20 mL) and aqueous KOH (20%, 10 mL) were added to a THF solution of **8** (2 g, 3.14 mmol) and stirred for 2 h at room temperature. After removal of the solvent under reduced pressure, **9** was obtained in 80% yield after purification by column chromatography using hexane as the eluent. m. p. 78-79 °C; ^{1}H NMR (300 MHz, $CDCl_3$, TMS) δ: 0.85-0.88 (t, 6H, -CH_3), 1.26-1.82 (m, 40H, -CH_2), 3.33-3.36 (s, 2H, -C≡C-H), 3.94-3.99 (t, 4H, -OCH_2), 6.84 (s, 2H, aromatic) ppm; ^{13}C NMR (75 MHz, $CDCl_3$): δ = 14.09, 22.66, 25.87, 29.10, 29.31, 29.54, 31.89, 69.62, 79.76, 82.37, 113.22, 117.70, 153.94 ppm; MS-FAB: calculated: $C_{34}H_{54}O_2$: 494.41, found: 494.29.

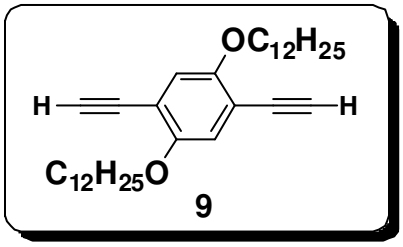

9

Synthesis of dimethyl 4, 4'-(2,5-bis(dodecyloxy)-1,4-phenylene)bis(ethyne-2,1-diyl)dibenzoate (10): To a solution of **9** (0.250 g, 0.500 mmol) in triethylamine

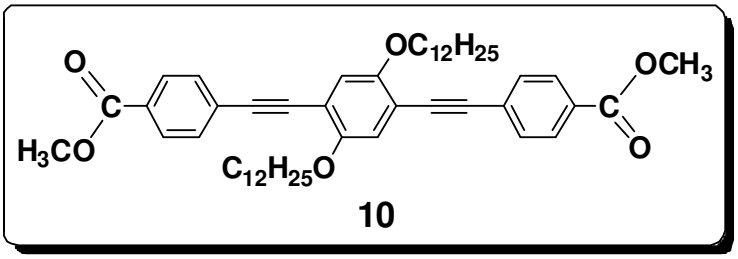

10

(20 mL), $Pd(PPh_3)_2Cl_2$ (0.082 g, 0.116 mmol) and CuI (0.022 g, 0.116 mmol) were added followed by dry THF (5 mL) as the co-solvent. 4-Iodobenzoate (0.262 g, 0.116 mmol) was then added and the reaction mixture was kept at ambient temperature (50 °C) for 12 h. After the completion of the reaction, the mixture was passed through a short celite column using CH_2Cl_2 as the eluent. The fractions were collected and the solvent was removed under reduced pressure. The crude product obtained was further purified by column chromatography (3% EtOAc/Hexane) to give the compound **10** as a yellow solid (Yield, 78%). m. p. 95-97 °C ^{1}H NMR (400 MHz, $CDCl_3$) δ : 8.03-8.01 (d, J = 8 Hz, 4H, aromatic), 7.79-7.75 (d, 4H, aromatic), 7.03-6.99 (d, 2H, aromatic), 4.06-4.02 (m, 4H, OCH_2), 3.97 (s, 6H, OCH_3), 1.87 (m, 6H), 1.55 (m,8H), 1.37 (m,22H), 0.87 (m, 10H) ppm; HRMS-FAB: $[M]^+$ Calcd for $C_{50}H_{66}O_6$, 762.49; found:763.01

Synthesis of 4, 4'-(2,5-bis(dodecyloxy)-1,4-phenylene)bis(ethyne-2,1-diyl)di-benzoic acid (11): To a solution of **10** (0.500 g, 0.650 mmol) in THF, 20% KOH

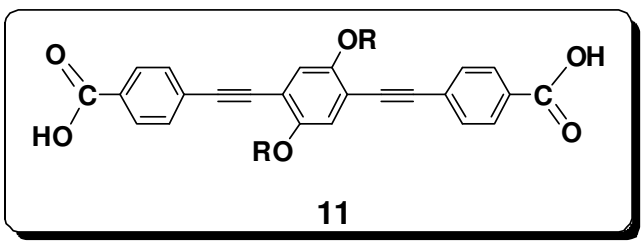

11

in methanol was added and refluxed for 3 h. The reaction mixture was tested for completion of the reaction by TLC. Subsequently, the reaction mixture was poured into 10% HCl, the precipitate

formed was filtered, dried and used for the next step (Yield, 61 %). ^{1}H NMR (400 MHz, $CDCl_3$) δ: 8.05-8.03 (d, J = 8 Hz, 4H, aromatic), 7.60-7.57 (d, J = 8 Hz, 4H, aromatic), 7.03-6.99 (d, 2H, aromatic), 4.04-4.01 (m, 4H, OCH_2), 1.85 (m, 4H), 1.35 (m, 32H), 0.85 (t, 12H) ppm; HRMS-FAB: $[M]^+$ Calcd for $C_{48}H_{62}O_6$, 734.65; found: 734.02

Synthesis of 6-chloro-N^2-dodecyl-N^4, N^4-dioctyl-1,3,5-triazine-2,4-diamine (13): To a mixture of **12** (6 g, 32.53 mmol) and DIPEA (15 mL) in dry THF (100 mL) was added dodecylamine (6.035 g, 32.53 mmol) drop wise in dry THF for 1 h in an ice bath. The reaction was allowed to continue for 1 h and brought to room temperature. To the reaction mixture, dicoctyl amine (7.85 g, 32.53 mmol) was added drop wise at room temperature and allowed to react for 2 h. The reaction mixture was filtered to remove the salt, and then evaporated. The residue was extracted with dilute HCl and water, dried over anhydrous sodium sulphate followed by removal of the solvent under vacuum. The product obtained was reprecipitated from methanol to yield the compound **13** in 80%. m. p. 75-77 °C; ^{1}H NMR (400 MHz, $CDCl_3$) δ: 6.61 (2H), 3.59 (m, 4H, NCH_2), 3.40 (m, 4H, NCH_2) 3.25-3.22 (m, 4H, NCH_2) (m, 4H), 2.16 (m, 3H), 1.5-1.57 (m, 9H) ppm; HRMS-FAB: $[M]^+$ Calcd for $C_{31}H_{60}ClN_5$, 537.45; found: 537.01.

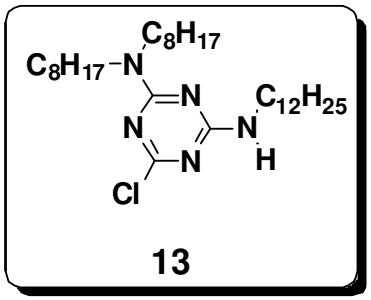

13

Synthesis of N^2-(2-aminoethyl)-N^4-dodecyl-N^6, N^6-dioctyl-1,3,5-triazine-2,4,6-triamine (14): To a solution of **13** (2 g, 3.72 mmol) in dry THF (30 mL), ethylene diamine (2.23 g, 37.5 mmol) was added drop wise and refluxed for 10 h. The

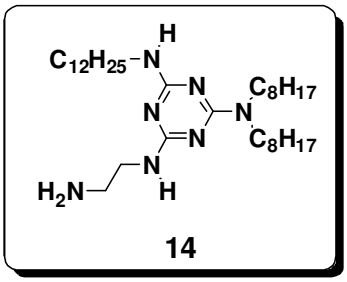

14

solvent was removed from the reaction mixture, the residue was dissolved in $CHCl_3$ and extracted with water. The organic layer was collected, concentrated under vacuum and purified by column chromatography with 2% MeOH in $CHCl_3$ to yield the compound **14** in 80%. m. p. 65-67 °C; ^{1}H NMR (400 MHz, $CDCl_3$) δ : 6.61(2H, 3.40 (m, 4H, NCH_2) 3.25-3.22 (m, 4H, NCH_2) (m, 4H), 2.16 (m, 3H), 1.5-1.57 (m, 9H) ppm; HRMS-FAB: $[M]^+$ Calcd for $C_{33}H_{67}N_7$, 561.55; found: 560.1.

Synthesis of 4'-(2,5-bis(dodecyloxy)-1,4-phenylene)bis(ethyne-2,1-diyl)bis-(*N*-(2-(4-(dioctylamino)-6-(dodecylamino)-1,3,5-triazin-2-ylamino)ethyl) benzamide) (BM-TPE): To a solution of **14** (0.150 g, 0.205 mmol) and alkyl substituted melamine (**14**) (0.240g, 0.428 mmol) in dry DCM, *N*-ethyl-*N*′-(3-dimethylaminopropyl)-carbodiimide (WSC) (0.196 g, 1.024 mmol) dissolved in 30 mL of dry DCM was added drop wise in cold condition. The reaction mixture was stirred at room temperature for 8 h, poured into water (500 mL) and extracted with dichloromethane. The organic fractions were collected and dried with anhydrous sodium sulphate. The crude product was purified by column chromatography (EtOAc: Hexane) followed by repeated precipitation from methanol (Yield, 53%). m. p. 102-104 °C; ^{1}H NMR (400 MHz,

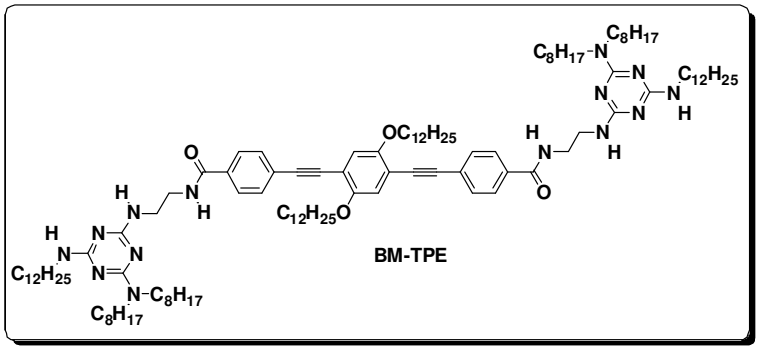

BM-TPE

$CDCl_3$) δ : 7.70-7.68 (d, J = 8 Hz, 4H, aromatic), 7.52-7.50 (d, J = 8 Hz, 4H, aromatic), 6.99 (s, 2H, aromatic), 4.96 (s, 2H), 4.63 (s, 2H), 4.04 (m, 4H ,OCH_2), 3.62 (s, 8H) , 3.43-3.32 (m, 12H), 1.85-1.82 (m, 5H), 1.54 (m, 24H), 1.25 (m, 99H), 0.86 (m, 26H) ppm; MALDI-TOF: $[M+H]^+$ Calcd for $C_{114}H_{192}N_{14}O_4$, 1821.53; found:1822.93

4.5.2. Description of Experimental Techniques

Details of the instrumentation are described in the experimental section of Chapter 2 (section 2.6.2).

Atomic Force Microscopy (AFM)

Samples for the AFM analyses were prepared as follows: Methylcyclohexane solutions of **BM-TPE** and **BM-TPE·dCA** assemblies were prepared by mixing chloroform solution of **BM-TPE** and chloroform/methanol mixed solution of **dCA** with a 1:1 molar stoichiometry and the solvent was evaporated thoroughly. The resulting solid was dissolved in methylcyclohexane by gentle heating to give methylcyclohexane solutions of the H-bonded assemblies of **BM-TPE** and **dCA**. In another method, compounds **BM-TPE** and **dCA** were taken in 1:1 molar ratio in a screw capped vial and dissolved in a mixture of chloroform and methanol (1:1) ($c = 1 \times 10^{-2}$ M in 1 mL) by sonication followed by heating, It was then flushed with nitrogen gas to remove the solvent and further dried in vacuum for 36 h. It was then dissolved in methylcyclohexane and diluted to required concentrations for each measurement. For all AFM analysis, only the aged solution (thermodynamically equilibrated solution) was used. Samples were

prepared by drop casting the diluted gel samples (**BM-TPE** or **BM-TPE·dCA** in methylcyclohexane) at a concentration of $c = 1 \times 10^{-5}$ M, on a freshly cleaved highly oriented pyrolytic graphite (HOPG). Samples were dried under vacuum for 24 h after spin coating. AFM images were acquired under ambient conditions using SII Nano Navi station (SII Nanotechnology Inc, Japan) with an SPA-400 Probe unit operated with dynamic force mode. Silicon cantilevers (OMCL-AC160TS-C2) with a spring constant of 42 N/m and frequency of 300 kHz (nominal value, Olympus, Japan) were used for the AFM observations in air. The scan rate was varied from 1 to 2 Hz.

Transmission Electron Microscopy (TEM)

The samples for TEM analyses were prepared by drop casting the diluted gel samples (**BM-TPE** or **BM-TPE·dCA**) in methylcyclohexane at a concentration of 1×10^{-5} M on to carbon coated copper grids (400 mesh). TEM images were obtained after drying the sample in vacuum for 24 h.

4.6. References

1 . (a) S. C. Zimmerman and P. S. Corbin, *Struct. Bonding*, **2000**, *96*, 63.
b) S. Yagai, *J. Photochem. Photobiol. C: Photochem. Rev,* **2006**,*7,* 164.

2. (a) G. M. Whitesides, E. E. Simanek, J. P. Mathias, C. T. Seto, D. Chin, M. Mammen and D. M. Gordon, *Acc. Chem. Res*. **1995**, *28*, 37; (b) P. Timmerman and L. J. Prins, Eur. *J. Org. Chem*., **2001**, 3191; (c) A. Ranganathan, V. R. Pedireddi, C. N. R. Rao, *J. Am. Chem. Soc*. **1999**, *121*, 1752.

3 . (a) Albertus P. H. J. Schenning, E. W. Meijer, *Chem. Commun*, **2005**, 3245; (b) A. Ajayaghosh, S. J. George , A. P. H. J. Schenning, *Top. Curr. Chem,* **2005**, *258*, 83; (c) M. Wolffs, S. J. George, Z. Tomovic, S. C. J.Meskers, A. P. H. J. Schenning and E.W. Meijer*, Angew. Chem. Int. Ed,* **2007***,46,* 8203.

4. (a) F. Würthner, S. Yao, B. Heise and C. Tschierske, *Chem. Commun*. **2001**, 2260; (b) F. Würthner, Z. Chen, F. J. M. Hoeben, P. Osswald, C.-C. You, P. Jonkheijm, J. V. Herrikhuyzen, A. P. H. J. Schenning, P. P. A. M. van der Schoot, E. W. Meijer, E. H. A. Beckers, S. C. J. Meskers and R. A. J. Janssen, *J. Am. Chem. Soc*. **2004**, *126*, 10611; (c) A. R. Hirst, J. F. Miravet, B. Escuder, L. Noriez, V. Castelleto, I. W. Hamley, D. K. Smith, *Chem. Eur. J*. **2009**, *15*, 372; (d) V. Percec, M. Peterca, M. E. Yurchenko, J. G. Rudick, and P. A. Heiney, *Chem. Eur. J*., **2008**, *14*, 909; (e) A. R. Hirst, and D. K. Smith; *Chem. Eur. J*. **2005**, *11*, 5496; (f) J. R. Moffat and D. K. Smith; *Chem comm*. **2009**, 316; (f) A. R. Hirst and D. K. Smith; *Top. Curr. Chem*. **2005**, *256*, 237.

5. (a) A. Ajayaghosh and S. J. George, *J. Am. Chem. Soc*. **2001**, *123*, 5148; (b) A. Ajayaghosh and V. K. Praveen, *Acc. Chem. Res*. **2007**, *40*, 644; (c) A. Ajayaghosh, V. K. Praveen and C. Vijayakumar, *Chem. Soc. Rev*., **2008**, *37*, 109; (d) S. S. Babu, V. K. Praveen, S. Prasanthkumar, A. Ajayaghosh, *Chem. -Eur. J*. **2008**, *14*, 9577; (e) S. S. Babu, S. Mahesh, K. K. Kartha, A. Ajayaghosh; *Chem. -Asian. J*. **2008**, *4*, 824;

(f) V. K. Praveen, S. S. Babu, C. Vijayakumar, R. Varghese, A. Ajayaghosh, *Bull. Chem. Soc. Jpn*. **2008**, *81*, 1196

6 (a) S. Yagai, T. Nakajima, K. Kishikawa, S. Kohmoto, T. Karatsu and A. Kitamura, *J. Am. Chem. Soc*. **2005**, *127*, 11134; (b) S. Yagai, M. Higashi, T. Karatsu and A. Kitamura, *Chem. Mater*. **2005**, *17*, 4392; (c) S. Yagai, M. Higashi, T. Karatsu and A. Kitamura, *Chem. Commun*. **2006**, 1500; (d) S. Yagai, T. Kinoshita, M. Higashi, K. Kishikawa, T. Nakanishi, T. Karatsu and A. Kitamura, *J. Am. Chem. Soc*. **2007**, *129*, 13277; (e) S. Yagai, Y. Monma, N. Kawauchi, T. Karatsu and A. Kitamura, *Org. Lett*. **2007**, *9*, 1137; (f) S. Yagai, T. Seki, T. Karatsu, A. Kitamura and F. Würthner, *Angew. Chem. Int. Ed*, **2008**, *47*, 3367; (g) T. Seki, S. Yagai, T. Karatsu and A. Kitamura, *J. Org. Chem*. **2008**, *73*, 3328.

7. (a) S. Yagai, S. Mahesh, Y. Kikkawa, K. Unoike, T. Karatsu, A. Kitamura A. Ajayaghosh, *Angew.Chem. Int. Ed*. **2008**, *47*, 4691; (b) A. Ajayaghosh, R. Varghese, S. Mahesh, V. K. Praveen, *Angew. Chem. Int. Ed*. **2006**, *45*, 7729; (c) A. Ajayaghosh, R. Varghese, V. K. Praveen, S. Mahesh, *Angew.Chem. Int. Ed*. **2006**, *45*, 3261.

8. a) K. Yoosaf, A. Belbakra, N. Armaroli, A. Llanes-Pallasb, D. Bonifazi, *Chem. Commun*. **2009**, 2830; (b) G. Fernández, F. García, L. Sánchez, *Chem. Commun*. **2008**, 6567; (c) F. García, G. Fernández, L. Sánchez, *Chem. Eur. J.* **2009** (In Press, DOI: 10.1002/chem.200900303); (d) F. García, F. Aparicio, G. Fernández, and L. Sánchez, *Org. Lett*. **2009**, (In

Press, DOI: 10.1021/ol900832e) (e) H. S. Seo, J. Y. Chang, G. N. Tew, *Angew. Chem. Int. Ed*. **2006**, *45*, 7526.

9 . S. Yagai, Y. Monma, N. Kawauchi, T. Karatsu and A. Kitamura, *Org. Lett*. **2007**, *9*, 1137.

10 . T. Seki, S. Yagai, T. Karatsu and A. Kitamura, *J. Org. Chem*., **2008**, *73*, 3328.

11. S. Yagai, S. Kubota, K. Unoike, T. Karatsu and A. Kitamura, *Chem. Commun*. **2008**, 4466.

12 . K. Sonogashira, Y. Tohda, N. Hagihara, *Tetrahedron Lett*. **1975**, *16*, 4467.

13. T. Seki, S. Yagai, T. Karatsu and A. Kitamura, *J. Org. Chem.* 2008, *73*, 3328.

14. Y. Jeong, K. Hanabusa, H. Masunaga, I. Akiba, K. Miyoshi, S. Sakurai, K. Sakurai, *Langmuir* **2005**, *21,* 586; b) M. Suzuki, Y. Nakajima, M. Yumoto, M. Kimura, H. Shirai, K. Hanabusa, *Langmuir* **2003**, *19,* 8622; c) X.-Q. Li, V. Stepanenko, Z. Chen, P. Prins, L. D. A. Siebbeles, F. Würthner, *Chem. Commun.* **2006**, 3871.

LIST OF PUBLICATIONS

1. Evolution of nano to microsized spherical assemblies of a short oligo(*p*-phenyleneethynylene) into superstructured organogels, A. Ajayaghosh, R. Varghese, V. K. Praveen, **S. Mahesh,** *Angew. Chem. Int. Ed.* **2006**, *45*, 3261-3264.

2. Vesicles to helical nanotubes: an unprecedented "sergeant and soldiers" effect in the self-assembly of oligo(*p*-phenyleneethynylene)s, A. Ajayaghosh, R. Varghese, **S. Mahesh**, V. K. Praveen, *Angew. Chem. Int. Ed.* **2006**, *45*, 7729-7732.

3. Toroidal nanoobjects from rosette assemblies of melamine-linked oligo(*p* phenyleneethynylene)s and cyanurates, S. Yagai, **S. Mahesh**, Y. Kikkawa, K. Unoike, T. Karatsu, A. Kitamura, A. Ajayaghosh, *Angew. Chem. Int. Ed.* **2008**, *47*, 4691-4694 (**article with cover page**).

4. Solvent-directed self-assembly of π-gelators to hierarchical macroporous Structures and aligned fiber bundles, S. S. Babu, **S. Mahesh**, K. K. Kartha, A. Ajayaghosh, *Chem.-Asian. J*. **2008**, *4*, 824-829.

5. Role of complementary H-bonding interaction of a cyanurate in the self-assembly and gelation of melamine linked tri(*p*-phenyleneethynylene)s, **S. Mahesh**, R. Thirumalai, S. Yagai, A. Kitamura, A. Ajayaghosh, *Chem*. *Comm,* **2009***,* 5984-5986 (**article with cover page**).

6. Reversible self-assembly of entrapped fluorescent gelators in polymerized styrene gel matrix: erasable thermal imaging via recreation of supramolecular architectures, S. Srinivasan, P. A. Babu**, S. Mahesh**, A. Ajayaghosh, *J. Am. Chem. Soc.*, **2009**, *131*, 15122–15123.

PAPERS PRESENTED AT CONFERENCES

1. Toroidal nanostructure from hydrogen-bonded rosettes of melamine-linked oligo(*p*-phenyleneethynylene)s and cyanurates, **S. Mahesh**, S. Yagai, A. Kitamura, A. Ajayaghosh, International symposium (Indo-Japan cooperative science programme) on "Recent Trends in Molecular Materials Research" January 20-22, 2008, Trivandrum, India

COVER PAGES

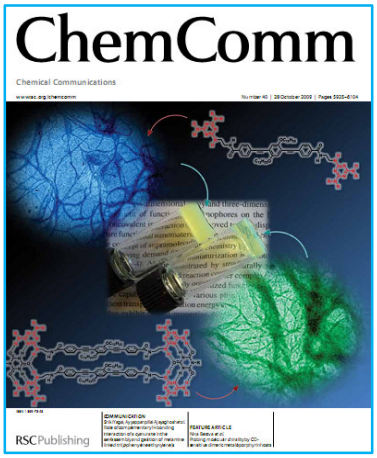


A Journal of the Gesellschaft Deutscher Chemiker
Angewandte Chemie
International Edition
www.angewandte.org
2008–47/25
GDCh
Rosette
Nanodonut
40 nm
Nanodonuts ...
WILEY-VCH

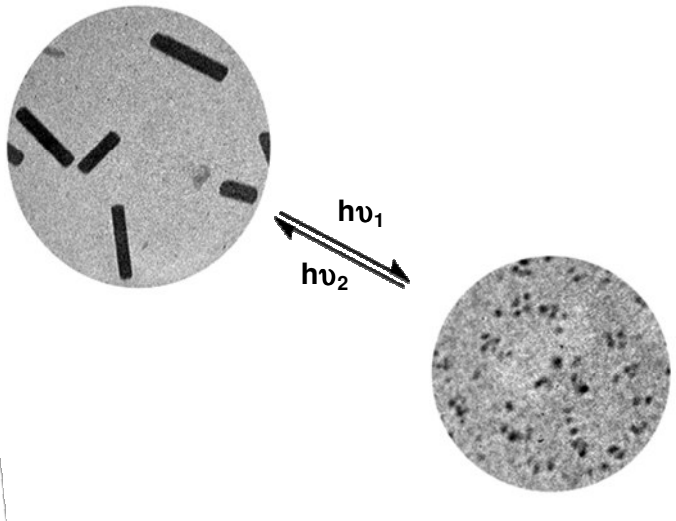
hυ1
hυ2

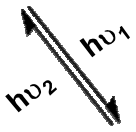
hυ1
hυ2

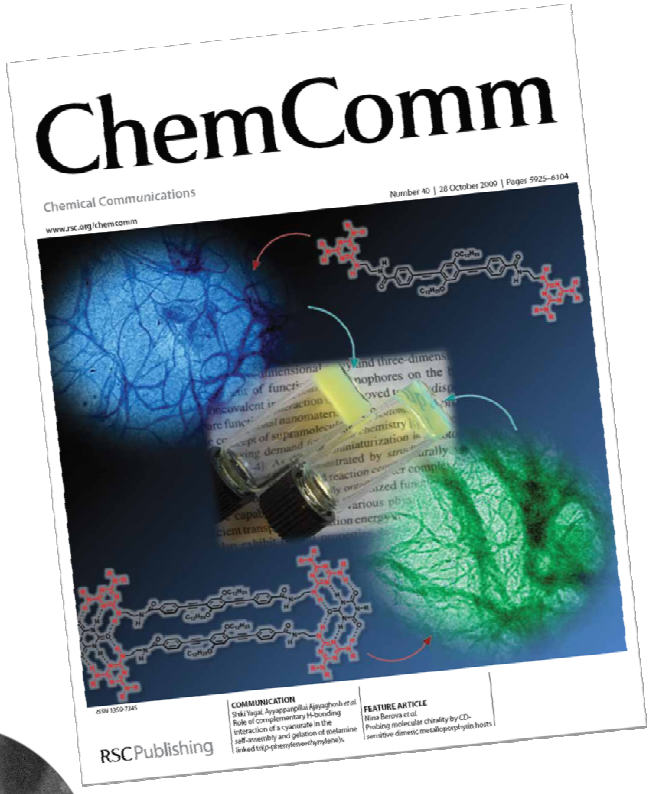
ChemComm
Chemical Communications
RSC Publishing

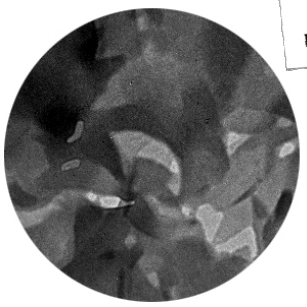

2009

NIIST